UNIVERSIDAD COMPLUTENSE DE MADRID
FACULTAD DE CIENCIAS MATEMÁTICAS
SECCIÓN DEPARTAMENTAL DE ASTRONOMÍA Y GEODESIA

UNIVERSITÉ DE STRASBOURG

ECOLE DOCTORALE DES SCIENCES DE LA TERRE, DE L'UNIVERS ET DE L'ENVIRONNEMENT
INSTITUT DE PHYSIQUE DU GLOBE DE STRASBOURG

ANALYSIS OF LONG-TERM GRAVITY RECORDS IN EUROPE; CONSEQUENCES FOR THE RETRIEVAL OF SMALL AMPLITUDE AND LOW FREQUENCY SIGNALS INCLUDING THE EARTH'S CORE RESONANCE EFFECTS

MEMORIA PARA OPTAR AL GRADO DE DOCTOR
PRESENTADA POR

Marta Calvo García-Maroto

Bajo la dirección de los Doctores:
José Arnoso Sampedro
Científico Titular - Instituto de Geociencias (CSIC-UCM)

Jacques Hinderer
Directeur de Recherches, EOST-IPGS-Université de Strasbourg

Madrid, 2015

UNIVERSIDAD COMPLUTENSE DE MADRID
FACULTAD DE CIENCIAS MATEMÁTICAS
SECCIÓN DEPARTAMENTAL DE ASTRONOMÍA Y GEODESIA

UNIVERSITÉ DE STRASBOURG

ECOLE DOCTORALE DES SCIENCES DE LA TERRE, DE L'UNIVERS ET DE L'ENVIRONNEMENT
INSTITUT DE PHYSIQUE DU GLOBE DE STRASBOURG

Thèse de doctorat présentée par :
Marta Calvo García-Maroto

ANALYSIS OF LONG-TERM GRAVITY RECORDS IN EUROPE; CONSEQUENCES FOR THE RETRIEVAL OF SMALL AMPLITUDE AND LOW FREQUENCY SIGNALS INCLUDING THE EARTH'S CORE RESONANCE EFFECTS

en vue de l'obtention du titre de Docteur de l'Université de Strasbourg
Spécialité : Sciences de la Terre

Thèse dirigée par :

Jacques Hinderer,   Directeur de recherches,
                        Université de Strasbourg
José Arnoso Sampedro, Científico Titular
                        Instituto de Geociencias (CSIC-UCM)

Soutenue publiquement, à l'Universidad Complutense de Madrid, Espagne, devant le jury composé de:

Mme. Mª Pilar Romero Pérez	Rapporteur externe
M. Nicolas Florsch	Rapporteur externe
M. Yves Rogister	Rapporteur interne
M. Jacques Hinderer	Directeur de thèse
M. Jose Arnoso Sanpedro	Directeur de thèse
M. Machiel Simon Bos	Examinateur

Madrid, 2015

Table of contents

Acknowledgements

Abstract

Temporal gravity variation measurements have been a long historical tradition in Central Europe, with some stations recording for decades. From the 80s, time varying gravity is permanently recorded at the Earth's surface by a worldwide network of superconducting relative gravimeters within the Global Geodynamics Project of the International Association of Geodesy.

In one of these stations, located in Strasbourg since the 1970s, the three main gravimeter types (relative spring gravimeter, relative superconducting gravimeter, and absolute gravimeter) have been set up. We use all these series to review the instrumental betterments. Studying the different improvements on gravimeters in the last years, mainly in terms of long term stability and instrumental drift, we show that the superconducting gravimeters can uniquely contribute to the study of the low frequency Earth's tides and small amplitudes waves. Also, the stability of the scale factor of the superconducting gravimeters is studied with the help of numerous calibration experiments carried out by collocated absolute measurements at Strasbourg Observatory.

Finally, after estimating the values of the Free Core Nutation parameters, we search for the rotational normal mode called Free Inner Core Nutation (FICN), the gravity effect of which has never been observed before. For this purpose we develop a methodology to constrain the possible frequency range, through the detailed tidal analysis in the diurnal frequency band, using the 27-year superconducting gravity series recorded at J9 observatory, to separate small amplitude waves that have never been studied before, and which could be close enough to the frequency range of the FICN to be affected in terms of resonant amplitude.

This work contributes to show the importance of not only the length, but also the quality of the data series to improve our knowledge of the Earth's dynamics.

Keywords: spring gravimeters, absolute gravimeters, superconducting gravimeters, Earth's tides, tidal potential of degree 3, long-period tides, time stability, instrumental drift, calibration, rotational normal modes.

List of figures

List of Tables

List of used abbreviations

AG	Absolute Gravimeter
AP	Air Pressure
BFO	Black Forest Observatory, Schiltach, Germany
C026	SG model at J9 Observatory (1996-present)
CAG	Cold-Atom Gravimeter
CMB	Core-Mantle Boundary
CPD	Cycle per Day
CPSD	Cycle per Sidereal Day
CW	Chandler Wobble
DAS	Data Acquisition System
ECGS	European Center for Geodynamics and Seismology
ECMWF	European Centre for Medium-Range Weather Forecast
EOST	Ecole et Observatoire des Sciences de la Terre
ET	Earth Tides
ETERNA	Eterna program package v. 3.30 (3.40), Wenzel, H-G, (1996)
FCN	Free Core Nutation
FICN	Free Inner Core Nutation
GGP	Global Geodynamics Project (since 1997)
GGP-ISDC	GGP Information System and Data Center (GFZ)
GGP2	Gravity card and filter in GGP (for SG C026 from 1997 to 2010)
GGP1	Gravity card and filter in GGP (for SG C026 since April 2010)
GPS	Global Positioning System
GRACE	Gravity Recovery and Climate Experiment, space gravimetry
GWR	Manufacturer of SGs (San Diego, California, USA)
HW95	Hartmann and Wenzel Catalogue, 1995
ICB	Inner Core Boundary
ICET	International Center for Earth Tides
ICW	Inner Core Wobble
IERS	International Earth Rotation and Reference Systems Service (http://www.iers.org/)
IGN	Instituto Geográfico Nacional - Spain
IPGS	Institut de Physique du Globe de Strasbourg
IUGG	International Union of Geodesy and Geophysics
LOD	Length of Day
LTM	Local Tidal Model
LP	Long Period
LS	Least Squares
LSSA	Least Squares Spectral Analysis
L&R	Lacoste&Romberg gravimeter
MGL	Micro-g LaCoste

MSD	Mean Square Deviation
NA	North American Gravimeter
NDFW	Nearly Diurnal Free Wobble
OSG	Observatory Superconducting Gravimeter
OTL	Ocean Tidal Loading
PDF	Probability Density Function
PET	Portable Earth Tide
PREM	Preliminary Reference Earth Model
PSD	Power Spectral Density
REN	Rigid Earth Nutation
SG	Superconducting Gravimeter
SNM	Seismic Noise Magnitude
SNR	Signal-to-Noise Ratio
SNREI	Spherically symmetric, Non-Rotating, perfectly Elastic and Isotropic Earth model
STDV	Standard Deviation
T005	T770 SG model at J9 Observatory (1987-1996)
TGP	Tide Generating Potential
TOM	Tilt-Over Mode
TSOFT	Software package for the analysis of time series and Earth tides (Van Camp and Vauterin, 2005)
VAV	Software package for the analysis of Earth tides (Venedikov, Arnoso, Vieira, 2001, 2003)
VLBI	Very Long Baseline Interferometry
μGal	microgal – acceleration unit (1μGal = 10 nm/s^2)

Chapter 1

General Introduction

General Introduction

Gravimetry is a relatively old discipline, with the first attempts to determine the gravity dating back to the 1700s. Since then, it has evolved in a very fast manner, in theoretical, instrumental and analytical ways.

The elasto-gravitational deformation of the Earth and the associated temporal gravity variations, measured on the surface of the Earth, are due to many geophysical phenomena with different periods and amplitudes, including among others, the Earth tides (which are the motions induced in the solid Earth, and the changes in its gravitational potential, induced by the tidal forces from external bodies) which have the strongest effect.

Many methods can directly measure gravity, but only a few obtain the accuracies needed by geophysicists and geodesists. The increasing interest in the study of temporal gravity changes is due to the improvements of gravimeters and to its usefulness in Earth sciences.

This study is motivated by the improvements on gravimeters in the last decades (especially after the development of the superconducting gravimeters), which allow us to have now, many years later, very long series of high quality data than can be exploited to benefit from the advantages of their unprecedented length.

This thesis is divided into five parts, summarized as follows:

The first one, as a necessary background, is devoted to remind some basic concepts of the tidal theory such as: the tidal forcing, the tidal accelerations, the tidal parameters, the tidal potential and the different tidal potential catalogues, the response of the solid Earth to the tidal forcing and associated resonance effects.

Besides, we present a brief description of the different instruments that have been historically used to record Earth tides (not only gravimeters); the operating principle and characteristics of resolution, coverage and specific accuracy of the more important ones are described.

We conclude by explaining the methods of signal processing that will be applied later on our data, and the most appropriate methods of analysis of Earth tide data.

The second part is focused on the 'study site' (Strasbourg Observatories) where the Earth tides observations, which were introduced by R. Lecolazet in the 1950s, have a long tradition of almost 60 years. The different locations, the gravimetric instrumentations and the historical results are mentioned.

In the third part, we use some of the longest European gravity records, registered by spring and superconducting gravimeters, to study the sensitivity of the instruments through the temporal evolution of the delta gravimetric factors for the

main tidal waves, as well as the $\delta M_2/\delta O_1$ ratio (main semi-diurnal over main diurnal amplitude responses). Several temporal variations appear, which are much lower in the case of the superconducting gravimeters, and we try to find an explanation. We describe the data sets that are used in this part and in the two following, together with the treatments applied to these studies and we finally synthesize the results. In this part we also perform a detailed study of the stability of the scale factor of the superconducting gravimeter installed at Strasbourg Observatory, through the numerous calibration experiments carried out by collocated absolute measurements since 1997.

In the fourth part we focus on the time series of superconducting (SG) gravity data, which we have shown to be better compared to the long spring gravimeter records, despite they are slightly shorter, to try to separate contributions of near-frequency waves, to detect very weak amplitude signals and also to detect low frequency signals, that was not possible with shorter time series of gravity data.

The fifth and final parts are devoted to the theory of two of the Earth's rotational modes (the Free Core Nutation (FCN), and the Free Inner Core Nutation (FICN)), which provide valuable information about the deep interior of the Earth. We also attempt to retrieve the surface gravity effects associated with these normal modes in the long-term gravity data used in previous sections. The results obtained using first the data from J9 Observatory, and then using data from several European SG stations, are provided.

This thesis entitled: *'Analysis of long gravity records in Europe; tidal stability and consequences for the retrieval of small amplitude and low frequency signals including the Earth's core resonance effects'* is hence located in the context of a thorough quest for knowledge of the interior of our planet Earth through the high quality gravity data. This became possible thanks to the huge efforts carried out by the different SGs stations to provide us with longer and better time series of data.

The completion of this thesis has been carried out under a joint supervision between Universidad Complutense de Madrid and Université de Strasbourg, thanks to the opportunity that the Spanish Instituto Geográfico Nacional offered me to spend the last years at École et Observatoire des Sciences de la Terre (EOST), Strasbourg.

Chapter 2

Earth tides: theory, instrumentation and analysis

2.1.1 Introduction

When we study a continuous time-record of a gravimeter, by far the tides are the dominant signal in the data (the semidiurnal and diurnal tides are especially evident). These variations can reach up to 300 µGal (1 µGal = 10 nm/s^2) peak to peak, depending on the coordinates of the station. The tides occur at fixed frequencies given by the combined spin and orbital dynamics of the Moon about the Earth, and the Earth and the other planets around the Sun. The largest components are at semidiurnal and diurnal periods, but there are also long-period components (fortnightly, monthly, half-yearly, yearly, and an 18.6 year nutation corresponding to the lunar nodal cycle). The tidal potential amplitude is latitude dependent; the diurnal tides are at maximum at $\pm45º$ latitude and zero at the equator and poles, whereas the semidiurnal tides are zero at the poles and at maximum at the equator and the long periodic tidal waves are a maximum at the poles.

Recently, Earth tides have become more important in geodesy as the increasing precision of measurements has required corrections for tidal effects that could previously be ignored. Tides affect gravity at about the 10^{-7} level, and tidal displacements (a few tens of centimeters) are about 10^{-7} of the Earth's radius. Later on in this study, we will try to analyze as many tidal waves as possible using different gravity series of high quality recorded in Europe.

To better understand the origin of tides, we should remember some basic concepts of the tidal theory; we describe first the tidal forcing, the tidal accelerations, the tidal parameters (which are our main study items in chapters 4 and 5), the tidal potential and the different tidal potential catalogues. We next consider how the solid Earth responds to the tidal forcing and what effects produces. Later in section 2.2 we conclude with brief descriptions of several instruments for measuring Earth tides (gravimeters), and in section 2.3 with the analysis methods appropriated to Earth-tide data.

Earth tides

The Earth tides are the motions induced in the solid Earth, and the changes in its gravitational potential induced by the tidal forces from external bodies. Tidal fluctuations have three roles in geophysics (Agnew 2007):

1. Measurements of them can provide information about the Earth (structure, rheology).

2. Models of them can be used to remove tidal variations from geodetic and geophysical measurements.

3. Models of them can be used to examine tidal influence on some natural phenomena (as for example, finding the tidal stresses to see if they trigger earthquakes).

First observations of tides phenomena date back to the beginning of the Christian era, when the *Naturalis Historia* of Pliny the Elder (AD 77-79) collates many tidal observations (as for example one on the banks of the Guadalquivir and other near to Seville). In his Natural History, Pliny describes the twice daily cycle and the occurrence of four maximum tidal ranges a few days after the new or full moon. He also identified that there is a locally fixed interval between lunar transit and the next high tide at a particular location. He further described how tides of the equinoxes in March and September have a larger range than those at the summer solstice in June and winter solstice in December.

Nevertheless, it took several centuries until Sir Isaac Newton published his universal theory of gravitation in 1687, to have a scientific explanation for the tidal phenomenon. He discovered the nature of the tide generating force.

$$F_1 = F_2 = G\frac{m_1 m_2}{r^2}$$
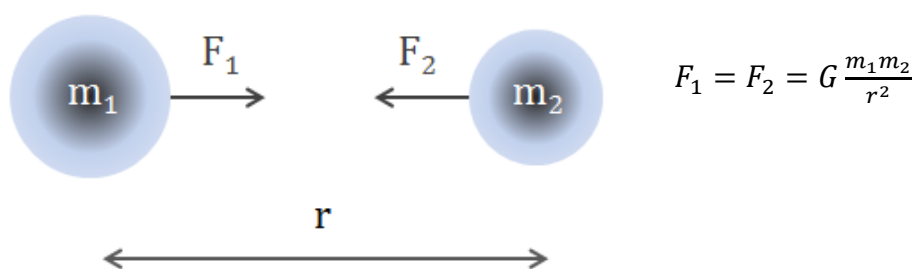
Fig. 2.1.1: Diagram of Newton's law of gravity.

He explained in his "Principia Mathematica" how the tides are originated from the gravitational attraction of the moon and the sun on the Earth. He also showed in his theory why there are two tides for each lunar transit, the reason why spring and neap tides occurred, why diurnal tides are largest when the moon was furthest from the plane of the equator and why the equinoxial tides are larger in general than those at the solstices.

2.1.2 The tidal force

The tidal force is a differential force appearing between a point P on the surface of the Earth and its center of mass O. The tidal forces arise from the gravitational attraction of bodies external to the Earth. Due to the high accuracy of astronomical theory, the tidal forcing can be described to much more precision than can be measured.

We consider first the gravitational forces applied to one body (the Earth, in this case) by another (the Moon). The points of the Earth nearest the Moon are attracted toward the Moon more than is the center of the Earth. And conversely, the points of the Earth farthest from the Moon are attracted less. Therefore, both the far and near sides of the Earth are pulled radially outward away from the center, while the regions that are at right angles to the Earth–Moon vector are pulled radially inward.
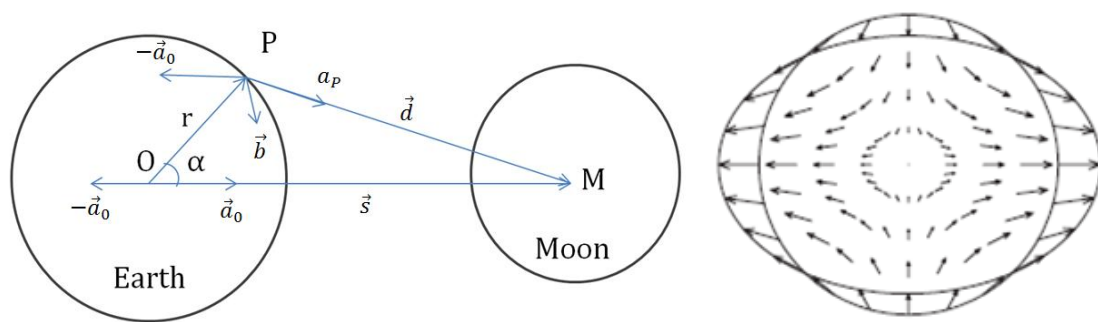
Fig. 2.1.2: Tidal forcing. The left plot shows the geometry of the problem for computing the tidal force at a point P on the Earth, given an external body M (Moon). The right plot shows the field of forces (accelerations) for the actual Earth–Moon separation. The elliptical line shows the equipotential surface under tidal forcing, greatly exaggerated (adapted from Agnew, 2007).

Because of the Earth's diurnal rotation, the tidal force at a fixed point varies through two complete cycles in 1 day. This semidiurnal time dependence is split into many periodic terms with frequencies closely spaced about 2 cycles per day due to the time variability of the orbital motion of the moon. Furthermore, because the moon is not always in the plane of the Earth's equator (the Earth–Moon vector is inclined, respect to the Earth's rotation axis) there is also significant variability at frequencies closely spaced about 1 cycle per day.

Earth also experiences a tidal force from the Sun and the planets. These tidal forces are defined in a similar way, and can also be decomposed into semidiurnal, diurnal, and long period terms.

As we will see in section 2.1.4, the tidal force can be written as the gradient of a tide-generating potential (TGP), consisting of a sum of terms with sinusoidal time dependences where the sines and cosines have arguments involving linear combinations of the orbital frequencies corresponding to the Sun, the Moon and planets.

2.1.3 The tidal accelerations

The tidal acceleration $\vec{b}$ at an observation point P on the Earth's surface (figure 2.1.2) results from the difference between the gravitational accelerations $\vec{a}_P$ generated by a celestial body at a point P, and the orbital acceleration $\vec{a}_0$ due to the motion of the Earth around the barycenter of the two-body system (the Earth and the Moon in our case). Because of the spatial extension of the body (the Earth), the gravitational accelerations due to others celestial bodies are slightly position dependent, whereas the centrifugal accelerations are constant within the body and on the surface of the body (Wenzel, 1997a).

In figure 2.1.2, on the left plot are represented the gravitational acceleration, orbital acceleration and tidal acceleration for the Earth-Moon system. Using Newton's gravitational law, the tidal acceleration vector $(\vec{b})$ for the Moon is given by:

(2.1)

$$\vec{b} = \vec{a}_P - \vec{a}_0 = \frac{GM_s}{d^2} \cdot \frac{\vec{d}}{d} - \frac{GM_s}{s^2} \cdot \frac{\vec{s}}{s}$$

Where,

$G = 6.6672 \cdot 10^{-11} m^{-3} kg^{-1} s^{-2}$ is the Newtonian gravitational constant

M_s is the mass of the Moon

$\vec{d}$ is the topocentric distance vector

$\vec{s}$ is the geocentric distance vector

For the Earth-Moon system the barycenter is located inside the Earth's body, and the orbital motion of the Earth around the barycenter generates orbital accelerations.

Similar considerations are valid for the other celestial bodies; the Sun and the nearby planets of our solar system also generate tidal accelerations on the Earth's surface, but slighter (Table 2.1.1).

The difference between the gravitational accelerations and the orbital accelerations generates small tidal accelerations; on the Earth's surface, these

accelerations correspond to about 10^{-7} of the Earth's gravity g. As we will see later in section 2.2, the resolution of high quality gravimeters is less than 10^{-11} m/s^2 ($\sim 10^{-12}$g), so when we analyze their records, the tidal accelerations due to the nearby planets have also to be considered.

The maximum tidal accelerations due to celestial bodies on the surface of the Earth are listed in Table 2.1.1.

Table 2.1.1: List of maximum values of the tidal accelerations exerted on the Earth, generated by the different celestial bodies.

Acceleration due to:	Maximum tidal accelerations
Moon	1.37 ·10^{-6} m/s^2
Sun	0.50 ·10^{-6} m/s^2
Mercury	3.64 ·10^{-13} m/s^2
Venus	5.88 ·10^{-11} m/s^2
Mars	1.18 ·10^{-12} m/s^2
Jupiter	6.54 ·10^{-12} m/s^2
Saturn	2.36 ·10^{-13} m/s^2
Uranus	3.67 ·10^{-15} m/s^2
Neptune	1.06 ·10^{-15} m/s^2
Pluto	7.61 ·10^{-20} m/s^2

2.1.4 Tidal potential

For a quantitative description it is useful to work with the tidal potential, which enables an expansion into scalar spherical harmonics. This potential V is defined so that its gradient is the tidal acceleration vector.

(2.2)

$$\vec{b} = grad\ V = \frac{\partial V}{\partial \vec{r}} \vec{r}\ \text{(vertical acceleration only)}$$

We can derive its expression following the development in Munk and Cartwright (1966). Considering M_{ext} as the mass of an external body, the gravitational potential V derivates from it at a point P in the Earth is:

$$V = \frac{GM_{ext}}{d} = \frac{GM_{ext}}{R} \frac{1}{\sqrt{1 + \left(\frac{r}{R}\right)^2 - 2\left(\frac{r}{R}\right)cos\alpha}} \qquad (2.3)$$

Where as shown in figure 2.1.2,

r is the distance of P from O

d is the distance from P to M

α is the angular distance between P and the sub-body point of M

Using Legendre polynomials, the more general tidal potential including all degrees can be written in his geometry (e.g. Agnew 2007) as:

(2.4)

$$V(r, \alpha) = \frac{GM_{ext}}{R} \cdot \sum_{n=0}^{\infty} \left(\frac{r}{R}\right)^n P_n(cos\alpha)$$

The $n = 0$ term is constant in space, so its gradient is zero and can be discarded.

The $n = 1$ term is

(2.5)

$$\frac{GM_{ext}}{R} r\, cos\alpha = \frac{GM_{ext}}{R} x_1$$

Where x_1 is the Cartesian coordinate along the OM axis. Its gradient is a constant, thus the tidal potential V_{tid} can be rewritten as the equation (2.4) with the two lowest terms removed:

(2.6)

$$V_{tid}(t) = \frac{GM_{ext}}{R(t)} \sum_{n=2}^{\infty} \left(\frac{r}{R(t)}\right)^n P_n(cos\alpha(t))$$

Where R and α are functions of time. $P_n(cos\alpha(t))$ are the Legendre polynomials, which are defined respectively for degrees n=2, 3, 4 as (Hobson, 1931):

$P_2(x) = \frac{1}{2}(3x^2 - 1)$

$P_3(x) = \frac{1}{2}(5x^3 - 3x)$

$P_4(x) = \frac{1}{8}(35x^4 - 30x^2 + 3)$

Because the relation r/R is about $1.6 \cdot 10^{-2}$ for the Moon and about $4.3 \cdot 10^{-5}$ for the Sun, the series expansion converges rapidly.

The tides of degree 4 ($n = 4$) are just detectable in very low noise gravimeters. In our case, as we will use some high quality data records in chapters 4, 5 and 6, we will consider $n = 2$, $n = 3$ and $n = 4$ terms. In that section, we will be able to retrieve in our data series some small amplitude waves in the major tidal group generated by the third-degree and fourth-degree potentials.

The largest contribution to the tidal potential results from degree 2 terms with about 98% of V, so for a first approximation it is justifiable to terminate the series expansion at $n = 2$. However, as we will see in section 2.1.5, for the most accurate

tidal potential catalogues we use $n_{max} = 6$ for the Moon, $n_{max} = 3$ for the Sun and $n_{max} = 2$ for the planets.

Sometimes it is convenient to express the relative position of the point P on the surface of the Earth and the celestial body as a combination of geocentric and celestial coordinates. The geocentric coordinates are the spherical co-latitude θ and spherical longitude λ. The celestial coordinates of the tide generating body are the declination δ (the angular distance north of the celestial equator) and the local hour angle τ (defined as the difference in longitude between P and the tide-generating body)

The potential can be rewritten then as:

$$(2.7)$$

$$V(t) = \frac{GM_{ext}}{R(t)} \sum_{n=2}^{\infty} \left(\frac{r}{R(t)}\right)^n \frac{1}{2n+1} \sum_{m=0}^{n} P_n^m(cos\theta) \cdot P_n^m(sin\delta) \cdot \cos(m\tau + m\lambda)$$

Where P_n^m is the associated Legendre function of degree n and order m (Hobson, 1931):

$$P_2^0(\theta) = \frac{1}{2}(3\,cos^2\theta - 1) \qquad\qquad P_3^0(\theta) = \frac{1}{2}(5\,cos^3\theta - 3cos\theta)$$

$$P_2^1(\theta) = 3sin\theta cos\theta \qquad\qquad P_3^1(\theta) = \frac{3}{2}(5\,cos^2\theta - 1)$$

$$P_2^2(\theta) = 3\,sin^2\theta \qquad\qquad P_3^2(\theta) = 15sin^2\theta cos\theta$$

$$P_3^3(\theta) = 15sin^3\theta$$

Due to the Earth's rotation, the hour angle τ of the celestial body varies from 0 to 2π in 24 hours.

Each term of the sum over m in the precedent equation has a certain spatial periodicity (figure 2.1.3). The potential V therefore has:

- A long period term connected to zonal harmonics P_n^0, $(m = 0)$

- A diurnal term connected to tesseral harmonics P_n^1, $(n > m)$

- A semi-diurnal term connected to sectorial harmonics P_2^2, $(m = n = 2)$
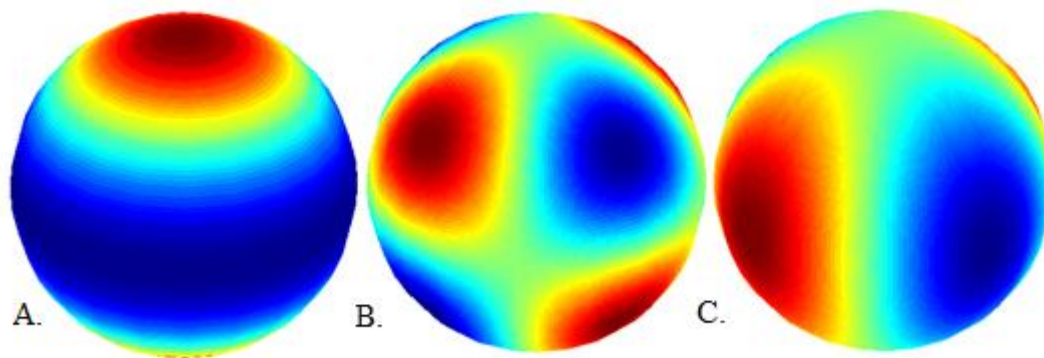
Fig. 2.1.3: Examples of some geographical distribution of tidal potential; A, zonal function (for n=2, m=0); B, tesseral function (for n=3, m=2); C, sectorial function (for n=m=2).

This will allow us the separation of the tidal potential into latitude dependent terms and time/longitude dependent terms, and the spectral representation of the tidal potential by a tidal potential catalogue, as we will see in section 2.1.5

Table 2.1.2: Major tidal harmonic components listed in order of increasing frequency (f). The corresponding period ($T = 1/f$) is also shown.

Symbol	Description	Period (T) hours	Frequency (cpd)
Sa	Second overtide of M_2 constituent, annual	8765.5223	0.0027
O1	First overtide of M_2 constituent	25.8193	0.9295
K1	Lunar declinational diurnal constituent	23.9345	0.9973
N2	Larger Lunar elliptic semidiurnal constituent	12.6583	1.8960
M2	Principal lunar semidiurnal constituent	12.4206	1.9323
S2	Principal solar semidiurnal constituent	12.0000	2.0000
K2	Luni-solar declinational semi-diurnal constituent	11.9672	2.0055

2.1.5 Tidal Potential Catalogues

The way for computing a theoretical gravity tide is using the catalogue of tide-generating potential (TGP). These catalogues consist of a table of amplitudes, phases and frequencies for a lot of tidal waves.

Sir G. H. Darwin (1883) was the first to have ever computed a catalogue of tidal waves. He also gave names to the main tidal waves which are still used today. Darwin's harmonic developments of the tide-generating forces were later improved by A. T. Doodson (1921), who developed the tide-generating potential in harmonic form, distinguishing a total of 378 tidal frequencies. In his development, he included only terms of degrees 1 to 3 (i.e. 24, 12, and 8 hour periods) using the orbital and rotational data for the Earth as forced by the Sun and Moon. Currently, the most recent and extensive tidal developments, as for example the Hartmann & Wenzel catalogue (1995) or the harmonic development of Kudryavtsev (2004), include the perturbation effects of all the major planets and terms up to degree 6 for the moon (4 hour period) as well as terms allowing for the non-spherical shape of the major bodies.

In the last decades several tidal potential catalogues have appeared (Table 2.1.3), in which the truncation level has continuously been decreased and the number of waves and coefficients has continuously been increased. The catalogue of Tamura (1993) includes coefficients due to the indirect tidal potential of the planets Venus and Jupiter. The catalogue of Roosbeek (1996) includes the lunar tidal potential of degree 5 and Hartmann & Wenzel (1995) reach the degree 6 respectively. Both of them also include coefficients due to the direct tidal potential of the nearby planets and due to the flattening of the Earth.

Table 2.1.3: List of different tidal potential catalogues available.

Author(s)	Year	Nº of waves	Nº of coeff.	Max. degree	Truncation (m^2/s^2)
Doodson	1921	378	378	3	$1.0 \cdot 10^{-4}$
Cartwright et al.	1971, 1973	505	1010	3	$0.4 \cdot 10^{-4}$
Büllesfeld	1985	656	656	4	$0.2 \cdot 10^{-4}$
Tamura	1987	1200	1326	4	$0.4 \cdot 10^{-5}$
Xi	1989	2934	2934	4	$0.9 \cdot 10^{-6}$
Tamura	1993	2060	3046	4	$0.4 \cdot 10^{-5}$
Roosbeek (RATPG95)	1996	6499	7202	5	$0.8 \cdot 10^{-7}$
Hartmann and Wenzel (HW95)	1995	12935	19271	6	$0.1 \cdot 10^{-9}$
Kudryavtsev (KSM03)	2004	26753	28806	6	$0.1 \cdot 10^{-9}$

There are two different approaches to cataloging the TGP; these catalogues have either been computed by underline analytical spectral analysis (e.g. Doodson, 1921; Xi, 1987; Roosbeek, 1996) or by numerical spectral analysis (Cartwright and Tayler, 1971,

Cartwright and Edden, 1973, Büllesfeld, 1985, Tamura, 1987, Hartmann and Wenzel, 1995) of the tidal potential generated by the celestial bodies.

The analytical spectral analysis method requires analytical ephemerides of the celestial bodies, whereas the numerical spectral analysis method needs numerical ephemerides only (*the ephemerides is a catalog of apparent positions of the bodies in the solar system as seen from a position and time on the Earth; each body is defined by a longitude, latitude, right ascension and declination*). For example, the HW95 has been computed using the DE200 numerical ephemeris of Jet Propulsion Laboratory, Pasadena (Standish, 1990), of the solar system bodies between 1850 and 2150.

All tidal potential catalogues use a representation of the tidal potential on a rigid Earth similar to (Wenzel, 1997a):

(2.8)

$$V_{(t)} = D \sum_{l=1}^{l=l_{max}} \sum_{m=0}^{m=l} \left(\frac{r}{a}\right)^l \Gamma(\theta) \cdot \bar{P}_{lm}(cos\theta) \cdot \sum_i \left[C_i^{lm}(t) \cos(a_i(t)) + S_i^{lm}(t) \sin(a_i(t)) \right]$$

where

$D, \Gamma(\theta)$ are the normalization constants

a is the semi-major axis of the reference ellipsoid

$C_i^{lm}(t), S_i^{lm}(t)$ are the time dependent coefficients, given by:

$$C_i^{lm}(t) = C0_i^{lm} + t \cdot C1_i^{lm}$$
$$S_i^{lm}(t) = S0_i^{lm} + t \cdot S1_i^{lm}$$

The arguments $a_i(t)$ are given by:

$$a_i(t) = m \cdot \lambda + \sum_{j=1}^{j=j_{max}} k_{ij} \cdot arg_j(t)$$

With $k_{ij} = m$

The integer coefficients k_{ij} are given in the specific catalogue, while the astronomical arguments $arg_j(t)$ can be computed from polynomials in time.

The catalogue that we will use later on in chapters 4, 5 and 6 for performing our tidal analyses, is the Hartmann and Wenzel catalogue (HW95) which is the most widely employed in the gravimetric community. For this catalogue, the normalization constants D and $\Gamma(\theta)$ have been set to unity.

Several comparisons between the different catalogues have been carried out; Merriam (1993) compared the catalogs of Tamura (1987) and Xi (1989) with GTIDE software concluding that although their differences should be detectable

using SGs, in practice either of the catalogs could be used for SG analysis. Wenzel (1996a) compared also the past catalogues and concluded that the HW95 was the most accurate for high precision work. Roosbeck (1996) noted that this is because HW95 is derived from one of the benchmark series itself and its only error should be computational. Finally, Kudryavtsev (2004) compared the KSM03 with the HW95 and the RATGP95 showing that its accuracy in the frequency domain is close to that of HW95 and RATGP95.

2.1.6 Tidal Parameters

For the main tidal waves, the purpose of the tide analysis is to determine the transfer function between the observed tidal amplitude (in the gravimetric records) and the theoretical amplitude of the astronomical tide for a solid Earth's model at the coordinates of the station, i.e. an amplitude ratio and a phase difference between the observed and the theoretical tidal vectors. These quantities are called tidal gravimetric factors and are commonly noted by δ (amplitude factor) and κ (phase difference). Through the tidal analysis, each analyzed wave furnishes an observed pair (A, α) at its tidal frequency ω, where $A = \delta \cdot A_t$ (being A_t the theoretical amplitude), and α is the phase. So for each wave, the amplitude factor δ is defined with respect to the theoretical tidal amplitude A_t as the ratio A/A_t (Melchior, 1978).
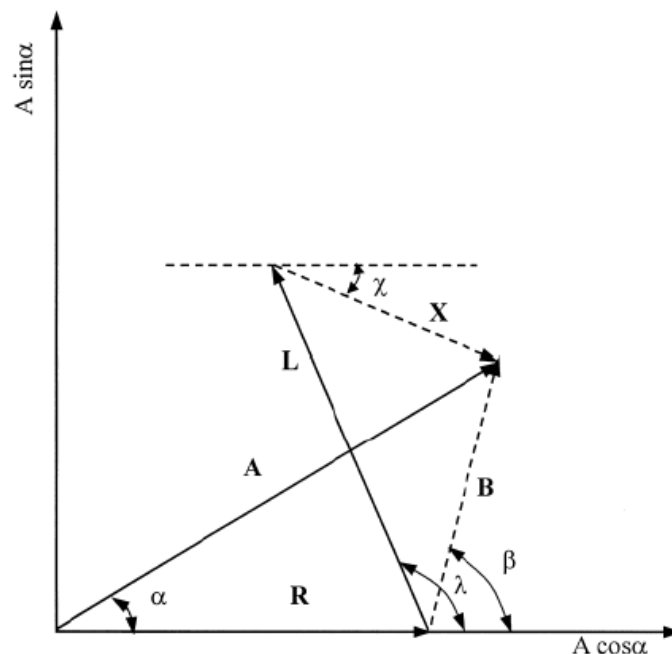
Fig. 2.1.4: For a given tidal frequency, phasor plot showing the relationship between the observed tidal amplitude vector $\boldsymbol{A}(A, \boldsymbol{\alpha})$, the Earth model $\boldsymbol{R}(\boldsymbol{R}, \boldsymbol{0})$, the computed ocean tides load vector $\boldsymbol{L}(\boldsymbol{L}, \lambda)$, the tidal residue $\boldsymbol{B}(B, \boldsymbol{\beta}) = \boldsymbol{A} - \boldsymbol{R}$ and the corrected residue $\boldsymbol{X}(\boldsymbol{X}, \chi) = \boldsymbol{B} - \boldsymbol{L}$, after Ducarme et al. (2009).

* The tidal gravimetric amplitude factor δ, which is one of the important tidal parameters for comparing with observations, is used to describe the transfer function for surface gravity variations. This factor is a frequency dependent coefficient. According to the conventions used for tidal data analysis (Dehant and Ducarme, 1987) we adopt the following definition of the gravimetric factor δ: *'In the frequency domain, the tidal gravimetric factor is the transfer function between the tidal force exerted along the perpendicular to the ellipsoid and the tidal gravity changes along the vertical as measured by a gravimeter'*

So, in the frequency domain, the amplitude factor as defined by the International Centre for Earth Tides (ICET) is then deduced by dividing the final amplitude by the vertical tidal force at the frequency ω:

(2.9)

$$\delta_{ICET} = \frac{\text{body tide signal measured by a gravimeter along the vertical}}{\text{gradient of the external tidal potential along the perpendicular to the reference ellipsoid}}$$

In the case of an Earth initially in hydrostatic equilibrium, the ellipsoidal normal is assumed to coincide with the local vertical. For a non-hydrostatic Earth the vertical is given by the perpendicular to the geoid.

* The phase factor κ_n, gives the delay or lead of the tidal response with respect to the phase of the tidal potential.

The gravimetric factors (δ, κ) can be used to construct the synthetic tide at any location. These synthetic tides are modeled by summing several wave groups with the specific gravimetric factors that usually have been determined in some prior tidal analysis at the station.

It is common for the gravimetric factors to differ from their theoretical values $\boldsymbol{R} = (A_t \delta_m, 0)$ (where δ_m is the theoretical gravimetric factor for a particular Earth model), due to two main reasons. Firstly, because the ocean tidal loading (OTL) is automatically incorporated into the estimated factors (when the synthetic tide is reconstructed from the empirical gravimetric factors both the ocean loading, and the system phase lag will be automatically included along with the solid Earth tide), while ocean tides are variables. Secondly, due to the Earth model used. Indeed the tidal gravimetric factors are expressed as a function of the Love numbers and depend on the Earth's model, as we will see in section 2.1.7.

2.1.7 Earth Response

Once that we have described the tidal forces, we consider now to the response of the solid Earth to these forces. The Earth, considered elastic at such frequencies, deforms under the tidal stress; the tidal force tends to deform the solid Earth into the elliptical shape (see Figure 2.1.2). This Earth's tidal deformation is caused by the gravitational attraction of the Sun and Moon and, to a much lesser extent, the other planets (Dehant et al. 1999).

The formalism for describing mathematically the tidal transfer functions for a spherical Earth was predicted by Love (1911). He showed that tidal effects could be represented using a set of dimensionless numbers, now called the Love numbers (or Love and Shida numbers, since the number l was introduced in 1912 by T. Shida of Japan).

Wahr (1979, 1981a) extended this formalism to an ellipsoidal, rotational Earth. His model contains an ellipsoidal, elastic, deformable inner core, an ellipsoidal liquid outer core and an ellipsoidal, elastic, deformable mantle without ocean and atmosphere. The Earth is assumed to be hydrostatically pre-stressed and uniformly rotating.

Later, the effects of mantle inelasticity in a rotating, elliptical Earth were included (Wahr and Berger 1986; Dehant 1986, 1987) resulting in the use of complex Love numbers.

Then, Dehant and Defraigne (1997) extended the tidal formalism to include effects of non-hydrostatic elliptical structure inside the Earth.

The real Earth is, of course, inelastic and non-hydrostatic, and it is likely that the effects of both inelasticity and non-hydrostatic structure are large enough to have a significant impact on tidal observations (Dehant et al., 1999).

The Earth's response to the tides can be well described with only a few parameters; first we can consider the Earth as an SNREI model (spherically symmetric, non-rotating, elastic and isotropic), of which the Preliminary Reference Earth Model (PREM) of Dziewonski and Anderson (1981) is the most widely used version. For this Earth's model it is simple to describe the response to the tidal potential (Jeffreys, 1976). Because of symmetry, only the degree n is relevant, and these parameters (Love numbers h_n, k_n and l_n for each of the n harmonics in the TGP) can be computed by solving the gravito-elastic equations of motion for the Earth and finding the surface displacement u_n and surface gravity potential ψ_n for any kind of forced deformation, as tides or tidal loading (e.g. Wang, 1997):

$$u_n = \frac{1}{g_0}[h_n\hat{r} + l_n\nabla_s]W_T$$

$$\psi_n = k_nW_T$$

$$\delta_n = 1 + \frac{2h_n}{n} - \frac{(n+1)}{n}k_n$$

where,

∇_s is the horizontal gradient operator in spherical polar coordinates

g_0 is the surface gravity.

W_T is the surface gravity potential

$\hat{r}$ is the unit radial vector

The Love numbers completely describe any kind of deformation, elastic or inelastic, and therefore contain all the complexity of the actual Earth, that is, resonances for all the Earth's normal modes, anelasticity and frequency dependency (Dickman, 2005). Tidal displacements of geodetic instruments on the Earth's surface are usually described by h (radial) and l (tangential) (see e.g., McCarthy, 1996; Mathews et al., 1997), while k is used to represent tidal effects on the orbits of Earth-orbiting satellites (see e.g., Yoder et al., 1983: McCarthy, 1996).

They have been frequently computed for seismic Earth models such as PREM and given in a number of different forms. They are in principle complex numbers because of the Earth's anelasticity (e.g. Mathews 2001).

The numerical values of the Love numbers depend on the Earth's internal properties. So it is possible to learn about some of those properties by comparing tidal observations with predictions based on theoretical results for the Love numbers; tidal observations have been used to place constraints on the Earth's anelastic properties, as we will point in chapter 6. We have already introduced the real gravimetric tidal factors (δ_n, k_n) in section 2.1.6. δ_n is found from a combination involving h_n and k_n, as above (l_n is not used in gravity as it corresponds to the Earth response in horizontal displacement).

Typical elastic values for a standard modern Earth model for $n = 2, 3$ and 4 respectively are $h_n = 0.6032, 0.291$ and 0.175; $k_n = 0.298, 0.093$ and 0.043; yielding $\delta = 1.155, 1.167$ and 1.121 (A nominal pair of values for n= 2 is taken as $\delta = 1.16, \kappa = 0^\circ$).

For more realistic Earth models, we should add the effects of rotation, ellipticity, inelasticity and anisotropy, moving away from a simple SNREI model (Crossley et al., 2013).

<u>Inelasticity</u> causes a small tidal phase lag (time delay) due to frictional deformation in the Earth's mantle, so δ becomes complex with an in-phase component $\delta\cos(\kappa)$ and an out-of-phase component $\delta\sin(\kappa)$. Although this effect

may produce a change in the amplitude of the Love numbers up to 7% at long periods, the effect is quite small for the body tides.

<u>The rotation and ellipticity</u> effects act to couple the Love numbers of neighboring harmonic degrees, so each δ_n factor is split into three components δ_0, δ_+ and δ_- (Dehant et al 1999). This yields a small latitude dependence where δ decreases by about 0.1% between the equator and the poles, consistent with older spring gravity measurements (Dehant and Ducarme 1987). Afterward Wang (1994) found that this latitude dependency should be even smaller and in 2007 Agnew quoted a variation between the equator and the 60ºN latitude of only $4 \cdot 10^{-4}$.

Finally, the <u>ocean tides load</u> the crust and lead to vertical deformation; the tides in the ocean cause time-varying pressure loads on the surface of the solid Earth with the same frequencies as the Earth tides. Typically, tidal displacements of the solid Earth are of the order of several tens of centimeters. However, unlike ocean tides, Earth tides cannot be observed without sensitive instruments, because they cause both the ground and the observer to be displaced by the same amount.

The most common way to detect Earth tides is with a gravimeter (i.e. gravimetric tide). There are three contributions to the observed tidal variations in the gravitational acceleration. All three contributions are roughly of the same order:

1.-The direct attraction of the Sun, the Moon and to a lesser extent the Planets.

2.-The change in the Earth's gravity field due to tidal deformation within the Earth.

3.-The change in the gravitational acceleration at the gravimeter due to the radial tidal displacement of the Earth's surface under the gravimeter (commonly referred as the free-air gravity effect).

Since some of the scientific results of our study will be the retrieval of small amplitude and low frequency signals including the core resonance effects, in the next section we will present the long-period tides.

2.1.8 Long-Period tides

As we have seen in section 2.1.4., the potential V has a long-period (LP) term connected to zonal harmonics P_n^0.

The long-period tides generated by this term have been studied since the time of Laplace (18th century). These tides are characterized as being zonally symmetric (similar as the example shown in figure 2.1.3.A.), by weak amplitudes and by periods longer than one day. They are generated by changes in the Earth's orientation relative to the Sun, Moon, and Jupiter;

- The declination of the Moon relative to the Earth gives rise to the lunar fortnightly tidal constituent Mf (period 13.6606 days).

- The ellipticity of the lunar orbit gives rise to a lunar monthly tidal constituent Mm (period 27.3216 days).

- The motion of the Sun and Jupiter, introduced additional fundamental frequencies, as the major solar contributions at 6 months Ssa (period 182.6211 days) and annual Sa (period 365.2596 days). These two contributions are dominated by thermal effects.

Due to the nonlinear dependence of the force on distance, additional tidal constituents exist with frequencies which are the sum and differences of those fundamental frequencies.

- At much longer periods there is a lunar tide at 9.3 year and 18.61 year periods which are extremely difficult to identify in gravity, and that we will try to detect in our gravimetric series in chapter 5.

- There is also an additional gravity change which results from the gravitational torque acting on the Earth by the Sun and Moon due to the fact that the Earth has a non-spherical shape. The presence of this torque causes the Earth to develop a free Eulerian nutation known as the Chandler Wobble with a period of about 433 days.

Figure 2.1.5 (up), extracted from Ducarme et al. (2004) shows the tidal spectrum in the LP band, according to the development of Tamura (1987) with periods between 4 days and 18.61 years. Most of the tidal constituents are generated by the Legendre polynomial P_2^0. It is easy to detect that the largest components are the fortnightly (Mf), monthly (Mm, Msm), semiannual (Ssa), annual (Sa) and 18.61 year nutation constituents.

There are also some 60 tides generated by P_3^0 , which are shown in figure 2.1.5 (down). The largest is the small declinational wave $3M_{md}$, corresponding to the tropic month.

The tides generated by P_n^0 with $n > 3$ are almost negligible.
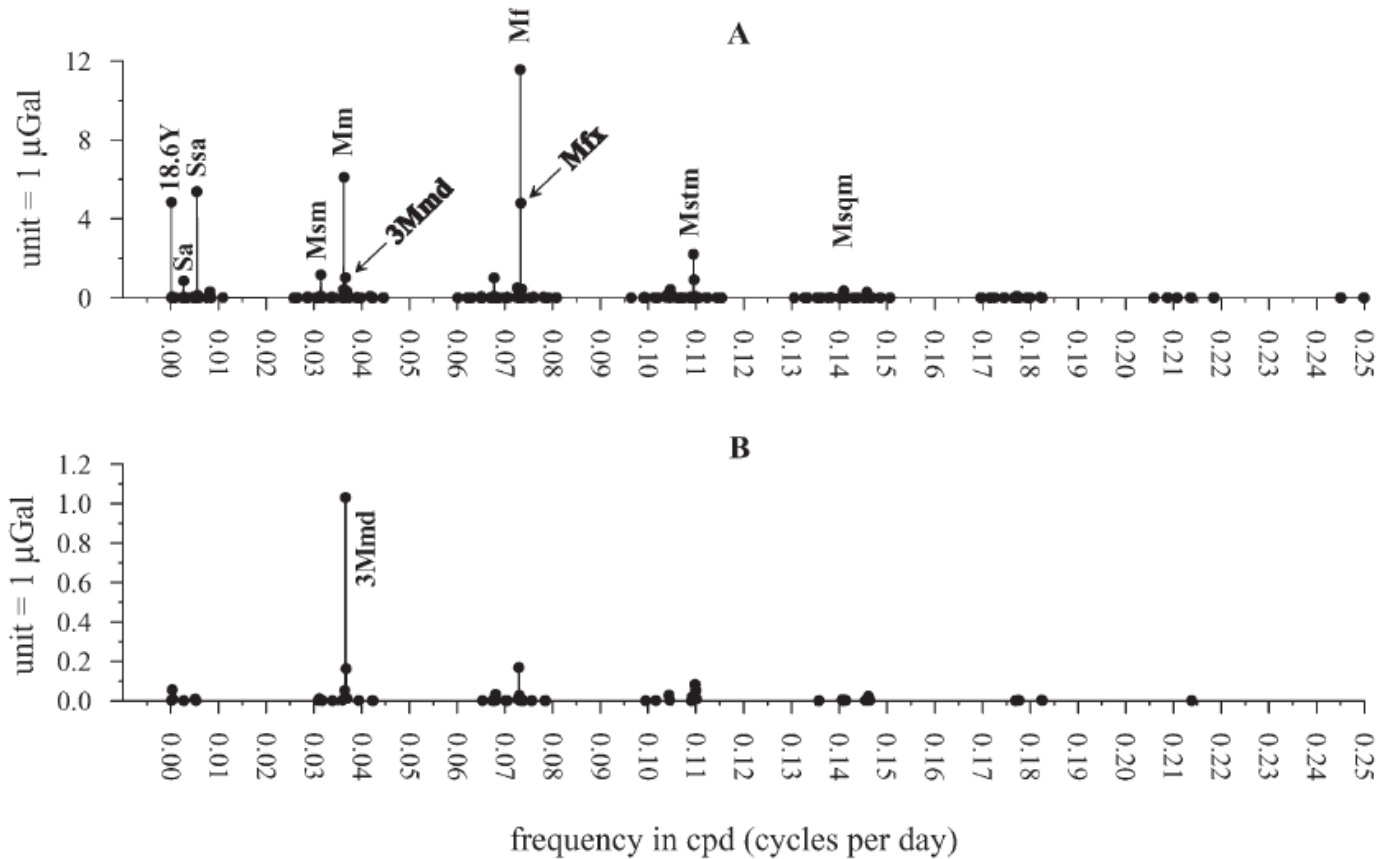
Fig. 2.1.5: Spectrum of the theoretical LP tidal gravity signal at latitude 75º (up) and P_3^0 tides at latitude 75º dominated by $3M_{md}$ (down), extracted from Ducarme et al., 2004.

Because a long-period tidal potential induces a second-degree zonal tidal response of the Earth, it causes not only the tides but also variations in the length of day (LOD) via conservation of angular momentum. In an elastic, spherically symmetric Earth, the induced variations (ΔLOD) should be proportional to the Love number k_2 (Munk and McDonald, 1960).

The tidal potential amplitude is latitude dependent so the long-period tides have their maximum values at the poles. Since tidal observations at high latitudes are advantageous for determining the LP tides, long-term observations with a LaCoste&Romberg ET gravimeter have been set up at the Antarctic Amundsen-Scott station (90º S) e.g. Rydelek and Knopoff (1982). However, as we will show later in section 2.2, the most serious limitation of spring gravimeters for LP tides remains in their inherent and unpredictable drift (even if their instrumental drift was considerably reduced recently). The much lower instrumental drift of SGs, and their higher sensitivity and stability (Richter et al. 1995), permits more precise studies of these LP tides (Sato et al., 1997a; Hinderer et al., 1998; Mukai et al., 2001; Ducarme et al., 2004; Boy et al., 2006a). Thus, a superconducting gravimeter (SG TT-70#016) was installed in 1993 at Syowa station, Antarctica, to observe Earth tides and Earth's free oscillation (Sato et al. 1993). In April 2003, this

gravimeter was replaced by a new SG CT#043 (Doi et al. 2008). Their data has also been used to study several long-period tides as Mm, Mf, Mqm, Msqm, Mtm, Mstm, Msf and Ms (Iwano et al. 2005).

To check the latitude dependent of these long-period tides and to obtain their expressions, we rewrite the potential as a function of the coordinates of the observation point.

If we consider the usual projection onto the celestial sphere from the center of the Earth (figure 2.1.6), where C is the celestial north pole, P the place of observation (geocentric latitude θ), CP its meridian and M the moon (declination δ, and zenital distance Ψ):
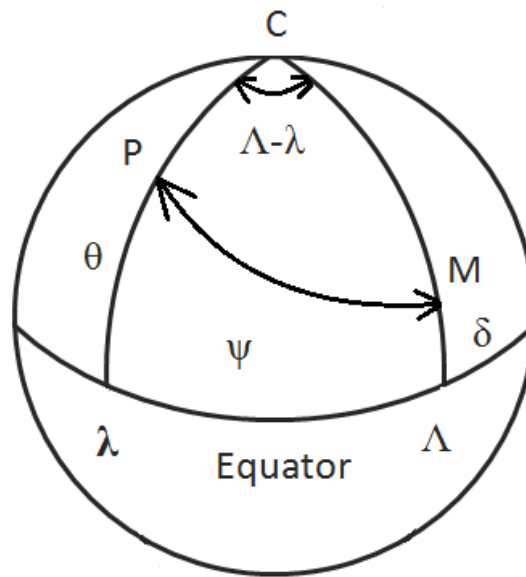
Fig. 2.1.6: Spherical triangle from positional Astronomy.

In the spherical triangle CMP (figure 2.1.6): (2.10)

$$\cos \Psi = \sin \theta \sin \delta + \cos \theta \cos \delta \cos(\Lambda - \lambda)$$

So the potential degree 2 (we have already mentioned in section 2.1.4 that the potential of degree 2 describes the 98%) can be rewritten as a function of θ, δ and Λ:

(2.11)

$$V_2 = G \left(\frac{c}{R}\right)^3 \left[(\cos{}^2\theta \, \cos^2\delta \, \cos2(\Lambda - \lambda)) + \sin 2\theta \, \sin 2\delta \, \cos(\Lambda - \lambda) + 3 \left(\sin^2\theta - \frac{1}{3}\right)\left(\sin^2\delta - \frac{1}{3}\right)\right]$$

where the first term, which is symmetrical about the equator, corresponds to the long-period. R, θ and Λ depend on the orbit of the Moon or the Sun, and also on the

Earth's rotation. We need to know the instantaneous zenith distances of the Moon and Sun and their distances from the place of observation. Their instantaneous position in relation to the Earth are given by their coordinates relative to the ecliptic (true longitude h_1 for the Sun; true longitude s_1 and latitude β for the Moon) and the reciprocal distances c_S/R_S and c/R.

Doodson (1921) expanded the equation (2.10) in a Fourier series. For this he chooses the 6 following independent variables, to express the arguments of the components of the tide, leading to a decomposition of tidal constituents into groups with similar frequencies and spatial variability.

τ, mean lunar time

s, mean longitude of the Moon

h, mean longitude of the Sun

p, longitude of Moon's perigee

N', longitude of Moon's ascending node

p_s, longitude of the perihelion

Using Doodson's expansion each constituent of the tide has a frequency

$$f = A\tau + Bs + Ch + Dp + EN' + Fp_s \tag{2.12}$$

Where the integers A, B, C, D, E and F are the Doodson numbers. So the total potential V_2 becomes a sum of terms of the form

$$K_{ABC \cdot DEF} G_i(\theta, R) \begin{bmatrix} cos, for\ i = 0,2 \\ sin, for\ i = 1 \end{bmatrix} (A\tau + Bs + Ch + Dp + EN' + Fp_s)$$

In table 2.1.4, we show a selection of the long-period tides from Doodson's full development.

Table 2.1.4: Tidal potential coefficients for the long-period tides.

Symbol	Doodson Argument	Astronomical Argument	Speed (º/hr)	Amplitude	Origin (L, lunar; S, solar)
M_0	055·555	0	0.000000	50458	L constant flattening
S_0	055·555	0	0.000000	23411	S constant flattening
S_a	056·554	$h - p_s$	0.041076	1176	S elliptic wave
S_{Sa}	057·555	$2h$	0.082137	7287	S declinational wave
S_{ta}	058·554	$2h + (h - p_s)$	0.123204	427	Elliptic tide from S_{Sa}
MS_m	063·655	$s - 2h + p$	0.471521	1587	Evectional tide from M_0
M_m	065·455	$s - p$	0.544375	8254	L elliptic wave
MS_f	073·555	$2(s - h)$	1.015896	1370	Variational tide from M_0
M_f	075·555	$2s$	1.098033	15642	L declinational wave
MS_{tm}	083·655	$2s + (s - 2h + p)$	1.569554	569	Evectional tide from M_f
M_{tm}	085·455	$2s + (s - p)$	1.642408	2995	Elliptic tide from M_f

The observation of long-period tides is believed to give us a good constraint for investigating the anelastic response of the Earth (Sato et al., 1997a). Compared to diurnal tidal periods where the Earth's rheology is predominantly elastic, on very long timescales (a few tens to thousands of years) the behavior of the mantle becomes viscoelastic. At long periods, polar motion (i.e. for a wobble period of 14 months) can again provide constraints on the Earth's rheology (the relationship between stress and strain), as any deviation from pure elasticity will increase with decreasing frequencies (Crossley et al, 2013).

In chapters 4 and 5 we will analyze the Earth tides using gravity records from different types of gravimeters. However, as we will see in section 2.2, there are several other kinds of instruments that can also be used to study the effects of Earth tides.

The first attempts to determine the gravity values date back to the 1600s (Crovini and Quinn, 1992). Since the first measurements with pendulums, there have been many different designs of gravity sensors proposed or built for measuring variations of the Earth's gravitational field.

These kinds of instruments are called **gravimeters**, and may be divided into portable or stationary devices, and into absolute gravimeters (which measure the exact value of gravity at a given point and a moment at the Earth's surface), and relative gravimeters (which measure only the temporal and/or spatial variations of gravity).

Since the appearance of the first devices, we have observed much evolution in the instrumental design resulting in an inexorable improvement in terms of precision and accuracy. Indeed the historical advancement of gravity instrumentation has been driven by the need of a combination of increase precision, increase portability, reduce time consuming for each measurement and improve the easy of handling (Torge 1989, Chapin 1998, Nabighian et al 2005).

Over the years the precision and accuracy of the gravimeters have been steadily enhanced; first gravimeters built in the sixteenth century were simple pendulums that could measure the value of g with an accuracy of about 10^{-5} g, while currently the most modern instruments, in specific measurement conditions, achieve sensitivities of one nanoGal (10^{-12} g).

Figure 2.2.1 (adapted from Torge, 1989) discloses the evolution of the measurement accuracy of the different systems used over the time.
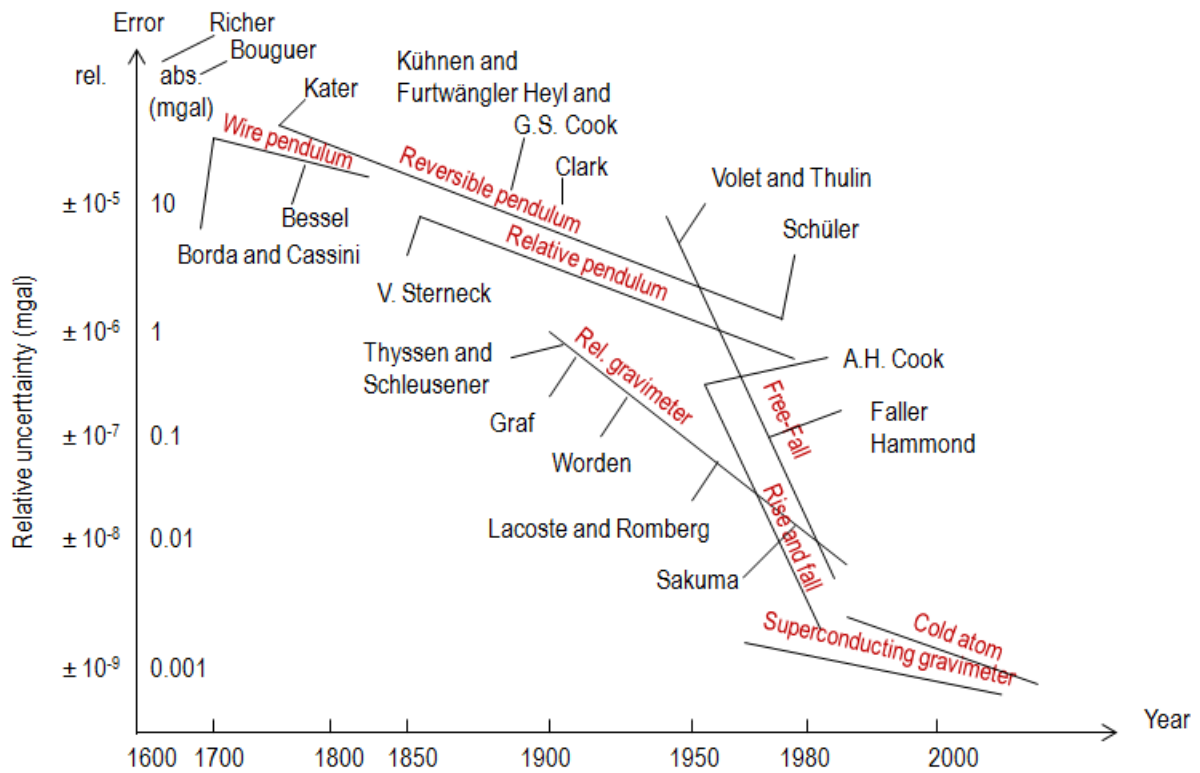
Fig. 2.2.1: Evolution of the accuracy of the gravity observation systems over time until 1980 *(adapted from Torge, 1989).*

2.2.1 Historical Instruments: Pendulums

Pendulums are the oldest type of gravimeters; the measurement of g exclusively depended on them until the beginning of the 20th century. They can be either absolute or relative instruments.

The principle of operation is simple; the period of swing of a simple gravity pendulum depends on its length, L, on the local strength of gravity g, and on the tilt angle of the pendulum away from vertical θ, called the amplitude. It is independent of the mass, m as shown by the equations hereafter.

26
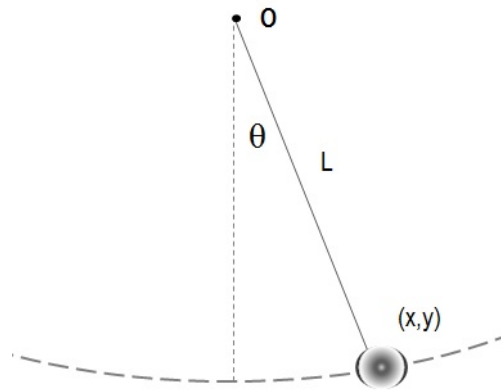
Fig. 2.2.2: Diagram of a simple gravity pendulum.

For small amplitudes, the period of such a pendulum depends only on the pendulum length and on the gravity.

$$T = 2\pi \sqrt{\frac{L}{g}}$$

(2.16)

So the gravity g, is inversely proportional to the square of the period of oscillation, T, and directly proportional to the length of the pendulum, L.

$$g = \frac{4\pi^2 L}{T^2}$$

(2.17)

If the same pendulum is swung under identical conditions at two locations, or at two different times, relative changes in g can be found through the corresponding change in T, that is, the ratio of the two values of g_1 and g_2; this ratio is related to the ratio of the two respective periods of oscillations T_1 and T_2

$$\frac{T_2^2}{T_1^2} = \frac{g_1}{g_2}$$

(2.18)

Thus, one can determine g_1/g_2 by simply measuring times.

Francis Bacon was one of the firsts who suggested the use of a pendulum to measure gravity (Bacon, 1620). He proposed to carry one up to a mountain to see

if gravity varies with altitude. But it was in the mid-seventeenth century when Dutch astronomer Christiaan Huygens inspired by investigations of pendulums by Galileo Galilei, invented the pendulum clock (1656) and was the first to use pendulum to measure g.

Until the early nineteenth century, all the pendulum measurements were absolute. The measurements were rather lengthy and complicated and were made mainly under laboratory conditions. In 1817 Kater designed his reversible pendulum (Kater, 1818), which simplified the implementation of the measurements and allowed greater accuracy. At that time, reversible pendulums were a fundamental improvement in absolute gravity measurement, with an initial precision of about 10 mGal (10^{-5} g). Several incremental improvements over the next 100 years brought this precision to about 1 mGal (10^{-6} g).

Kater also introduced the idea of relative gravity measurements, by comparing the gravity at two different points. Relative gravimetry was born after this achievement. Since then, its use has increased rapidly.

First precise gravimetric measurements were made in 1864 in Switzerland by Plantamour, using a pendulum based on the idea of Bessel's pendulum, constructed by A. Repsold. The first gravity measurements approaching modern precision were made in the early decades of the nineteenth century.

Fig. 2.2.3: Repsold's absolute pendulum used by Joaquín Barraquer y Rovira to realize the first absolute measurements of gravity in Spain (1982, National Astronomic Observatory of Madrid). Pendulum owned by The National Geographic Institute of Spain (IGN).

Pendulum measurements were affected by several sources of errors such as the vibration of the pendulum support, the change in the pendulum length and the influences of different non-gravitational forces and environmental conditions. In 1887 Von Sterneck developed a small nonreversible gravimeter pendulum that

was not affected by the effects of temperature and pressure and which was used for relative gravity measurements.

Pendulums, used for either absolute or relative measurements, were the initial standard instruments of gravimetry. They have been used in various configurations, dominating the field until the 1930's and playing an important role until the 1970's; the relative pendulum gravimeters were superseded by the spring gravimeters in the 1930's. The absolute pendulums were the standard in the measurement of absolute gravity until free-fall devices were developed in the 1960s. Since then, pendulum devices have rarely been used.

Bifilar Gravimeters

We should also do a brief remark on the bifilar gravimeters, even if these gravimeters were not widely used (almost all the results were obtained before 1957, Melchior (1966)).

Their great interest is that this kind of gravimeter has been used in the first attempts to measure the luni-solar variation of gravity by W. Schweydar (1914a, 1914b) at Potsdam, and by R. Tomaschek and W. Schaffernicht (1932, 1937) at Marburg. A scheme of the bifilar suspension is shown in figure 2.2.4.
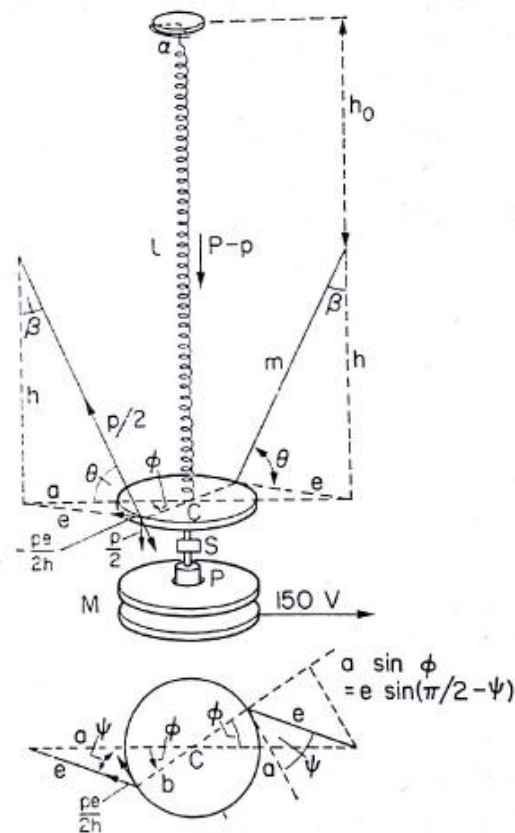
FIG. 85. Principle of bifilar gravimeter.

Fig. 2.2.4: Simplified scheme of a bifilar gravimeter, after Melchior (1966), and picture of bifilar gravimeter owned by IPGS.

In this kind of gravimeters, a mass of weight P (377 g in Schweydar's apparatus and 52.5 g in that of Tomaschek–Schaffernicht) is suspended from a spiral spring which supports most of the weight $(P - p)$ while a small part p is held up by two wires of equal length: a rotation through an angle α of the attachment point of the spiral spring is brought about a with a twisting screw and this turns the mass through an angle φ and twists the two suspensory wires; this angle φ will always be such that there is an equilibrium between the moment of rotation of the spiral and that of the bifilar suspension (Melchior, 1966).

2.2.2 Relative gravimeters

Relative gravimeters measure variations of the gravity field between two different points or between two times, so they are suitable for either spatial surveys or time-variable gravity monitoring at a fixed point.

Different models have been developed over the last century. In a relative gravimeter, the measurement of the variation of gravity is based on the principle of a mass subjected to the acceleration of gravity; the displacements of the mass are proportional to the variations of g. The mass can consist of a weight suspended to a spring, which is the case of mechanical models where variations in gravity cause variations in the extension of the spring. Or it may consist in a magnetic levitation of a superconducting sphere, as for the superconducting gravimeters.

Spring gravimeters

The relative pendulum measurements were difficult and time consuming. This led to the development of more accurate and portable gravity meters, the spring gravimeters which replaced the pendulums in the 1930's (Harrison and Sato, 1984).

A basic example of a mechanical relative gravimeter is typically composed of a weight attached to a spring. Variations in gravity cause variations in the extension of the spring, so the change in gravity force is linearly proportional to the change in the length of the spring.

Historically, we can consider that the spring gravimeters have been divided in two types: linear or stable type, in which the equilibrium conditions are between two forces (elastic and gravitational) and unstable or astatized type, in which a condition close to equilibrium is reached by equating the momentum of the gravitational and elastic forces. Mostly, these types of gravimeters are mobile instruments dedicated to field measurements.

<u>Stable-type spring gravimeters</u> were much used in early times. The principle of measurement is based on Hooke's law. The simplest way to represent this physical concept is to consider a mass suspended to a vertical spring (as in figure 2.2.4(a)). The extension of the spring is related to gravity changes through the equation:

$$F = mg = -k \cdot (s - s_0),$$ (2.19)

where k is the elastic constant of the spring, s_0 is the initial position of the spring and s its new position.

For two different stations or two different times, we can then compute the relative gravity change by: (2.20)

$$\Delta g = g_2 - g_1 = \frac{k \cdot (l_2 - l_1)}{m} = c \cdot \Delta l,$$

where l denotes the length of the spring, $(l_i = s_i - s_0)$, So the changes in gravity forces are linearly proportional to the changes in the length of the spring.

The major disadvantage of stable gravimeters is the great difficulties in measuring small displacements. While the advantage of unstable type is that their sensitivity can be greatly increased through the use of astatization, where a small change in force results in a large change in position.

a   b
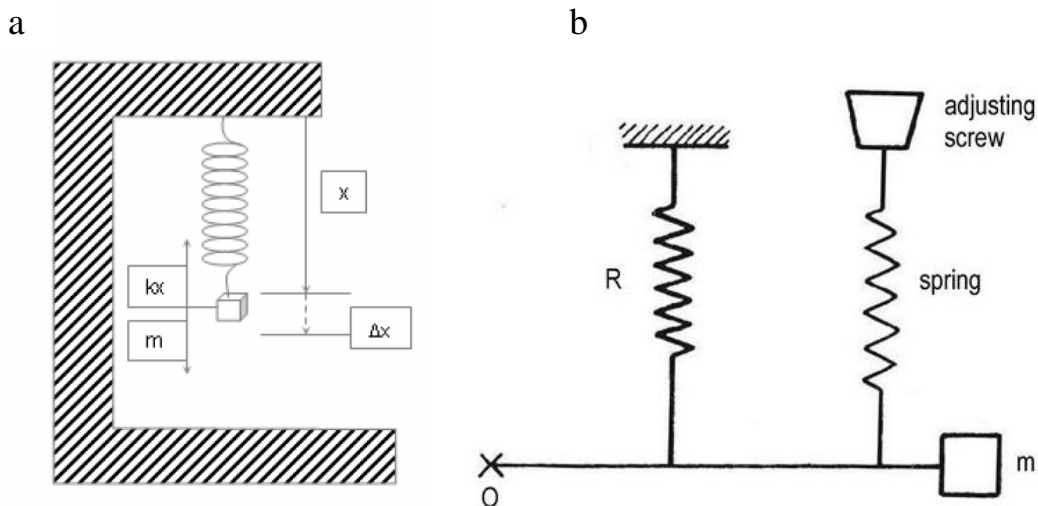
Fig. 2.2.5: Simplified scheme of stable gravimeter principle (a), and of unstable gravimeter principle (b), after Steiner (1988).

Unstable-type spring gravimeters are innovative with respect to stable-type gravimeters in the way that an additional force acting in the same direction as gravity is applied, resulting in a state of unstable equilibrium. Usually a proof mass is attached to a horizontal beam which is suspended by a main spring, and additional springs are applied to return the sensitive measuring part to equilibrium (as in figure 2.2.4 (b)). Therefore, changes in gravity are measured in terms of the restoring force (feedback) needed to return the mass to its standard null position.

More than 30 different types of spring gravimeter were designed from 1930 to 1950, but an important break-through in relative gravimetry resulted from the introduction of the **zero length spring,** invented by Lucien LaCoste (LaCoste, 1934). The characteristic of this type of spring is that the restoring force is proportional to the entire length of the spring.

The zero length spring was first introduced in the LaCoste-Romberg (LCR) gravimeter. And thanks to it, relative gravimeters become much easier to build, to calibrate and to use (LaCoste, 1988). Since 1934 when LaCoste designed his first gravimeter based on the zero length spring, this type of gravimeter has dominated the scene of relative gravimetry for about 50 years. Gravimeters with a zero-length spring have a larger sensitivity (~0.01 mGal) than previous spring gravimeters and the measurement can be made quicker, in a few minutes. Figure 2.2.3 shows a schematic diagram of a LaCoste-Romberg gravity meter.
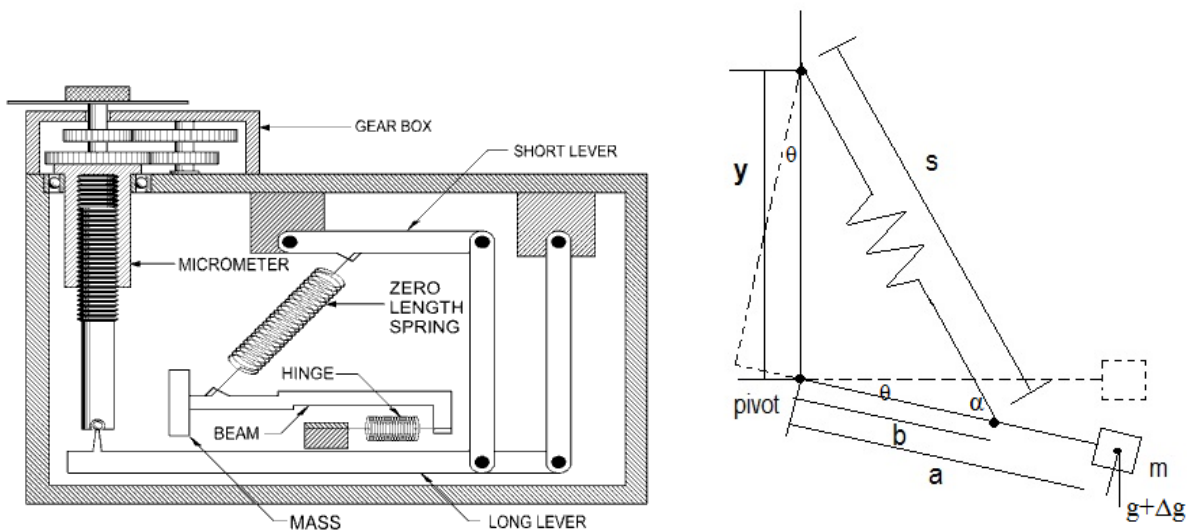
Fig. 2.2.6: Schematic diagram of a LaCoste-Romberg gravity meter, based on a Zero Length Spring, LR instruments.

In that case, the tension in the spring of length s, is given by the expression;

$$(2.21)$$

$$F = k \cdot (s - z),$$

where k is the spring constant and z is the unstretched length.

The moment balance about the pivot in figure 2.2.6, gives;

$$(2.22)$$

$$m \cdot g \cdot a \cdot cos\theta = k \cdot (s - z) \cdot b \cdot sin\alpha$$

using the law of sines;

$$m \cdot g \cdot a \cdot cos\theta = k \cdot (s - z) \cdot b \cdot \frac{y \cdot cos\theta}{s}$$

Then,

$$g = \frac{k}{m} \cdot \frac{b}{a} (1 - \frac{z}{s}) \cdot y$$

When g increases by δg, the spring length increases by δs where

$$\delta g = \frac{k}{m} \cdot \frac{b}{a} \cdot \frac{z}{s} \cdot \frac{y}{s} \cdot \delta s$$

More recently, different easy-to-use automatic gravimeters have been developed (as for example Scintrex CG-3 and CG-5 which have a resolution of 1 µGal and a field repeatability of 5 µGal, and which were the first self-leveling instruments), or the gPhone Gravimeter, which has very high resolution (0.1 µGal). In these gravimeters, the most critical components are housed in an insulated double-oven for better temperature stability.

Unfortunately, despite the most recent advances, the spring gravimeters have still some serious limitations. The principal problem is the elastic variability of the spring; the calibration factor often suffers from time variations and the measurements present a strong time drift, which depends as well on temperature changes. Also, these kinds of gravimeters suffer from the effects of mechanical shocks and vibrations.

But, despite all these limitations, most practical measurements of gravity are still made with these relative spring gravimeters since they are small, light, easy and quick to operate (they are currently the only portable relative gravimeters used for repetitive structural gravimetry), and are cheaper compared to the absolute or the superconducting gravimeters.

Superconducting gravimeters

Superconducting gravimeters (SGs) are also relative devices. Here, the spring suspension of the mass is replaced by the magnetic levitation of a superconducting sphere (which is a niobium sphere), where the magnetic field is generated by two induction coils, being superconducting themselves. The sphere and the coils are temperature regulated. To maintain this state of superconductivity, it is necessary to immerse the assembly in a liquid helium bath (temperature 4.2 Kelvins). The relative motion between the ground and the sphere, or any other perturbation of the gravity potential, moves the sphere away from its equilibrium position. The position of the sphere is detected by a phase-sensitive lock-in amplifier in conjunction with a capacitance bridge. Three capacitor plates surround the sphere with 1 mm clearance (Figure 2.2.7).

The AC signal from the center ring plate is proportional to the displacement of the sphere from the center of the bridge. The sensor is operated in feedback mode to take advantage of the increased linear dynamic range and rapid response compared to open-loop operation. The AC signal is amplified, demodulated, filtered, and applied to an integrator network. The DC output is connected to a precision resistor in series with a five-turn coil wound on the copper magnetic form below the sphere. The resulting feedback force is proportional to the product of the feedback current and the current on the surface of the sphere. This force is given by (Hinderer et al, 2007):

$$F = CI_F(I_{IC} + I_{IF})$$

where I_F is the feedback current, I_{IC} is the current induced on the surface of the sphere by the levitation field, I_{IF} is the current induced on the surface of the sphere by the feedback field, and C is a constant.

Because I_{IC} is proportional to g and I_{IC} is almost the maximum amplitude of the tides, the maximum nonlinearity is $(I_{IF}/I_{IC})_{MAX} \sim 10^{-7}$.

Therefore, the sensor is extremely linear. The gain (scale factor) of the sensor is determined by the geometry, the resistor size, the number of turns on the coils, and the mass of the sphere (usually 4 to 6 g for standard Observatory SGs).

First superconducting gravimeters were developed by William Prothero and John Goodkind (1968) and were manufactured since then by GWR Instruments Inc. The introduction of SGs in the 1980s drastically improved all studies of temporal gravity variations over a wide range of frequencies, ranging from minutes to years, compared to conventional spring gravimeters (Crossley et al., 1999).

The superconducting gravimeter can measure variations of gravity continuously with a precision a hundred times better than the spring instruments. They are the most sensitive and stable gravity sensors currently available for ground-based measurements. But in contrast with spring gravimeters, the SGs are not mobile so they are used as stationary observatory instrument.

The characteristics of the construction and operation of SGs are described in details in Goodkind (1999). The basic principle for the essential sensor elements is shown in figure 2.2.7.

Labels on the figure (left side, top to bottom):
Tilt meter
Vacuum can lid
Insulating support rods
Silicon diode thermometer
Vacuum can
Superconducting shield
Germanium thermometer
Capacitative plate leads
Capacitative sensing plate
Magnetic feedback coil
Shield support

Labels on the figure (right side, top to bottom):
Electrical lead to room temperature
Getter
Vacuum can support rod
MU – metal
Body heater
Electrical feedthrough
Heater for temperature control
Copper magnet form
Upper superconducting coil
Superconducting sphere
Lower superconducting coil
He gas fill crimp

Fig. 2.2.7: Main components of the superconducting gravimeter dewar and sensor (extracted from GWR website, http://www.gwrinstruments.com).

These gravimeters have a very small and linear instrumental drift, greatly improving the problem of spring gravimeters. Also by using magnetic levitation rather than a mechanical device, the problems of mechanical and thermal effects are avoided (Crossley et al., 2013).

Compared to mechanical spring instruments, SGs are characterized by a higher accuracy (in the range of the nGal (1 nGal $=0.01$ nm/s^2) in the spectral domain after time integration of a year long record) and a significantly lower instrumental drift (of the order of few µGal per year (1 µGal $= 10$ nm/s^2)). They also provide unprecedented long term stability. All these improvements allow the study of gravity variations related to geophysical phenomena over a very broad band of periods ranging from minutes to years (Richter et al. 1995; Hinderer and Crossley 2004).

During the last years, major improvements that have been conducted are: significant reduction in size of the dewar and sensor, removal of the need for liquid helium refills and availability of sophisticated data acquisition system that allow remote monitoring. Also some dual-sphere gravimeters have been manufactured, which are equipped with two vertically aligned sensor units. These gravimeters were developed in order to detect small (a few nm/s^2) instrument-induced offsets in the gravity data, (Richter and Warburton, 1997). Recently, GWR has introduced a new model of SG, called *i*Grav (figure 2.2.8) which is much smaller and more portable than previous models (Warburton et al 2010a, 2010b). The *i*Grav was designed to reduce size and weight of the SG, to make it more portable and to be much less complicated for field setup and use.

Fig. 2.2.8: New *i*Grav superconducting gravimeter, manufactured by GWR Instruments (extracted from GWR website, http://www.gwrinstruments.com).

In view of the worldwide development of SG sites and in order to coordinate SG-based research works, the pioneer SG groups decided to form the GGP (Global Geodynamics Project). This project began in 1997 as a long term initiative to establish a worldwide network of SG stations, with an open database and unified data formats. It aims to exchange data gravity, atmospheric pressure and sometimes environmental parameters, to facilitate studies on a global scale (Crossley et al., 1999). The high accuracy and time stability of these gravimeters are useful to study a wide range of geophysical applications (Hinderer et al., 2007) ranging from seismic modes, tides and seasonal to long-term tectonic processes.
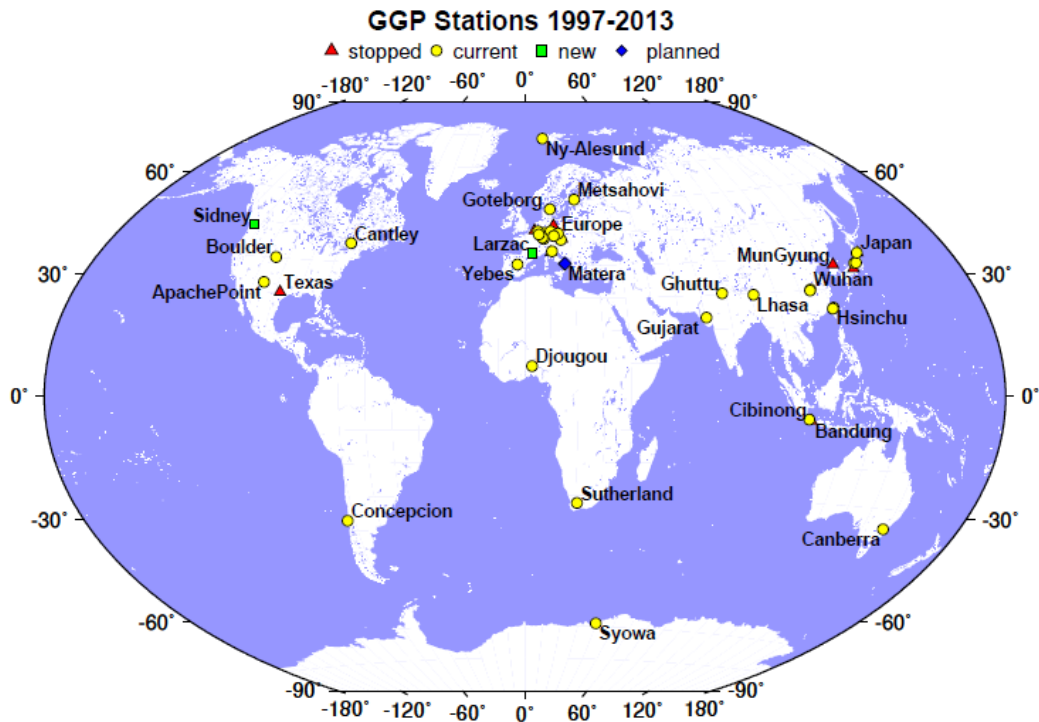
Fig. 2.2.9: Map of the global network of superconducting gravimeters grouped within the GGP project for the period 1997-2013, including new sites. (Extracted from GGP website, http://www.eas.slu.edu/GGP/ggphome.html).

All relative gravimeters, spring or superconducting models, require to be accurately calibrated in order to determine how changes of spring length or of electrical current, correspond to given gravity changes. This is usually performed using parallel absolute gravity measurements.

2.2.3 Absolute gravimeters

A distinction is drawn between relative gravimeters, which measure local variations of gravity in time or gravity differences between observation sites, and absolute gravimeters (AGs), which measure the local and instantaneous gravity value.

The advantage of such measurements is that they are independent of a reference system; they can determine the gravity at any location to a known accuracy. Besides they are not affected by instrumental drift. But on the other hand, they are very sensitive to site-specific conditions; indeed the accuracy of AG measurements is highly dependent on the quality of the site (level of microseismic noise, thermal stability, earthquakes, etc...). Moreover, because of mechanical degradation (dropping object) and logistical reasons, AGs are rarely used for continuous monitoring.

As previously mentioned, absolute pendulum gravimeters were largely replaced by instruments using the free-fall method. First AG built in the sixteenth century

(pendulums) could measure the value of g with an accuracy of about 10^{-5}g. While now, the most accurate AGs are able to measure the acceleration of a falling body with a relative accuracy of about 10^{-9}g.

In **1946**, the first free-fall measurements were carried out in Sevres by C. H. Volet. In **1963**, after the first instruments which used geometrical optics (Martsyniak (1956), Preston-Thomas et al. (1960) and Thulin (1960)), J. E. Faller developed the first free-fall interferometric instrument. The same year also appeared the rise-and-fall interferometric instrument designed by A. Sakuma. In **1967**, the absolute gravimeter of Alan H. Cook was presented, and also the first transportable AG of the free-fall type, from Hammond and Faller. By the early 1970s the best measurements were in the range of 0.01 to 0.05 mGal (Sakuma 1973).

The first commercial AGs were produced in **1986,** when 6 identical AGs were constructed by the Joint Institute for Laboratory Astrophysics (JILA) (Niebauer, 1987), reaching a precision of a few μGal. At the same time, the National Institute of Standards and Technology (NIST), the National Oceanic and Atmospheric Administration (NOAA), and the Institute for Applied Geodesy (IFAG), Germany, joined forces to develop the ballistic FG5 device. This new instrument appeared in the **1990s** and became the worldwide standard for absolute gravimetry. It is manufactured by Micro-g-solutions (USA) and routinely provides 1–2 μGal accuracy measurements at a site with runs lasting from a few hours to several days (Niebauer et al 1995).

This type of AG is based on measuring the acceleration of a body in free fall, where g can be directly determined by measuring length and time. A freely falling reflective test mass is dropped into a vacuum chamber (figure 2.2.10.). The trajectory of the mass is determined with a precision of about $\sim 10^{-6}$ m by laser interferometry, while the fall time is measured by a Rubidium atomic clock (sometimes controlled by GPS) with a precision of $2 \cdot 10^{-12}$Hz. The height of the fall is about 0.2 m and it takes around 0.2 s for the test mass to fall.
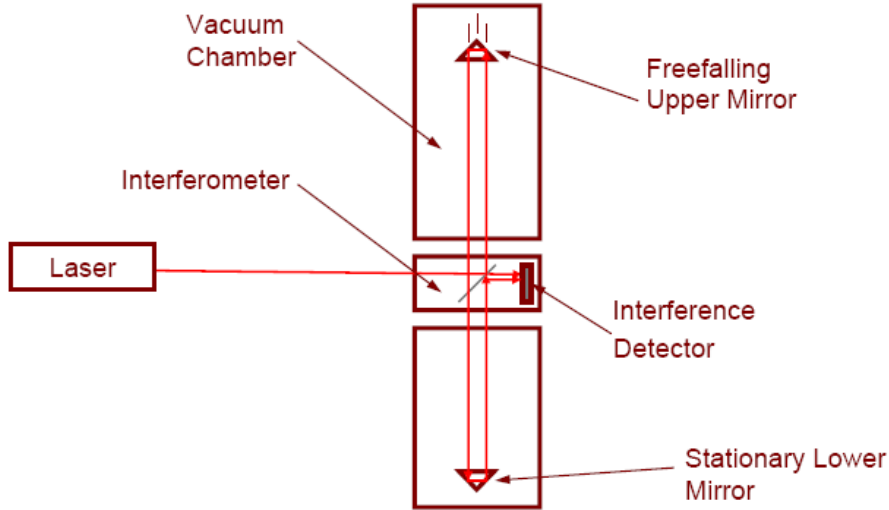
Fig. 2.2.10: Simplified scheme of measure principle of a FG5 free-fall absolute gravimeter. Copyright © 2008 Micro-g LaCoste, Inc.

For each drop, the value of g is determined by a least squares fit of the trajectory data using approximately 700 pairs of time and distance traveled by the mass. The trajectory of the test mass at the time t is given by (FG5 absolute gravimeter user's manual, microglacoste, 2008):

(2.23)

$$x_i = x_0 + v_0 t_i + \frac{1}{2} g_0 t_i^2$$

where x_0, v_0 and g_0 are the initial position, velocity and acceleration of the mass at $t = 0$

In practice, this situation is more complex due to the local vertical gradient of gravity γ (which is usually $\sim$ -3 μGal/cm, corresponding to the free-air gravity gradient $2g_0/r$) that generates changes in the value of g during the trajectory of the mass. So, the standard equation should be modified as follows:

(2.24)

$$x_i = x_0 + v_0 t_i + \frac{1}{2} g_0 t_i^2 + \frac{\gamma x_0 t_i^2}{2} + \frac{\gamma v_0 t_i^3}{6} + \frac{\gamma g_0 t_i^4}{24}$$

and taking into account the different time delays:

$$x_i = x_0 + v_0 t_i + \frac{1}{2} g_0 \widetilde{t_i^2} + \frac{\gamma x_0 \widetilde{t_i^2}}{2} + \frac{\gamma v_0 \widetilde{t_i^3}}{6} + \frac{\gamma g_0 \widetilde{t_i^4}}{24}$$

with:

$$\tilde{t}_i = t_0 - \frac{(x_i - x_0)}{c}$$

where c is the speed of the light.

A mean value of g is given for each set (about 100 drops are averaged to give a set value). Several sets must be performed. The whole measurement system is isolated from seismic noise by using a "superspring" unit that compensates the high-frequency ground vibrations.

In the following years, the time of the falling distances got smaller and the number of drops per set increased, appearing the A10 gravimeter which is a portable AG developed also by Micro-g LaCoste, Inc. (MGL) designed for use in the field. It has the same working principle and processing than the FG5, but is lighter, has a smaller drop chamber, and is easier to use. The A10 measurement possesses an accuracy of 10 μGal, mainly due to the use of a less stable laser. Also, more recently, some modifications of the FG5 have been introduced to give birth to the smaller FG5-L and extended FGX devices.

Even if the absolute gravity world is dominated by free-fall-type instruments (FG5, A10, JILAg), other AG prototypes have been developed over the years, as for example the IMGC-02 developed by the Italian Institute for Metrological Research-INRIM (D'Agostino et al., 2002), a memory of the original IMGC instrument which is based on the principle of Sakuma's instrument.

But the most relevant ones are based on cold-atom interferometry (CAG), which opens up a new way to perform the free-fall experiment (Peters et al. 1999). In this new kind of instruments there is no dropping or launching mechanisms of a solid body in free fall but atoms are dropped. So there is no mechanical friction and hence no mechanical limitation in the duration of measurements, except for the laser power. Another important advantage is that CAG can measure more frequently (several times a second) than the optical types. Initial results compared with the FG5, by B. Desruelle et al. at the 2013 AGU meeting, seem promising even if no complete precise inter-comparison has been performed yet.

Since 1981, periodic inter-comparisons of AG campaigns are conducted in order to detect possible systematic errors and to define the accuracy level of the methodology. The Bureau International des Poids et Mesures, Sèvres, France, has hosted eight campaigns (1981, 1985, 1989, 1994, 1997, 2001, 2005, 2009), and also several comparisons were held in Walferdange, Luxemburg at the European Center for Geodynamics and Seismology (ECGS) (2003, 2007, 2011, 2013).

Not only gravimeters have been used for measuring variations of the Earth's gravitational field, but there have been several other types of instruments, less used or very specific, such as the torsion balance developed by Baron Roland van

Eötvös in 1896 and used to measure the gradients of gravity and differential curvature. Also the vibrating string gravimeter (Lozhiskaya, 1959, Breiner et al., 1981) was used in Russian and in China. The borehole gravity meters, which were first developed in the 1950s in response to the need by the petroleum industry for accurate down-hole gravity data. The underwater gravity instruments, the shipborne gravity instruments and the gravity gradiometers can also be quoted.

2.2.4 Instruments used in this study

Throughout this thesis, we have used data recorded by different types of relative and absolute gravimeters.

Regarding the relative gravimeters, data from several models of spring gravimeters have been analyzed. Most of these mechanical models are astatized, such as the Lacoste and Romberg (L&R) or the North-American gravimeters. Data from stable types have been used too, like the Askania model.

A large number of superconducting gravimeters has also been used; few of them belong to the first models built in the 1980s, although most of them belong to the compact type (like the SG C026 at J9) or to the new generation of OSG (Observatory SG). There are even a few double-sphere instruments among them.

Regarding the absolute gravimeters, only records from FG5 models have been analyzed in detail, though data from JILAg instrument, already treated, have been also used.

Table 2.2.1: General specifications of different gravimeters used in this study.

Instrument	Resolution (µGal)	Precision (µGal)	Drift rate (µGal/period)
Spring*	1.0	0.1	~15/day
Superconducting	0.01	0.001	few/year
Absolute	10.0	2.0	NO

(*) As several types of spring gravimeter have been used, with different specifications, in the table we have only indicated the characteristics of a Lacoste and Romberg type, since we have mainly used data from two gravimeters of this type, the L&R ET005 and the L&R ET19 installed at J9 Observatory and Black Forest Observatory respectively.

A list of relevant papers on the use of superconducting gravimeters can be found at: http://www.gwrinstruments.com/published-papers.html

A list of relevant papers on the use of absolute gravimeters can be found at:

http://www.microglacoste.com/grav bib.php

As a large part of this thesis is devoted to data treatment and analyses of relative gravimeters, in the next part we will detail the pre-processing of raw data and then the analysis methods used to retrieve some information on the Earth's response to tidal forcing.

2.3 Gravimetric data analyses

The classical analysis tools (tidal analysis software, spectral FFT methods) require having relatively clean data series. So before introducing the tidal analysis software, we present the pre-processing method which aims at preparing data before exploitation.

2.3.1 Pre-processing of both spring and SG records

As most of the geophysical signals, any gravity time series requires specialized pre-processing before we can use it with fullest advantage. Indeed, some tools can deal with irregularly sampled data or series with missing samples (gaps) such as statistical spectral method (for instance the Lomb-Scargle periodogram, Lomb, 1976). Nevertheless, we will show in the following that our pre-processing does not impact our tidal analysis results, but, on the contrary, by filling up gaps with a well-known local tidal model (inferred from long-term observations at the station) we will be able to take full advantage of the length of our time-series.

So, in this section we will explain the methodology that we have applied to all the series from different gravimeters that we will use in the next sections.

The main disturbances contained in the raw gravity series are spikes, steps (sudden offsets) and gaps (missing samples), which are mainly due to instrumental problems, human intervention, and also from true geophysical signals such as earthquakes. These corrections are done to avoid that the disturbances alter any treatment realized on these series, such as tidal analysis or spectral estimation. A simple example of preprocessing is shown in figure 2.3.1.
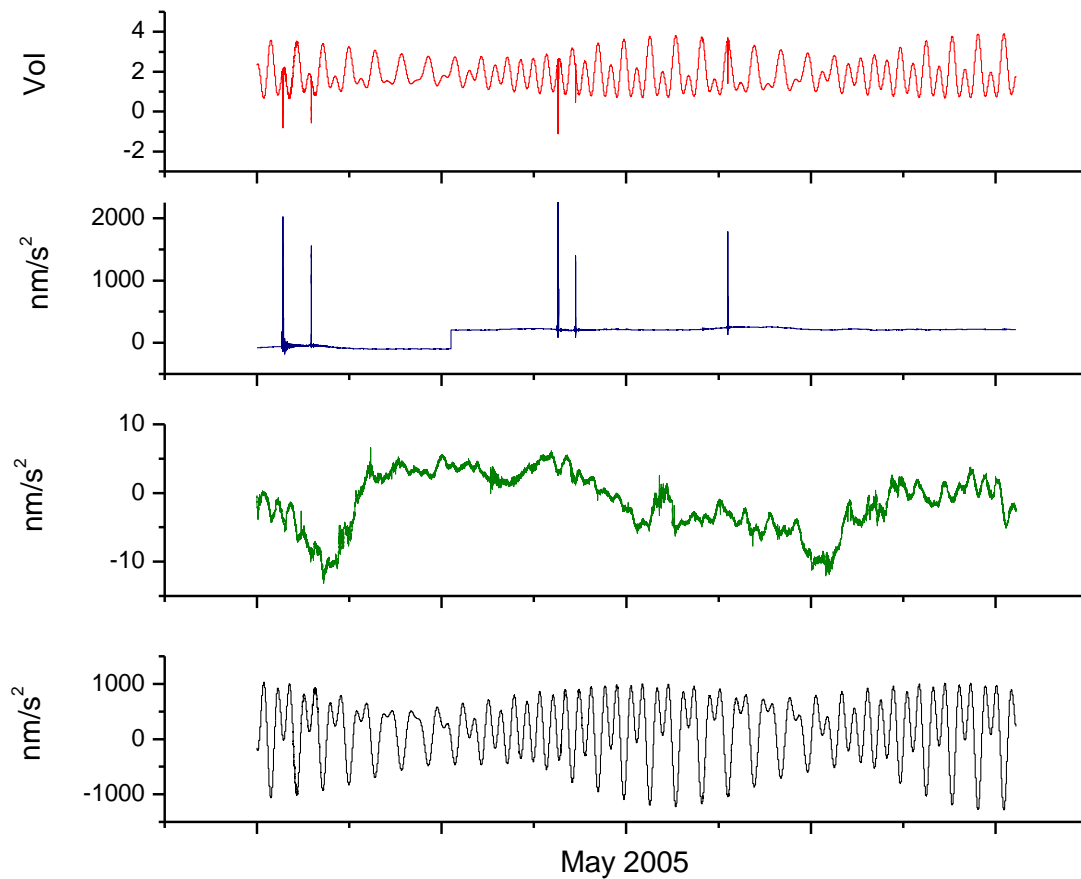
Fig. 2.3.1: Example of correction of gravity residuals. Upper plot shows 1 month (May 2005) of SG raw data at J9 Observatory. Second plot shows g (residuals) when g (removed) consists of a local tide model + a nominal pressure correction. Third plot shows the cleaned residuals, where all the spikes and earthquakes were previously replaced by a simple linear interpolation. And finally, corrected series is shown in the bottom.

As it is well described in Hinderer et al. (2002), many different processing methods are available and almost any user group possesses its own strategy to pre-process the data. They also show that not just the applied methodology is significant, but there are also 'human factors', because even when using the same processing tool, personal factors can enter into the treatment leading to significant long period changes in the gravity signal after different cumulative corrections.

Independently of the treatment used later to clean them, first we have to compute the gravity residuals from our raw data series. Usually, the classical preliminary step consists of subtracting from the gravity series, g (observed), all the contributions that can be modeled with some confidence g (removed), leading to the gravity residual series, g (residual).

g (residual) = g (observed) – g (removed),   (2.25)

where

g (removed) = contributions than we can model at our station   (2.26)

These gravity residuals are usually small amplitude signals which permit us to detect and correct more easily any kind of disturbance than if we use the original observed gravity series. When all problems have been fixed in g (residual), we just have to add back the previously removed signals, to obtain the corrected gravity series, g (corrected).

g (corrected) = g*(residual) + g (removed)   (2.27)

where g*(residual) is the g (residual) corrected ("clean residuals").

Removed Effects

Depending on the quality of the data and the auxiliary information available at each station, we are able to model the contributions of the largest amplitude signals that can be removed from the observed gravity series. We can decompose our temporal gravity observed series into a series of additive effects:

$g(observed)$ = g(disturbances)   (instrument and site origin, earthquakes)

$+g$(tides)   (solid Earth, ocean) the largest periodic contribution

$+g$(non-tidal loading)(atmosphere, ocean currents) *second largest effect*

$+g$(polar)   (polar motion effect)

$+g$(drift)   (instrument drift function)

$+g$(hydro)   (rainfall, soil moisture, groundwater, surface water, ice)

$+g$(other) (tectonics, deformations, slow earthquakes and all other possible signals)

(2.28)

We can divide all these contributions into two types of signals:
- ✓ Periodic signals: tides, polar motion (annual forced motion and Chandler wobble), seismic elastic normal modes.
- ✓ Non periodic signals: atmospheric pressure, hydrology, volcanic, non-tidal ocean circulation and general Earth deformation.

In our case, to calculate the residual gravity data we have only subtracted the standard models (local tides, local atmospheric pressure effect, polar motion and instrument drift). For each series of this study we have performed the following steps:

* We have first calibrated the raw gravity records by using the appropriate amplitude calibration factor (expressed in μGal/V or nms^{-2}/V) for each instrument to convert the observed gravity to their equivalent gravity values. Calibration issues are discussed in more detail in <u>section 4.5.</u>

* We have subtracted the body tides and the ocean tidal loading using a local tidal model. In some of the stations, this model could be computed from the luni-solar tidal potential using tidal parameters (amplitude and phase factors) originating from a previous tidal analysis at the same station. In the stations where such previous analysis was not available, we have computed a synthetic local tidal model using latitude dependent tidal factors, obtained for an inelastic non-hydrostatic Earth model like DDW99 model (Dehant et al., 1999).

Gravity data are principally dominated by the tidal signal. The amplitude of this contribution usually varies between 100 and 300 μGals, depending mainly on the station latitude and the phase of the luni-solar cycle.

* We have subtracted the local pressure effects using a standard empirical barometric admittance of – 0.3 μGal/hPa (e.g., Spratt, 1982; Müller and Zürn, 1983; Richter, 1983, Crossley et al. 1995) for the spring gravimeter series (because sometimes the pressure series are also affected by gaps or offsets, they should be corrected before removing their effects to the gravity series, in order to avoid introducing artificial signals in the gravity residuals). For the SG stations we have used the complete (local + non-local) atmospheric loading effects estimated at each GGP station by Jean-Paul Boy, available at <u>http://loading.u-strasbg.fr/GGP/</u>. These atmospheric loading effects are computed by convolving surface pressure fields provided by the European Centre for Medium-Range Weather Forecasts (ECMWF) and the appropriate Green's functions (Boy et al., 2002) describing the elastic Earth response and the direct Newtonian attraction to the atmospheric pressure loading.

Up to 10% of the signal may come from the atmosphere. Atmospheric effects on gravity became an important consideration with the higher precision and lower noise of the SG compared to previous instruments (Warburton and Goodkind 1977). A number of well-studied empirical and physical methods exist for making a pressure correction to the gravity data, but even with the most sophisticated treatments it is not possible to completely remove the atmospheric pressure effect. Among the different approaches used to correct gravity changes for the effects of atmospheric pressure changes we can find (Hinderer et al., 2014):

- A first option (which we have used for all the spring gravimeter stations) is to use a single barometric admittance (Crossley et al., 1995). This coefficient is computed, in the time domain, by minimizing (in the least squares sense) the difference between observed gravity residuals $g(t)$ and the observed barometric pressure $p(t)$ and solving for the real coefficient α (which means no phase lag) to determine the corrected gravity residual:

$$g_c(t) = g(t) - \alpha p(t)$$

(2.29)

Minimizing $\left| g_{c(t)} \right|^2$ assumes that errors in $g(t)$ and residuals $g_c(t)$ are uncorrelated.

The nominal value of α is close to – 0.3 µGal/hPa and corresponds to a model where pure attraction (– 0.42 µGal/hPa for a Bouguer plate) is partly reduced by crustal elastic deformation and the Earth's curvature (Niebauer, 1998; Warburton and Goodkind, 1977).

We should point out that in this case there is no change either in time or in frequency of this factor; however this simple model is able to cover 90% of the total air pressure effect.

- A second option is the frequency-dependent admittance (Neumeyer, 1995; Kroner and Jentzsch, 1999; Abd El-Gelil et al., 2008).

A frequency dependent correction coefficient can be estimated by cross spectral analysis, a method to determinate the frequency response function for a single input – single output model. For this model, the frequency response function $H(f)$ can be calculated after Bendat and Piersol (1986) by:

(2.30)

$$\widehat{H}(f) = \frac{\widehat{G}_{xy}(f)}{\widehat{G}_{xx}(f)}$$

where G_{xx} is the auto spectral density and G_{xy} the cross spectral density of the input series $x(t)$ and the output series $y(t)$, sampled at equally spaced time intervals ($n = 0,1, \dots, N-1$).

The gain factor $H(f)$ and the phase factor $\phi(f)$ of the frequency response function can be estimated at a frequency f, varying from 0 to Nyquist, by:

$$\left|\hat{H}(f)\right| = \frac{\sqrt{Re\hat{G}_{xy}(f)^2 + Im\hat{G}_{xy}(f)^2}}{\hat{G}_{xx}(f)}$$

$$\phi(f) = arctan\left(\frac{Im\hat{G}_{xy}(f)}{Re\hat{G}_{xy}(f)}\right)$$

After determination of the frequency response function, the frequency dependent atmospheric pressure correction can be carried out for the gravity data, using FFT techniques in the frequency domain, or using convolution techniques in the time domain (Neumeyer, 1995).

This approach is still constant in time, and some studies have shown that the admittance may also vary as a function of time (Merriam, 1995; Crossley et al., 2002). An approach based on a wavelet technique to filter out the atmospheric pressure effect simultaneously in time and frequency was proposed by Hu et al. (2005). Such approaches remain incomplete as they deal only with the local atmospheric pressure effect.

- The last option, which we have used for the SG stations, is to consider not only local pressure changes but rather a pressure distribution around the gravity station which may not be uniformly distributed. This leads then to a loading computation including both Newtonian attraction and elastic deformation (Farrell, 1972; Spratt, 1982). There are several loading approaches; from 2D pressure loading (Sun, 1995; Boy et al., 1998, 2001, 2002; Mukai et al., 1995) to the full 3D atmospheric models, where the atmospheric parameters are available at different vertical levels (Swenson and Wahr, 2002; Boy and Chao, 2005; Neumeyer et al., 2004; Kroner and Jentzsch, 1999; Klügel and Wziontek, 2009; Abe et al., 2010).

In this approach, the response of the Earth to pressure forcing is expressed using Green's functions (Farrell, 1972).

** The Newtonian effect corresponds to a direct gravitational attraction by air masses on the gravimeter (Merriam 1992):

$$GS(\psi, z) = \frac{G[a - (a+z)cos\psi]}{[a^2 + (a+z)^2 - 2a(a+z)cos\psi]^{3/2}}$$

(2.31)

where z is the altitude of the atmospheric elementary volume of density ρ_A and spherical coordinates (θ', λ'), G is the Newtonian constant of gravitation, ψ is the angular distance between the gravimeter of coordinates (θ, λ) and the elementary atmospheric mass.

** The elastic effects at (θ, λ) is equal to:

$$GE(\psi) = -\frac{G}{g_0 a^2} \sum_{n=0}^{\infty} [2h'_n - (n+1)k'_n]P_{n(}cos\psi)$$

(2.32)

For a comparison of 2D (surface loading), 2.5D and 3D models at two SG locations, Strasbourg (France) and Djougou (Benin), we refer the reader to Hinderer et al. (2014).

These loading computations are usually based on global models whose data assimilation systems contain observations from ground stations, radiosondes, satellites and many other sources; as for example the reanalysis models from the ECMWF, http://www.ecmwf.int/.

* We have corrected for the gravity effect induced by polar motion using IERS data (http://www.iers.org/). This signal, mainly composed of an annual term and the 14-month oscillation of the rotation pole (Chandler Wobble) is very well defined by IERS data, although at a level of only 5 µGal/yr (or 0.01 µGal/day) it is not important for gaps of less than a week or so.

A simple conversion is usually made between the coordinates' (x, y) amplitudes of polar motion (m_1, m_2) in radians and the gravity effect δg in µGal through the centrifugal effect (Wahr, 1985):

$$\delta g = \delta \, \Omega^2 r sin2\theta[\cos(m_1\lambda) - \sin(m_2\lambda)]$$

(2.33)

where (θ, λ) are station latitude and longitude, Ω the Earth's rotation rate. δ is the gravimetric factor of degree-2, expressing the response of the Earth to the variation of rotational potential and is equal to 1.16 for a purely elastic Earth, whereas fitted solutions are usually closer to $\delta = 1.18$ (e.g. Loyer et al, 1999, Harnisch and Harnisch 2006), that is to say closer to the response of an elastic Earth with a static global ocean.

* We have finally subtracted the instrument drift. From an instrumental point of view (e.g. Goodkind 1999) drift is likely to be either a linear or exponential function of time, but its amplitude is not easy to predict. Drift in the spring gravimeters is irregular and strong, even though in the 1980s they have incorporated electrostatic feedback that considerably improved their linearity and drift performance (Larson and Harrison 1986). For the SGs, drifts are characterized by a small initial exponential followed by a small linear term.

Representative values of instrument drift are usually less than 4 µGal/yr for the linear part where these have been checked carefully with AGs.

Instrument drift is not to be confused with a secular change of gravity, even though the two cannot be separated except using combined SG-AG observations. An example of SG drift correction using parallel AG measurements at J9 is shown in figure 2.3.2.

All these steps lead us to the gravity residuals series, which we then have to clean from disturbances (as shown in figure 2.3.1).
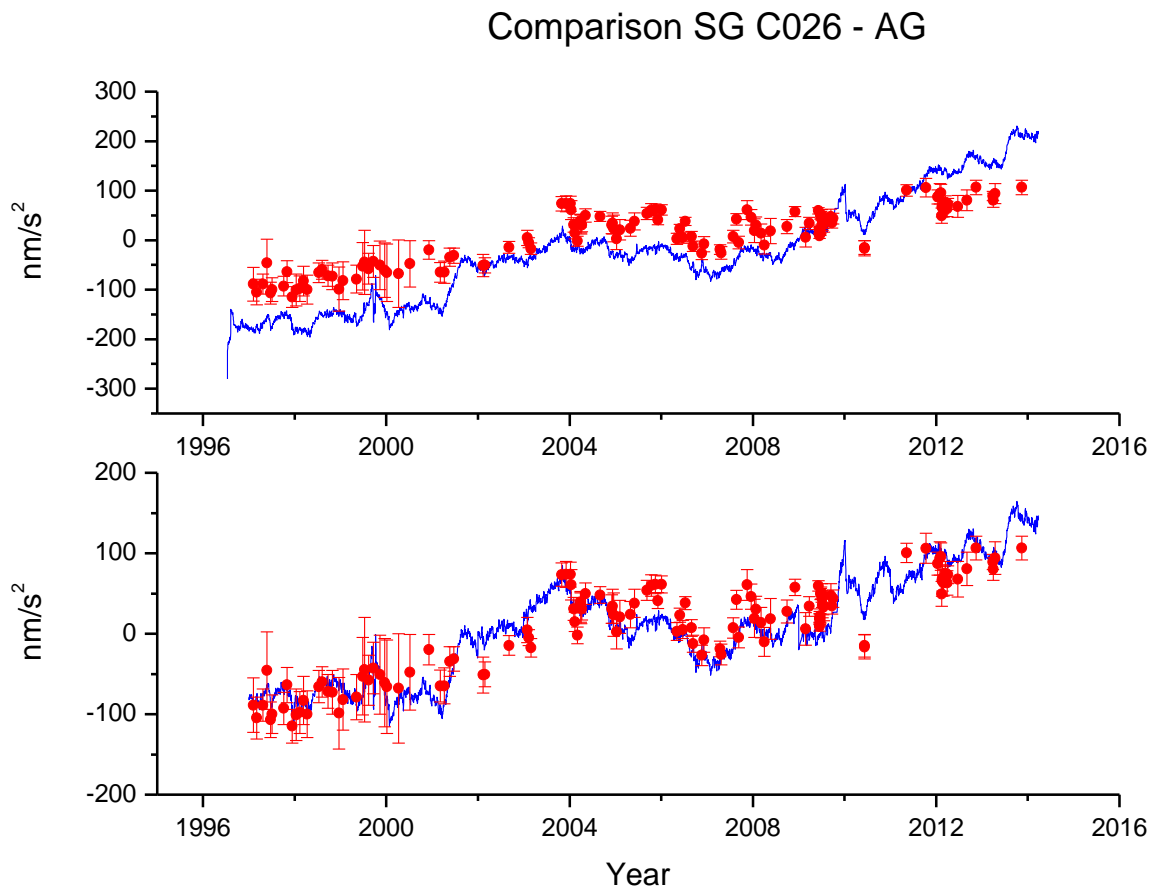
Fig. 2.3.2: Correction of the SG drift using 132 independent absolute measurements, recorded in parallel at J9 Observatory. Upper plot: superposition of AG measurements (red dots with the respective error bars) and the C026 residuals (blue line). Lower plot: superposition of AG measurements and the C026 residuals corrected from the estimated instrumental drift.

Once we have obtained all our gravity residuals series, we carried out the treatment of the disturbances with the help of the TSOFT pre-processing package developed by the Royal Observatory of Belgium (Van Camp and Vauterin, 2005) to

detect and visualize the disturbances in the data series, and to apply different manual corrections to remove spikes and offsets, reduce the earthquake perturbations and fill up gaps.

This software offers us the possibility of applying several manual corrections such as linear and cubic interpolations, or removing steps or gaps.
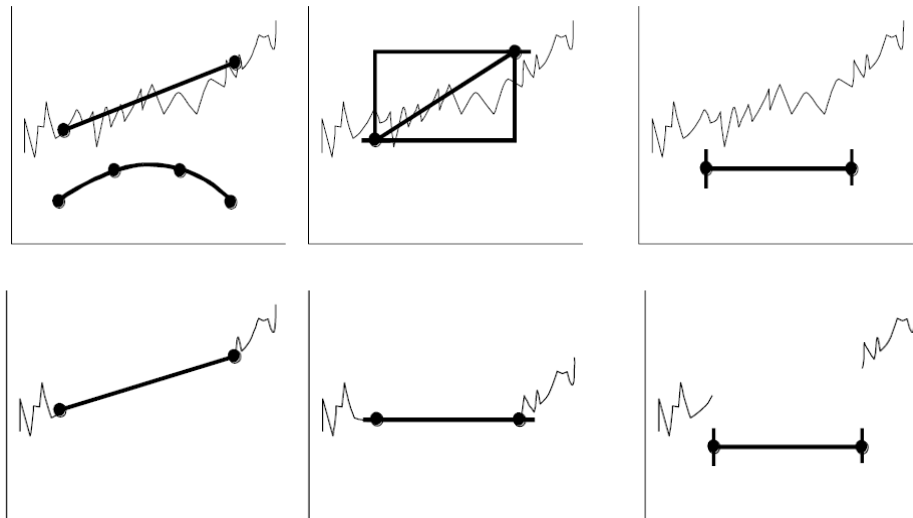
Fig. 2.3.3: Graphical representation of the different correctors offer by TSOFT, in unapplied state (upper) and in applied state (bottom). Left: linear and cubic interpolations; middle: step; right: gap (from TSOFT manual).

Earthquakes: we corrected the residuals for any earthquake disturbance by replacing it by a linear segment or by a cubic interpolation, depending on its length.

Spikes: we also removed spikes contained in the signal by replacing them by a linear interpolation.

Offsets: the offset correction (especially the one with small amplitude) is the most delicate step and has always been debated because sometimes it is impossible to decide without auxiliary information whether they are purely instrumental or due to geophysical phenomena (e.g. rain). The consequences are important for the study of the long term gravity changes because of the cumulative effect of the offset corrections. In particular, the drift estimate of the SG will be affected by this effect. One constraint can be introduced by repeating absolute gravity measurements at the same site which will clearly help in determining the physical long term gravity evolution (Hinderer et al., 2002).

Gaps: in our series, the smaller ones (up to some hours) have been filled up using the local tidal model for the station, and the longer ones (from few days up to 10 months for the L&R ET005) were not filled up at all. In this case, the total series remained divided into several blocks.

The problem of data gaps is in fact different for spikes and offsets because the information is missing rather than corrupted, leading to unevenly spaced data sets with all the inherent restrictions in using standard codes such as ETERNA (Wenzel 1996b) or simply an FFT (Hinderer et al, 2002).

The processing explained above has been applied with several small differences depending on the raw data and information available to us for each station:

- For the superconducting gravimeter stations, data were obtained from the GGP database (http://isdc.gfz-potsdam.de/), so we disposed both of raw gravity and pressure data, and all the necessary information such as the calibration factor and the time delay specific for each gravimeter. Also some of the stations provided information files indicating instrumental problems, offsets due to helium refills, changes in the electronics, etc. This information is very useful when deciding which type of corrections should apply to the series.

- Regarding the data from spring gravimeters, we had the air pressure measurements at the different stations except at Walferdange, where 40 year reanalysis data from the ECMWF were used (Uppala et al., 2005).

For these types of instruments, data were calibrated by comparing with theoretical tides as suggested by (Goodkind 1996) (while the SGs were calibrated using parallel absolute gravity measurements). Because these gravimeters underwent several improvements during our study period, it was necessary to re-estimate the amplitude calibration factors and the phase lags for each time block, while for SG data a single value was used for the total series (except for stations where the acquisition system has been updated and new phase lag had to be estimated for the new system). Moreover the irregular and strong instrumental drift affecting the spring gravimeters requires careful modeling, because of its impact on the calibration errors.

Since the spring gravimeters are very sensitive to the changes of temperature and air pressure, the thermal and atmospheric contributions are important for the noise in the diurnal and semidiurnal bands. So to avoid these perturbations the spring gravimeters should be installed in particular conditions. For example, at Potsdam, the Askania GS15 222 gravimeter was installed in an insulating chamber inside an airtight container, with a temperature stabilized about 23 ºC and a relative humidity not higher than 40%. The ET-19 at Black Forest Observatory is installed behind two airlocks in a container with an air-drying system, at a constant temperature of 10 ºC stable to 0.003 ºC in the gravimeter vault. And the ET-005 was installed in an isolated box thermostatically controlled at 35 ºC. The box was located in a room at 25 ºC inside an old underground fort (J9 Observatory). The sealed box protected also the sensor against the direct influence of barometric pressure variations.

There are two different approaches used to solve problems in the data: the first one consists on leaving gaps in the series when there is a problem in a segment. The second one consists on removing the disturbances in the residuals and to fill the gaps with a synthetic signal using a local tidal model.

In our case we have chosen the second approach (except for the really large gaps), which indeed is the preferred approach within the gravity community, although it requires more caution about what level of disturbances to correct or not. We have chosen it in order to have a uniformly sampled time series for applying, as much as possible, the same treatment to all gravity series (filtering, tidal analysis and spectral comparisons). Mainly because it is more convenient dealing with continuous data rather than series of data divided in sequences of blocks and gaps and because computer algorithms are also easier to implement for continuous data than for discontinuous ones.

The question of filling gaps and removing disturbances rather than maintaining the integrity of the signal with a Least Square Spectral Analysis (LSSA) technique like in Pagiatakis (2000) or with BAYTAP-G, which is a tidal analysis code using Bayesian information adapted to data with irregularities in drift, occasional steps and other disturbances (Tamura et al. 1991), is often a matter of debate, even if the percentage of the disturbances and gaps is very small with respect to the data length (mainly in the SGs series where the gap proportion is almost negligible, of about ~2% for J9 series).

To estimate the impact that the manual correction of these disturbances (using Tsoft) could have on the stability of the tidal analysis that we will compute in chapter 4, we have performed the following test, which is shown in detail in **Annex A**:

- ✓ We have generated a synthetic series for J9 station using DDW99 non hydrostatic Earth's model (Dehant et al., 1999) and NAO99 ocean model (Matsumoto et al. 2000).
- ✓ This series has been degraded by adding Gaussian white noise (with a standard deviation of 10 nm/s^2), random gaps (up to 2500h in total, corresponding to about 3% of our time length), 4 offsets of different size (5, 10, 15 and 20 nm/s^2) and 10% of spikes distributed all along the series.
- ✓ Finally, we have corrected this degraded series manually with the help of TSOFT, in a similar way as we have done for all the observed series used in this study.

We have performed similar tidal analysis on all these synthetic signals (pure synthetic tides, synthetic tides degraded with white noise, synthetic tides degraded with disturbances, synthetic tides degraded with both white noise and disturbances and finally the worst degraded synthetic signal after manual correction with TSOFT package). These tidal analyses have been performed using

ETERNA 3.4 software on yearly segments shifted month by month, in all the series and they have been used to compute the variability of the main diurnal and semi-diurnal tides.

From the obtained time variability of the main diurnal and semi-diurnal tidal as computed in Annex A, we can infer the following remarks:

- We found that the variations due to numerical effects in the tidal analysis are almost negligible.

- We found that the presence of disturbances (offsets, spikes and gaps) increases the variability. This variability is much higher when white noise is added.

- We found that the variations of delta-factors after manual corrections (pre-processing) are similar to the variations obtained from the noisy series before pre-processing. So no variability is added by the pre-processing itself.

Therefore, we can conclude that the corrections applied to our observed series do not distort the tidal results that will be shown in the following sections. Thus, the variations that we will study in chapter 4 on the tidal parameters, can neither be due to numerical and analysis noise, nor to the pre-processing of gaps, spikes and offsets. Rather, we will see that they are related to the noise contained in the signal (Calvo et al. 2014a).

We then present the tidal analysis methods that were developed in the past and the one that will be employed in this thesis.

2.3.2 Earth tides analysis

The Earth tides have been studied in different ways, although the background of all analyses is based on the early development of tidal potential by George Darwin (1883). About 1867, William Thomson (Lord Kelvin) introduced the method of harmonic analyses, and it was Laplace who realized that tides might be expressed by the cosine of an angle increasing uniformly with time, applying the essential principles of the harmonic analysis to the reduction of high and low waters. In the 20th Century different methods appeared, such as the combinations of Doodson (1921, 1954), the summations of Lecolazet (1956b, 1958a), the Pertsev's method (1958, 1961), before the development of the least squares method with Chjonicki (1972) or Venedikov (1961, 1966a). Throughout the century, the tidal analysis techniques evolved from the use of complicated analysis tables to determine a restricted number of tidal parameters, to the modern tidal analysis, which are computational methods. Nevertheless, most of the past and present methodologies kept the basic Darwin principle unchanged (Melchior 1966).

Essentially, tidal analysis consists of determining the tidal parameters (observed amplitudes and phases) of tidal waves at specific frequencies using observed data. An Earth tides analysis method basically establishes a comparison between the theoretical gravity signal at a station (which is computed for a given Earth's model; for example the Wahr-Dehant-Zschau Earth model (Dehant 1987) is used in ETERNA software) using the coordinates of the station and a tidal potential catalogue and the cleaned observed tidal gravity signal, to estimate a suite of tidal parameters for the station. However, as the oceanic tidal waves have practically the same spectrum, they cannot be separated from the body tides and what we get in our results is the superposition of both solid Earth and ocean tide effects.

The number of tidal waves that can be determined and the precision obtained in our analyses depend on the record data length and on the noise characteristics of the instrument used.

Spectral separation of tidal waves

The number of tidal groups that can be separated depends on the data length. However, even if we have very long records it is not possible to determinate the tidal parameters for each wave listed in the tidal potential catalogue. So, following the Rayleigh-criterion we assemble the closest waves in groups assumed to have similar properties. For each of these groups the tidal parameters are then estimated.

In principle, two tidal frequencies w_1 and w_2 can be separated on an interval of n equally spaced observations if their angular speeds differ at least by $360º/n$ (Rayleigh criterion).

$$(w_2 - w_1)T \geq 360º$$

where T is the data length (number of samples n times the sampling rate Δt). It is equivalent to request that their periods are within the interval $T = n \cdot \Delta t$

$$T \geq \frac{T_1 \cdot T_2}{T_1 - T_2}$$

Sampling rate

Besides, the sampling interval of the records, Δt, limits the maximum frequency that can be achieved because of the Shannon-Nyquist theorem. Hence a two-hour interval between samples is well sufficient for the Earth tides analysis, although the usual procedure is to use hourly readings. Because of the Nyquist-Shannon criterion, for $\Delta t = 1h$, the maximum frequency is 12 cpd (Nyquist frequency).

The 1 minute sampling rate has been conventionally adopted by the GGP network of superconducting gravimeters, even if most of the stations use higher sampling rates from 1 to 10 seconds. A first decimation (after applying a low-pass filter to avoid aliasing of high-frequency content) is then performed on the original data to get one minute sampled data.

2.3.3 Modern tidal analysis software

As said before, an analysis program basically establishes a comparison between the theoretical gravity signal for the station and the corrected observed tidal gravity signal to estimate a set of tidal parameters for the station.

Currently, three programs are mainly used for Earth tidal analysis within the SG community; two of them are based on the least squares approach: ETERNA (moving window filtering and global evaluation of the tidal families following T. Chojnicki) and VAV (non overlapping filtering and separation of the tidal families following A. P. Venedikov), and the third one is based on a Bayesian method (BAYTAP-G).

ETERNA. This package became the most popular one and its associated data format became the official transfer format adopted by the International Centre for Earth Tides (ICET). It was developed over many years by H. G. Wenzel (1994a, 1994b, 1996b), who generated a set of several FORTRAN codes for dealing with all the common aspects of processing gravimeter data. Among these codes, **ANALYZE** is the one used for tidal analysis, which is based on a method first developed by Chojnicki (1972) and improved later by Schüller (1977).

It is based on a least squares adjustment to estimate simultaneously the tidal parameters, the meteorological and hydrological regression parameters, the pole tide regression parameters and the Tschebyscheff polynomial bias parameters for drift determination. It is valid for all tidal components: potential, gravity, tilt, strain, displacements. The user can decide to use different sampling rates, and also can choose among different tidal development catalogues: from less than 400 waves (Doodson's catalogue) up to more than 10,000 waves for the tidal potential catalogue of Hartmann and Wenzel (1995).

The model used for least squares adjustment is:

$$l(t) + v(t) = \sum_{j=1}^{q} (\hat{X}_j \cdot CO_j + \hat{Y}_j \cdot SI_j) + \sum_k \hat{D}_k \cdot T_k(t_n) + \sum_m \hat{R}_m \cdot z_{m(t)}$$

Where

(2.34)

$l(t) =$ Observed gravity signal

$v(t)=$ Improvements to the observations

$X_j, Y_j=$ Linear form of unknown parameters (amplitude factor (H_j) and phase differences, (dF_j) for each wave group j:

$$X_j = H_j \cdot \cos dF_j$$

$$Y_j = H_j \cdot \sin dF_j$$

$CO_j, SI_j=$ Factor of theoretical tidal parameters A_j (amplitude) and Φ_j (phase) for each wave of frequency f_i in the wave group j, starting with wave a_i and ending with wave e_i:

$$CO_j = \sum_{i=a_i}^{e_i} H_i^* A_i \cdot \cos(2\pi f_i t + \Phi_i)$$

$$SI_j = \sum_{i=a_i}^{e_i} H_i^* A_i \cdot \sin(2\pi f_i t + \Phi_i)$$

$H_i^* =$ Amplification factor from digital highpass filter (equal to 1 if the drift is approximated by polynomials)

$D_k, T_k =$ Coefficients (D_k) of TSCHEBYSCHEFF-polynomials T_k of degree k

$R_m, z_m=$ Regression coefficients (R_m) of additional channel number m (z_m)

A possible drift in the data can be eliminated by highpass filtering (the filter coefficients for different numerical digital filters are included in the ETERNA-package) or is approximated by TSCHEBYSCHEFF–polynomials (T_k) whose coefficients (D_k) are also estimated in the least square adjustment.

VAV. It is based on the method of tidal harmonic analysis called MV66, developed by Angel P. Venedikov (1966a, 1966b), and its improvements through the successive program code SV and NSV (Venedikov et al., 1997). VAV is also widespread used for tidal analysis purposes. The last version of VAV was described most recently by Venedikov et al. (2003; 2005). In addition to the modelling of the tidal signal, according to the last published version, the following features of VAV can be highlighted:

- Transformation of the observed data from the time domain into a time/frequency domain and application of the method of least squares on the transformed data, allowing frequency-dependent estimates of the tidal parameters.

- A flexible model of the drift calculated using low power polynomials in the filtered data.

- A model for the estimation and/or elimination of the effect of perturbing signals such as the air pressure effect, through the own filtering process.

- Processing of data with arbitrary time step, and also with gaps without the need of interpolation.

As it is explained in Venedikov et al. (2001), the fundamental idea of the program consists in 2 steps:

1. Filtering of the original data on independent (without overlapping) intervals to eliminate the drift and to transform the data in separate pairs of series, each pair corresponding to one of the tides the user is interested in (a wide spectrum of frequencies can be chosen by the user).

2. Processing of the filtered numbers by the method of the Least Squares applied in the time/frequency domain. The series are processed independently, and the parameters for each tidal species are determined individually, although simultaneously (using all the separated tidal species in a single least squares adjustment).

The original data set Y is divided into N intervals $I(T)$ of central epochs $T = T_1, T_2 \ldots T_N$

Each interval contains n data points($n \cdot N = M$ = total number of data points), n differs between the intervals if the data are unequally spaced.

In a first stage of VAV, the hourly data $y(t)$ in every $I(T)$ are transformed by filtering into even and odd filtered numbers(u, v), as shown by (2.33):

$$(u_f(T), v_f(T)) = \sum_{\tau=-\theta}^{\theta} F_f(\tau)y(T + \tau)$$

(2.35)

For hourly data we can define 12 frequency bands $0 \leq f \leq 11 \ cpd$

Due to the use of a time window ΔT we can relate the processing in an initial stage to a limited number of basic frequencies that we denote as $\Omega = \Omega_1, \ldots \Omega_\mu$.

For evenly spaced data, VAV uses the same filters for all $I(T)$ while for unevenly spaced data, the filters are built up separately for every $I(T)$:

The transformation in the time/frequency domain of the tidal data is a classical idea which was already used by Doodson (1928) and Lecolazet (1958a). These methods applied narrow band-pass filters, aimed to separate perfectly the main tidal species, concentrated at the first frequencies. The VAV program applies more simple filters that used in MV66 and NSS, closer to cosine/sine Fourier filters, which do not attempt to get a complete separation of the main tidal species.

VAV constructs the filters as follows; first stage consists in the creation of the cosine/sine complex vectors, for a given $I(T)$ and all frequencies Ω

$$c(T,\Omega) = (Exp(i\Omega t_1) \ldots Exp(i\Omega t_n))^T, \qquad \Omega = \Omega_1, \ldots, \Omega_\mu$$

(2.36)

Later, VAV transforms the $c(T,\Omega)$ into the filters $f(T,\Omega)$; which are vectors with the same structure as $c(T,\Omega)$: The transformation is made as follows:

(i) $f(T,\Omega)$ is a linear combination of $p(T), c(T,\Omega_1), \ldots, c(T,\Omega_\mu)$,

(ii) $f(T,\Omega_1), \ldots, f(T,\Omega_\mu)$ are orthonormal, so that;

$$Ref(T,\Omega_i)^T \, Ref\,(T,\Omega_j) = Imf(T,\Omega_i)^T Im(T,\Omega_j) = \begin{cases} 0 \; for \; i \neq j \\ 1 \; for \; i = j \end{cases}$$

(iii)   with respect to the matrix of drift coefficients $p(T)$, $f(T,\Omega)^T p(t) = 0$

when $\Delta T = 24 \, h; \; \Omega = 15, 30, 45, 60, 75, 90 \; deg/h$, for evenly hourly data we have the trivial transformation:

$$f(T,\Omega) = c(T,\Omega)\sqrt{2/\Delta T}$$

These are pure cosine/sine filters, having also the property.

$$f(T,\Omega_i)^* c(T,\Omega_j) = \begin{cases} 0 \; for \; i \neq j \\ \sqrt{\Delta T/2} \; for \; i = j \end{cases}$$

Which implies that the filter $f(T,\Omega_i)$ amplifies its corresponding frequency $\Omega = \Omega_i$ and eliminates all other main frequencies.

For other situations, we have some deviations from this last equation.

The application of the filters $f(T,\Omega)$ on the $I(T)$ consists in the computation of the complex filtered numbers

$$u(T,\Omega) = f(T,\Omega)^T y(T)$$

(2.37)

Once that filters have been applied, VAV implements the least squares on (u,v) as if (u,v) are the observations. As a result, it provides the estimates of the unknowns, in which we are interested, the adjusted $(\hat{u},\hat{v})$ of the observed (u,v) and the residuals

$$\Delta u_f(T) = u_f(T) - \hat{u}_f(T)$$

$$\Delta v_f(T) = v_f(T) - v_f(T)$$

for all the values of T and f.

<u>BAYTAP-G.</u> This method was developed by Tamura et al., (1991) during the 1980s. It is based on a method called Bayesian prediction from Harrison and Stevens (1976) adapted to the use of Earth tide data. The user can choose between the tidal potential catalogues of Tamura (Tamura 1987) or Cartwright-Taylor-Edden (1973).

It is a hybrid method using a combination of harmonic series and the response method (Lambert 1974) to estimate the various components of a gravity record. These components (tidal parameters, drift and meteorological parameters) are estimated through an iterative method similar to least squares adjustment, by minimizing the term (Tamura 1990) using Akaike's Bayesian Information Criterion (Akaike, 1979, Tamura et al. 1991):

$$\sum_{i=1}^{n} [y_i - \sum_{m=1}^{M} (A_m \cdot C_{mj} + B_m \cdot S_{mj}) - d_i - \sum_{k=0}^{k=m} b_k \cdot x_{i-k}]^2$$

$$+ D^2 \sum_{i=1}^{n} [d_i - 2d_{i-1} + d_{i-2}]^2$$

$$+ WEIGHT^2 \sum_{m=2}^{M} ((A_m - A_{m-1})^2 + (B_m - B_{m-1})^2)$$

(2.38)

where:

A_m and B_m are the linear expressions of the unknowns amplitude factor and phase lead for each m of the M groups at all.

C_{mj} and S_{mj} are computed from the tidal potential catalogue using all j waves contained in the mth wave group.

The tidal part is subtracted from each observation y_i (n datapoints in total) together with the drift-value d_i and the term describing the influence of additional channels $x(t)$ onto the measurement. D and WEIGHT are called hyperparameters and can be defined in the parameters file.

2.3.4 Comparative analysis ETERNA 3.4/VAV

Dierks and Neumeyer (2002) compared all three programs using both synthetic data and a 1-year observed SG data set from station Sutherland (SU). They found the performance of the three programs to be similar, but with different treatments of the statistics between signals (tides, air pressure, and drift) and residual gravity. Also, several comparisons exist between ETERNA and VAV programs (Ducarme et al. 2006b). Ducarme pointed out that the computation of the root mean square errors (RMS) carried out by ETERNA was not done in the most appropriate way in the least square method. Wenzel improved the program, and here we used the latest version, ETERNA 3.4, which was corrected for the error in the SNR computation.

In our case, we have realized several comparisons between ETERNA 3.4 and VAV 06 software to compare their results in terms of delta amplitudes and phase differences. We don't take into account the differences obtained in term of error evaluations, because both programs estimated them in a different way; VAV evaluate it through the RMS error on the unit weight S_0, while least square solutions generally underestimate the errors as they suppose a white noise structure and uncorrelated observations i.e. a unit variance-covariance matrix (Ducarme e al. 2006b).

Program BAYTAP-G was discarded because it is not able to use more than 31 wave groups, and in the next sections we will be interested in analyzing as many waves as possible using very long records.

Synthetic data; first, we have generated synthetic series for J9 station using an elastic DDW99 non hydrostatic Earth's model (Dehant et al., 1999) and the tidal potential catalogue from Hartmann and Wenzel (1995):

- ✓ A short series of 1 month data
- ✓ A medium series of 1 year data
- ✓ A long series of 10 years data

Observed data; we have selected data intervals from the total record in J9 Observatory, with the same length as the theoretical records:

- ✓ A short series of 1 month data   (2001/01/01 – 2001/01/31)
- ✓ A medium series of 1 year data   (2000/01/01 – 2000/12/31)
- ✓ A long series of 10 years data   (1997/01/01/ - 2006/12/31)

All these series have been analyzed using ETERNA 3.4 and VAV 06 software. The wave grouping used was the same in both cases.

- In a first step, all analyses have been carried out using Tamura's catalogue in both software.

- In a second step, new ETERNA analyses have been carried out with Hartmann and Wenzel's (HW) catalogue.

The obtained results for 1 month data are compared in Table 2.3.1 for the synthetic data and in Table 2.3.2 for the observed data. The results for the more detailed analysis of 1 year and 10 year data are shown in **Annex B**.

* 1 month data

Table 2.3.1: Comparison of the results (amplitude factor, phase differences and standard deviations) obtained in the diurnal band (up) semi-diurnal band (middle) and ter-diurnal band (down) for the same synthetic data series (1 month data) using VAV 06 (left columns), ETERNA 3.4 with TAMURA catalogue (middle columns) and ETERNA 3.4 with HW catalogue (right columns).

Diurnal	VAV 06				ETERNA (TAMURA)				ETERNA (HW)			
	δ	MSD	κ	MSD	δ	stdv	κ	stdv	δ	stdv	κ	stdv
Q1	1.1510	0.0008	0.0220	0.0370	1.1533	0.0001	-0.0068	0.0064	1.1534	0.000001	0.0001	0.0001
O1	1.1523	0.0002	0.0070	0.0090	1.1532	0.0000	-0.0074	0.0016	1.1532	0.000000	0.0002	0.0000
K1	1.1363	0.0001	-0.0970	0.0110	1.1322	0.0001	-0.0162	0.0061	1.1322	0.000001	0.0002	0.0001
J1	1.1579	0.0016	0.2870	0.0810	1.1558	0.0004	-0.0152	0.0180	1.1552	0.000004	0.0001	0.0002
OO1	1.1753	0.0064	-0.5920	0.3100	1.1542	0.0012	0.2339	0.0616	1.1545	0.000013	0.0008	0.0006

Semi diurnal	VAV 06				ETERNA (TAMURA)				ETERNA (HW)			
	δ	MSD	κ	MSD	δ	stdv	κ	stdv	δ	stdv	κ	stdv
2N2	1.1570	0.0006	-0.0430	0.0320	1.1569	0.0003	-0.0230	0.0137	1.1575	0.000001	0.0004	0.0001
N2	1.1573	0.0002	0.0130	0.0090	1.1575	0.0001	-0.0168	0.0036	1.1575	0.000000	0.0004	0.0000
M2	1.1571	0.0000	0.0050	0.0020	1.1574	0.0000	-0.0066	0.0009	1.1575	0.000000	0.0004	0.0000
L2	1.1543	0.0016	0.1720	0.0810	1.1583	0.0007	0.0500	0.0363	1.1575	0.000003	0.0003	0.0002
S2	1.1575	0.0001	0.0260	0.0110	1.1574	0.0001	-0.0118	0.0069	1.1575	0.000001	0.0004	0.0000

Ter diurnal	VAV 06				ETERNA (TAMURA)				ETERNA (HW)			
	δ	MSD	κ	MSD	δ	stdv	κ	stdv	δ	stdv	κ	stdv
M3	1.0697	0.0015	0.2890	0.0790	1.0695	0.0003	-0.0529	0.0172	1.0694	0.00001	0.0005	0.0003

* 1 month data

Table 2.3.2: Comparison of the results (amplitude factor, phase differences and standard deviations) obtained in the diurnal band (up) semi diurnal band (middlel) and ter diurnal band (down) for the same observed data series recorded at J9 (1 month data, 2001/01/01–2001/01/31) using VAV 06 (left columns), ETERNA 3.4 with TAMURA catalogue (middle columns) and ETERNA 3.4 with HW catalogue (right columns).

Diurnal	VAV 06				ETERNA (TAMURA)				ETERNA (HW)			
	δ	MSD	κ	MSD	δ	stdv	κ	stdv	δ	stdv	κ	stdv
Q1	1.1476	0.0019	-0.2520	0.0930	1.1495	0.0006	-0.3116	0.0287	1.1496	0.0005	-0.3048	0.0271
O1	1.1495	0.0005	0.0770	0.0230	1.1503	0.0001	0.0629	0.0070	1.1503	0.0001	0.0704	0.0066
K1	1.1422	0.0002	0.1920	0.0290	1.1383	0.0005	0.2763	0.0272	1.1383	0.0005	0.2927	0.0257
J1	1.1667	0.0041	0.3470	0.2040	1.1631	0.0017	0.1266	0.0803	1.1625	0.0016	0.1417	0.0757
OO1	1.1793	0.0161	-0.4320	0.7770	1.1611	0.0056	0.4141	0.2742	1.1613	0.0052	0.1801	0.2584

Semi diurnal	VAV 06				ETERNA (TAMURA)				ETERNA (HW)			
	δ	MSD	κ	MSD	δ	stdv	κ	stdv	δ	stdv	κ	stdv
2N2	1.1529	0.0016	2.6560	0.0810	1.1544	0.0011	2.6306	0.0545	1.1549	0.0012	2.6538	0.0600
N2	1.1733	0.0005	2.6330	0.0220	1.1730	0.0003	2.6043	0.0140	1.1730	0.0003	2.6214	0.0154
M2	1.1880	0.0001	2.1680	0.0050	1.1883	0.0001	2.1523	0.0034	1.1884	0.0001	2.1593	0.0037
L2	1.2079	0.0041	3.5600	0.1960	1.2076	0.0029	3.2865	0.1379	1.2068	0.0032	3.2380	0.1522
S2	1.1901	0.0003	0.6720	0.0280	1.1893	0.0006	0.6723	0.0268	1.1893	0.0006	0.6847	0.0296

Ter diurnal	VAV 06				ETERNA (TAMURA)				ETERNA (HW)			
	δ	MSD	κ	MSD	δ	stdv	κ	stdv	δ	stdv	κ	stdv
M3	1.0664	0.0033	0.9630	0.1690	1.0633	0.0063	0.4561	0.3411	1.0632	0.0062	0.5098	0.3351

In both cases, using theoretical or observed data, the numerical results for the amplitude ratio and phase difference obtained with VAV 06 do not significantly differ to those obtained with ETERNA 3.4. (<0.08% for O_1 and 0.02% for M_2 for theoretical data, and <0.07% for O_1 and 0.02% for M_2 for observed data) Also the results from ETERNA 3.4 using different tidal potential catalogues (TAMURA or Hartmann & Wenzel) are almost same, being the ones with HW potential the more accurate.

We can conclude that none of these softwares is clearly better than the other. Nevertheless, we have chosen to use ETERNA 3.4 all along this thesis instead of using VAV 06, mainly due to the fact that ETERNA 3.4 allows us to use the newest tidal potential catalogue from Hartmann and Wenzel (1995), which is not possible with VAV.

We have finished introducing the theory, the methods and the instruments. Before turning to the analyses of real data and to the results we have obtained during this thesis, we will present the gravimetric observatory in Strasbourg which has been our reference site for various studies.

Chapter 3

Gravimetric Observation in Strasbourg (1954-2014)

Throughout this thesis we analyze data recorded by different types of gravimeters installed in several gravimetric stations located in Europe. The gravity records at the station in Strasbourg will be studied more in detail and we will use this station as comparison site to study the differences and improvements between data sets obtained from different kinds of gravimeters. Therefore in this section we will deal with some historical aspects and will show some major results obtained at the two Gravimetric observatories, belonging to the EOST (Ecole et Observatoire des Sciences de la Terre), located in Strasbourg along the last six decades.

There is a traditional gravity recording of Earth tides at Strasbourg which was initiated by Pr. Robert Lecolazet (1910 – 1990) in the 50s. Since 1937 he was working at the 'Institut de Physique du Globe de Strasbourg (IPGS)'. After 1948 he focused his work in the gravity field, especially devoted to the study of Earth tides.

Hence since the 1950s, the surface time gravity changes have been measured locally using different kinds of gravimeters (spring, absolute and superconducting types) at two different stations (figure 3.0); first in the Seismological Observatory of Strasbourg for almost 20 years and later on in the 70s at the J9 Observatory, 10 km far away from Strasbourg city. Over these years many kinds of improvements have been observed in terms of instrumentation, of tidal potential developments and more specifically in terms of data analysis techniques, which have allowed obtaining some fundamental results as we will see later.
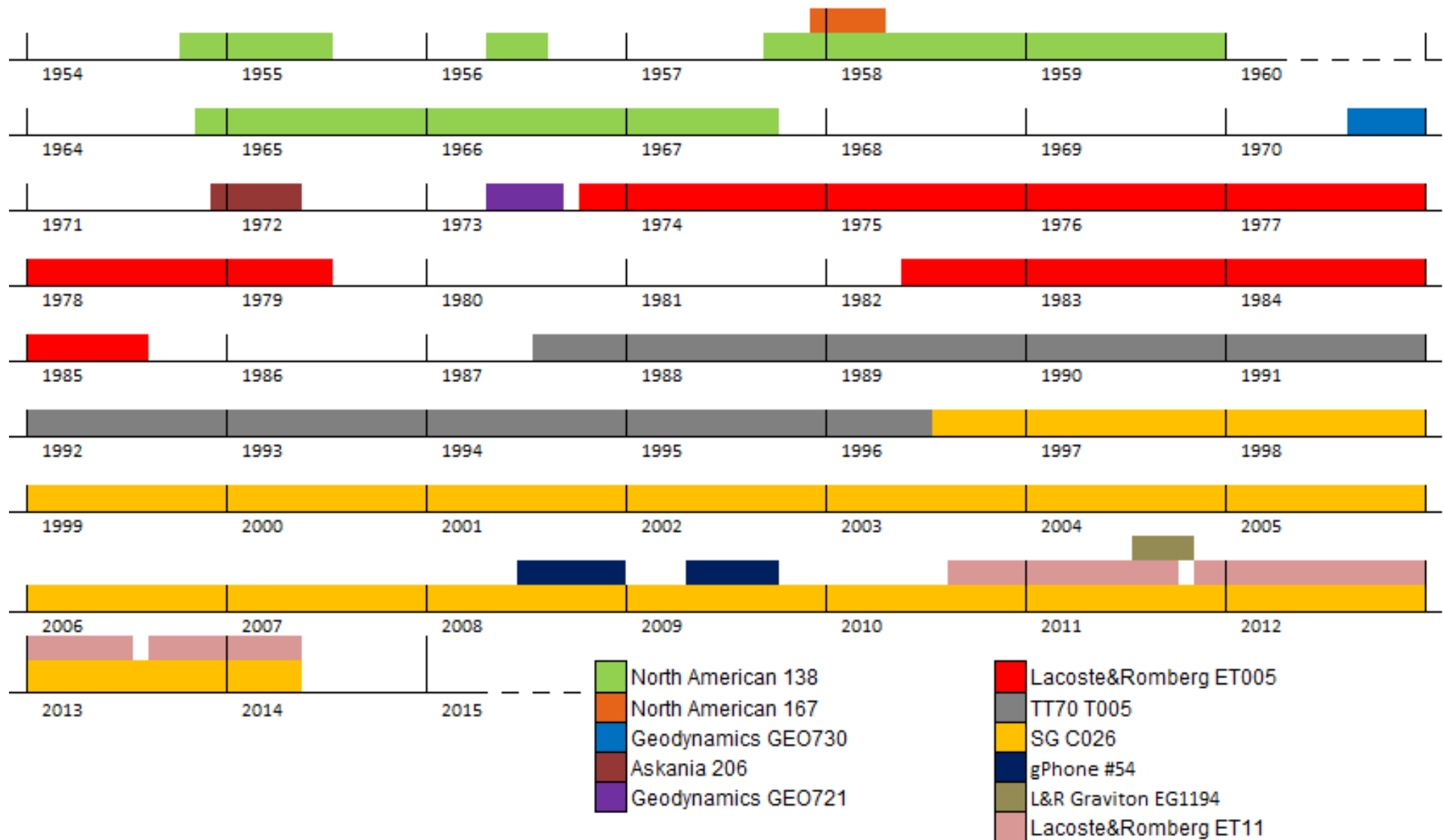
Fig. 3.0: Summary of the time periods when various gravimeters have been recording at the Seismological Observatory of Strasbourg (1954-1967), and later at J9 Observatory (1970-today).

3.0 Gravimetric tides before 1954

ʹLe Bureau des Recherches Géologiques et Géophysiques a fait procéder durant quatre jours, du 5 au 9 juillet 1948, à une longue série de mesures de la gravité en un même point. Les déterminations, effectuées d'heure en heure, avaient un double objet : d'une part, examiner le comportement du gravimètre 'North-American' au point de vue de la stabilité et de la sensibilité ; d'autre part, étudier l'influence de l'action luni-solaire sur les mesures gravimétriques de précision. Le Service Hydrographique de la Marine, en se chargeant du dépouillement des résultats, a permis de donner à cette expérience une portée plus générale.ʹ

We transcribed in this epigraph the beginning of the text from Bollo and Gougenheim (1949). This text, which is one of the first texts published in Europe, describes the state of the study of tidal gravity at that date. It even reproduces the same title as an article of Truman (1939) published in the United States, which somehow marked the renewal of the instrumentation developed since the design of the zero-length spring gravimeter, invented by Lucien Lacoste in 1934.

The data shown by Bollo and Gougenheim were not, of course, the first measurements of the Earth's tides. It is easy to scan the previous results, through the reports on the tides of the Earth's crust presented by W. D. Lambert, in the reports of the International Union of Geodesy and Geophysics (IUGG).

Rebeur (1882) estimated a γ factor using a pendulum measurement, registered at Strasbourg. But the first measurement using data recorded by gravimeters was made in 1913 by Schweydar with a bifilar gravimeter in Potsdam. He found a value of $\delta=1.20$ for the gravimetric factor (Schweydar, 1914a).

Almost 20 years later, there were new observations by Tomaschek and Schaffermigh at Marburg, using also a bifilar gravimeter. Unfortunately their results were not good and they found $\delta < 1$ (Lambert, 1936).

These early works seem to have been intended for research on the Earth's elasticity and especially to improve the knowledge of Love numbers insofar as the combination $(1 + k \cdot h)$, which were already known from the observation of the deflection of the vertical.

From the 1935s began a study of gravity anomalies to better constrain geophysical exploration using more accurate and portable instruments. However, to achieve greater precision it was also necessary to correct the measurements of tidal effects. This was a major cause to boost interest in the study of Earth's tides.

There were many trials, but the most significant results were those of Truman between 1936 and 1937 (Lambert 1939), where he found an average δ=1.13. And also the works performed in USA by the 'Gulf Research and Development Corporations' in 1939, described by Eckhardt (Lambert 1939) where using 11 gravity records, they found an average δ=1.57, ranging from 1.36 to 2.25.

In France, the first campaigns to obtain a map of gravity anomalies began in 1940 and persisted after the 2nd World War. This led to the paper cited above (Bollo and Gougenheim, 1949) where they presented a four day series registered at Chambon la Forêt, 100 km south of Paris, using a North American gravimeter. These results were indicative of the state of the art (figure 3.1)
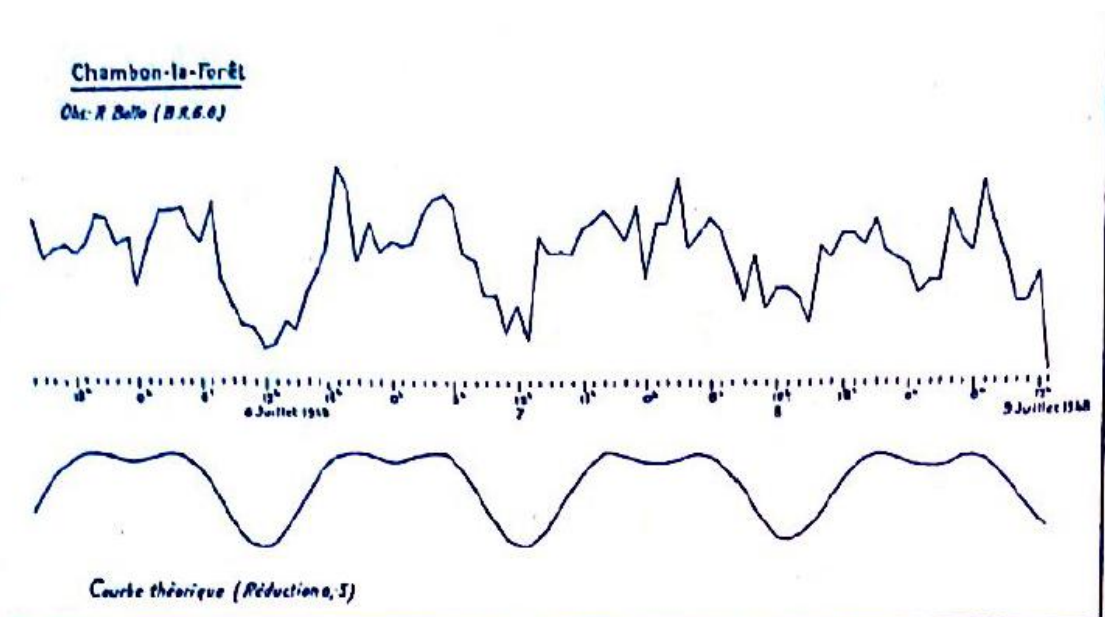
Fig. 3. 1: Theoretical (lower plot) and observed (upper plot) gravity variations from 5/07/1948 to 9/07/1948 at Chambon la Forêt Observatory.

Few years later, in 1953 Prof. R. Lecolazet from IPGS acquired a North American gravimeter to be used for teaching geophysics, but also for the study of tidal gravity. Thereby, the studies of Earth's tides begun in Strasbourg.

3.1. Seismological Observatory of Strasbourg (1950-1970)

The first location where Pr. R. Lecolazet chose to install permanent gravimeters to record Earth tides was inside the Seismological Observatory of Strasbourg (figure 3.2), a building belonging to the University of Strasbourg in the city center (48.583 N, 7.767 E, 138 m). The first observations were carried out in 1954 using a spring gravimeter, the North American 138, which was equipped with a photographic recording device (figure 3.3).

Fig. 3.2: Building of the Seismological Observatory of Strasbourg, where was installed the first spring gravimeter devoted to record gravity Earth tides.

Fig. 3.3: North American 138 which was installed at the Seismological Observatory of Strasbourg in consecutive periods from 1955 until 1967.

Pr. Lecolazet and co-workers obtained more than 5 months of consecutive record, precisely 163 days from October 1954 to March 1955. This series was published as the longest series recorded at that time (Lecolazet, 1956a, Melchior 1957). Since then, they continued to gradually improve their equipment obtaining longer and better data series. In November 1964 they installed the sensor in an isolated box thermostatically controlled. The gravimeter was equipped, among other improvements, with a permanent electrostatic calibration device. Moreover the photographic recording system was highly improved. As expected, the instrumental drift became much more regular and decreased, making it possible to study long-period waves.

3.1.1. Observation of Long Period tidal waves

Since November 1964 this gravimeter was continuously recording for almost 3 years. Using the first 13 months of this series, they were able to observe for the first time the monthly, fortnightly and ter-monthly tidal waves Mm, Mf and Mtm (figure 3.4 - Lecolazet and Steinmetz, 1966). These first results were still not precise enough but were very encouraging. Such observations were possible not only because of the data quality, but also because of the use of new techniques of signal processing.
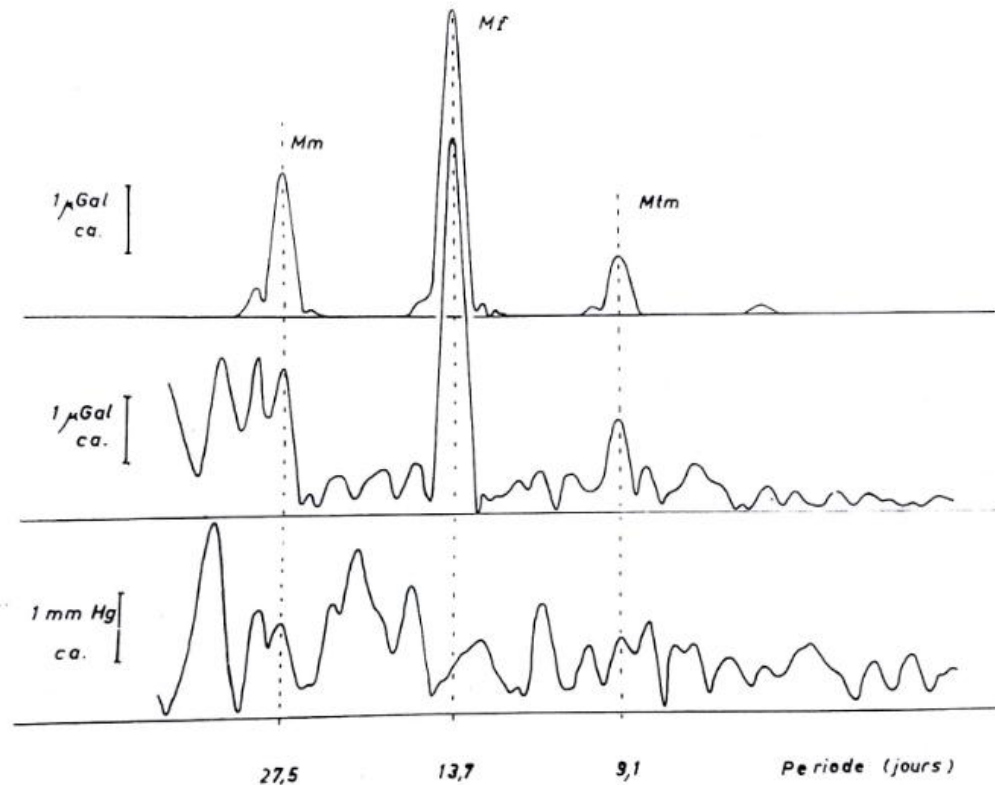
Fig 3.4: First observation of the monthly, fortnightly and ter-monthly waves Mm, Mf and Mtm, using the 3 year series recorded by the North American 138 gravimeter installed in Strasbourg from 1964 until 1967 (extracted from Lecolazet and Steinmetz, 1966). Upper plot: theoretical waves. Medium plot: observed waves. Lower plot: observed air pressure variation.

The North American 138 continued recording at the same site until 1967. Another North American gravimeter (NA 167) was recording in parallel during 82 days at the end of 1957 and beginning of 1958. The aim was to study and compare the sensitivity and accuracy of both instruments (Lecolazet 1958b). Using the last period of data recorded by the North American 138 (1012 days between November 1964 and August 1967) they were able to observe the Free Core Nutation resonance (section 3.1.2).

Finally, we have to mention that a Geodynamics model, the GEO730 owned by J.T. Kuo, recorded during 79 days between September and December 1970. Within the international context of the station, these data were included in different international tidal gravimetry profiles and networks (Melchior et al., 1976, Melchior et al., 1981).

3.1.2. First observation of Free Core Nutation resonance with gravimetric data

As previously described in section 2.1.9, the fluid core resonance phenomenon affects the amplitude of the tidal waves close to the Free Core Nutation (FCN) period in the diurnal frequency band. As the rest of the gravity community, Lecolazet became interested in searching evidence for the FCN in gravity records after the theoretical works of Jeffreys, Vicente and Molodensky in the middle of last century, concentrating much effort to try to detect it in the data series recorded at Strasbourg station.

In a first step, the study of the existence of the Earth's FCN focused on the relative values of the gravimetric delta factors δ of the main diurnal tides (O_1 and K_1). Lecolazet initiated the search for a clear evidence of the FCN by its associated resonance effects on the diurnal tides using the 5-month data recorded with the North American AG 138 from October 1954 until March 1955. Unfortunately, the first results he published were in disagreement with the theoretical models (Lecolazet 1957, Melchior 1957). Two years later, using the series from 1957 to 1958, he published the first clear observation of $\delta(O_1) > \delta(K_1)$ in agreement with Jeffreys' theory (Lecolazet, 1959). Then Lecolazet (1960) obtained even better results using the complete series of 860 days of the NA 138 registered between August 1957 and December 1960.

In a second step, once the existence of this resonance was confirmed, efforts were focused on the search for its frequency. After some failed attempts (Lecolazet and Steinmetz, 1973) where they were not able to locate correctly the frequency, Lecolazet and Steinmetz published in 1974 the first results of the discovery of the resonance of the core (Lecolazet and Steinmetz, 1974) determining that it would be either between K_1 and PSI_1, or between K_1 and PHI_1. In both publications they used the same dataset, i.e. almost 3 continuous years between 1964 and 1967 obtained with the North-American AG 138 installed at the Seismological Observatory in Strasbourg. The major difference in the results was then due to the different methodology used in the data analysis; in 1974 they performed a tidal analysis using an improved least-squares method proposed by T. Chojnicki (Chojnicki, 1972), which is based on Venedikov's method of tidal analysis (Venedikov 1961, 1966b).

These results were then much improved by using a longer series recorded between 1973 and 1975 with a LaCoste-Romberg Earth-Tide gravimeter (LR-ET005), equipped with a feedback system installed at the J9 Gravimetric Observatory of

Strasbourg, definitively confirming that the FCN frequency lies between K_1 and PSI_1 frequencies (Abours and Lecolazet, 1978, Lecolazet and Melchior, 1977).

The instrumental precision of the LR-ET005 was not only better than that of the North American, but also the tidal analysis technique was improved with the help of computer processing conducted at the International Center for Earth Tides, where the Chojnicki's least-squares procedure was applied and complemented with a spectral analysis of the residuals.

Since then, developments in both theory and observations have allowed substantial improvements in the estimation of the FCN resonance parameters, especially with the development of the superconducting gravimeters (SGs) in the 80s.

3.2. Gravimetric Observatory of Strasbourg J9 (1970s - today)

At the beginning of the 70s, R. Lecolazet and co-workers decided to move the gravimetric observatory to a quietest place situated outside the city. The chosen place is located about 10 km from Strasbourg in a bunker named J9 (figure 3.5) built by the Germans after the 1870 war on the top of a sedimentary hill (48.622 N, 7.684 E, 180 m).

Fig. 3.5: Pictures of the outside and the inside corridor of the bunker J9, where the gravimetric observatory is located.

The new gravimetric observatory is settled at J9 since 1970. Thereafter, time-variable gravity variations have been observed and recorded at J9 with various spring and superconducting gravimeters (figure 3.6). Besides, since 1997, absolute gravity measurements are also performed regularly. During this long period, the relative gravimeters (sensors and electronics) and the acquisition systems were drastically improved. These improvements allowed increasing the measurement accuracy by more than 10 times (Calvo et al. 2014b).
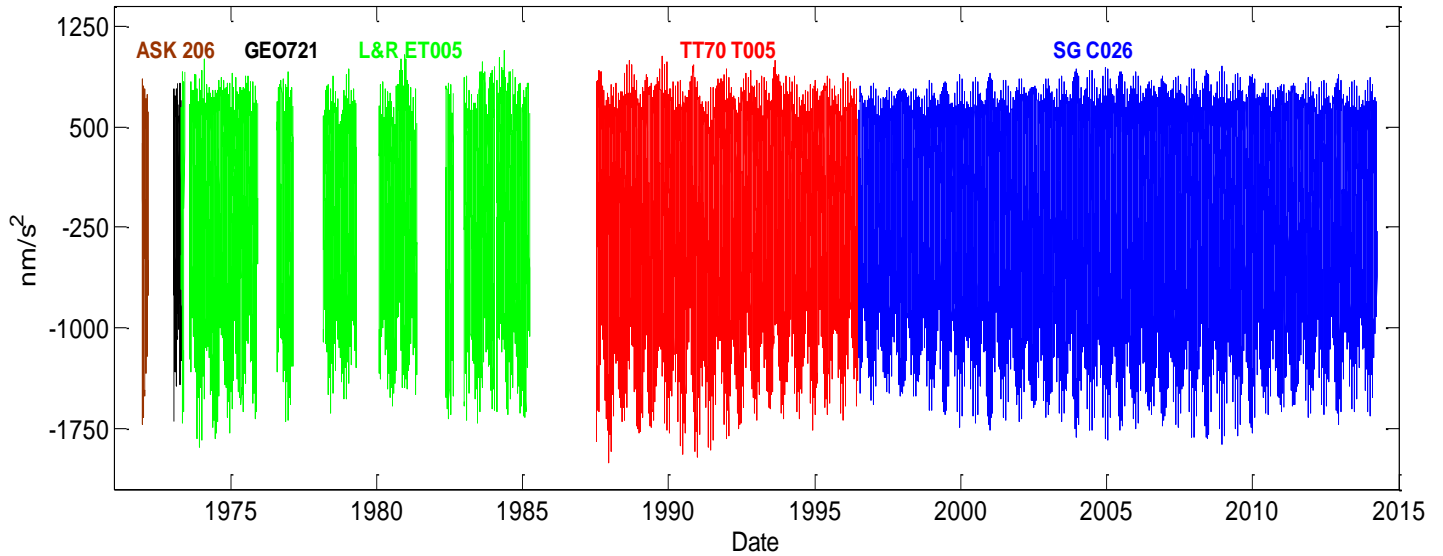
Fig. 3.6: Time-varying gravity measured at the Gravimetric Observatory J9, located near Strasbourg, from 1970 to 2013. The first 3 series were recorded by spring gravimeters: Askania model in brown, Geodynamics model in black and Lacoste and Romberg model in green. The last 2 series were obtained by superconducting gravimeters: TT70 model in red and C026 model in blue.

3.2.1. Spring gravimeters

The first 10 years of observations were carried out by different models of spring meters: the first one was an Askania gravimeter belonging to M. Bonatz, ASK206, which was recording for 77 days at the end of 1971 and beginning of 1972. After that, a Geodynamics gravimeter GEO721, was installed by P. Melchior and J.T. Kuo during 82 days in 1973. Later a Lacoste&Romberg ET005 (figure 3.7) modified in order to record Earth tides by R. Lecolazet and J. Gostoli in 1970 with an electrostatic feedback system and a digital recording, was recording with a sampling rate of 1 hour (J. Gostoli, 1970). This later gravimeter was operational during two periods of 2100 and 1120 days respectively from October 1973 until middle 1985. This series was used in several studies, including the observation of the FCN resonance as seen in section 6.3.

As we have already explained in section 2.2.2, the spring meters are too sensitive to the changes of temperature, so to avoid such perturbations the L&R ET005 was installed in an isolated box thermostatically controlled. The box was located in a room itself thermally stable of the underground fort; the sealed box protected also the sensor against the direct influence of barometric pressure variations. This gravimeter was calibrated by a direct comparison with an Askania gravimeter GS15 in 1972 (Abours, 1977).

Fig 3.7: Pictures of the isolated boxes where the spring gravimeters L&R ET005 (left picture) and the L&R ET11 (right picture) were installed at J9 Observatory.

More recently, there have been also different spring gravimeters temporarily installed in J9, such as the Microg-LaCoste gPhone 054 owned by IGN-Spain (figure 3.8) and which was recording for almost 1 year between 2008 and 2009 (Riccardi et al., 2011). A LaCoste & Romberg Graviton-EG1194 from Instituto de Geociencias (CSIC, UCM) of Spain was operating there for 3 months during 2011, aiming to check its instrumental response, both in amplitude and phase as well as its time stability (Arnoso et al., 2014). Currently a Lacoste-Romberg ET11, belonging to BFO was installed by W. Zürn and is recording since 2012 (figure 3.7- right).

Fig 3.8: Spring gravimeter Microg-LaCoste gPhone 054 owned by IGN-Spain, installed at J9 Observatory between 2008 and 2009.

3.2.2. Superconducting gravimeters

Since 1987 two different superconducting gravimeters have been recording in two consecutive periods at J9. The first superconducting gravimeter was a TT70 model from GWR Instruments installed in 1987. This meter was recording for almost 10 years. Using the first 8 years of this series, Florsch et al. (1995) were able to observe for the first time 3 of the quart-diurnal tidal waves M_4, N_4, K_4 (degree 4 and order 4) with extremely small amplitude. Later on, Boy et al. (2004) definitively confirmed these observations by comparing observed gravity changes with loading estimates using different models of non-linear tides over the North-Western European shelf. The loading contribution of non-linear oceanic tides has already been clearly observed using measurements from spring gravimeter (Baker, 1980). In 1990, Wenzel and Zürn identified tidal terms of 4th order in the 1 to 3 cycle/day frequency bands using the data from the Lacoste-Romberg ET19 installed in the Black Forest Observatory (Wenzel and Zürn, 1990) but thanks to the high precision of SG data, Florsch et al. (1995) could also identified quarter-diurnal tidal waves (degree and order 4) of lunisolar origin (figure. 3.9).
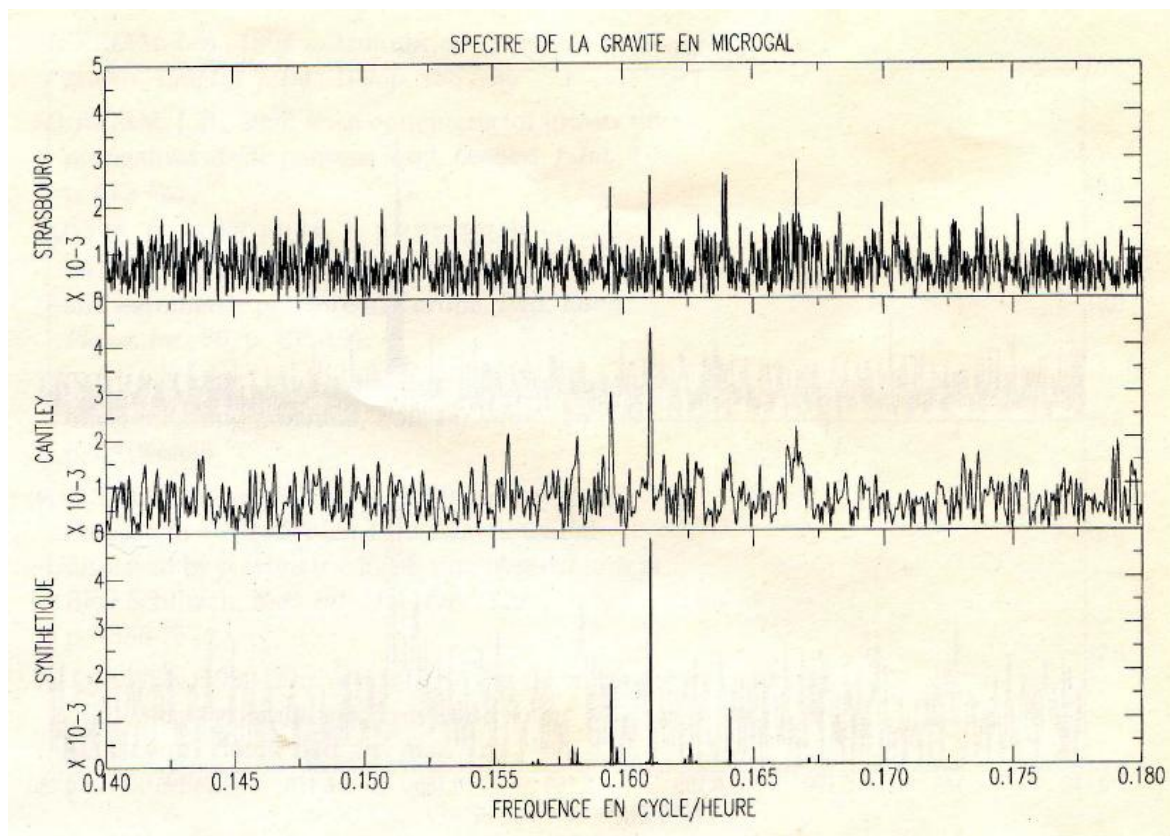
Fig. 3.9: Gravity spectra recorded by the T005 SG at Strasbourg (France) and Cantley (Quebec) and comparison with that of the theoretically predicted tide calculated at Strasbourg, highlighting 3 of the quart-diurnal tides waves M_4, N_4, K_4. Extracted from Florsch et al. 1995.

In 1996 this SG was replaced by a more compact model, the C026, which is still recording. These data are continuously collected within the global GGP (Global Geodynamics Project) network (Crossley et al., 1999). As explained in section 2.2.2, SGs are using magnetic levitation against gravity on the contrary to the mechanical meters which use a spring. The SG long term stability is hence much better than in the case of spring meters mainly because of the unavoidable creep of the spring whatever its constitutive material (Torge 1989). The high sensitivity of the SGs is achieved by an efficient adjustment of the vertical magnetic gradient, so compared to the spring instruments, the superconducting gravimeters are characterized both by a higher accuracy and a significantly lower instrumental drift.

Fig. 3.10: Superconducting gravimeters installed at the J9 Observatory. Left one: TT70 model (T005). Right one: compact SG model (C026).

As we will see later on in section 4.3, the model C026 was also improved with respect to the previous T005 version in terms of noise levels (Rosat et al., 2002) and drift rates (Amalvict et al., 2001) both because of the instrument itself and also the data acquisition system upgrade. The high quality of this gravimeter records has allowed to carry out extensive researches on different topics in global geodynamics such as the study of global Earth deformation (tides, loading, etc.), non-linear ocean tides (Boy et al. 2004), hydrology (Longuevergne et al., 2009, Rosat et al., 2009a) and metrological aspects such as calibration (Amalvict et al., 2002), long-term drift determination (Amalvict et al., 2001; Boy et al., 2000), noise level estimates (Rosat et al., 2004; Rosat and Hinderer, 2011) and comparisons with other temporarily

instrumentation like the gPhone previously mentioned (Riccardi et al. 2011) and the L&R Graviton-EG (Arnoso et al., 2014; Rosat et al., 2014).

Considering only the J9 Observatory, we have almost 40 years of time-varying gravity record, more than 26 years of which have been registered with superconducting gravimeters, leading to the longest series ever recorded by SGs.
Later on, in chapter 5 (Contribution of long series to tides studies) we will show the importance of long records.

3.2.3. Absolute gravimeters

Since 1997, there is also a portable absolute gravimeter FG5 # 206 manufactured by Micro-g Solutions which is regularly measuring at the J9 Observatory in parallel with the SG, but also at different sites in France and abroad. The main purposes of these AG measurements performed at J9 are the drift control and the calibration of the superconducting gravimeter (C026).

To determinate the instrumental drift of SGs, the long-term behavior is constrained by regular absolute gravity measurements, which are performed in parallel. For the T005, the absolute measurements were carried out by J. Mäkinen with the absolute gravimeter JILAg-5 belonging to FGI (Finnish Geodetic Institute). We only dispose of 6 measurements for all the T005 period. For the C026, there have been numerous absolute measurements since its installation with instruments of the new generation of ballistic gravimeters, mainly the FG5#206. There was also one measurement realized in parallel with both instruments (JILAg-5 and FG5#206) in 1996 for comparison.

Fig. 3.11: Picture of both absolute gravimeter models, JILAg-5 and FG5#206 during the co-located measurement made in 1996 at J9 Observatory.

The SG gravity residuals obtained after removing the local tides, polar motion and atmospheric pressure effects are plotted in figure 3.12 with the corresponding parallel absolute gravity measurements.
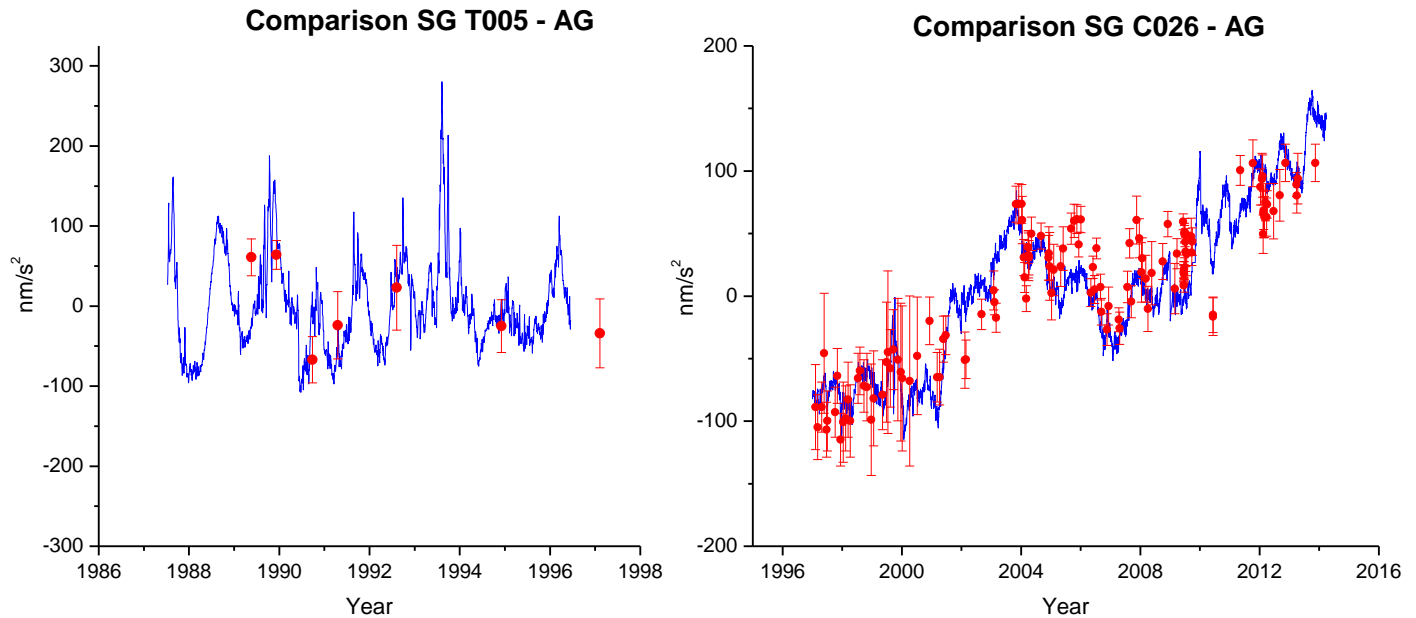
Fig. 3.12: Superposition of SG gravity residuals (continuous line) with AG measurements (dots with error bars) (left) between SG (T005) and AG (JILAg-5) for the period 1987–1996, (right) between SG (C026) and AG (FG5#206) data for the period 1996–2014. Please note that the instrumental drift was removed from these superpositions.

We have also used the AG measurements to determine the SG amplitude scale factor. Several scale factor experiments of different durations (from several hours to 9 days) were regularly performed since 1996. These results allow us to discuss the time stability of the calibration of the SG (Hinderer et al., 1991a; Amalvict et al., 1999, 2001, 2002; Calvo et al., 2014b). Due to the importance of the time stability of the scale factor of the SGs, a detailed study using these experiments is carried out in section 4.5.

Furthermore, these absolute measurements have been combined with GPS data or hydrological data in different studies to investigate the long term evolution of gravity that was observed at J9 (Amalvict et al., 2004; Rosat et al., 2009).

In addition to all the gravimetric instrumentation, there are other auxiliary instrumentation installed at the observatory, such as a weather station, GPS permanent antenna, and different hydrological sensors (piezometers, soil moisture sensors).

Chapter 4

Time stability of tidal parameters in Europe

4.1. Introduction

As we will see in section 5, long gravity records are of great interest when performing tidal analyses. Indeed, long series enable to separate contributions of near-frequency waves (the frequency resolution is the inverse of the data length) and also to detect low frequency signals (e.g. long period tides and polar motion) (the lowest detectable frequency is also the inverse of the data length). In addition to the length of the series, the quality of the data and the temporal stability of the noise are also very important.

In this section we use some of the longest gravity records available in Europe to study the time stability of the response (instrument + Earth) to tidal forcing. We expect this response to be solely dependent on the stability of the instrument and merely to geophysical phenomenon. The stability at each station is investigated using the temporal variations of the tidal parameters (amplitude factor and phase difference) for the main diurnal and semidiurnal tidal waves (O_1, P_1, K_1, M_2, S_2 and K_2) as well as for the M_2/O_1 delta factor ratio. This ratio, being independent of the instrumental calibration, is a very good indicator of the stability of the instrument. Once the time variability of these temporal series has been estimated, we have to consider the possible origins of time varying tidal parameters (instrumental noise, numerical effect, analysis effect, pre-processing effect, geophysical effects, etc...).

Most of the results described in this chapter have been published in Calvo et al. 2014a.

To carry out these studies, we used 3 data sets recorded with different models of spring gravimeters in Black Forest Observatory (Germany, 1980-2012), Walferdange (Luxemburg, 1980-1995) and Potsdam (Germany, 1974-1998) as well as several superconducting gravimeters (SGs) data sets, with at least 9 years of continuous records, at different European GGP (Global Geodynamics Project) sites (Bad Homburg, Brussels, Medicina, Membach, Moxa, Vienna, Wettzell and Strasbourg).

The long term stability of the tidal observations is also dependent on the stability of the scale factor of the relative gravimeters. Unluckily, we only have a long series of calibration experiments for the SG C026 installed at the J9 Gravimetric Observatory of Strasbourg. Therefore we have checked the time stability of the scale factor for the SG C026 using numerous calibration experiments carried out by co-located absolute gravimeter (AG) measurements during the last 15 years. The reproducibility of the scale factor and the achievable precision are investigated by comparing the results of all these calibration campaigns.

Temporal gravity variation measurements have been a long historical tradition in Europe with some sites recording for decades. Among the oldest gravity stations we can quote Walferdange (Luxembourg), the Black Forest Observatory (BFO, near Schiltach, Germany), Potsdam (in Germany) and J9 (10 km north of Strasbourg, France) where various kinds of gravimeters have been recording. Since the development of the Global Geodynamics Project in 1996 (Crossley et al. 1999), many Superconducting Gravimeter (SG) stations were installed in Europe. For the oldest ones, the gravity data sets have reached more than 9 years of continuous records for instance at Bad Homburg, Moxa and Wettzell in Germany, Brussels in Belgium, J9, Medicina in Italy, Membach in Belgium, and Vienna in Austria (Fig. 4.1). We have chosen all these stations to realize our stability study not only because of their length, but also because of their quality in terms of noise.

Fig. 4.1: Map of the location of the permanent gravity stations in Europe used in this study (blue, SG gravimeter stations, brown, spring gravimeter stations). BFO: Black Forest Observatory, BE: Brussels, MB: Membach, BH: Bad-Homburg, MC: Medicina, MO: Moxa, VI: Vienna and WE: Wettzell.

In view of the long duration of these continuous records, we can investigate the question of the stability in time of the instruments, particularly in terms of noise level and of response function (calibration factor).

<u>4.1.2. Time stability</u>

When dealing with long gravity records, time stability is very important because temporal changes of the instrumental sensitivity may introduce a related systematic error in tidal analysis. Therefore it is essential to ensure that the sensitivity of the instrument is as stable as possible to avoid possible errors arising from these temporal changes.

For each station the sensitivity of the instrument is investigated through the temporal variations of the tidal parameters (amplitude factor and phase difference) for the main tidal waves in the diurnal and semi-diurnal frequency bands (O_1, P_1, K_1, M_2, S_2 and K_2), as well as for the M_2/O_1 ratio of gravimetric factors. To evaluate these temporal variations we have performed for each data series a tidal analysis using ETERNA 3.4 software (Wenzel, 1996b), applied to segments of one year data, shifted month by month (there is hence an overlap of 11 months between two consecutive analyses). Here we have used the HW95 catalogue which predicts gravity tides with an error of 0.1 nGal ($\sim 10^{-12}g$) in frequency (Hartmann and Wenzel 1995). A barometric admittance is also retrieved using a least-square fit to barometric records available at the station. As we fit a tidal model to the observed gravity records, both the solid and the oceanic tides are adjusted together. We refer to section 2.3 for a description of ETERNA.

For all the tidal analyses presented in the next two sections, the ETERNA software is applied on 1 h data using 23 groups of waves between 0.000146 cpd and 4 cpd (cycle per day). These groups can be found in **Annex C.**

Using all these tidal analyses we can easily compare the different evolutions of the amplitude factors and phase delays of the major semi-diurnal and diurnal tides obtained for each type of gravimeters. However, before performing the tidal analysis in our series, they have to be pre-processed. In section 2.3, we have already explained the pre-processing steps that we have performed on all the observed data series to correct them from the different kinds of disturbances that could be contained in the signal. We refer the reader to the section 2.3.1, where a detailed description of the gravity data pre-processing is given. In particular, in Annex A, we recall the fact that the pre-processing does not affect the time-stability of the retrieved gravimetric factors.

To analyze the time stability of these series, we suppose that any time variability in the Earth's response to tides (gravimetric Love numbers) cannot be induced by internal process inside the Earth but could be due to some variability in the surface loading (oceanic load, atmospheric load). In fact, the tidal parameters being the transfer function of the Earth to tidal forces should be constant in time (at least on our investigated time-spans). We will try to find out if the tidal parameters from different waves vary in time in the same way and why.

4.2 Time variation of tidal parameters in spring gravimeter series

We first use the data series which have been recorded by different models of spring gravimeters (Fig. 4.2): 1.) The Askania GS15 222 gravimeter was installed during almost 24 consecutive years in the Gravimetric Observatory in Potsdam, obtaining what was at that time the longest gravimetric series in the world digitally recorded from a spring gravimeter. 2.) The LaCoste-Romberg Earth-Tide gravimeter ET-19 is installed since 1980 inside an abandoned mine that was transformed into a seismological observatory (Black Forest Observatory). 3.) The Askania GS15 233 gravimeter was installed during 16 years in an old gypsum mine, north of Luxemburg city, in the Walferdange Underground Laboratory for Geodynamics.
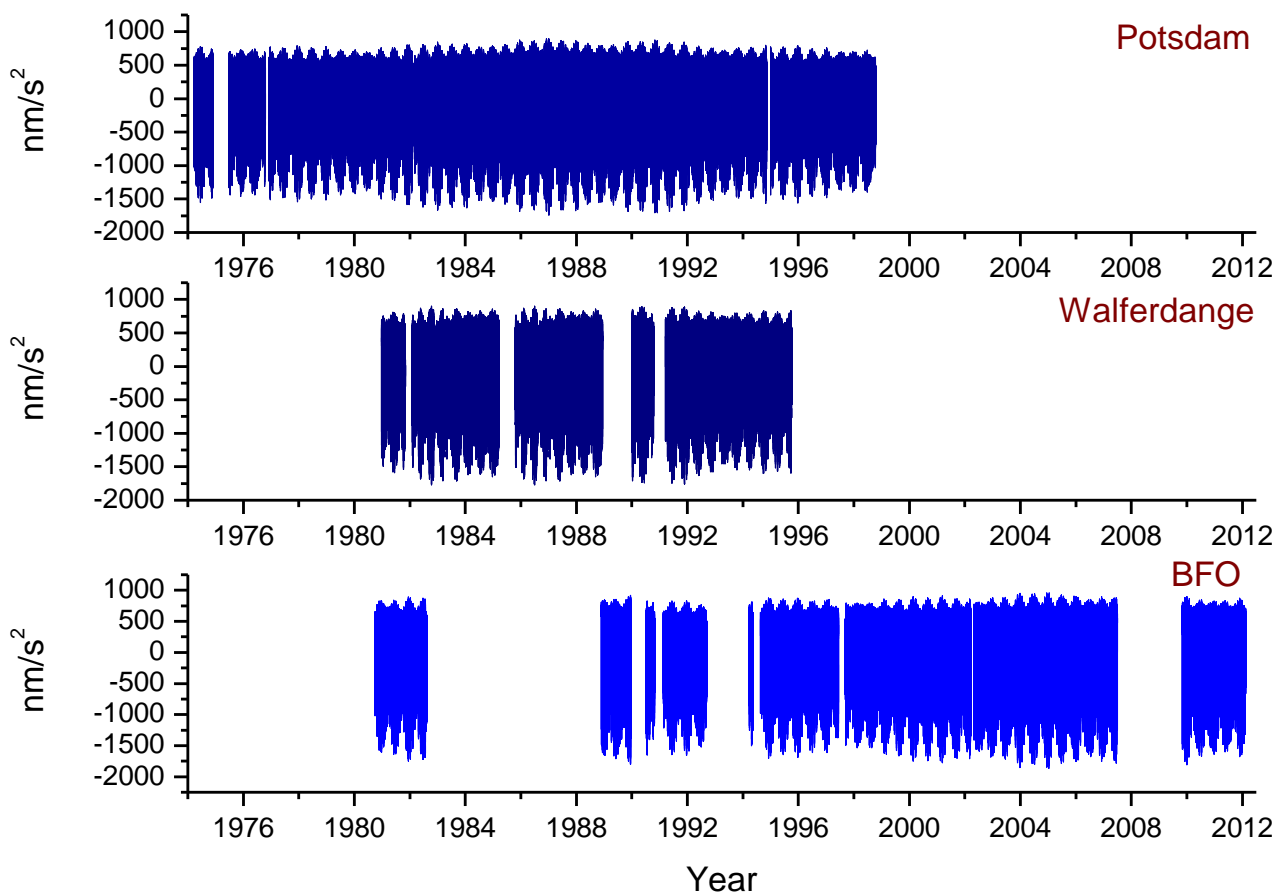
Fig. 4.2: Temporal gravity variations recorded with spring gravimeters at the Gravimetric Observatory Potsdam, Walferdange Observatory and Black Forest Observatory. The complete time series have been corrected for any disturbance, and we have also removed a linear (Walferdange and BFO) or exponential (Potsdam) instrument drift.

Once these three raw datasets have been pre-processed to obtain clean series, we have performed tidal analyses as mentioned above (using ETERNA 3.4 software, applied on 1 h yearly segments shifted month by month, using 23 groups of waves), obtaining temporal series for the amplitude factors and phase differences of the main tidal waves in the diurnal and semi-diurnal frequency bands. Those temporal series are represented in figures 4.3a and 4.3b.
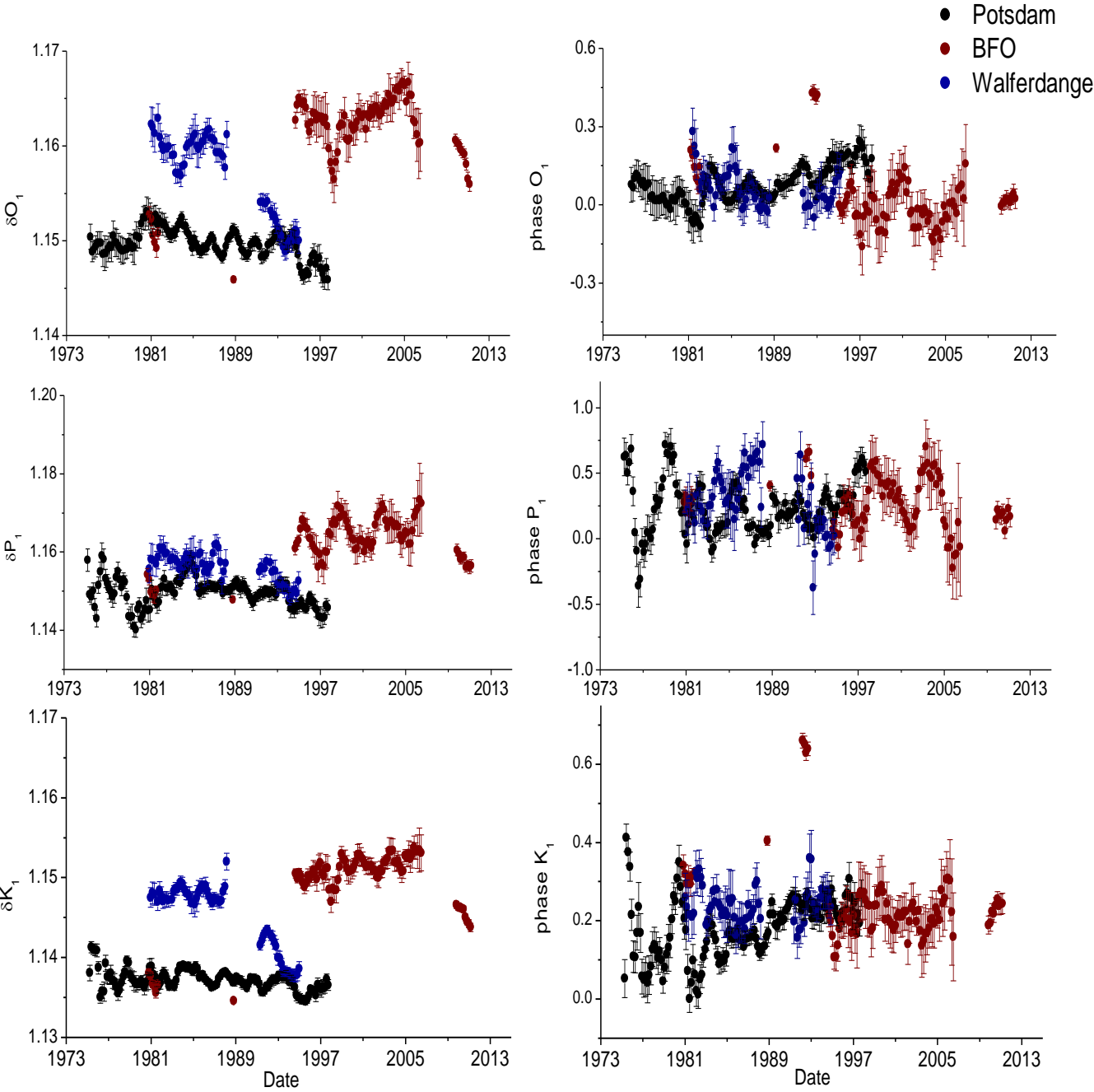
Fig. 4.3a: Temporal variations of the tidal amplitude factors and phase differences (in degrees) for the 3 main diurnal waves (O1, K1 and P1), obtained from the tidal analysis using ETERNA 3.4 software on yearly segments shifted month by month of 3 spring gravimeters at Potsdam, BFO and Walferdange. The resulting tidal parameters are associated to the central epoch of the analyzed interval. The gravimetric factors have not been corrected for any ocean tide loading.
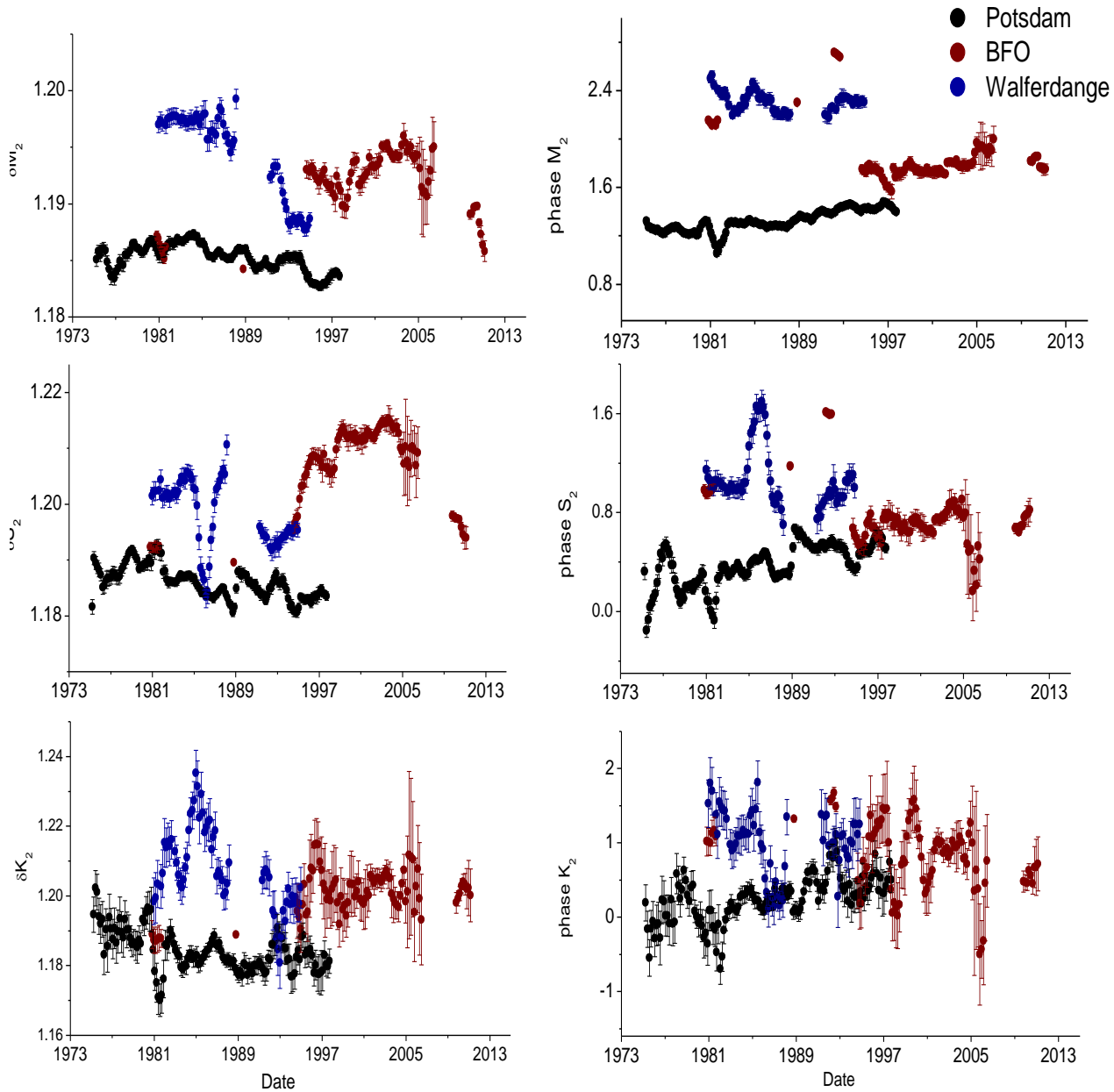
Fig. 4.3b: Temporal variations of the tidal amplitude factors and phase differences (in degrees) for the 3 main semidiurnal waves (M_2, S_2 and K_2), obtained from the tidal analysis using ETERNA 3.4 software on yearly segments shifted month by month of 3 spring gravimeters at Potsdam, BFO and Walferdange. The resulting tidal parameters are associated to the central epoch of the analyzed interval. The gravimetric factors have not been corrected for any ocean tide loading.

We have removed certain intervals of the series, where data were affected by purely instrumental problems, as for instance when the instruments were updated. Some of the eliminated intervals were detected thanks to information provided by the gravimeter's owners. When this information was not available, we easily detected them by looking for anomalies in the residual gravity signal that correspond to abnormal values in the tidal amplitudes and phases, as shown in the example for Walferdange in figure 4.4.
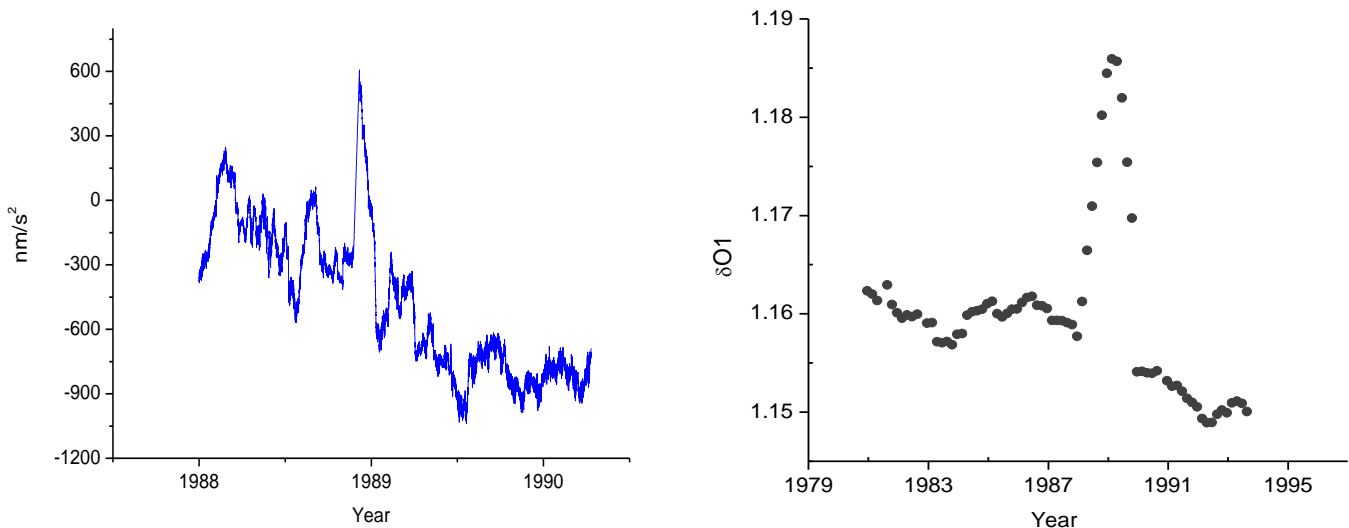
Fig. 4.4: Example of how anomalies found in the residual gravity signal (left plot) correspond to abnormal values in the tidal amplitudes. In that case, the tidal amplitude obtained from the tidal analysis made on yearly segments where the affected interval (December 1988-January 1989) is included, are influenced.

The variations of amplitude factors for the three spring gravimeter stations (Fig. 4.3a and 4.3b) around the mean value, are of the order of 1% for the diurnal waves (O_1, P_1, K_1) and slightly higher for the semidiurnal waves (M_2, S_2, K_2) (Table 4.1). These variations are estimated using the statistics toolbox from Matlab 7.5., by computing for each of the main tides the distribution of the delta values (examples of the distribution are shown in figure 4.5). This leads to a mean value (δ_m) and to a standard deviation (σ) for each tide. We will use this standard deviation as a stability criterion and compute the ratio σ / δ_m for each tide.
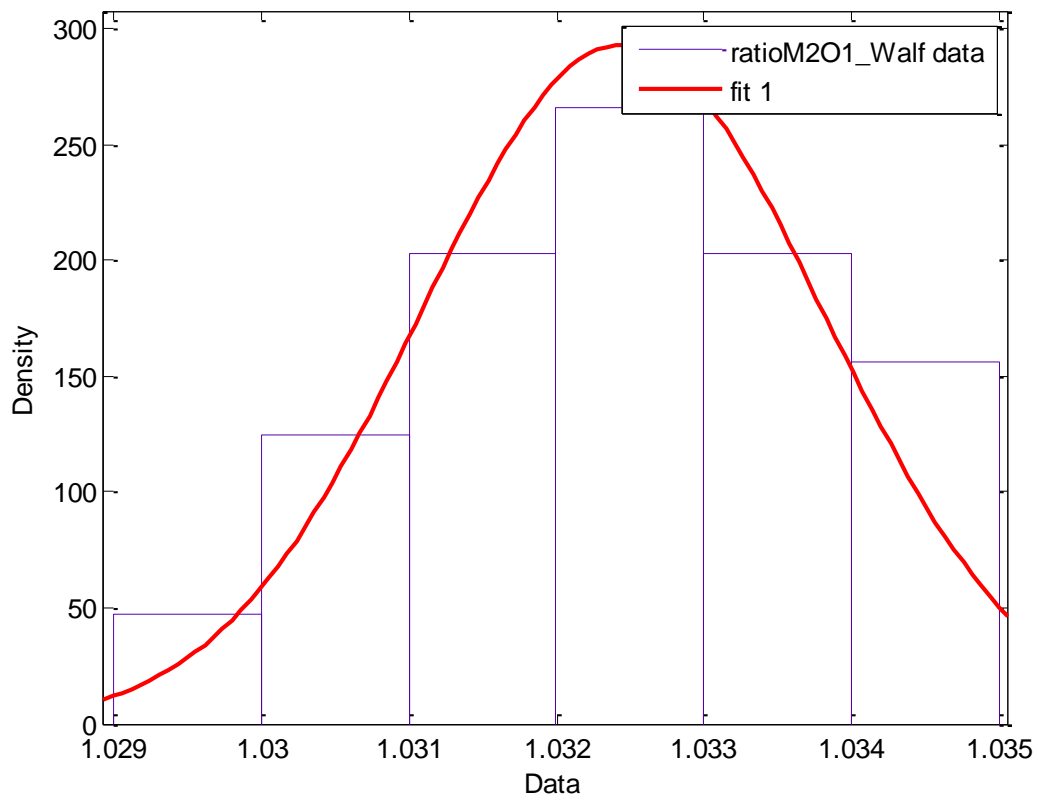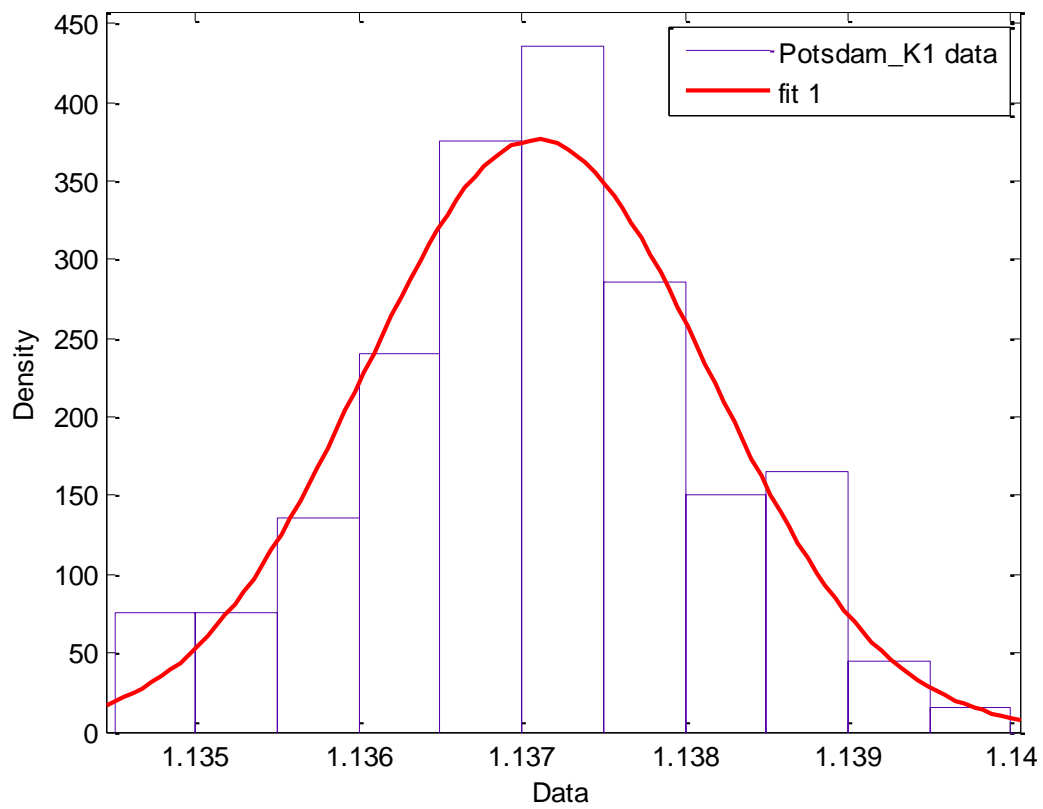
Fig. 4.5: Example of distribution of the delta values for a diurnal wave (O1 at Potsdam station), upper plot, and distribution for the delta factor ratio M2/O1 at Walferdange station, lower plot.

As the tidal amplitude factor distribution is close to a Gaussian, 95% of the tidal factor variations are within the $\pm 2\sigma$ quoted intervals. In table 4.1 we indicate the time stability for each of the four main tides, assuming $\pm 2\sigma$ confidence interval.

Table 4.1: Time stability ($\pm 2\sigma$ confidence interval) computed for the main tidal harmonic components based on their amplitude factors and the respective gravimetric factor ratios M_2/O_1 for the 3 spring gravimeter stations BFO, Potsdam and Walferdange. Periods with instrumental problems were not taken into account in the computation.

Spring grav. Stations	O_1	P_1	K_1	M_2	S_2	K_2	M_2/O_1
Black Forest Observatory	0.85 %	1.50 %	0.80 %	0.71 %	1.93 %	1.67 %	0.56 %
Potsdam	0.52 %	1.26 %	0.44 %	0.39 %	0.94 %	1.93 %	0.33 %
Walferdange	1.49 %	1.19 %	1.39 %	1.25 %	1.96 %	1.99 %	0.51 %

As mentioned before, the variations in amplitude and phase are larger mainly within the intervals where instrument problems or changes in the instrument insulation occurred. So, such periods were dismissed when computing these variations, in order to check the time stability during quieter time intervals.

We have also computed for each instrument the temporal variations of the ratio $\delta M_2/\delta O_1$. From the distribution of values around the mean value, we found temporal variations of the order of 0.3% for Potsdam and almost 0.5% for BFO and Walferdange stations (figure 4.6).

M_2 and O_1 are chosen because they are waves of the largest amplitude in their respective frequency bands. This ratio, being independent of the gravimeter's calibration, is a very good indicator of the stability of the instrument. Thanks to its stability, we can detect if there is any inconsistency at some point between these two waves, independent from variations (if any) on instrument calibration.
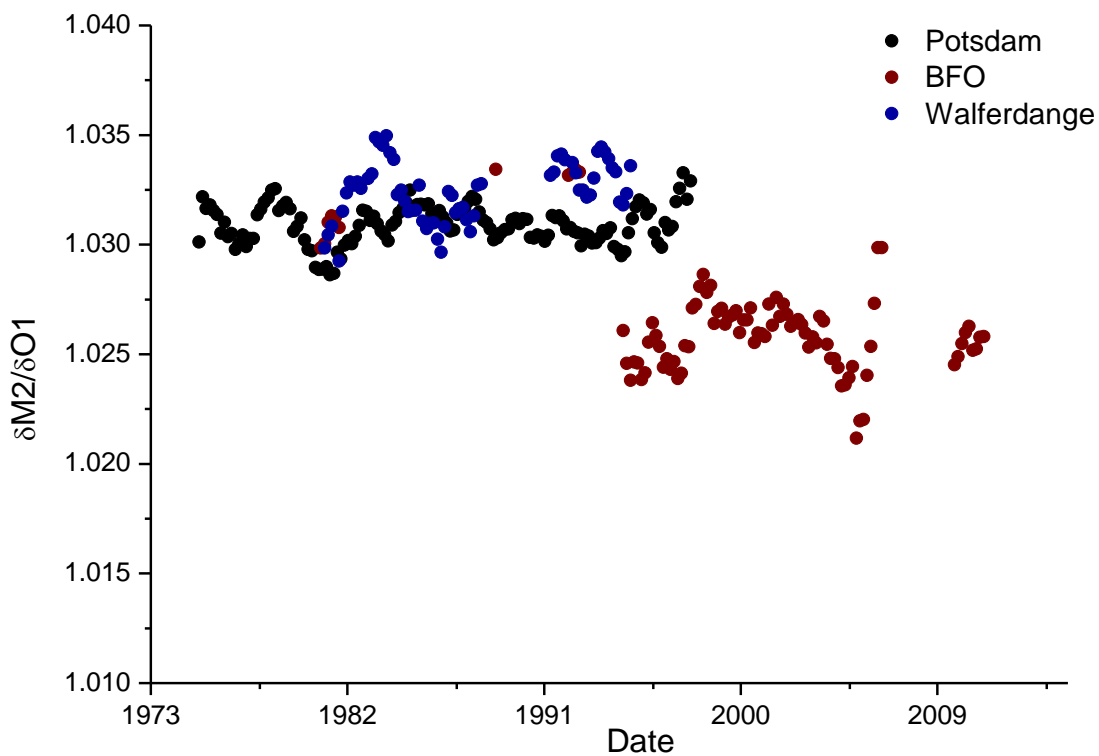
Fig. 4.6: Temporal variations of the gravimetric factor ratio $\delta M_2/\delta O_1$, derived from the results of the tidal analysis using ETERNA 3.4 software on yearly segments shifted month by month for the 3 spring gravimeters at Potsdam, BFO and Walferdange.

Some periodic fluctuations seem to appear in the individual gravimetric factors, and also in their respective $\delta M_2/\delta O_1$ ratios, best visible in the longest and less noisy Potsdam series (see figure 4.9 for comparison of the noise) at diurnal and semi-diurnal frequencies. The origin of such fluctuations, if geophysical, could be due for example to some time-variations in the oceanic or atmospheric loading, which have never been really observed or computed.

Before interpreting any time variability in the delta factors as being geophysical, it is important to check if there is any correlation with the remaining noise (including instrumental and environmental noise). We compare then, the time evolution of two of the main waves (O_1 and M_2) with respect to the time evolution of the noise level in their respective frequency band (diurnal and semidiurnal) in figure 4.7. The corresponding noise levels were calculated with ETERNA 3.4. ETERNA computes the average noise levels from the mean FFT of the estimated residuals, in several frequency bands.
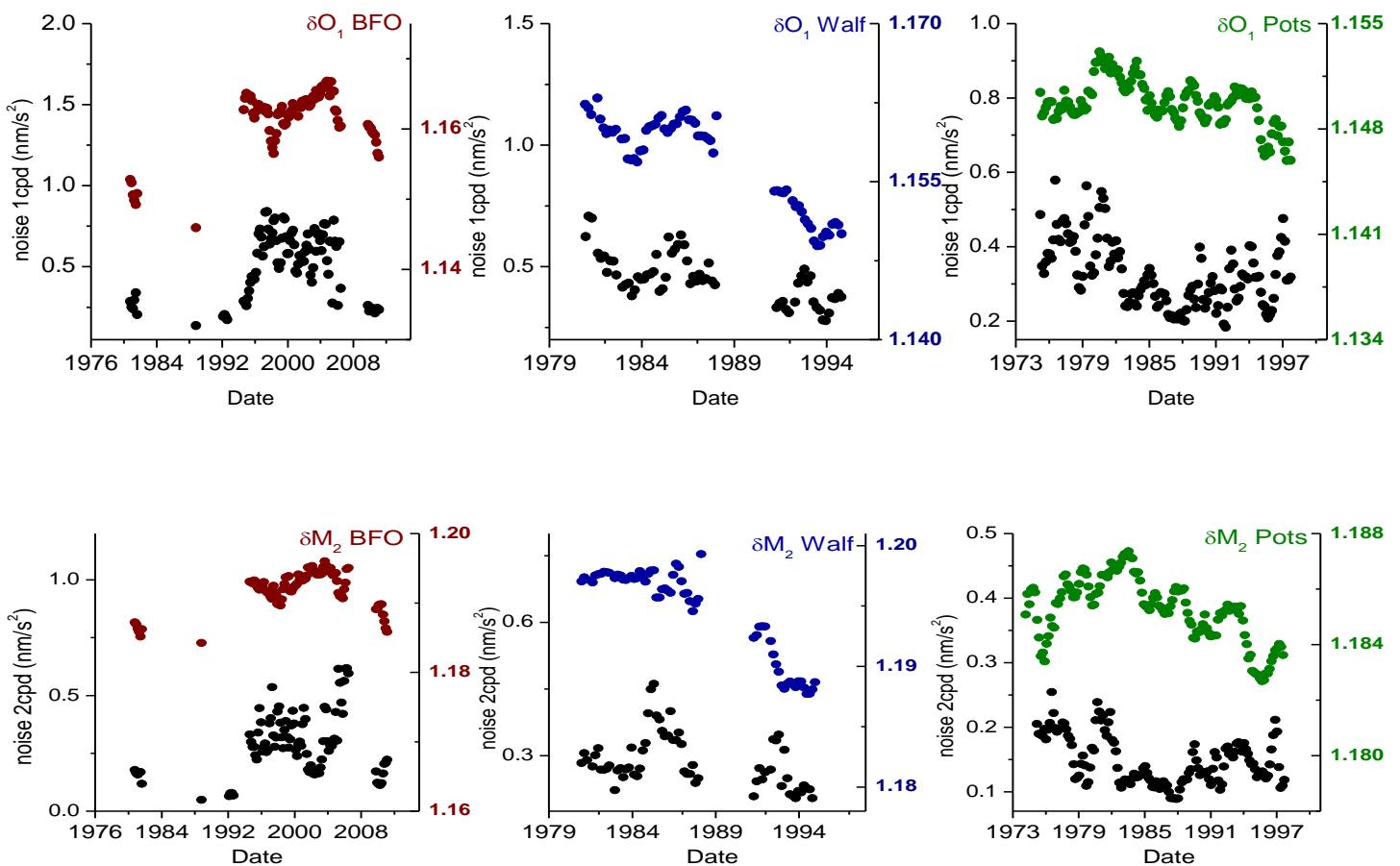
Fig. 4.7: Time evolution of diurnal gravimetric factor (O1) compared with time evolution of the noise level in the 1 cpd frequency band (upper plots), and of semidiurnal gravimetric factors (M2) compared with noise level in the 2 cpd

frequency band (lower plots), for the spring gravimeters recording at BFO (left), Walferdange (middle) and Potsdam (right) stations.

In some of the cases, the correlation between the periodic fluctuations observed in the time variability of the delta factors and the time evolution of the noise in the tidal frequency bands (1 and 2 cpd respectively) is weak. However, if we compare the noise with the absolute differences of the delta factors (e.g. $|\delta_{01}-$ mean $\delta_{01}|$), these correlations are higher for all the waves in the three stations (Fig 4.8).
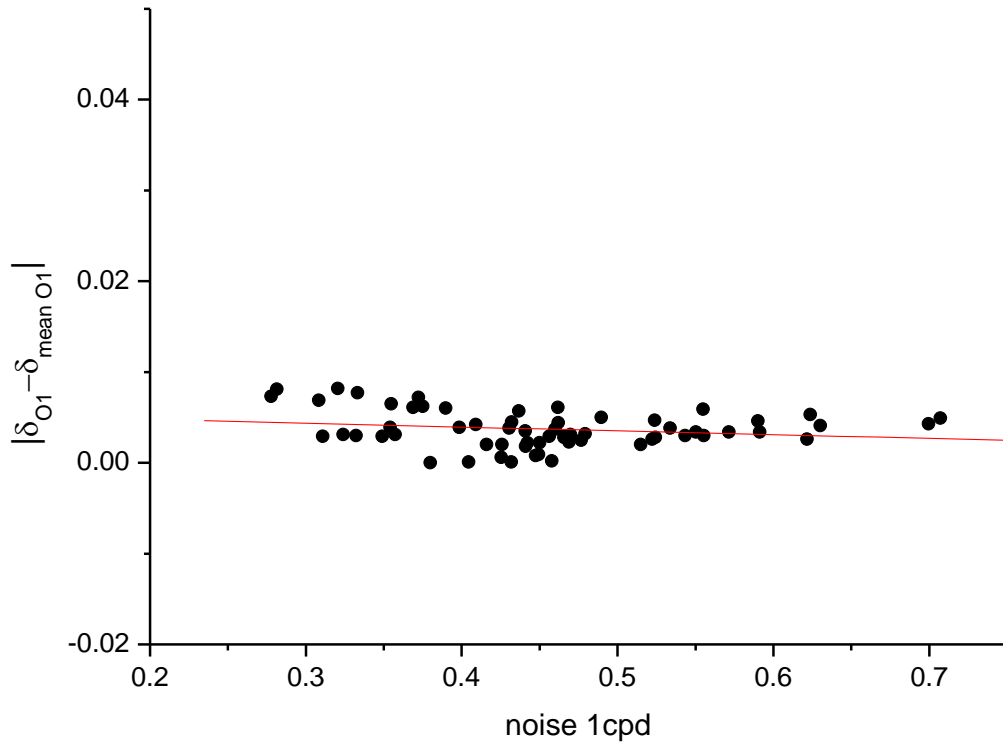
Fig. 4.8: Example of correlation between the noise level in the 1 cpd frequency band and the variation of the tidal amplitude factor for O1 ($|\delta O1 -$ mean $\delta O1|$) at Walferdange Observatory (correlation coefficient = 0.73).

Also, for all three spring gravimeters, the greatest variations in tidal parameters (either positive or negative) are indeed related to the noisiest periods (see figure 4.7).

We also check if similar variations in tidal factors appear in SG data, since, as already shown in section 2.2, SGs are instruments with a better precision than spring gravimeters. In the next section we will emphasize the better performances of SGs with respect to spring gravimeters.

As the ambient noise is one of the possible sources than can affect the tidal parameter stability, we have also calculated the time evolution of the noise amplitude for the three spring gravimeters and also for the SG C026 at J9, using the same time-windows

as for the stability of the gravimetric factors (figure 4.9) to compare them. It is obvious that the amplitude of SG noise is not only much smaller than the noise amplitude from the spring gravimeters, but it is also much more stable.

We will push forward this comparison at J9 between spring gravimeters and SGs in the next part.
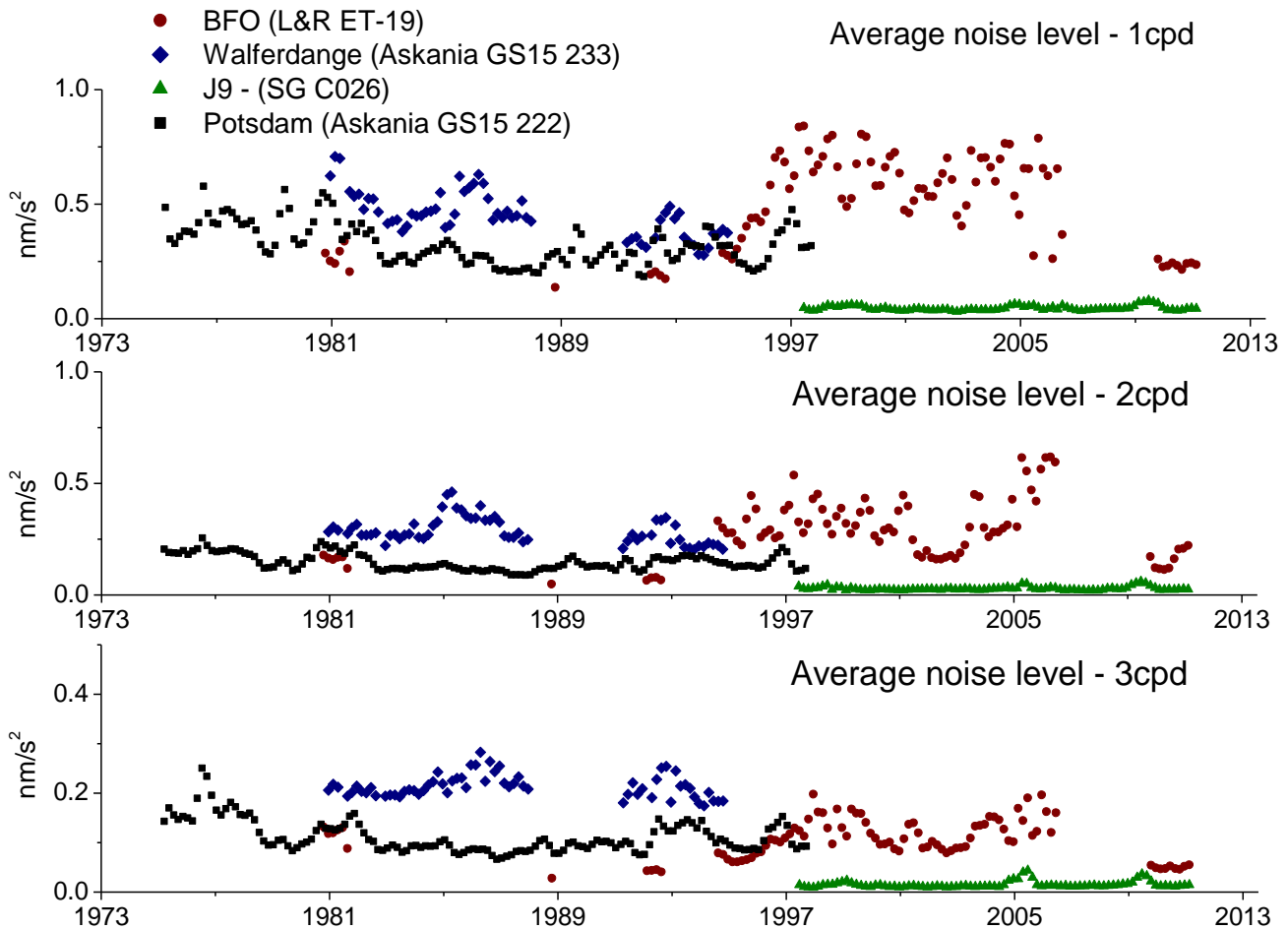
Fig. 4.9: Time evolution of the amplitude of the noise levels in various frequency bands (1, 2 and 3 cpd) obtained from the tidal analysis calculated using ETERNA 3.4 software on yearly segments shifted month by month of 3 spring gravimeters at Potsdam, BFO and Walferdange, and of the superconducting gravimeter C026 at J9 site.

4.3 Comparison of spring and superconducting gravimeters at J9

As previously mentioned in section 2.2.2, the first superconducting gravimeter was installed in the early 80s. Since then, numerous instruments have been installed worldwide providing us with long gravity records of excellent quality (higher sensitivity with a smaller and more stable instrument drift than spring gravimeters) that allow us to carry out investigations in a wide range of geophysical phenomena (Richter et al., 1995, Hinderer et al., 2007).

We compare now the average noise levels in the main tidal bands computed using ETERNA 3.4 software (ETERNA computes the average noise levels from the mean FFT of the estimated residuals in a given frequency band) of the 3 spring gravimeters which data has just been discussed in the previous section 4.2, with the average noise level of the SG C026 of Strasbourg (Fig. 4.10) to demonstrate the improvement from a mechanical spring gravimeter to a modern cryogenic instrument. The noise levels have been roughly decreased by a factor 5 in amplitude.
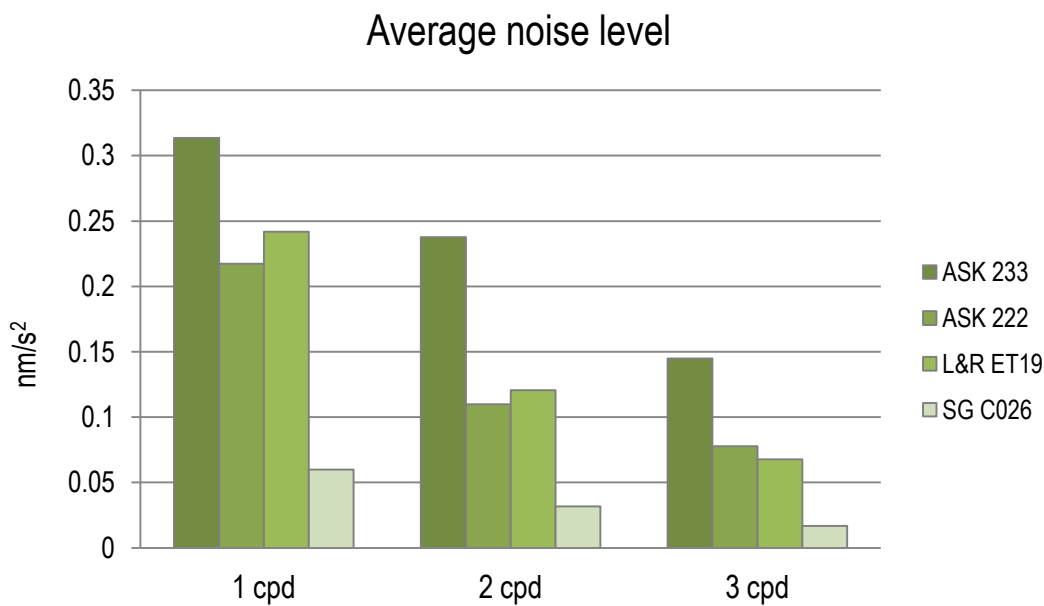
Fig. 4.10: Comparison of the amplitude of noise levels for the 3 spring gravimeters (Askania GS15 222 at Potsdam, LaCoste-Romberg ET-19 at BFO, Askania GS15 233 at Walferdange) and the superconducting gravimeter C026 at J9 station. The average noise levels were calculated with ETERNA for every instrument in the tidal frequency bands 1, 2 and 3 cpd, normalized by the record length.

However, it is not possible to separate the environmental noise from the instrument noise using a single instrument at a single site (environmental noise, as opposed to instrumental noise, is due to unmodeled geophysical phenomena at the observing site, as well as local noise created by some other instrumentation installed beside like air conditioning, human noise generated around the site, nearby traffic, oceanic micro-seismic noise, etc...). So to better compare the noise levels of the spring

gravimeters with respect to the noise levels of the SGs we use the two series of spring gravimeters (Askania and LaCoste-Romberg models) and the two series of SGs (T005 and C026), which have been recording at the same place (J9 Observatory), although during different epochs. Thus, we can compare their respective instrument noise assuming no difference due to site noise (some differences would occur because of the varying oceanic noise, although this part was filtered out as we are using low-pass filtered 1h-decimated data), to highlight the improvement in instrument noise (the last includes sensor, electronics and acquisition system). The resulting average noise levels are plotted in figure 4.11 for the 1, 2 and 3 cpd frequency bands.

Average noise level
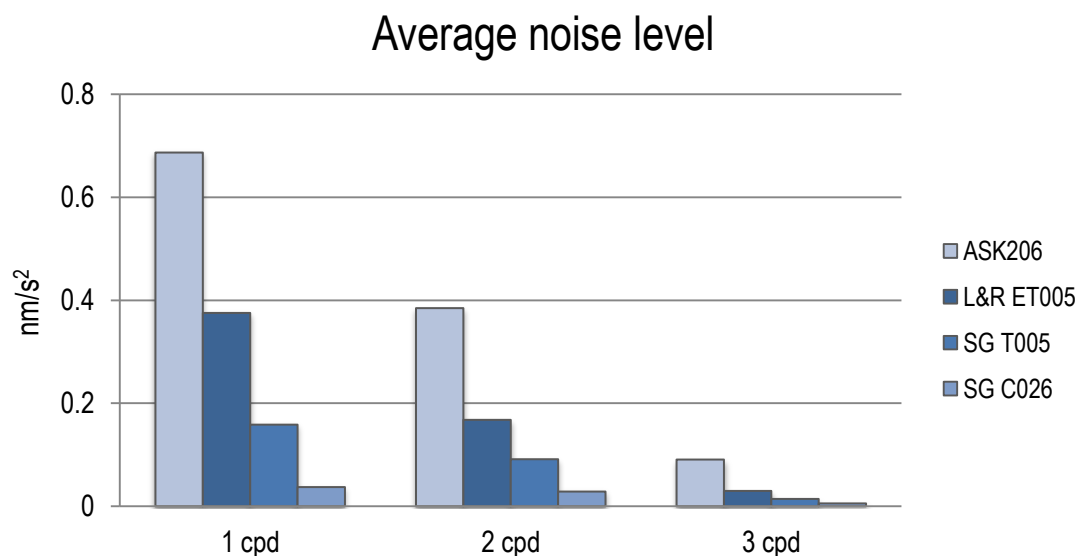
Fig. 4.11: Comparison of the amplitude of noise levels for 2 spring gravimeters (Askania 206 and L&R ET005) and 2 superconducting gravimeters (SG T005 and SG C026), all of them installed at observing site J9. The amplitudes have been normalized by the record length.

Major improvements in terms of noise level of the SGs over the spring gravimeters have already been shown in Riccardi et al. 2011 and Rosat el al. 2014. It has also been shown that L&R Earth Tide gravimeters (Fig. 4.12 for the ET-005 and ET-11 at J9, or ET-19 at BFO in Zürn et al. 1991) perform better than the Portable Earth Tide (PET) spring gravimeters at periods shorter than 3 h. They are comparable, however, to good isolated ET (like ET-005 or ET-19) at tidal frequencies. The later can even compete with SGs (Zürn et al. 1991a). Concerning the L&R ET-11, which is still recording at J9, its higher noise level at sub-seismic frequencies is due the fact that the sensor is not air-tight any more (Rosat et al. 2014).

Banka (1997) developed a standard procedure to estimate the noise level at an observing site. This procedure was generalized to compute the noise levels of SG sites belonging to the GGP by Rosat et al. (2004), and in 2011 an updated comparison of the SG seismic noise was published showing that the noise at the GGP sites was quite stable in time (Rosat and Hinderer 2011). In Fig. 4.12, the procedure summarized in

Rosat et al. (2004) has been used for each data series. This procedure is based on the computation of the residual power spectral densities (PSDs) over a quiet time period in the seismic (periods smaller than 1h) and in the sub-seismic (between 1h and 6h) frequency bands. Using the raw calibrated gravity records from each gravimeter, the residual data is computed by removing a local tidal model and the local atmospheric pressure effect (by a nominal admittance of -3 (nm/s^2)/hPa). The quietest periods of 15 continuous days are considered and a linear drift is removed before applying a high-pass filtering with a cut-off period of 8 h. The PSD is then estimated using a smoothed periodogram.

From the mean of the Fourier transforms of the 15 quietest days, we estimate the PSD using the periodogram definition:

$$P(f) = \frac{|X(f)|^2}{T}$$

where T is the time duration and $X(f)$ is the Fourier transform of the signal.

The PSDs are then normalized according to Parseval's theorem, meaning that the integrated PSD from zero to Nyquist frequency corresponds to the variance of the time series. Then we apply a smoothing of the periodogram using a Parzen window of 101 points. The smoothing does not affect the PSD level and makes the periodogram consistent (Rosat and Hinderer, 2011). Following Banka (1997), from the mean PSD in the period range 340–600 s, we can compute the seismic noise magnitude (SNM) defined by:

$$\text{SNM} = log_{10}[\text{meanPSD}(\mu Gal^2/Hz)] + 2.5$$

where the mean PSD is defined in $\mu Gal^2/Hz$
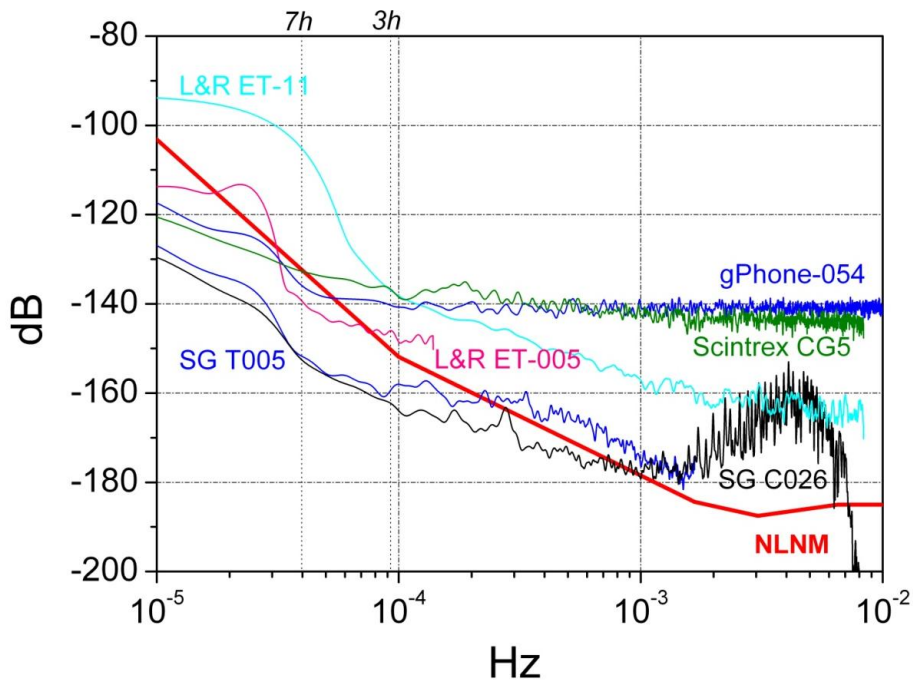
Fig. 4.12: Power Spectral Densities on the quietest period of 15 days of L&R ET005, L&R ET-11, SG T005, SG C026, Scintrex CG5 and gPhone-054. The NLNM (New Low Noise Model) of Peterson (1993) is plotted for reference (after Rosat et al. 2014).

As for the tidal analysis, we can check that the variability in the barometric admittance decreases in time when moving from the spring meter L&R ET005 to the SG T005 and SG C026. This is most likely due to lower noise in the gravity and pressure data (fig. 4.13).
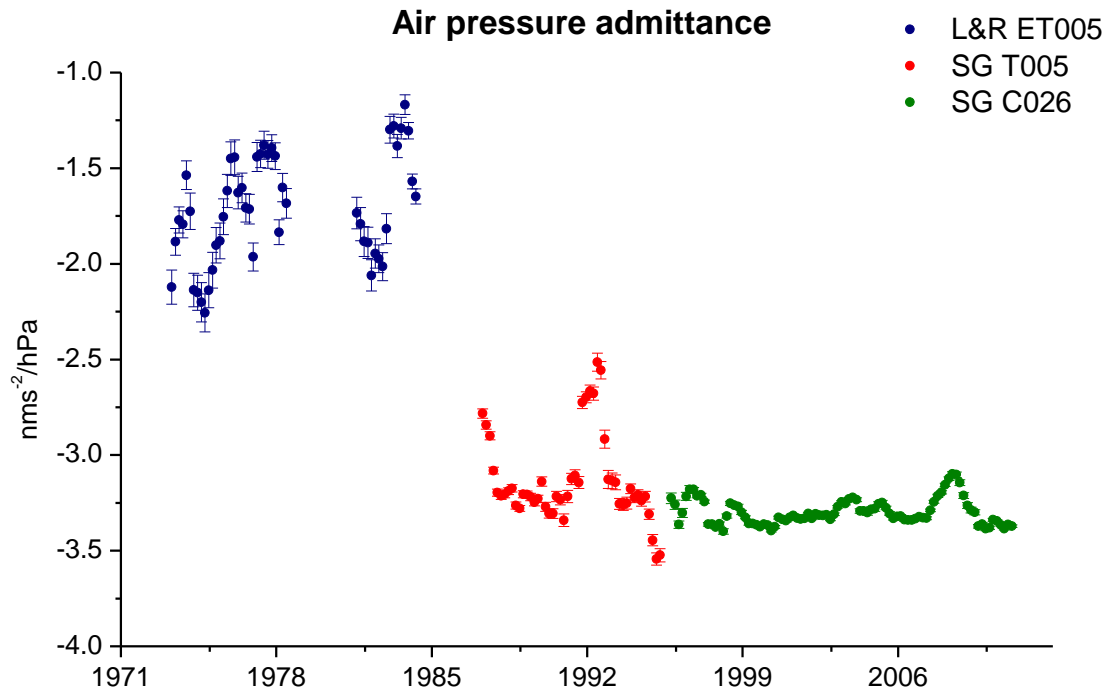
Fig. 4.13: Temporal changes of the yearly atmospheric gravity-pressure admittance, derived from the results of the tidal analysis using ETERNA 3.4 software on yearly segments shifted month by month for the L&R ET005, SG T005 and SG C026 recording at J9.

To have more insight on the question of the stability in time of the SG data, we will first focus on the 2 SG series recorded at the Gravimetric Observatory of J9. As said in section 3, at this station two different superconducting gravimeters have been recording consecutively since 1987 until nowadays. The first SG was a TT70-T005 model from GWR Instruments installed in July 1987. This gravimeter was recording for almost 10 years. In 1996 this gravimeter was replaced by a more compact type, the C026, which is still recording. As both instruments have been installed not only in the same observatory, but also on the same pillar, we can merge them into one single series of almost 26 years of data. Both series have been pre-processed and corrected independently (using for each one its own calibration factor and phase delay) before merging them. The gap (several days) between the removal of the old gravimeter and the installation of the new one was filled using a local tidal model obtained from tidal analyses at J9.

The phase lag for the C026 was determined experimentally in 1999 (Van Camp et al. 2000), while that of T005 was determined from the phase differences of the eight major diurnal and semidiurnal waves between tidal analyses of the C026 and T005. For the C026 a linear instrumental drift was removed while for the T005 an exponential drift model was fitted.

101

As for the spring gravimeter series of the previous section, we check the time stability of the tidal parameters by performing for each data series a tidal analysis using ETERNA 3.4 software over periods of one year, shifted month by month. The obtained time-varying gravimetric factors and phase differences are plotted in Fig. 4.14.
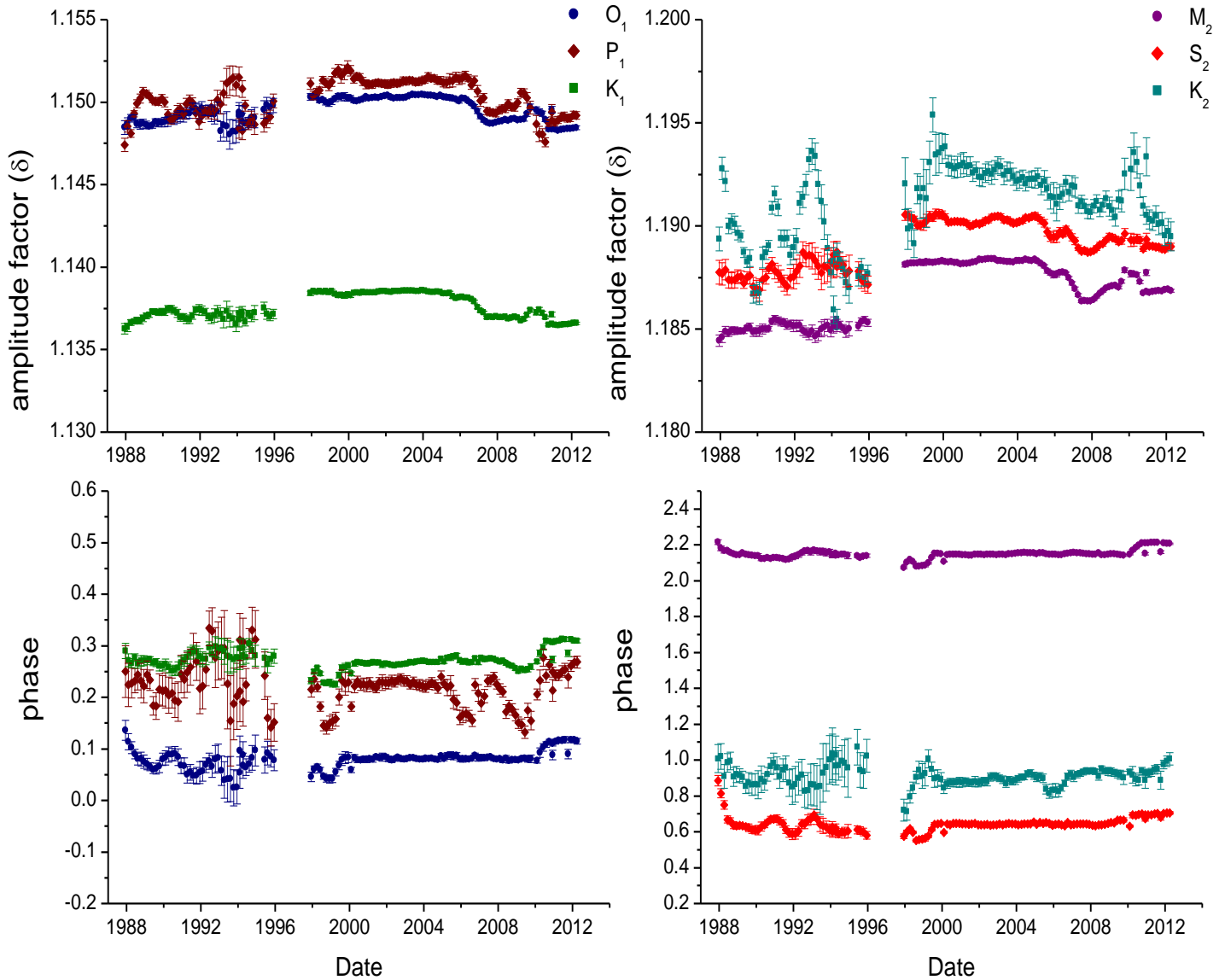
Fig. 4.14: Temporal variations of the gravimetric factors and phases differences (degrees) for the main diurnal and semidiurnal waves (O1, P1, K1, M2, S2, K2), obtained from the tidal analyses using ETERNA 3.4 on yearly segments shifted month by month of the merged series of 2 superconducting gravimeters recording at J9 station. The resulting tidal parameters are associated to the central epoch of the analyzed interval. The gravimetric factors and phase differences were not corrected for any ocean tide loading.

Similar study has been carried out with the delta factor ratio $\delta M_2/\delta O_1$ and the respective temporal variation is shown in figure 4.15.
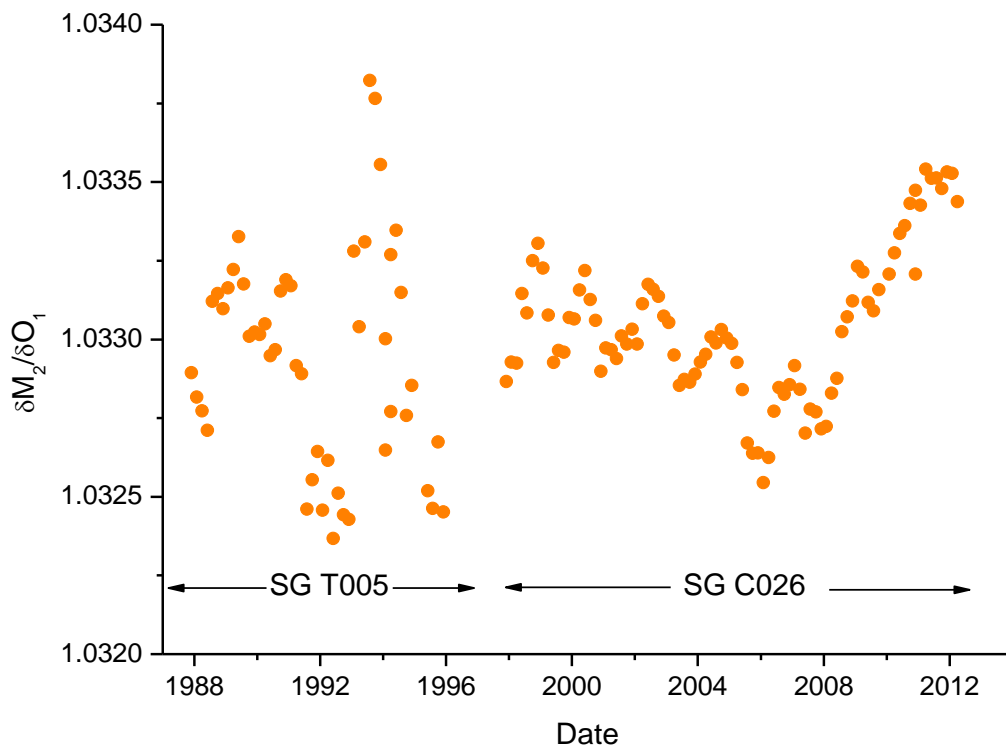
Fig. 4.15: Temporal variations of the delta factor ratio $\delta M2/\delta O1$, computed from the tidal analyses using ETERNA 3.4 software on yearly segments shifted month by month of the merged series of 2 superconducting gravimeters (SG T005 & SG C026) at J9 site.

At a first glance, we can notice the large improvement in the stability of the SG series with respect to the results from the different spring gravimeters that we have presented in section 2.2. The SG compact model C026 has also improved with respect to the previous version of SG, T005, not only in terms of stability, but also in terms of noise levels (Rosat et al. 2004, Rosat and Hinderer, 2011), and drift rates (Amalvict et al.,2001) due to both instrument and data acquisition system upgrades. Despite the high temporal stability that is achieved, we can still observe some temporal variations with an annual periodicity, particularly visible on the variations of the ratio $\delta M_2/\delta O_1$ after 1996 (series of SG C026) in Fig. 4.15.

These variations must be carefully interpreted because it is difficult to distinguish whether they are due to geophysical processes or to instrumental noise and/or numerical effects. For example, large fluctuations in noise levels and in delta factors for the C026 occur around early 2007, when the tilt-compensation system failed and in 2010 when the electronics was changed. Apart from these known troubles, some correlation appears between the variations of the noise level (fig. 4.16) and the variations of the delta factors. For the rest of the series the variations are extremely

small, reaching stability around 0.1% for the diurnal band, 0.16% for the semidiurnal band and 0.5 % for the ratio $\delta M_2/\delta O_1$ (see Table 4.3).

We check that, as for spring gravimeters, the greatest variations in tidal parameters for the SG C026 are also related to the noisiest periods. For this purpose, we compare the time variations of the delta factor for the main diurnal and semidiurnal waves (O_1, P_1, K_1, M_2, S_2 and K_2), to the time evolution of the noise level in their respective frequency bands (1 cpd and 2 cpd). Results are plotted in figure 4.16.
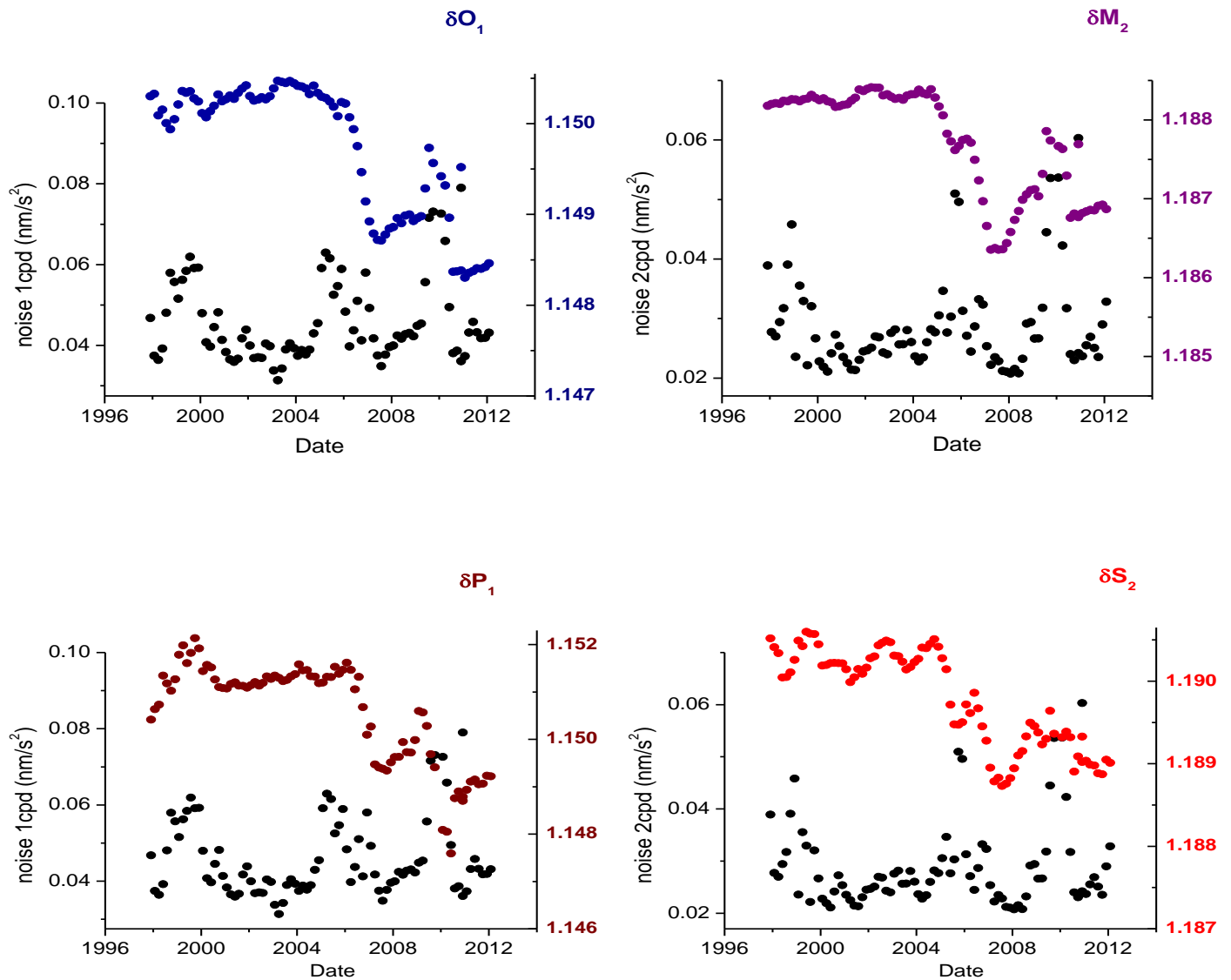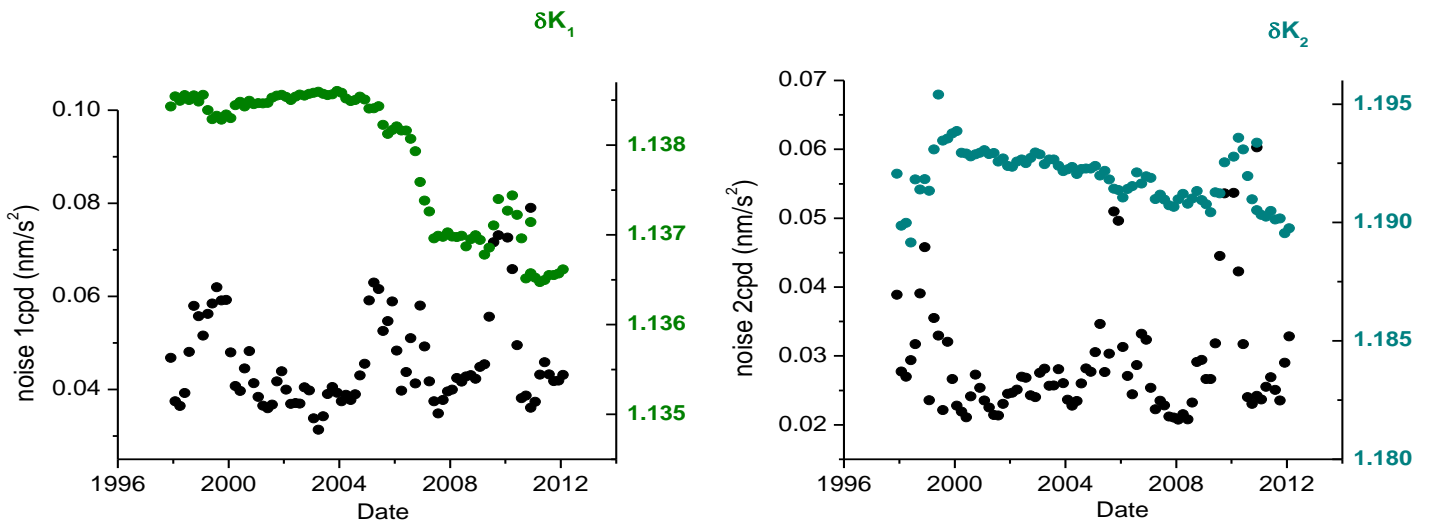
Fig. 4.16: Time evolution of diurnal delta factors (O1, P1, and K1) compared with time evolution of the noise level in the 1 cpd frequency band (left plots), and of semidiurnal delta factors (S2, M2 and K2) compared with noise level in the 2 cpd frequency band (right plots) for the superconducting gravimeter C026 recording at J9.

The comparison of the time variations of the delta factors for the main diurnal and semidiurnal waves with the time evolution of the noise level computed in their respective frequency bands, shows that when the noise is increasing, the corresponding delta factor is varying much more (towards either larger or smaller values than the mean value) than during quieter periods. Also, if we compare the noise with the absolute differences of the delta factors (e.g. $|\delta_{O1} -$ mean $\delta_{O1}|$) similar as we have done previously with the spring gravimeters (Fig 4.8), we obtained correlation coefficients between 0.59 and 0.79.

We have shown the improvements from a spring gravimeter to an SG and found some time variability in the gravimetric tidal response of the Earth. These variations seem to be mostly related to noise variability. In order to check if these time-variations of gravimetric factors are local, we consider now other SG sites in Europe to verify if we can find similar trends in the variability of the delta factors.

4.4 Superconducting gravimeters in Europe

Before interpreting the time variations of the delta factors at J9 station as being geophysical, similar variations should be observed at other European sites. Hence we analyzed also the time-variations of the gravimetric factors for the main diurnal and semi-diurnal tidal waves using the SG data from several European GGP stations: Bad-Homburg (10 years), Brussels (18 years), Medicina (14 years), Membach (16 years), Moxa (11 years), Vienna (9 years) and Wettzell (13 years). These European sites were chosen because of the length of their records and because they are far from the oceans. The scale factors and phase lags of their respective instruments are summarized in Table 4.2.

The analysis procedure is the same as the one used before for the spring gravimeter data and for the SG data at J9 station. The results are presented in Fig. 4.17 for the diurnal and in Fig 4.18 for the semidiurnal main waves. The time fluctuations of the ratio $\delta M_2/\delta O_1$ are presented in Fig. 4.19 for the 8 European stations.

Table 4.2: List of superconducting gravimeter stations and their respective period of observation used in this study. The corresponding scale factors and phase lags for each instrument are also given.

Superconducting gravimeter Stations	Period	Scale Factor (μGal/V)	Phase Lag (s)
Bad Homburg	2001-2011	-73.95	45.0 / 10.09
Brussels	1982-2000	-58.15	30.0
J9 (T005)	1987-1996	-76.02	36.0
J9 (C026)	1996-2013	-79.20	17.18 / 9.7
Medicina	1998-2012	-74.82	43.0 / 11.1
Membach	1995-2012	-78.42	9.9
Moxa	2000-2011	-60.65	12.0
Vienna	1997-2007	-77.82	9.36
Wettzell	1998-2011	-81.58	45.0 / 14.17
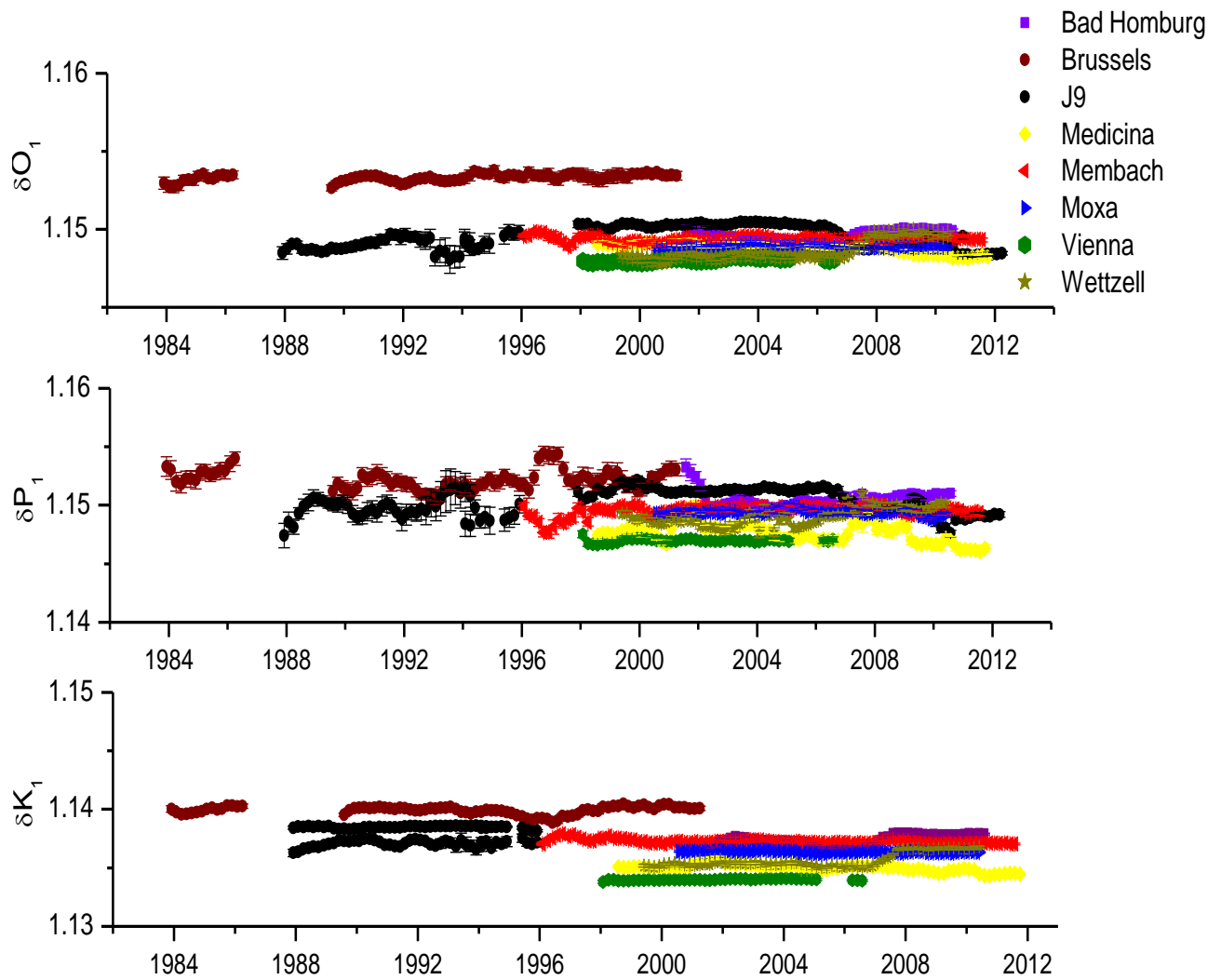
Fig. 4.17: Temporal variations of the tidal amplitude factors for the main diurnal waves (O1, P1, K1), obtained from the tidal analysis using ETERNA 3.4 software on yearly segments shifted month by month for 8 European SGs, with no ocean loading correction applied. The resulting tidal parameters are associated to the central epoch of the analyzed interval.
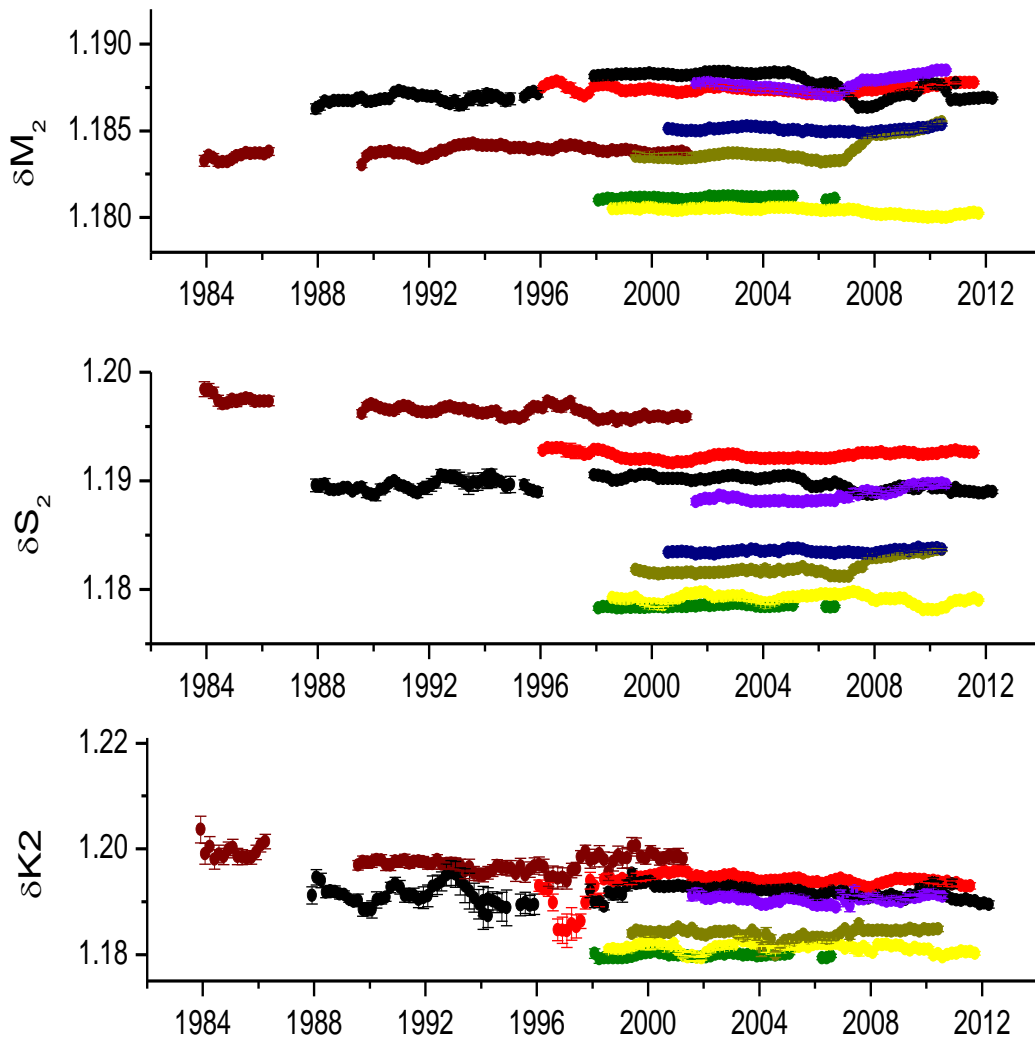
Fig. 4.18: Temporal variations of the tidal amplitude factors for the main semidiurnal waves (M2,S2, K2), obtained from the tidal analysis using ETERNA 3.4 software on yearly segments shifted month by month of 8 European SGs, with no ocean loading correction applied. The resulting tidal parameters are associated to the central epoch of the analyzed interval.
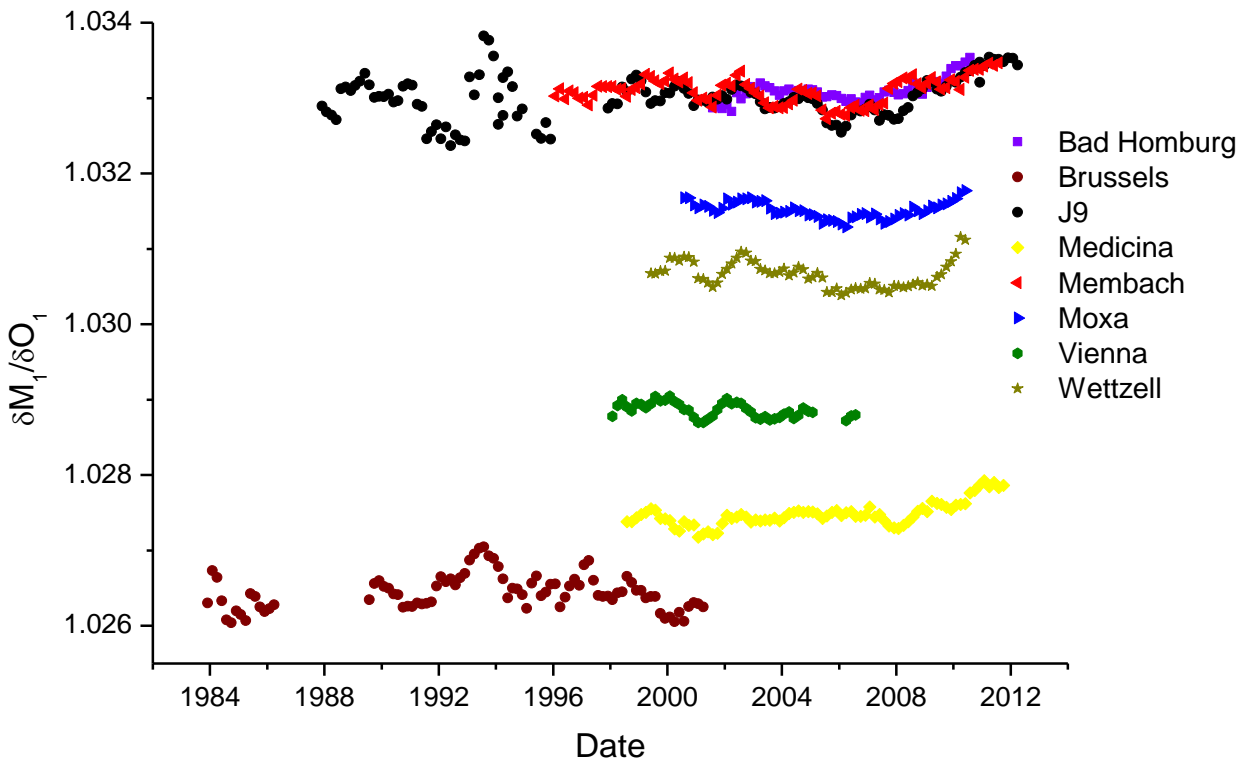
Fig. 4.19: Temporal variations of the delta factor ratio δM2/δO1, calculated from the results of the tidal analysis using ETERNA 3.4 software on yearly segments shifted month by month of 8 superconducting gravimeter stations in Europe.

There is no clear correlation between the time variations of the delta factors at the different SG sites, even if some common fluctuations are visible at several sites. So it is hard to interpret the time variations of the delta factors at these stations as being caused by global or regional geophysical effects. Examples of these weak correlations for a diurnal (O_1) and semidiurnal (M_2) waves between different SGs are shown in figure 4.20.
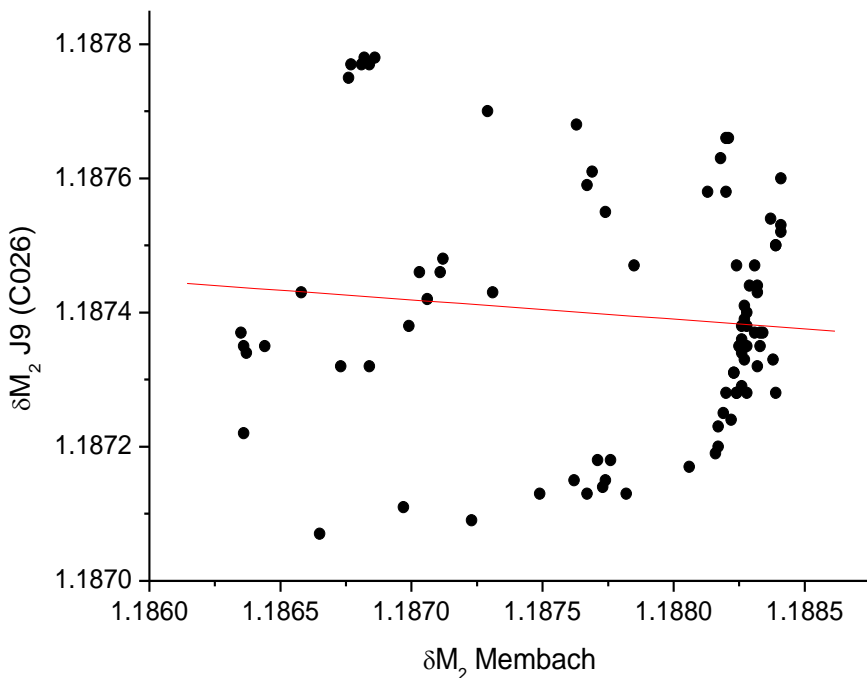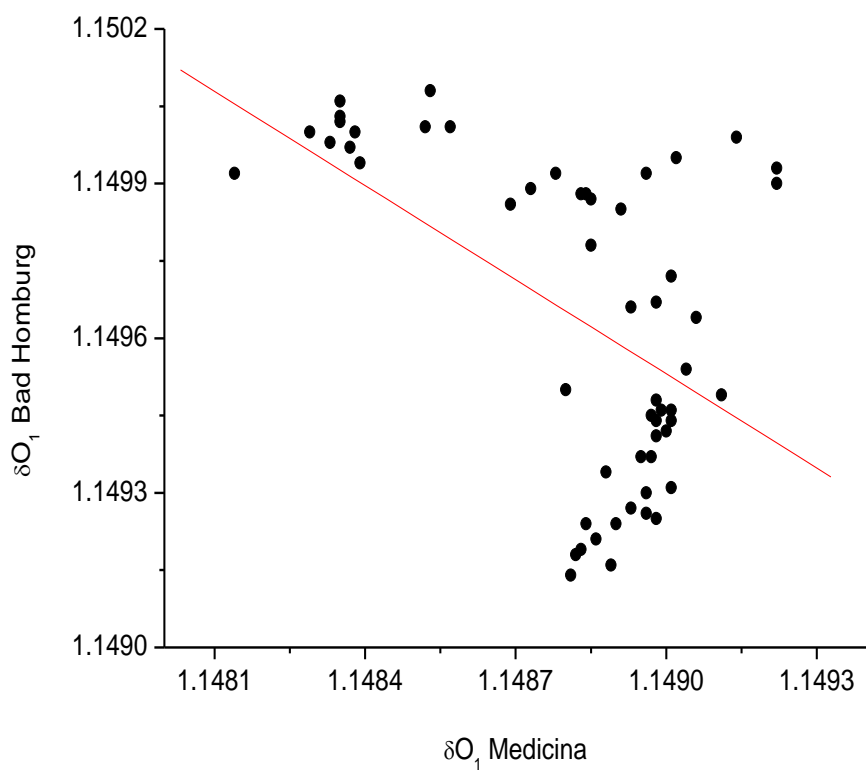
Fig. 4.20: Example of weak correlation between time variations of delta gravimetric factors at different SG sites. For O1, between Bad Homburg and Medicina, during their 10 years common period, left plot (correlations coefficients=-0.39). For M2, between Membach and J9 (C026), during their 14 years in common, on the right plot (correlations coefficients= -0.11).

In Table 4.3 we compare the stability of the observed temporal evolution of the tidal delta factors at Strasbourg with results from other European SG stations, proving that all stations have almost the same rate of variation. These stabilities are calculated in the same way as for the spring gravimeter series of the previous section 4.2. We compute for each of the main tides the distribution of the delta values, leading to a mean value (δ_m) and to a standard deviation (σ) for each tide, using the statistics toolbox from Matlab 7.5. We use then this standard deviation as a stability criterion and compute the ratio σ / δ_m for each one. As the tidal amplitude factor distribution is close to a Gaussian, 95% of the tidal factor variations are within the $\pm 2\sigma$ quoted intervals. In table 4.3 are indicated the time stability for each of the six main tides, as well as for the M_2/O_1 delta factor ratio, assuming a $\pm 2\sigma$ confidence interval.

These variations, ranging from 0.03% to 0.18% in the diurnal band and from 0.05% to 0.29% in the semidiurnal band, show the strong stability reached by SGs in general, much better than the stability obtained with series from spring gravimeters. For instance, the stability for the most stable spring gravimeter (Potsdam) is nearly four times lower than the worst stability of the results obtained with SGs. It is well known that noise in the diurnal and semidiurnal bands has an important thermal and atmospheric contribution (Crossley et al., 2013). Despite the fact that the spring gravimeters were installed as stable and thermally isolated as possible, the changes in pressure and temperature have still a much larger effect than on SGs.

Managers of some of the SG stations (Wettzell and Medicina) gave us very useful auxiliary information to safely interpret some of these variations as being purely instrumental (for instance changes in the electronics).

Table 4.3: Time stability ($\pm 2\sigma$ confidence interval) of the main tidal parameters and the delta factor ratio for the 8 SG European stations with at least 9 years of continuous data. Periods with instrumental problems were not taken into account in the computation.

SG Stations	O_1	P_1	K_1	M_2	S_2	K_2	M_2/O_1
Bad Homburg	0.10%	0.25%	0.14%	0.13%	0.19%	0.23%	0.03%
Brussels	0.12%	0.28%	0.13%	0.14%	0.24%	0.46%	0.07%
J9 (T005)	0.15%	0.31%	0.11%	0.16%	0.51%	0.63%	0.11%
J9 (C026)	0.09%	0.11%	0.09%	0.08%	0.12%	0.29%	0.06%
Medicina	0.10%	0.28%	0.11%	0.06%	0.13%	0.26%	0.05%
Membach	0.06%	0.16%	0.06%	0.07%	0.11%	0.29%	0.05%
Moxa	0.03%	0.07%	0.02%	0.04%	0.05%	0.19%	0.03%
Vienna	0.04%	0.05%	0.02%	0.02%	0.04%	0.12%	0.03%
Wettzell	0.09%	0.12%	0.11%	0.09%	0.13%	0.16%	0.05%

In Table 4.4, we list the respective average noise level calculated for 1, 2 and 3 cpd, with ETERNA 3.4 software, for the 8 SG stations.

Table 4.4: Amplitude of the average noise levels calculated with ETERNA for every instrument in the tidal frequency bands 1, 2 and 3 cpd.

SG Stations	1cpd (nm/s^2)	2cpd (nm/s^2)	3cpd (nm/s^2)
Bad Homburg	0.01765	0.00929	0.00445
Brussels	0.03366	0.01544	0.00834
J9 (T005)	0.05993	0.03388	0.01719
J9 (C026)	0.01107	0.00750	0.00348
Medicina	0.02247	0.00962	0.00462
Membach	0.01357	0.01357	0.00284
Moxa	0.01516	0.00899	0.00386
Vienna	0.01534	0.00619	0.00356
Wettzell	0.02553	0.01347	0.00378

The temporal variations of the main tidal parameters were previously investigated (Meurers 2004, Harnisch and Harnisch, 2006) using SG records. Meurers (2004) focused on small amplitude variations in the time domain by analyzing gravity data sets of 1995 hour long, shifted by steps of 332 hours over the entire records, using different GGP stations. He found that most of the stations showed a distinct seasonal variation in the tidal amplitude factors, especially for M_2, concluding that the observed amplitude factor variations are caused less by numerical deficits of the analysis procedures than by physically meaningful loading processes.

In our investigation, we have not found any clear annual modulation in the M_2 tidal amplitude factors for the European SGs studied. However, an annual modulation of K_2 appears indeed in some of the European SGs (Vienna and Membach stations), although with amplitudes (less than 3. 10^{-4}) smaller than the variations obtained by Meurers (2004) and never during the entire series (see an enlargement of delta K_2 for Vienna station in Fig. 4.21). At other SG sites such seasonal variability is not seen. Therefore, it is difficult to interpret such modulation as being geophysical (Membach is close to the ocean while Vienna is far; maybe some atmospheric or hydrological effects, although in that case they should also appear at nearby sites, which is not the case). Note that we rely on successive analyses performed with one year of data, while Meurers (2004) performed its analysis on periods of 2.5 months. Any annual modulation in the tides hence cannot be separated by analyses of 2.5 month duration, on the contrary to our case.
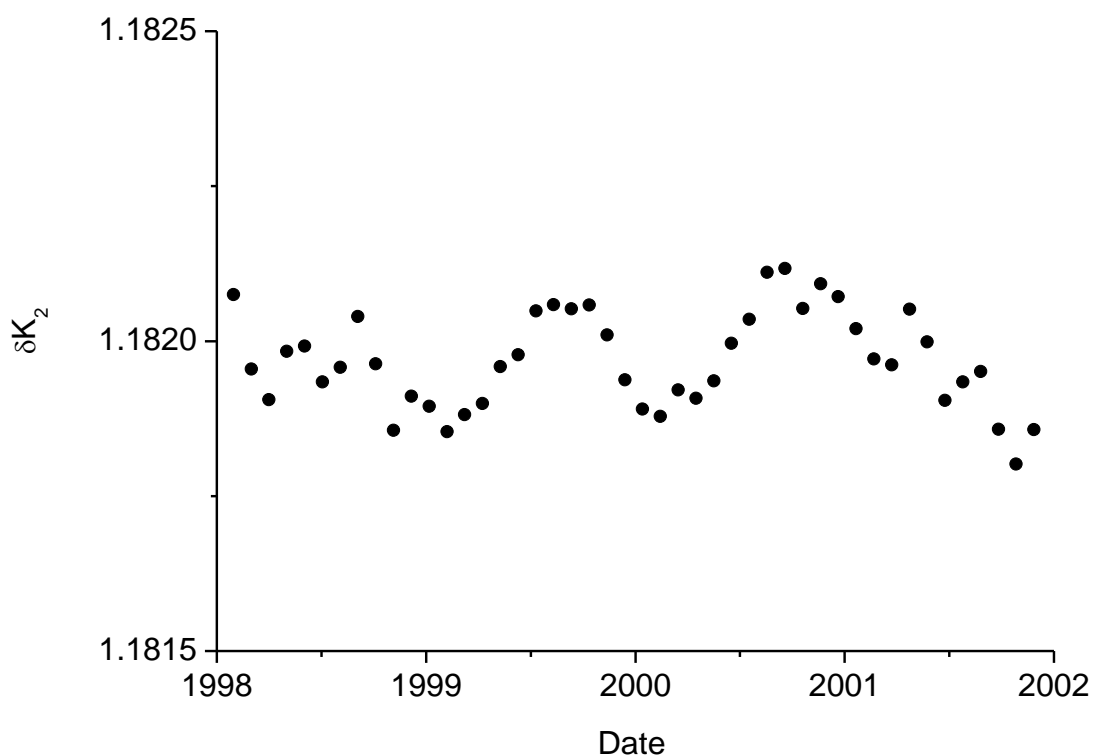
Fig. 4.21: Temporal variation of the K2 amplitude factor in Vienna from 1998 to 2002, obtained from the tidal analysis using ETERNA 3.4 software on yearly segments shifted month by month, exhibiting a small annual modulation.

More generally, the interpretation of these temporal variations in the tidal parameters is hard to carry on; it is difficult to distinguish whether they could reflect a geophysical meaningful process or if they are only due to instrumental instability and/or numerical effects. Atmospheric loading is one of the candidates for influencing the amplitude factors, as well as long term amplitude changes in ocean tides and hence in ocean tide loading (see Müller et al., 2011; Meurers 2012; Tai & Tanaka 2014).

It is known that tidal amplitude factors and phase delays may vary according to the location (see Melchior & de Becker 1983) because of ocean tidal loading (e.g. Baker & Bos 2003), Earth's ellipticity (Wang 1997), large scale mantle heterogeneities (Métivier and Conrad, 2008). However, possible changes in time of the Earth's tidal response are almost never mentioned except in some seismotectonic studies where there is a change in the ambient stress field (Westerhaus 1997).

The fact that any temporal variation in the tidal amplitude factor is highly improbable from a physical point of view and that the ratio $\delta M_2/\delta O_1$ is much smaller, it leads us to consider changes of instrumental origin, namely the scale factor converting observed feedback voltages to gravity, which may vary in time. For all the SG stations used in this study (for J9 two scale factors were used, one for each SG according to the

113

period of observations) we have assumed that the instrumental scale factor was constant during the total period.

In section 4.5 we will check the time stability of the instrument scale factor for the SG C026 installed at J9 Observatory, for which we possess a large number of parallel absolute gravity measurements spanning a large time interval (1997-2012).

4.5. Time stability of SG instrumental scale factor at J9

The long-term tidal stability is directly dependent on the stability of the scale factor of the relative gravimeters. This stability is even more critical for the spring gravimeters than for the SGs.

For each of the spring gravimeters used in this study the scale factors were obtained by different methods. The Askania gravimeter of Potsdam was calibrated in 1975 on the Czechoslovak Gravimetric Calibration Base and in 1992 by intercomparison with two LaCoste-Romberg G-meters, 156 and 249, belonging to the Geodetic Institute of Karlsruhe University. The L&R ET-19 installed at BFO was calibrated in 1988 using the same gravimeters L&R-G156 and L&R-G249. These instruments were repeatedly calibrated on the Hannover vertical calibration line. The Askania gravimeter in Walferdange was calibrated by adjustment with a Scintrex CG3M -265. We could check that these values did not fit well throughout the entire records, especially after some technical improvements of the instruments. Therefore, we decided to re-estimate the scale factors by comparing with theoretical tides as suggested by Goodkind (1996).

For SGs, the scale factor is much more stable in time than for the spring-type gravimeters. However, even for such a precise instrument the stability should be checked. It depends on specific properties of the gravity sensor and it is variable among different instruments so it must be determined experimentally for each one (GWR Instruments 1985). This factor is typically of the order of 10^{-6} ms^{-2}V^{-1}; this means that a signal as small as 10^{-12}m s^{-2} could be recorded with a nominal resolution of 1 μV. It is usually derived from a direct comparison with repeated absolute gravity (AG) measurements, which is the most widely used method (e.g. Francis, 1997, 2002; Tamura et al., 2001; Imanishi et al., 2002, Fukuda et al., 2005), although it can be done in several other ways, as for example by moving the instruments using an acceleration platform (Richter et al. 1995), by moving an external mass (Achilli et al. 1995, Falk et al. 2001) around the sensor or even using spring gravimeters (Riccardi et al., 2012; Meurers, 2012). It has been demonstrated repeatedly (e.g. Goodkind et al. 1991; Hinderer et al. 1994) that SG calibrations are very stable over time. It is known that the instrument can keep its calibration to better than one part in ten thousand (10^{-4}) over periods as long as several years (Merriam, 1993).

To have more insight on this effect, we have focused on the long (1996-2013) series recorded by the SG C026 installed at the J9 Gravimetric Observatory of Strasbourg, checking the stability of its instrumental sensitivity with the help of numerous calibration experiments of different durations (from 2 to 10 consecutive days) carried out by co-located AG measurements since 1997. I have been directly involved in the experiments conducted from June 2008.

Fig. 4.22: Pictures of both, the superconducting gravimeter SG C026 (left) installed at the J9 Gravimetric Observatory of Strasbourg, and the absolute gravimeter FG5#206 (right), used in most of the calibration experiments carried out at J9 Observatory since 1996.

The usual procedure to estimate the scale factor is by linear least-squares adjustment of the SG gravity data (usually in volts) with an absolute gravimeter used as reference. The method relies on the basic assumption that both sensors experience exactly the same gravity variations.

We have already mentioned in section 2.2 how is the raw data recorded by each kind of gravimeter. These raw SG and AG records must be corrected for any earthquake occurring at the time of calibration and cleaned for spikes, gaps and offsets if any. No other correction is applied (data from AG is treated with **g v.8** software, developed by Micro-g Solutions). Then, we fit the two raw data sets using a least squares approach according to the linear relation:

$$y_n = ax_n + b$$

where;

y_n represents the AG data and is expressed in μGal,

x_n represents the SG feedback output and is expressed in volt,

a represents the scale factor and is expressed in μGal/volt,

b is the offset and is expressed in μGal.

Assuming that the measurement error of y_n follows a normal distribution, we find the values of a and b that minimize the weighted sum of the squared residuals:

$$S_1 = \sum_{i=1}^{N} w_n (y_n - a x_n - b)^2$$

where N is the number of data values and w_n is the weight. We minimize S_1 with respect to the unknown parameters leading to the well-known normal equations.

We calculate the scale factors considering two different kinds of AG raw measurements (an example of each raw AG data, drop values and set values, is shown in Fig. 4.23):
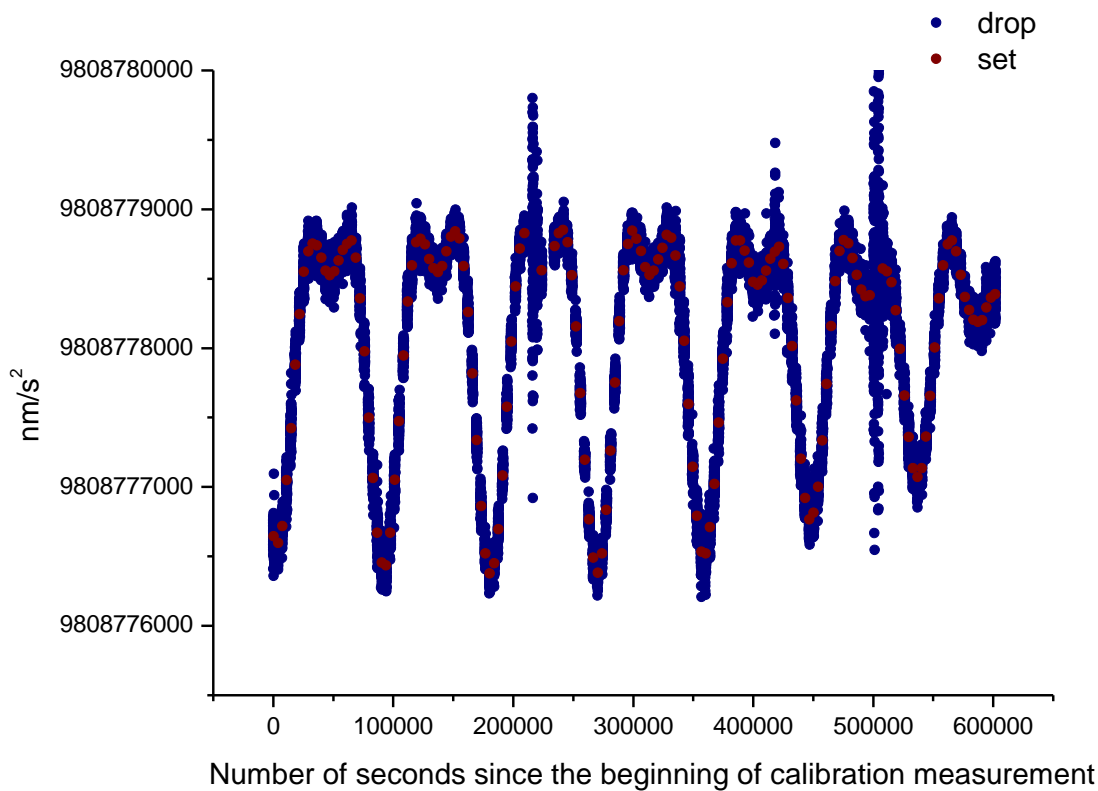
Fig. 4.23: Example of raw drop data (blue dots) and raw set data (red dots) from one of the AG measurements used in one of the SG calibration experiments carried out by direct comparison at J9 observing site (June, 2009).

* First we used the individual drop gravity values of the AG measurement (as we have explained in section 2.2, each drop corresponds to an individual free fall experiment, where the value of g is determined by a least squares fit of the trajectory data using approximately 700 pairs of time and distance traveled by the mass, using the equation 2.24) and we superimpose the SG output by comparing each drop of the AG to the closest sample of the SG and then apply the linear least squares method. In this case we have a large number of points for the adjustment but with large error bars on

the AG drop values. Usually, there is one drop every 10 s, during sessions which last from 3 to 8 days.

* Second we use the set gravity values of the AG, (each 'set value' represents the gravity averaged over the set interval (typically up to 60 min)). From the 1 or 2 second sampled SG records (depending of the available data acquisition system) we pick up the SG values for all the time interval corresponding to each set, and we estimate the average values for each of these set periods (same averaging length for SG and AG) before applying the linear least squares method. In this case, we have less data for the adjustment but with smaller error bars on the AG set values as previously on the drop values.

Once we have estimated for each experiment the scale factors using each of the two kinds of AG data (drop/set values), we investigate their temporal evolution from 1997 to 2012. The values of the scale factors estimated using either the drop or the sets are close, with a better standard deviation when using individual drops method, although with a slightly better time stability in case of the sets (Table 4.4).

Other experiments have been conducted to estimate the temporal evolution of these scale factors at several stations. Meurers (2004, 2012) found that for the GWR C025 installed in Vienna the scale factor was temporarily stable with a maximum variation less than 0.01%. Also Kroner et al. (2005) obtained a variation in the range of 0.01% for the dual-sphere SG sensor in Jena. For Strasbourg variations of about 0.3 % were found (Amalvict et al. 2001; Rosat et al. 2009) using the AG set values and their error bars. Our results agree with these previous two studies (Fig. 4.24). The mean scale factors with their uncertainty and their stability are given in Table 4.5. The first column is the weighted mean value and uncertainty computed from all the individual scale factors including their error bars. The second column is the relative uncertainty and, as before for the tidal factors, we use the distribution of the scale factors to compute the time stability at 2σ.
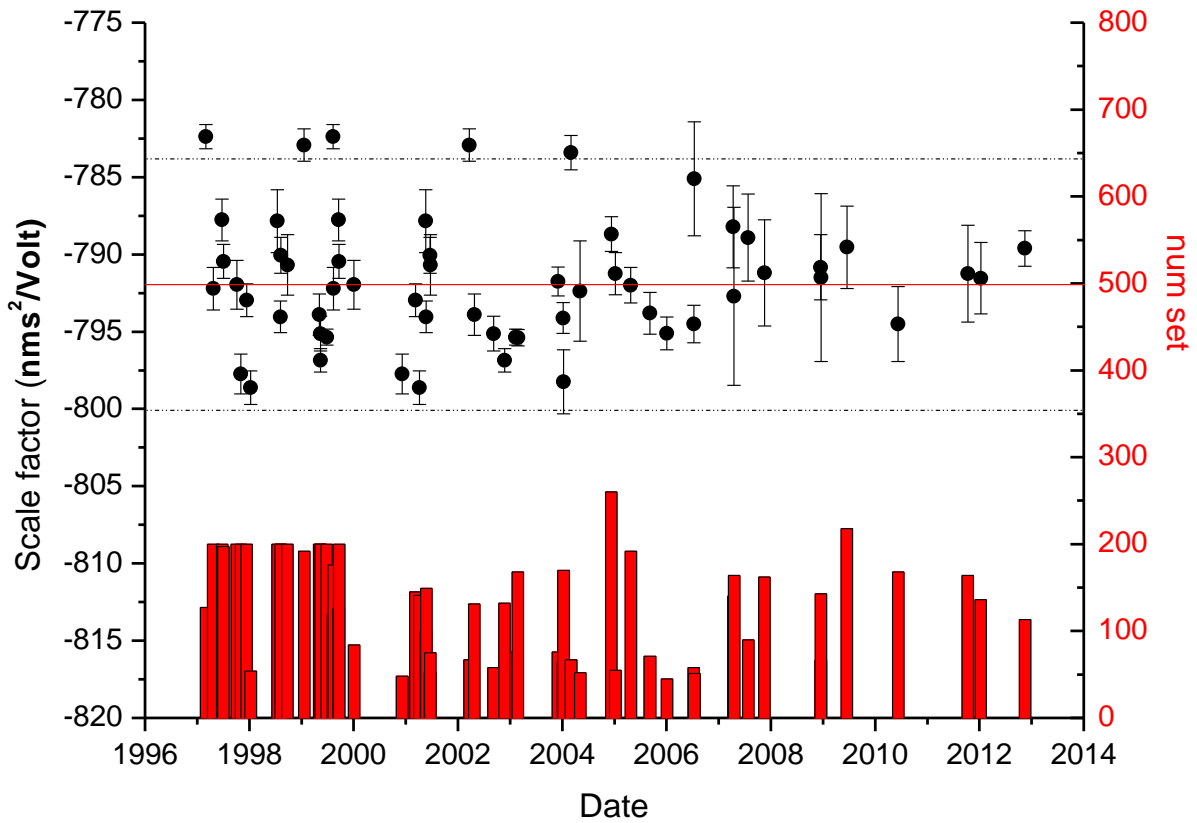
Fig. 4.24: Time stability of the scale factors of the SG C026 at J9 station, from 1997 to 2012. The numbers of sets used for the intercomparison with the AG measurements are represented by the column bars. These calibration factors have been calculated using the individual drop values. Mean weighted value is indicated by a red line and the dotted lines represent the $\pm 2\sigma$ confidence interval.

For the SG C026, we usually employ a constant scale factor of -792 nm/s^2/V, corresponding to the mean value plotted in figure 4.24.

Table 4.5: Scale factor determinations (mean weighted value, absolute and relative uncertainty and time stability ($\pm$ 2σ confidence interval) according to the AG set by set or AG drop by drop processing of SG/AG data at J9 station.

Methodology	Scale factor (nm/s^2/V)	uncertainty	Stability (2σ)
Set by set	-790.76 $\pm$ 2.34	0.29 %	1.48 %
Drop by drop	-791.96 $\pm$ 0.91	0.11%	1.55 %

Notice that we have weighted the AG measurements using the set errors from AG measurements in the fit of the scale factor, even if the resulting uncertainty is larger than without weights (Table 4.6). The calibration accuracy is in fact limited by the AG drop to drop scatter.

Table 4.6: Scale factor determinations (mean weighted value) with (left) and without (right) the errors from AG measurements in each individual calibration experiment at J9 station.

Methodology	Scale factor (nm/s²/V) *with AG errors*	Scale factor (nm/s²/V) *without AG errors*
Set by set	-790.76 ± 2.34	-789.98 ± 0.74
Drop by drop	-791.96 ± 0.91	-792.27 ± 0.23
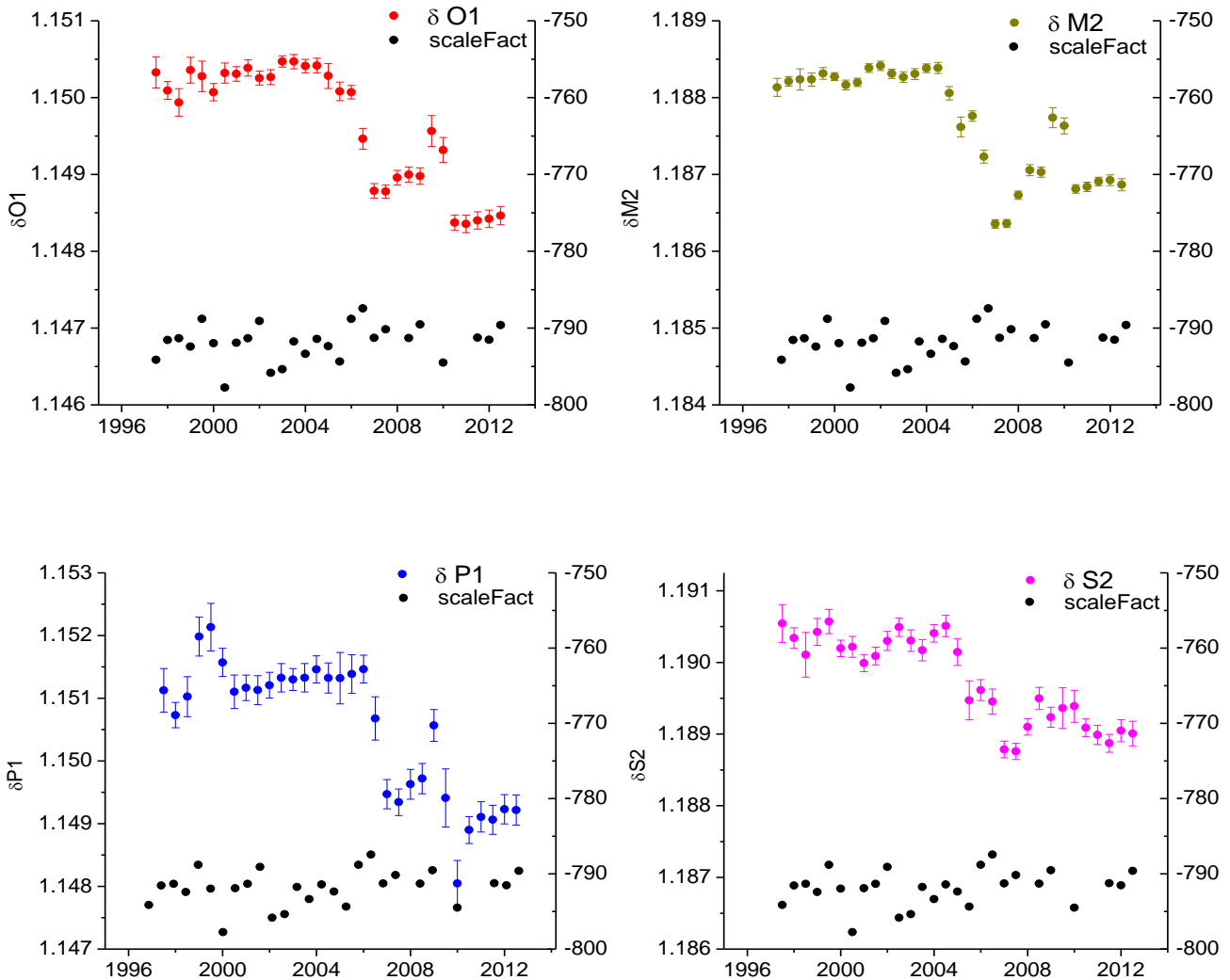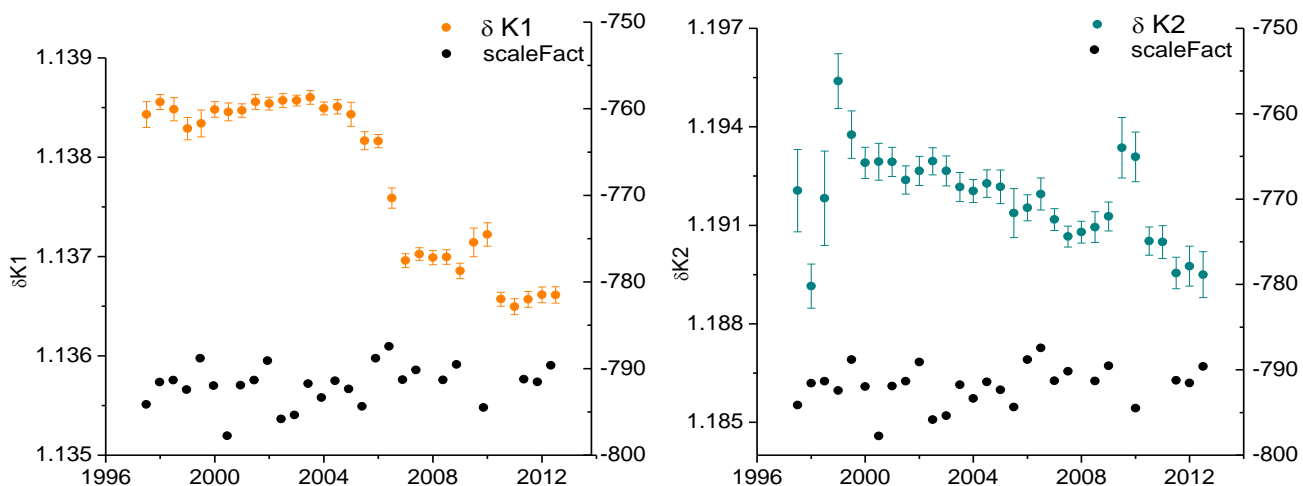
Fig. 4.25: Temporal variations of the tidal amplitude factors for the main diurnal and semidiurnal waves (O1, P1, K1, M2, S2 and K2) compared to the temporal variations of the scale factor at J9 station.

To check any possible correlation between the time variations of the scale and delta factors, we have superposed them in Fig. 4.25. There is no clear correlation between any of them (as show the examples in figure 4.26 where the correlation coefficients are -0.25 and 0.09 respectively).
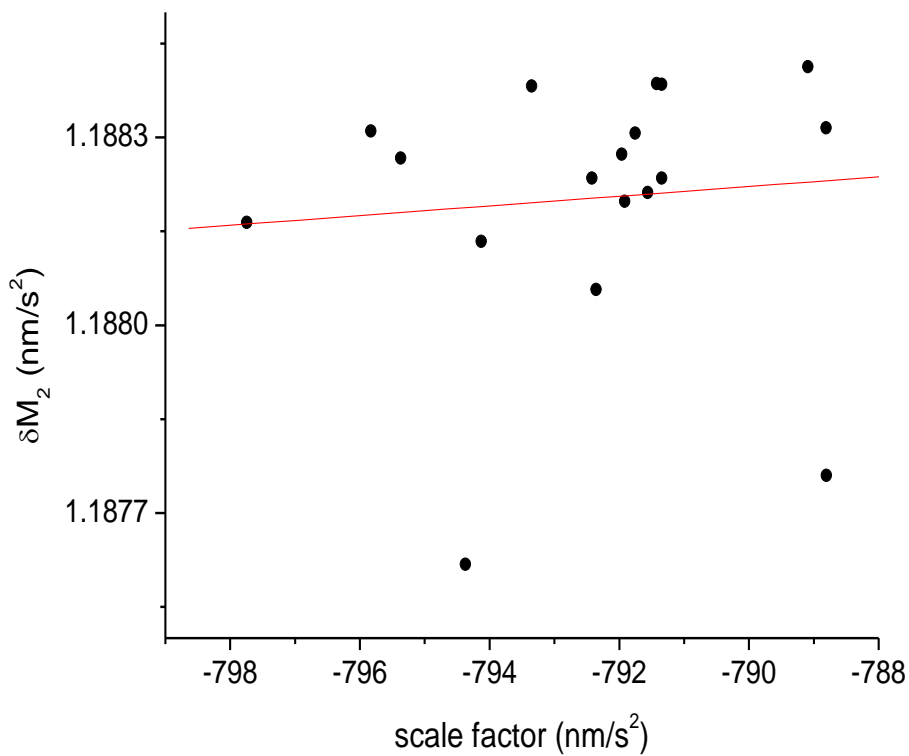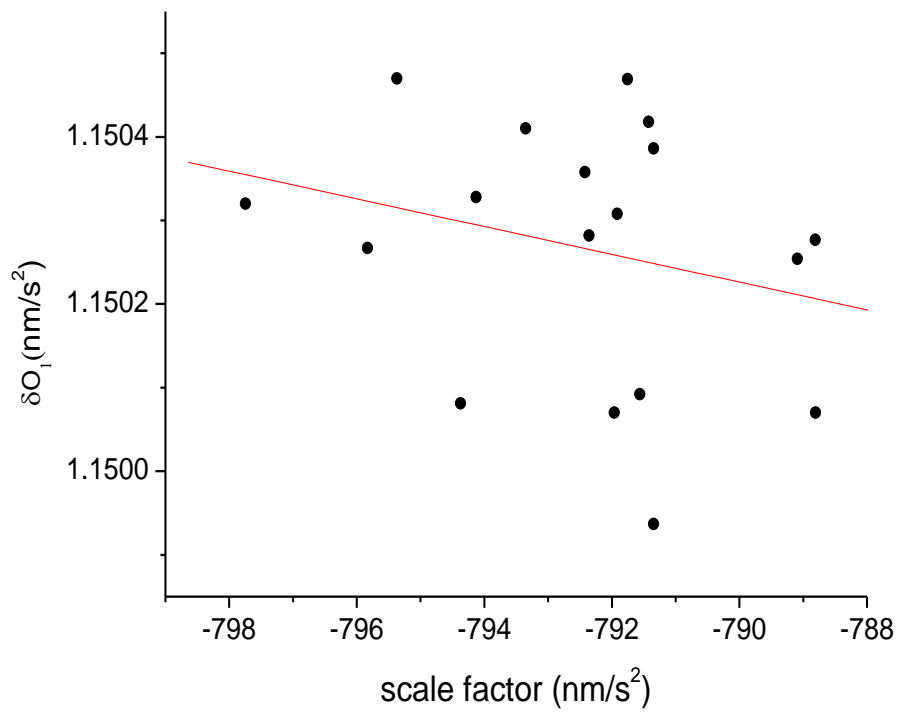
Fig. 4.26: Example of weak correlation between the temporal variations of the tidal amplitude factors and the temporal variation of the scale factors at J9 station, for a diurnal wave (O1, left plot, (correlation coefficient = -0.25)) and for a semidiurnal wave (M2, right plot (correlation coefficient = 0.09)).

Therefore, the observed time variations of delta factors may be mainly due to noise variations, as suggested in section 4.3. It turns out that the internal SG C026 stability ($\sim$ 0.10%) we derived by averaging the values obtained for the diurnal and semidiurnal tidal bands is much better than the one that can be achieved by SG calibration repetitions using AG data ($\sim$ 1.4%).

Since a clear part of the time changes of the delta factors is due to variable noise content, we can infer that the intrinsic instrumental stability of the SGs is very high, at least better than 0.15% in general or even 0.05% for some SGs (as in Moxa or Vienna stations).

We used very long gravity records available in Europe: 3 data sets recorded by spring gravimeters at BFO, Potsdam and Walferdange, and 8 long SG data sets recorded at different European GGP sites with at least 9 years of continuous data to investigate the sensitivity of each instrument, using the temporal variations of the delta factors for the main tidal waves (O_1, P_1, K_1, M_2, S_2 and K_2) as well as the $\delta M_2/\delta O_1$ ratio. These tidal analyses have been performed on the gravity records rearranged in temporal subsets (yearly data sets, shifted month by month) to check the time stability of the tidal responses. For each instrument, the temporal evolutions of the tidal parameters were investigated in detail and compared among them. We also retrieved the evolution of the ratio $\delta M_2/\delta O_1$, which is independent of the calibration. One of the main limitations in the use of spring gravimeters is their large irregular instrumental drift (see figure 4.27).
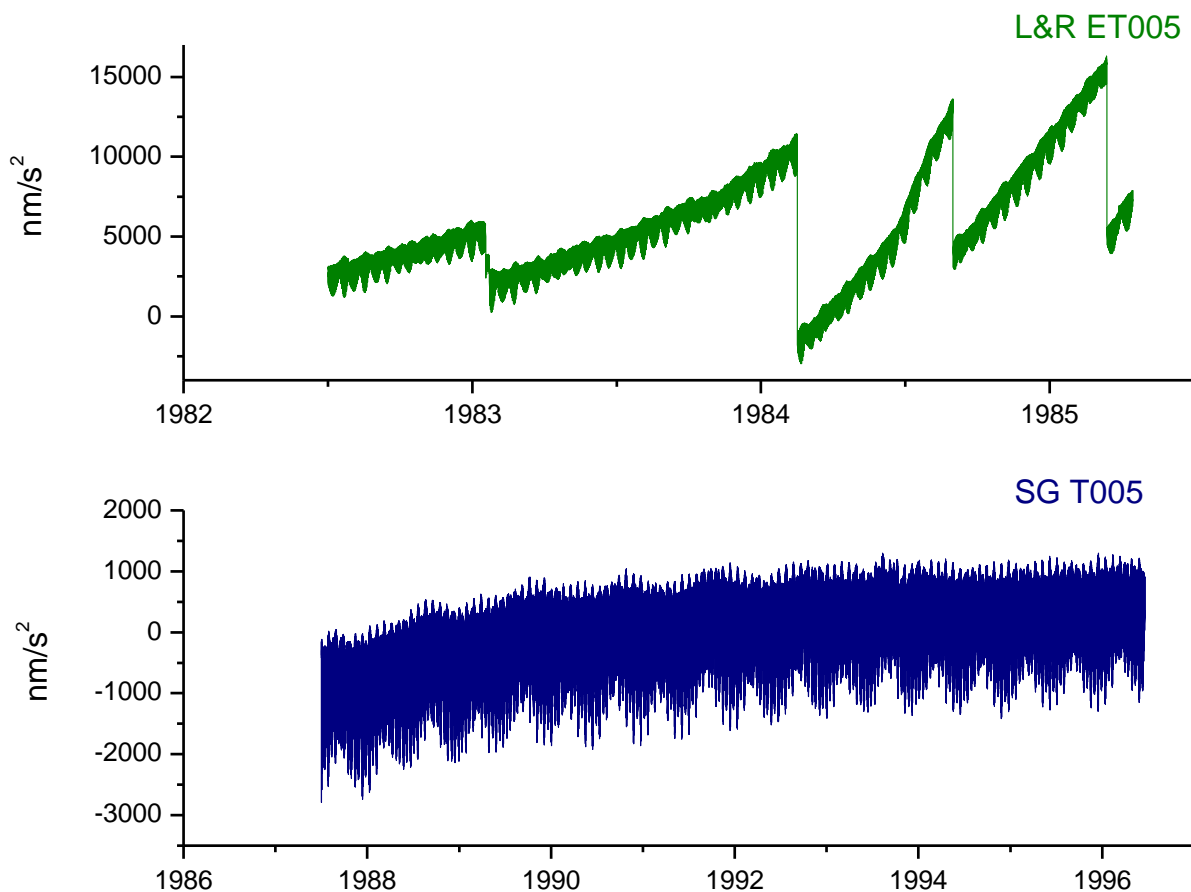
Fig. 4.27: Comparison of the instrumental drift of a spring gravimeter, the L&R ET005 (upper plot) and a superconducting gravimeter, SG T005 (lower plot) both of them installed at J9 Observatory.

Compared to the spring gravimeters, the superconducting gravimeters provide unprecedented long term stability (for instance, the stability for the most stable spring gravimeter (Potsdam) is nearly four times lower than the worst stability of the results obtained with SGs). The observed temporal evolution of the tidal delta factors in Strasbourg is found to be very similar to other European SG stations with stability between 0.03% and 0.3%, and some time fluctuations with a seasonal oscillation at a few sites.

In case that these temporal variations reflect a geophysical process, they should reflect it similarly at most European sites, which is not the case in our results. It is possible that variations in ocean loading could generate small variations in the delta factors at some European stations (for which ocean loading is similar). It may be more or less hidden by ambient noise, instrumental problems, hydrological effects, etc.

As the variations of the ratio $\delta M_2/\delta O_1$ are much smaller than the variations for each individual gravimetric factor, it led us to consider that some part of the tidal factor fluctuations could be due to changes of instrumental origin (e.g. calibration). Therefore, we investigated the long-term stability of the scale factors of the gravimeters. In particular, we checked the stability of the scale factor for the SG C026 installed at J9 for the period 1997-2012 where numerous AG/SG calibration experiments were available. It turns out that the internal SG C026 stability ($\sim 0.1\%$) as derived from the tidal analyses is more than 10 times better than the one that can be achieved by SG/AG calibration repetitions ($\sim 1.4\%$), no matter which AG/SG fitting method have been used to calculate the values of the scale factors. We do not find any clear correlation between variations of tidal factors and variations of scale factors. Consequently, it is highly possible that the observed time variations of delta factors are due mostly to the noise variations as shown by the correlation found between delta factor deviations and noise level changes.

Chapter 5

Contribution of long data series to tidal gravimetry

Some of the results presented in this chapter (sections 5.2 and 5.3) have been published in Calvo et al. (2014a).

5.1. Introduction

Long term gravity records are of great interest when performing tidal analyses. Indeed, long series enable to separate contributions of near-frequency waves (the frequency resolution is the inverse of the data length) to detect very weak amplitude signals and also to detect low frequency signals (e.g. long period tides and the gravimetric effect of the pole tide) (the lowest frequency in the spectrum is also the inverse of the data length). In addition to the length of the series, the quality of the data and the temporal stability of the noise are also very important. As we have seen in previous chapter the long superconducting gravimeter records are preferred to the long spring gravimeter records, even when they are slightly shorter, mainly because of their long-term stability, lower noise level and very small linear instrumental drift.

Previously in chapter 3 we have already referred to the long tradition of recording solid Earth tides at Strasbourg, and we have also mentioned the gravimeters of different types that have been recorded at J9 Observatory. Considering only the longest series, we have therefore almost 40 years of consecutive gravimetric records (from 1973 when the L&R ET005 was first installed, to nowadays) at J9. Among these data, over 27 years have been registered by two models (T005 and C026) of superconducting gravimeters consecutively installed there, leading after merging to the longest available series ever recorded by SGs at the same site.

As both SGs have been installed not only in the same observatory but also on the same pillar, and that there were only few days between the removal of the old gravimeter and the installation of the new one (11 days compared to 27 years, almost negligible), we can merge the SG T005 and SG C026 series into one series filling up the gaps between instruments using a local tidal model obtained from tidal analyses at the station. Before merging them, both series have been pre-processed and corrected independently (using for each one its own calibration factor and phase shift).
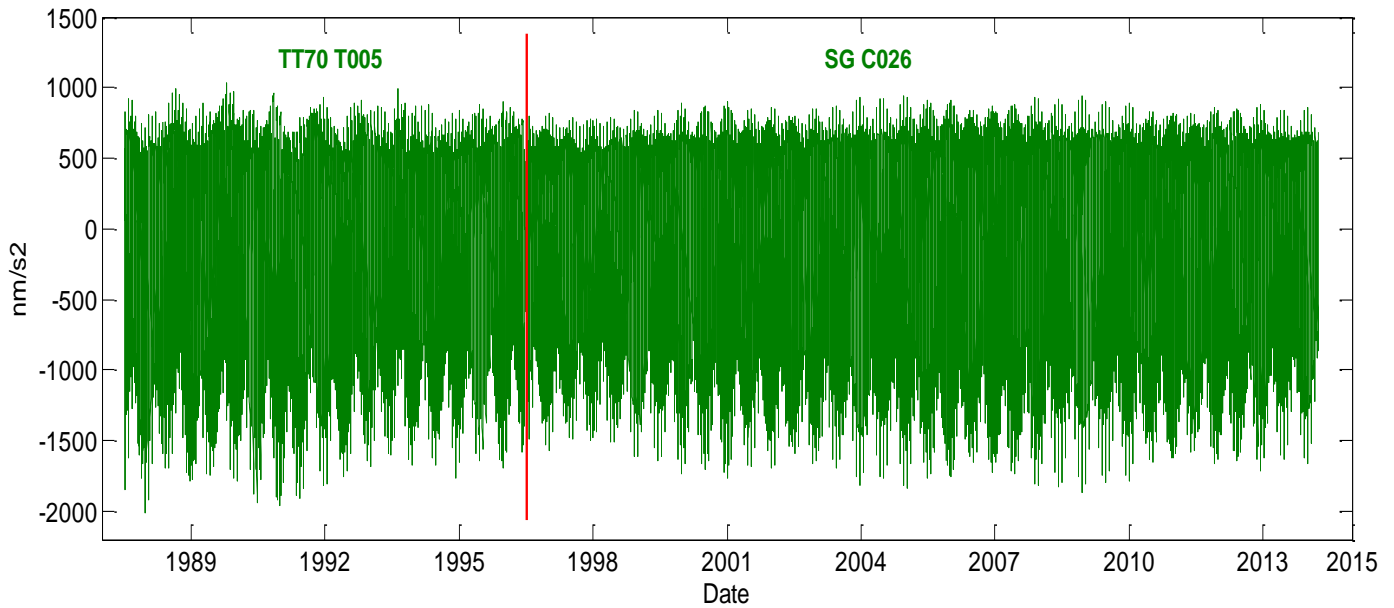
Fig. 5.1: Temporal gravity recorded by superconducting gravimeters at the Gravimetric Observatory J9, from 1987 to 2014.

We expect to benefit from this unprecedented length both in achieving high spectral resolution in the tidal bands and also in obtaining higher precision in the tidal determination. Thus, we will attempt to retrieve small amplitude waves in the major tidal groups (e.g. tides generated by the third-degree potential), to separate waves close in frequency and to detect very low frequency signals that have never been observed in gravity data of shorter duration.

5.2 Analysis of small-amplitude tidal constituents

Firstly we are going to investigate some of the very **weak amplitude tidal signals** contained in the gravity data that can be observed using long gravity records. Thus, we compare the spectral analysis from two of the observed gravity series that we have already studied in section 4.2 and 4.3; the spring gravimeter series recorded at Black Forest Observatory (L&R ET19) and the SG series recorded at J9 with two SGs (T005&C026).

We use 8400 days (~23 years) of data for each station, corresponding to the common interval between both stations (1988-2012). Even if the length is the same for both series, the lower noise level of the SG series with respect to the spring gravimeter allows us to detect some low-amplitude tidal waves. An example is given in the diurnal tidal band with the tidal wave $2NO_1$ (amplitude 1.98 nm/s^2), and in the semi-diurnal tidal band with the waves BET_2 (amplitude 1.2 nm/s^2) and LAM_2 (amplitude 3.5 nm/s^2). These tidal waves are clearly hidden in the instrumental noise of the spring gravimeter (figure 5.2). Our noise analyses in previous section and the knowledge that BFO is a low-noise site over a wide frequency range (Zürn et al., 1991a; Widmer et al, 1992) enable us to state that the observed noise is mostly instrumental.
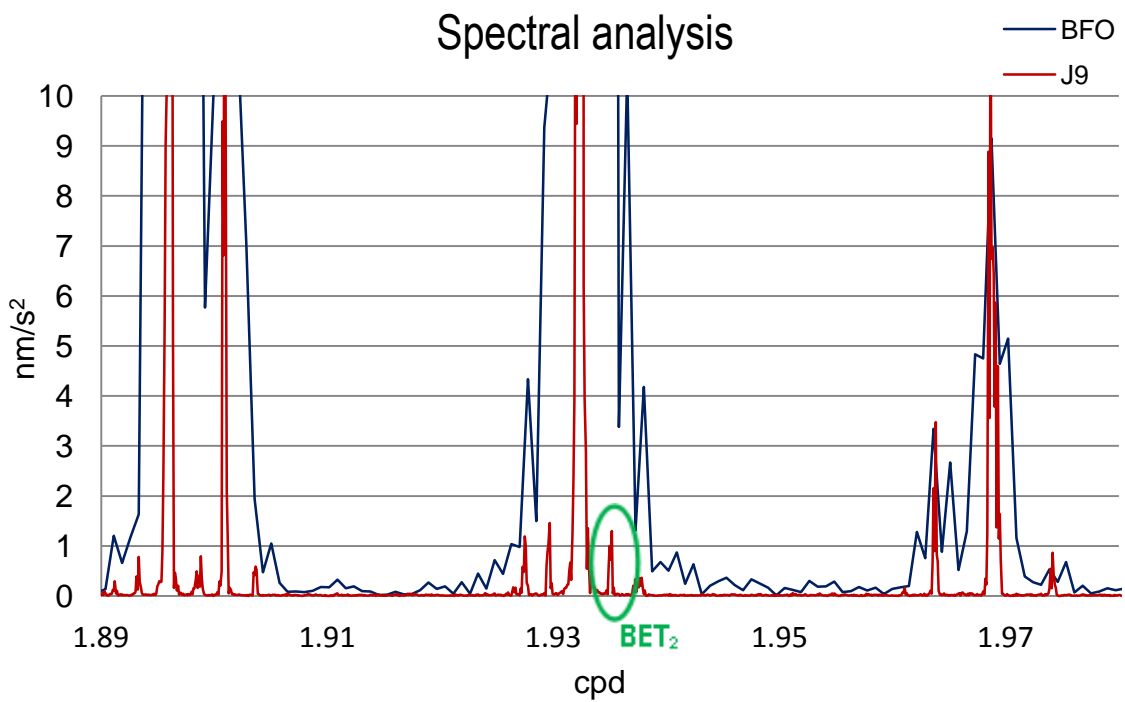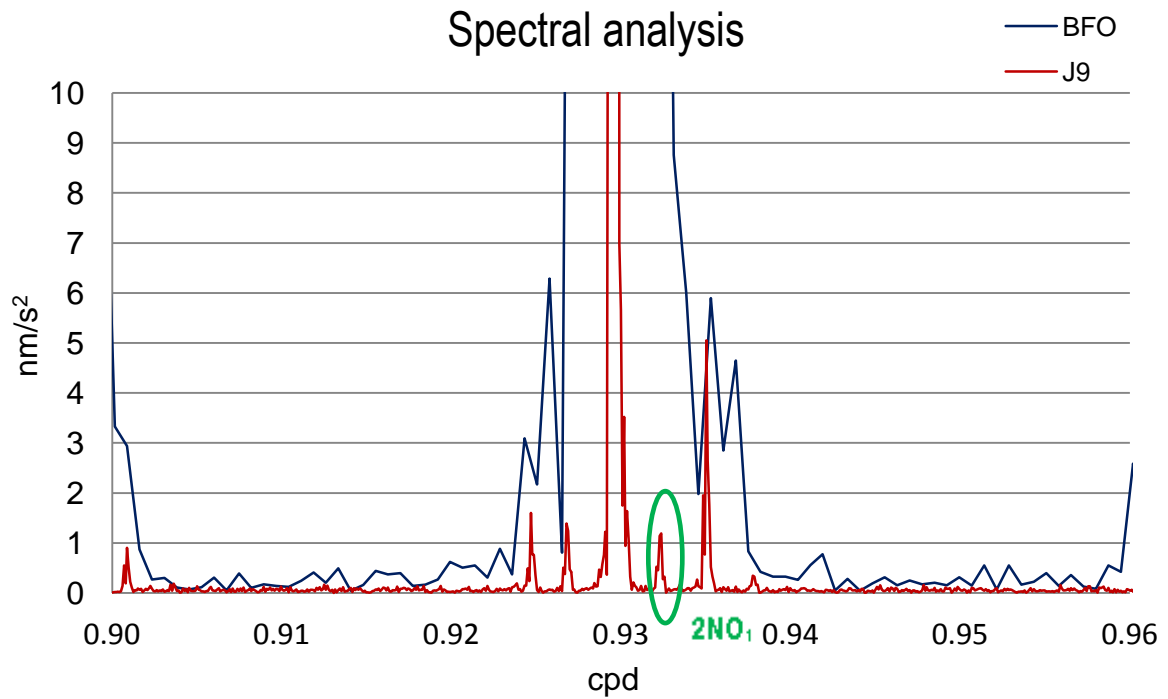
Fig. 5.2: Amplitude spectra of J9 gravity series (SG) and BFO series (L&R) from the same time span (8400 days) in the diurnal (up) and in the semi-diurnal (down) tidal bands.

Now that the advantage of using SG series instead of spring series has been clearly demonstrated, we will focus for the rest of this chapter on the 2 SG series recorded at J9. If we compare the spectral analysis from the 9 year series of the SG T005 to the merged 27-year series recorded by T005 and C026 at J9, we observe that the total length of the series allows us to detect some new low-amplitude tidal waves that were hidden in the shorter series such as the diurnal k1x- (amplitude 8.5 nm/s^2), and the semi diurnal $3KM_2$ (amplitude 0.51 nm/s^2) tidal waves (figure 5.3).
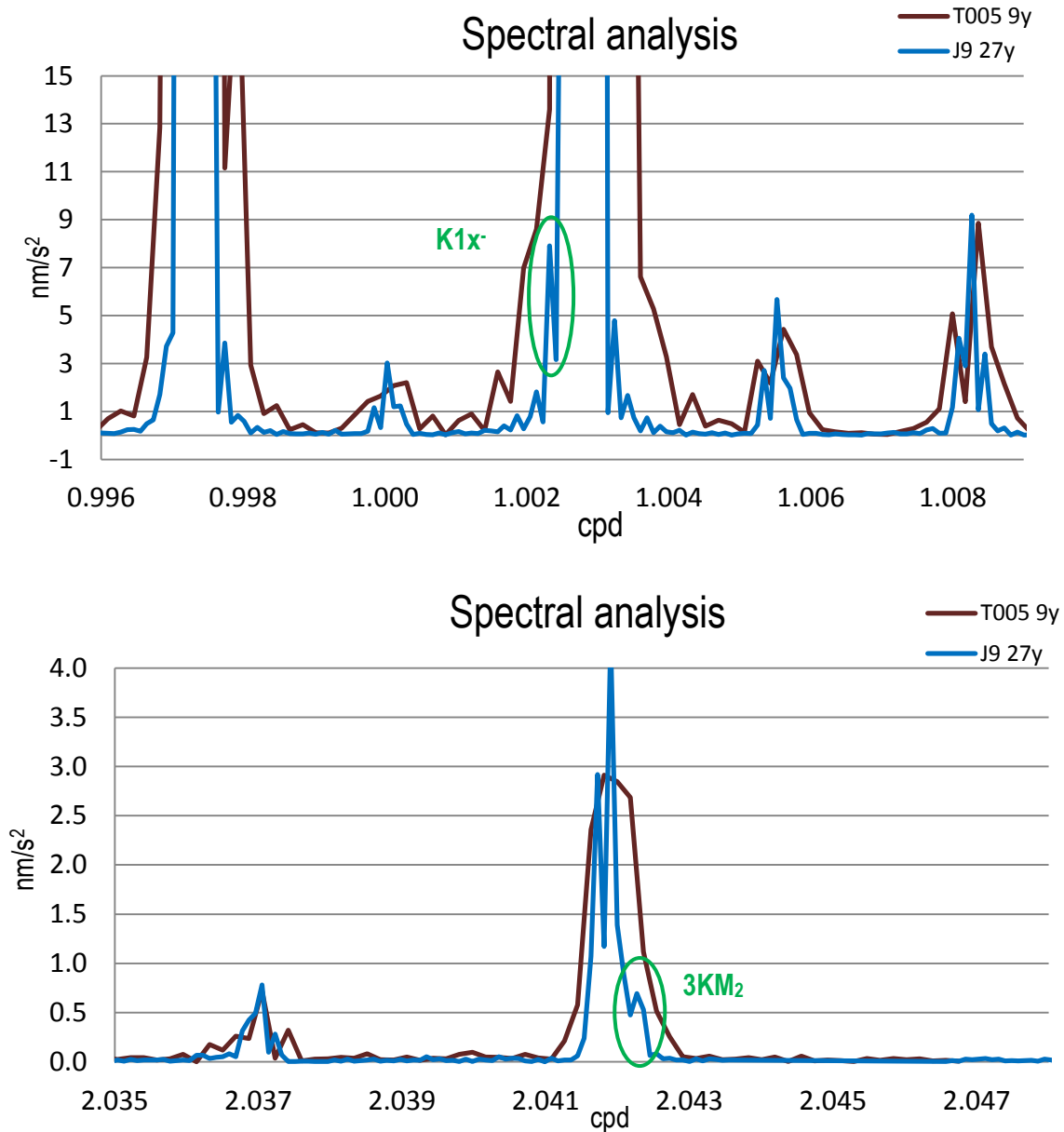
Fig. 5.3: Amplitude spectra of J9 gravity series, 9 year of T005 in brown, and 27 years of T005&C026 in blue, in the diurnal (up) and in the semidiurnal (down) tidal bands.

However, the signal-to-noise ratio (SNR) is not only improved by increasing the length of the data set, but it is also strongly influenced by the quality of data.

In our case the C026 series is 9 years shorter than the total series (T005+C026), although being less noisy than the total series (due to noise contributed by the T005) we are able to detect in the spectral analysis of C026 series some low-amplitude tidal waves that are hidden by the instrument noise in the total (T005+C026) series as for example SO_1 (frequency = 1.0704 cpd) and $2NO_1$ (frequency = 0.93015 cpd) (cf. figure 5.4).
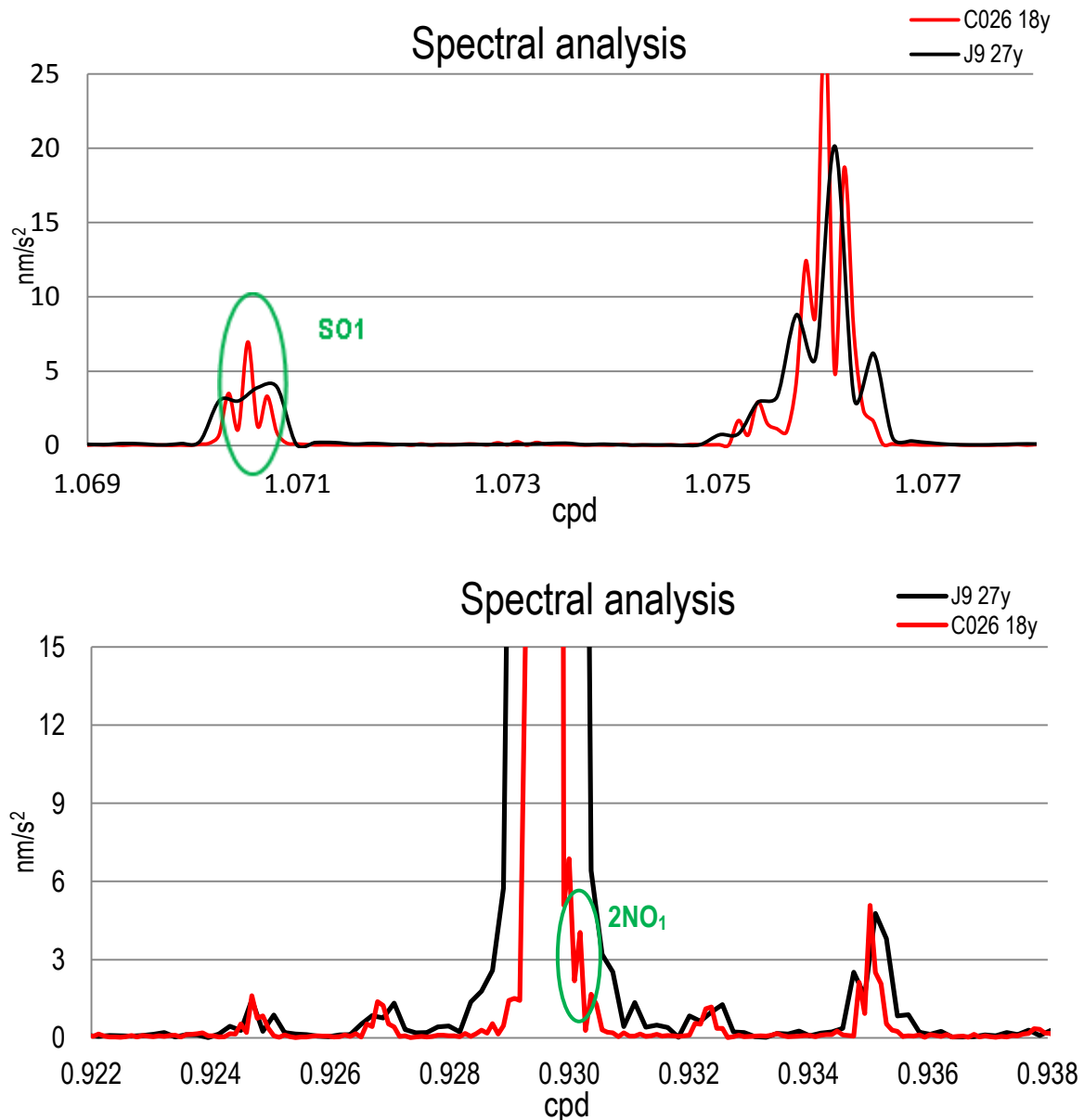
Fig. 5.4: Spectral analyses in the diurnal frequency band of the 18 years series of the SG C026 in red, and of the merged 27 year series recorded both by T005 and C026 in black, at Strasbourg J9 Observatory.

We have determined that we still have to wait 5 more years until the SNR of the full series is larger than the SNR of the C026 alone. This comes from the fact that the SNR of an undamped harmonic signal is given by:

$$\text{SNR} = A \sqrt{\frac{N}{2 \cdot \sigma}}$$

where:

A is the amplitude of a periodic signal,

N the number of samples

σ the white noise amplitude (root mean square).

In our case, $\sigma_{T005} \sim 2\sigma_{C026}$

Then, to achieve a $SNR_{TOTAL} \geq SNR_{C026}$ being

$$\sigma_{TOTAL}^2 = \frac{N_{T005}\sigma_{T005}^2 + N_{C026}\sigma_{C026}^2}{N_{T005} + N_{C026}}$$

We need the length of the C026 series to be $N_{C026} = 23$ years. That is, 5 more years that we have currently available.

In **Annex E** some other examples of detection of weak amplitude tidal signal are shown.

Another example of small tidal wave detection is given in figure 5.5, which exhibits the delta factors of the diurnal tidal waves ($3MK_1$, M_1 and $3MO_1$) caused by the potential of degree 3 around the FCN (Free Core Nutation) resonance frequency. It is interesting to note that the resonance only alters the amplitude of the degree 2 tides as expected from the theory (e.g. Hinderer & Legros 1989). Small amplitude tides of degree 2 that can be separated thanks to the length of the data nicely superimpose onto the resonance curve (least squares fitted) in a way similar to the more classical waves like O_1, K_1, PSI_1 and PHI_1 (Florsch & Hinderer 2000; Rosat et al. 2009b).
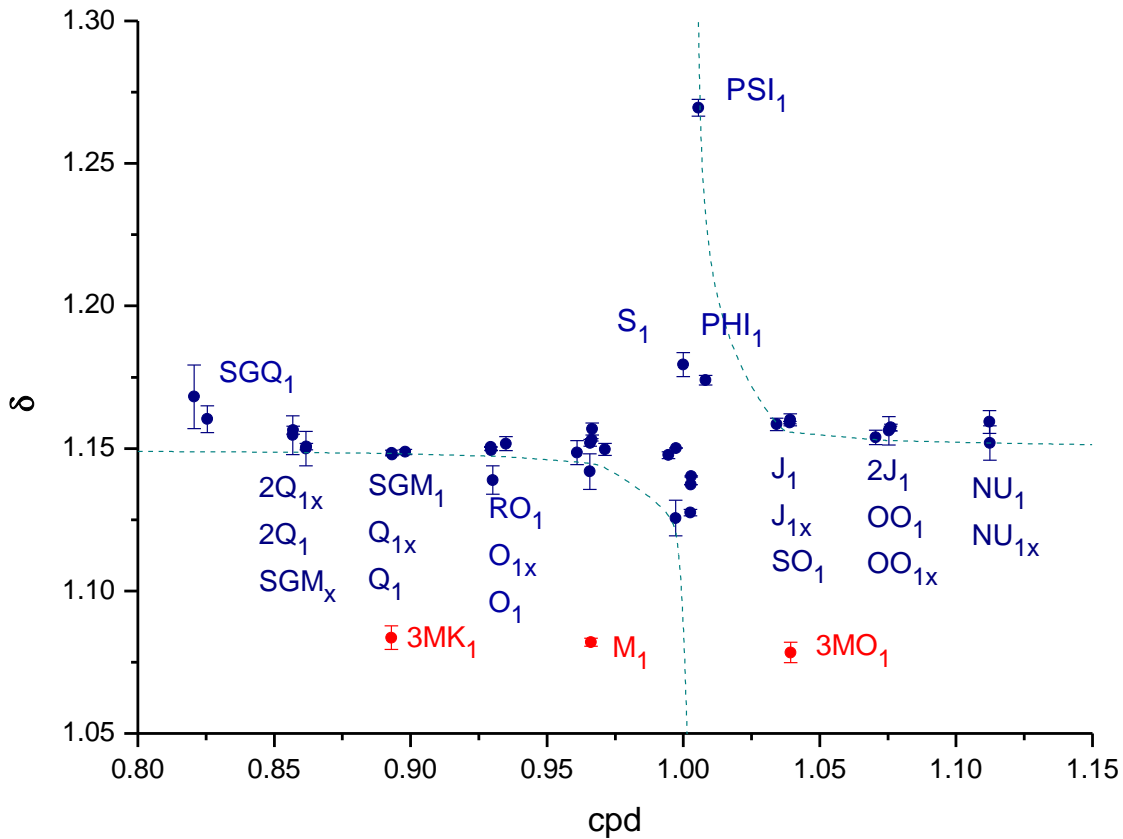
Fig. 5.5: Amplitude factors in the diurnal frequency band using the complete (9760 days, 26.7 years) SG record (T005 + C026) in Strasbourg J9 Observatory. Degree-2 tidal factors are shown in blue dots and degree-3 tidal factors (3MK1, M1, 3MO1) in red dots.

Some of the main tidal waves generated by the tidal potential of third degree in the diurnal, semi diurnal and ter diurnal bands have already been determined. The ter diurnal M_3 was determined very early (Melchior and Venedikov, 1968), despite of its small amplitude. Using the 17 year long observation at Potsdam (Askania 222), Dittfeld (1991) succeeded for the first time in separating the diurnal (M_1) and two semidiurnal ($3MK_2$ and $3MO_2$) waves from their neighboring second degree terms. Melchior et al (1996) used 12 year series of observations with the SG T003 at Brussels to separate M_1, $3MK_2$ and $3MO_2$ with a precision better than 0.5%. More recently, Ducarme (2011) was able to determinate M_1, $3MK_2$, $3MO_2$ and M_3 with a precision of 0.1%, using long series from 17 SGs.

If we consider the development of the tidal potential expressed as a function of the coordinates of the observation point on the surface of the Earth and the celestial body as a combination of geocentric and celestial coordinates (equation 2.7), we can see

that the tidal potential of degree 3 is generating tidal waves in the Long Period (m=0), Diurnal (m=1), semi diurnal (m=2) and ter diurnal (m=3) frequencies.

Expressing the potential as a function of the astronomical arguments, it can be developed in a sum of harmonic constituents (equation 2.8). In table 5.1 we show a selection of the third degree tides from Doodson's full development.

Table 5.1: Principal constituents deriving from W_3 in the diurnal and semidiurnal frequency bands.

Symbol	Doodson Argument	Astronomical Argument	Angular speed (º/h)	Amplitude (nm/s²)	Origin (L, lunar; S, solar)
$3MK_1$	135·555	$\tau - 2s$	13.394020	2.01	L decl.
$3ML_1$	145·655	$\tau - s + p$	13.947677	1.03	Ellipt. M_1
M_1	155·555	τ	14.492052	6.28	1st order elliptic tide from K_{1m}
$3MO_1$	175·555	$\tau + 2s$	15.590085	2.29	L decl.
$3MJ_2$	235·655	$2\tau - 2s + p$	27.890713	1.78	Ellipt. $3MK_2$
$3MK_2$	245·555	$2\tau - s$	28.435088	6.47	L decl.
$3MO_2$	265·555	$2\tau + s$	29.533121	5.97	L decl.
$3MQ_2$	275·455	$2\tau + 2s - p$	30.077495	0.33	Ellipt. $3MO_2$
$3KM_2$	285·555	$2\tau + 3s$	30.631154	0.55	L declinational wave
MN_3	345·655	$3\tau - s + p$	42.931782	1.44	Ellipt. M_3
M_3	355·555	3τ	43.476156	5.23	Principal terdiurnal lunar tide.

5.3 Analysis of near frequency tidal components

Another benefit provided by the long term data series is that they allow us to separate contributions of near frequencies (e.g. the annual and the Chandlerian components of the Earth's polar motion). The minimum frequency resolution required to separate two neighboring waves is inversely proportional to the length of the data set. Now we have nearly 10.000 days of data recorded continuously at J9 by SGs, leading to a frequency resolution of 10^{-4} cpd.

As shown in figure 5.5 for the diurnal band, performing a tidal analysis on the total length series enables to separate several groups of tidal waves that were not separable before with shorter data series. There are also several new tidal waves that can be separated in the semi-diurnal, ter-diurnal and quart-diurnal frequency bands, as shown respectively in figures 5.6, 5.7 and 5.8.
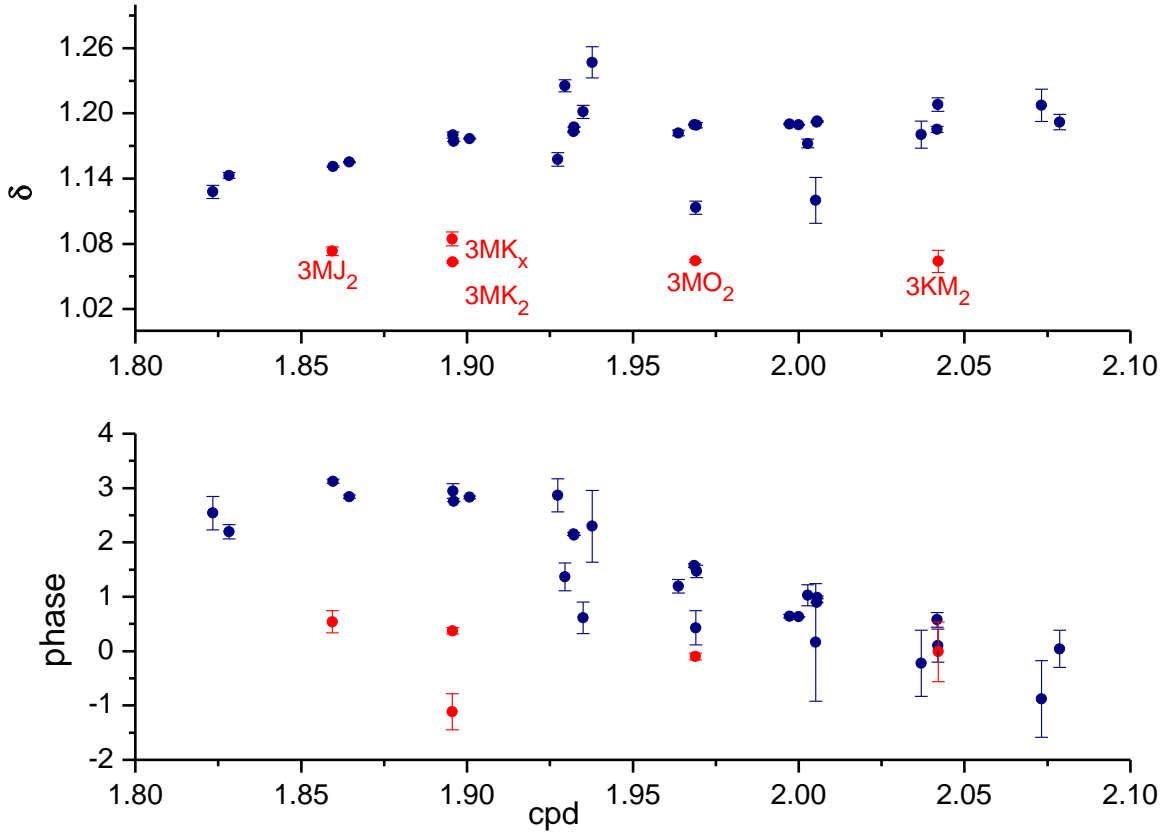
Fig. 5.6: Amplitude factors in the semi diurnal frequency band using the complete (9760 days, 26.7 years) SG record (T005 + C026) in Strasbourg J9 Observatory. Degree-2 tidal factors are shown in blue dots and degree-3 tidal factors ($3MJ_2$, $3MK_x$, $3MK_2$, $3MO_2$, $3KM_2$) in red dots.
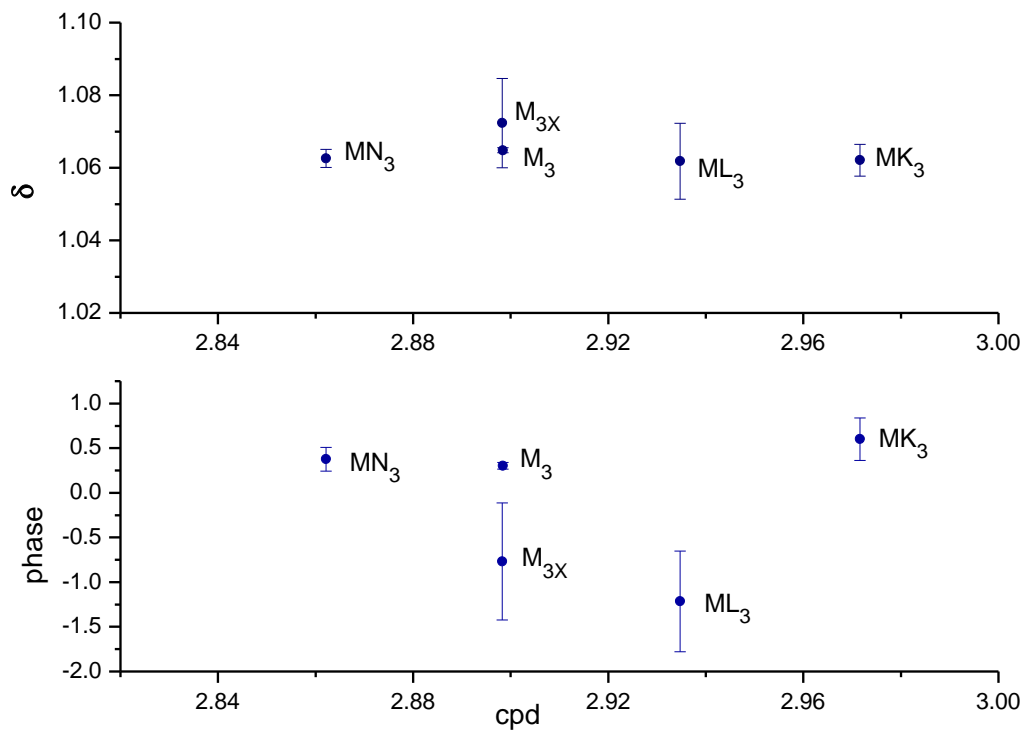
Fig. 5.7: Amplitude factors in the ter diurnal frequency band using the complete (9760 days, 26.7 years) SG record (T005 + C026) in Strasbourg J9 Observatory.
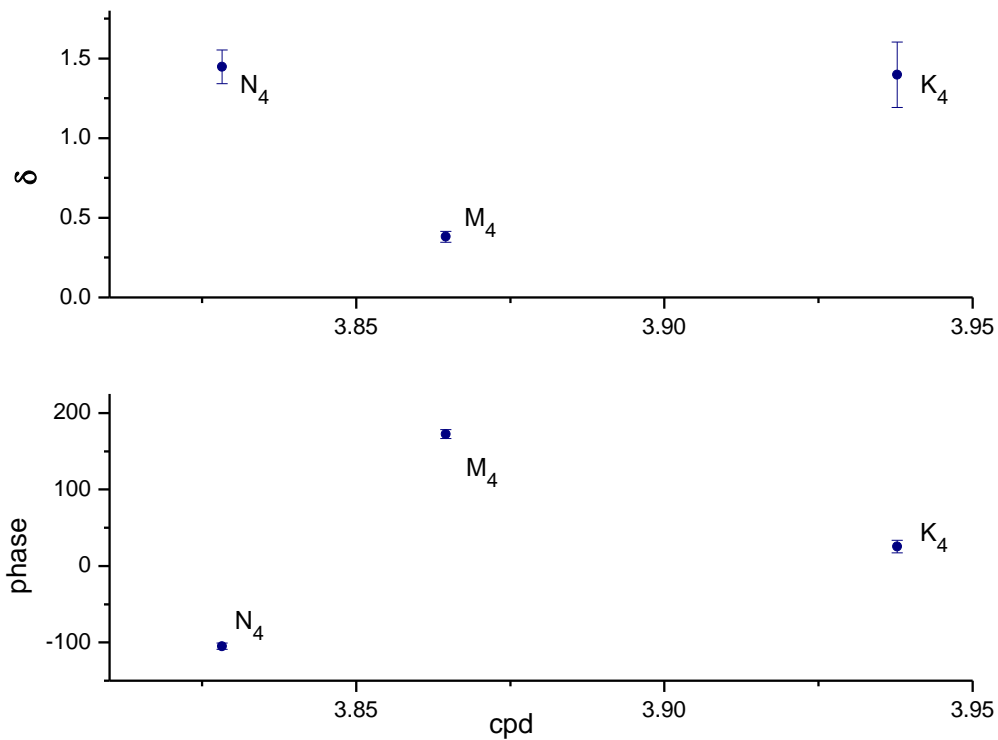
Fig. 5.8: Amplitude factors in the quart diurnal frequency band using the complete (9760 days, 26.7 years) SG record (T005 + C026) in Strasbourg J9 Observatory.

A complete list of the different groups of tidal waves that we have separated by performing a tidal analysis on the complete data series using ETERNA 3.4, is shown in Tables 5.2, 5.3, 5.4 and 5.5, respectively for the diurnal, semi-diurnal, ter-diurnal and quart-diurnal groups.

Unfortunately, the phase values for $2J_1$, LK_{1x} , NU_{1x} , TET_1, $3KM_2$, and $2K_2d$ waves are not properly estimated.

Table 5.2: Tidal amplitudes, gravimetric factors (δ) and phases (κ, with respect to local tidal potential and lags negative) with their respective uncertainties obtained for the diurnal groups using ETERNA 3.4 software on the complete SG data series at J9 Observatory. The tidal potential used is Hartmann and Wenzel (1995).

Frequency (cpd)	Wave	Observed amplitude (nm/s²)	δ	stdv	κ (deg)	stdv
0.8234	1158	1.0260	1.1679	0.0098	-0.1053	0.4812
0.856497	SGQ_1	2.6408	1.1604	0.0041	-0.9205	0.2027
0.856806	$2Q_{1x}$	1.7013	1.1549	0.0059	-0.0879	0.2948
0.859691	$2Q_1$	9.0330	1.1564	0.0012	-0.6764	0.0602
0.861663	SGM_x	2.0446	1.1507	0.0053	-0.7929	0.2634
0.892332	SGM_1	10.8381	1.1506	0.0010	-0.5208	0.0496
0.892951	$3MK_1$	2.4655	1.0848	0.0036	1.5651	0.1900
0.893098	Q_{1x}	12.7893	1.1489	0.0008	-0.4252	0.0410
0.89613	Q_1	67.7533	1.1478	0.0002	-0.2811	0.0077
0.906316	RO_1	12.8713	1.1488	0.0008	-0.2071	0.0393
0.92939	O_{1x}	66.9471	1.1511	0.0002	-0.0199	0.0077
0.929846	O_1	354.3307	1.1493	0.0000	0.0785	0.0014
0.93045	$2NO_1$	2.2684	1.1421	0.0044	1.2396	0.2197
0.940488	TAU_1	4.6281	1.1517	0.0021	0.0855	0.1051
0.963857	NTAU	2.6113	1.1486	0.0037	0.2364	0.1864
0.965681	LK_{1x}	1.8429	1.1425	0.0055	-0.0753	0.2750
0.965828	LK_1	10.0408	1.1520	0.0010	0.2291	0.0504
0.966285	M_1	7.6918	1.0818	0.0012	0.8654	0.0653
0.966447	NO_1	27.9417	1.1530	0.0004	0.1859	0.0181
0.966757	NO_{1x}	5.6226	1.1561	0.0018	0.2508	0.0902
0.974189	CHI_1	5.3310	1.1496	0.0018	0.1942	0.0916
0.995144	PI_1	9.6243	1.1478	0.0011	0.1386	0.0525
0.997116	P_{1x}	1.7953	1.1135	0.0055	3.2266	0.2828
0.998029	P_1	164.9565	1.1501	0.0001	0.2103	0.0031
1.002445	S_1	3.9923	1.1774	0.0037	2.0137	0.1830
1.002592	K_{1x-}	9.6301	1.1220	0.0010	1.2057	0.0527
1.002739	K_1	492.9588	1.1374	0.0000	0.2556	0.0010
1.003652	$K1_{x+}$	67.0119	1.1393	0.0002	0.5420	0.0076
1.005624	PSI_1	4.3061	1.2693	0.0026	0.3289	0.1162
1.01369	PHI_1	7.2447	1.1738	0.0015	0.2687	0.0707
1.034468	TET_1	5.3707	1.1585	0.0019	0.0850	0.0926
1.039031	J_1	28.0974	1.1590	0.0004	0.1377	0.0183
1.039193	J_{1x}	5.5709	1.1594	0.0019	0.3450	0.0919
1.039649	$3MO_1$	2.7974	1.0779	0.0031	0.7709	0.1654
1.071084	SO_1	4.6393	1.1539	0.0022	0.1454	0.1089
1.075779	$2J_1$	2.2975	1.1561	0.0044	-0.0739	0.2176
1.075941	OO_1	15.3445	1.1571	0.0007	0.0928	0.0343
1.080945	OO_{1x}	9.8319	1.1571	0.0011	0.1280	0.0519
1.112233	NU_1	2.9440	1.1593	0.0035	0.4437	0.1736
1.216398	NU_{1x}	1.8727	1.1517	0.0053	0.2149	0.2630

Table 5.3: Tidal amplitudes, gravimetric factors (δ) and phases (κ, with respect to local tidal potential and lags negative) with their respective uncertainties obtained for the semi-diurnal groups using ETERNA 3.4 tidal analysis software on the total SG series at J9 Observatory.

Frequency (cpd)	Wave	Observed amplitude (nm/s^2)	δ	stdv	κ (deg)	stdv
1.8234	$3N_2$	1.0591	1.1310	0.0059	2.3595	0.2977
1.856954	EPS_2	2.7671	1.1401	0.0025	2.3772	0.1278
1.859382	$3MJ_2$	1.7644	1.0707	0.0037	0.2700	0.1979
1.862429	$2N_2$	9.5911	1.1524	0.0007	3.1155	0.0370
1.89507	MU_2	11.5958	1.1544	0.0006	2.8257	0.0303
1.895526	$3MK_x$	1.1014	1.0796	0.0059	0.3904	0.3149
1.895689	$3MK_2$	6.4015	1.0661	0.0010	0.2236	0.0549
1.895836	N_{2x}	2.7686	1.1791	0.0026	3.3458	0.1258
1.896749	N_2	73.8431	1.1741	0.0001	2.7579	0.0047
1.906463	NU_2	14.0534	1.1763	0.0005	2.7759	0.0246
1.927418	GAM_2	1.1607	1.1771	0.0060	3.0630	0.2904
1.930155	ALF_2	1.3788	1.2214	0.0053	0.8927	0.2477
1.932128	M_{2x}	14.4286	1.1772	0.0005	2.2672	0.0238
1.933188	M_2	389.9426	1.1871	0.0000	2.1274	0.0009
1.935322	BET_2	1.1851	1.1917	0.0059	1.5735	0.2811
1.942754	DEL_2	0.4809	1.2488	0.0124	3.8036	0.5708
1.963709	LAM_2	2.8647	1.1827	0.0025	1.4722	0.1190
1.968566	L_2	11.0564	1.1907	0.0006	1.5157	0.0309
1.968876	$3MO_2$	5.8996	1.0652	0.0011	-0.2635	0.0579
1.96917	$3MO_x$	1.1517	1.1039	0.0058	0.8611	0.3008
1.976927	KNO_2	2.7606	1.1893	0.0023	1.4079	0.1096
1.998288	T_2	10.6265	1.1895	0.0007	0.6081	0.0323
2.000767	S_2	181.7413	1.1893	0.0000	0.6219	0.0020
2.003033	R_2	1.4877	1.1662	0.0038	0.7217	0.1863
2.005167	$3MQ_2$	0.3371	1.1175	0.0200	-1.8150	1.0251
2.005477	K_2	49.4807	1.1916	0.0001	0.8782	0.0070
2.01369	K_{2x}	14.7552	1.1923	0.0005	1.0320	0.0231
2.037206	ZET_2	0.5235	1.1787	0.0123	0.2766	0.5955
2.041768	ETA_2	2.7604	1.1884	0.0026	0.3930	0.1274
2.041931	ETA_x	1.2119	1.1981	0.0061	0.3363	0.2891
2.042387	$3KM_2$	0.5438	1.0656	0.0101	0.2882	0.5416
2.07366	$2S_2$	0.4621	1.1997	0.0146	-0.7022	0.6977
2.182844	$2K_2$	0.7241	1.1913	0.0071	0.1291	0.3412

Table 5.4: Tidal amplitudes, gravimetric factors (δ) and phases (κ, with respect to local tidal potential and lags negative) with their respective uncertainties obtained for the ter-diurnal groups using ETERNA 3.4 tidal analysis software on the total SG series at J9 Observatory.

Frequency (cpd)	Wave	Observed amplitude (nm/s^2)	δ (nm/s$^{2)}$	stdv	κ (deg)	stdv
2.86212	MN$_3$	1.2446	1.0637	0.0023	0.3108	0.1240
2.89826	M$_{3x}$	0.2558	1.0706	0.0113	-0.8831	0.6070
2.89841	M$_3$	4.5471	1.0649	0.0006	0.3024	0.0344
2.93470	ML$_3$	0.2556	1.0572	0.0094	-1.0707	0.5069
2.97161	MK$_3$	0.5906	1.0617	0.0042	0.5355	0.2261

Table 5.5: Tidal amplitudes, gravimetric factors (δ) and phases (κ, with respect to local tidal potential and lags negative) with their respective uncertainties obtained for the quart-diurnal groups using ETERNA 3.4 tidal analysis software on the total SG series at J9 Observatory.

Frequency (cpd)	Wave	Observed amplitude (nm/s^2)	δ (nm/s$^{2)}$	stdv	κ (deg)	stdv
3.82826	N$_4$	1.7222	1.4718	0.1057	-104.9288	4.1157
3.86455	M$_4$	0.0910	0.3808	0.0397	172.5050	5.9709
3.93775	K$_4$	5.9660	1.3972	0.2052	25.4002	8.4141

5.4 Observation and search for very low frequency signals

In addition to exhibiting small amplitude signals and near frequency groups, another advantage of the length of J9 SG record is to enable us to study also long-period signals. In this part we will focus on the low frequency terms, such as the long period tides (18.6 year, 9.3 year, annual to ter-monthly) and the Chandler Wobble (CW, period of 435 days).

The theoretical aspect of these long period signals have already been explained in the section 2.1.8.

We have already pointed out in section 2.2 that the SGs have a very small instrumental drift compared to spring gravimeters. This is the main reason why studies about long period tides are particularly suited to SG data. However, the presence of long term drift leads to spectral noise which increases with decreasing frequency (colored noise). This means that the detection of signals is more and more difficult when the frequency of the signal decreases, even if the data set is long enough to allow the spectral detection.
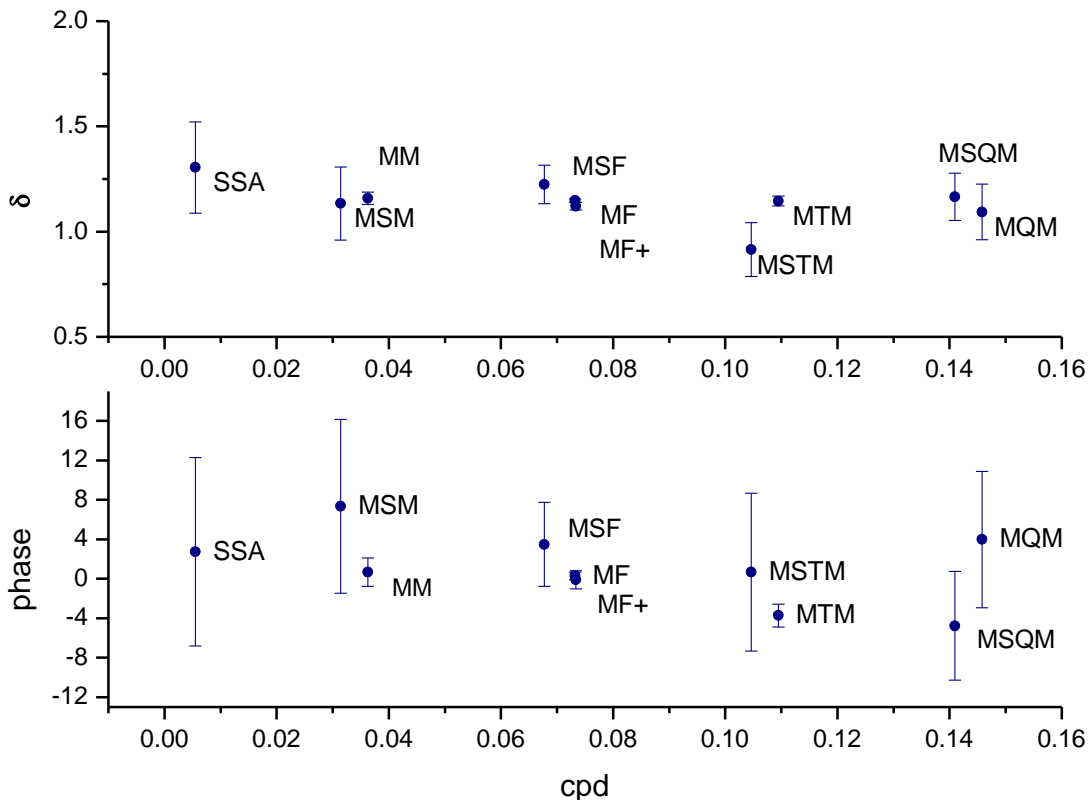
Fig. 5.9: Amplitude factors in the long period tidal frequency band using the complete (9760 days, 26.7 years) SG record (T005 + C026) in Strasbourg J9 Observatory.

Studies of long period (LP) tides (usually M_f and M_m) using SGs can be found elsewhere. In a recent paper, Boy et al. (2006c) analyzed long series from 18 GGP stations to estimate the ocean tide loading for the monthly (M_m) and fortnightly (M_f) tides. Also, Ducarme et al. (2004) determined different LP tidal waves using data from different GGP superconducting gravimeter data. The determination of the tidal parameters for all these tidal waves is very useful to retrieve some information on the Earth's rheology at such frequencies (e.g. Wahr and Bergen, 1986), as any deviation from pure elasticity will increase with decreasing frequencies (Crossley et al., 2013). The observation of these tides is believed to give us a good constraint for investigating the anelastic response of the Earth (Sato et al., 1997a). Compared to diurnal tidal periods where the Earth's rheology is predominantly elastic, on very long timescales the behavior of the mantle becomes viscoelastic.

In figure 5.10, we compare the spectral analyses for the observed and theoretical signals in Strasbourg using the Hartmann and Wenzel (1995) tidal potential development. The length of the data series allows us to separate some of the long period signals that were not visible with shorter series. An example is given by the separation of the annual term Sa and the Chandler component (CW), which requires at least 6.5 years of data. The spectral agreement between the CW signature and the prediction of the gravity change due to the polar motion (not shown here) is the basis of more detailed studies on the amplitude factor of the pole tide that can be found elsewhere (e.g. Ducarme et al. 2006).
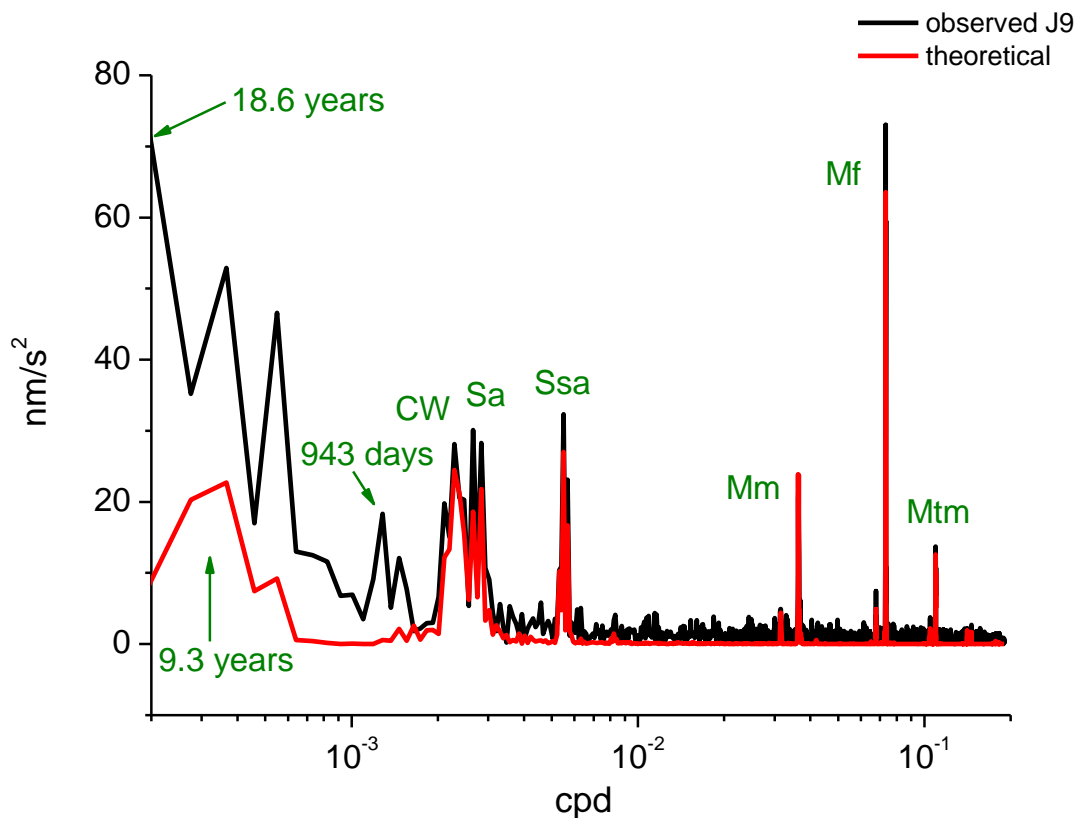
Fig. 5.10: Spectral amplitude of the merged 27 year series (T005 & C026) at Strasbourg J9 Observatory showing the Chandler Wobble (CW) and the long-period tides: the ter-monthly (Mtm), fortnightly (Mf), monthly (Mm), semi-annual (Ssa), annual (Sa), 9.3-year and 18.6-year components.

Unfortunately, despite the 27-year length of our data series we are still not able to retrieve the tidal waves of 9.3 and 18.6 year periods, which are of special interest for investigating the rheological behavior of the solid Earth at such periods. Our spectral peaks are obviously biased by the large noise still present in the SG data in the low frequency band. In a few more years, the SNR of the complete data series should be improved and we may expect to eventually detect the 18.6-yr tide. Finally, the long term gravity time series retrieved from SG observations are crucially depending on the amount of corrected offsets, for the determination of the polar motion and the seasonal components. That is why we must pay a close attention to this point, when correcting the raw gravity data, as already explained in section 2.3.1 (pre-processing).

However, it is evident that the ability of SGs to reliably measure effects at the 0.1 μGal level has opened up many interesting scientific possibilities.

The search of 18.6 and 9.3 year period signals

We have already indicated that the much lower instrumental drift of SGs versus mechanical spring meters has enabled more precise studies of long period tides (M_f, M_m, SSa, Sa) (Sato et al. 1997a; Hinderer et al. 1998; Mukai et al. 2001; Ducarme et al. 2004; Boy et al. 2006). However, at even longer periods, there are lunar nodal tidal waves at 9.3 and 18.61 year period which are extremely difficult to identify in gravity. The lunar nodal tide amplitude represents only about 5% of the amplitude of the daily diurnal tide from the Moon.

The Earth's nutation is a predictable cycle of the Earth's spin in space, which has inertial space periods equal to the orbital periods of the Sun and Moon. The four dominant periods are cycles of 18.61 years, 9.3 years, 182.6 days and 13.66 days. Unfortunately, the large tidal variations at annual and semiannual periods are obscured in Earth rotation observations by meteorological effects, while those having periods of 9.3 and 18.6 years are obscured by the decadal variations in the Earth's rotation (Gross, 2007). We will try to search any evidence of the presence of the 18.6 and 9.3 year lunar nodal tides in our long gravity records.

*Observations

5.4.1. Search of the 18.6 year period signal

The largest nutation term (18.6 y period) is of lunar origin. It arises from the precession of the lunar orbit around the ecliptic and will be extremely difficult to identify in gravity (Doodson & Warburg, 1941). We use first the long gravity record form J9 Observatory (only the 27 year record with SGs from 1987 to 2014).

In figure 5.10, we have already shown that despite the 27-year length of our series recorded at J9, we were not able to retrieve the tidal waves of 9.3 and 18.6 year periods from the spectral analysis. We will try to check now if there is any clear evidence of this signal in the residuals of our data series.

We have computed the theoretical 18.6 year wave for J9 station using PREDICT (Wenzell, 1996b), which is a FORTRAN code contained in ETERNA package, used for the computation at a specific station of Earth tide signals with constant time interval. As with ANALYZE code, we can choose between seven different tidal potential catalogs. We used here again Hartmann and Wenzel (1995) tidal potential. As shown by figure 5.11, superposing this theoretical signal with the gravity residual series, we cannot find any kind of correlation between both signals (correlation coefficient = -0.34), mostly because the residuals are too noisy, even for the second part inferred from C026 (after the vertical blue line).
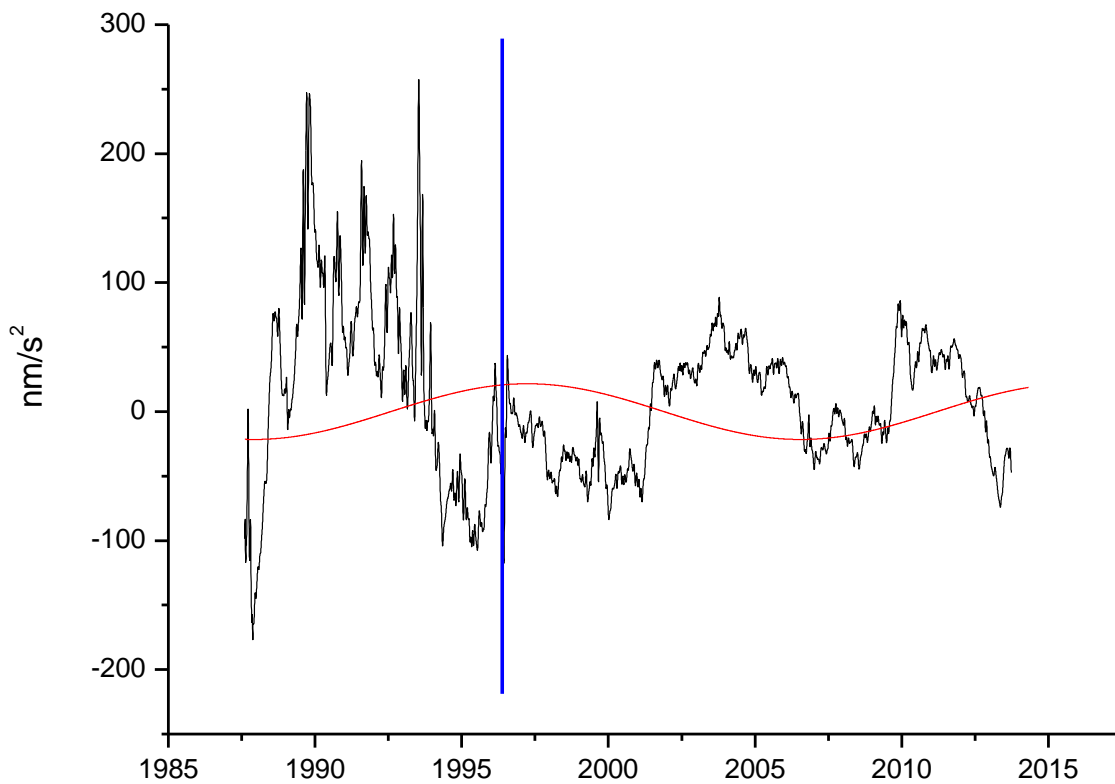
Fig. 5.11: Superposition of the 27 year gravity residuals (in black) at J9 Observatory: T005 (before vertical blue line) + C026 (after vertical blue line), and the theoretical 18.6y wave at the same location (red) (correlation coefficient = -0.34).

We have made similar comparisons with all the European SGs series previously treated in section 4. The only station in which the residuals seem to have a better correlation with the theoretical 18.6y wave is Membach (figure 5.12). But even at this station, where the amplitude of the residuals is almost half of the amplitude from the residuals from C026 at J9 and is also less noisy, the correlation is still not clear enough (correlation coefficient = 0.47).
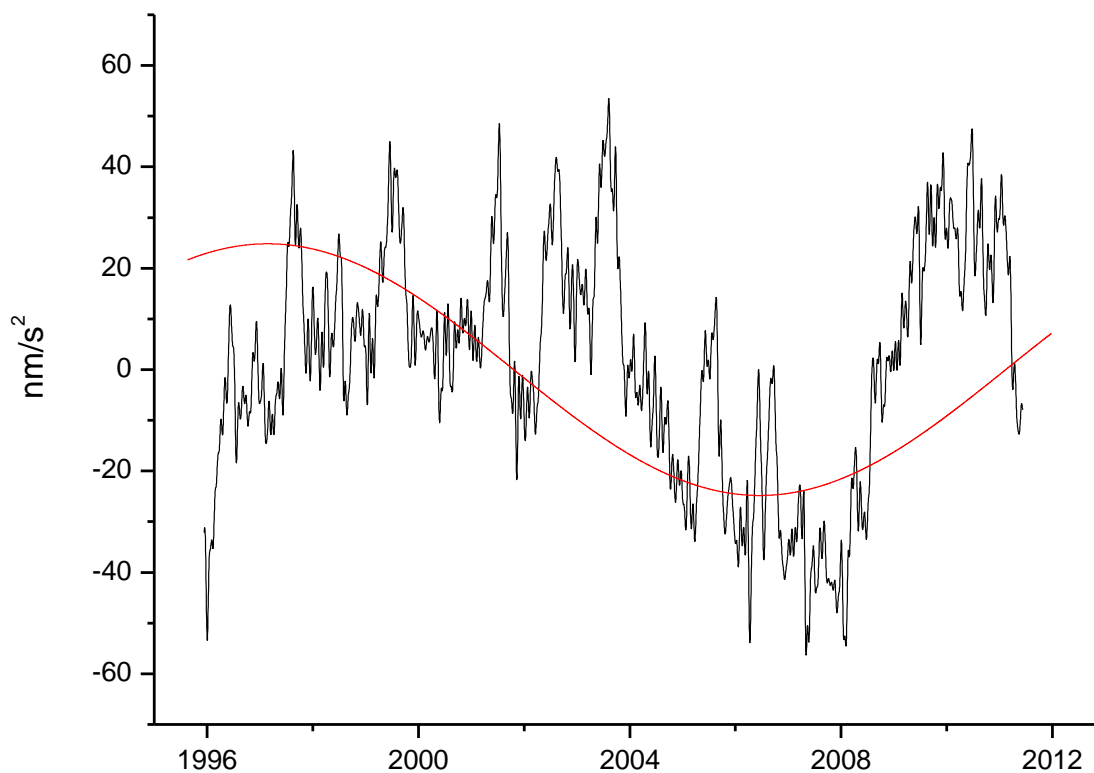
Fig. 5.12: Superposition of the 16 year gravity residuals (in black) at Membach Observatory (GWR C021) and the theoretical 18.6y wave at the same location (red) (correlation coefficient = 0.47).

It will be really interesting to check if actually this correlation continues when more years are available for this station, because currently the total series do not cover the whole period of the principal nutation term.

The tidal potential amplitude is <u>latitude dependent</u>; the long-period tides have their maximum values at the poles. So, since tidal observations at high latitudes are advantageous for determining the LP tides, long-term observations with a LaCoste&Romberg ET gravimeter have been set up at the Antarctic Amundsen-Scott station (90º S), see e.g. Rydelek and Knopoff (1982). However, because of the large drift inherent to spring gravimeters the very long period tides are unreachable.

Due to this latitude dependence, we have also checked using the series from Metsahovi station, in Finland, which was not previously used in this study, but whose latitude is higher than that of the other stations analyzed in this study (60.22º N). Unfortunately, the result was deceiving as shown by figure 5.13 (correlation coefficient = 0.02).
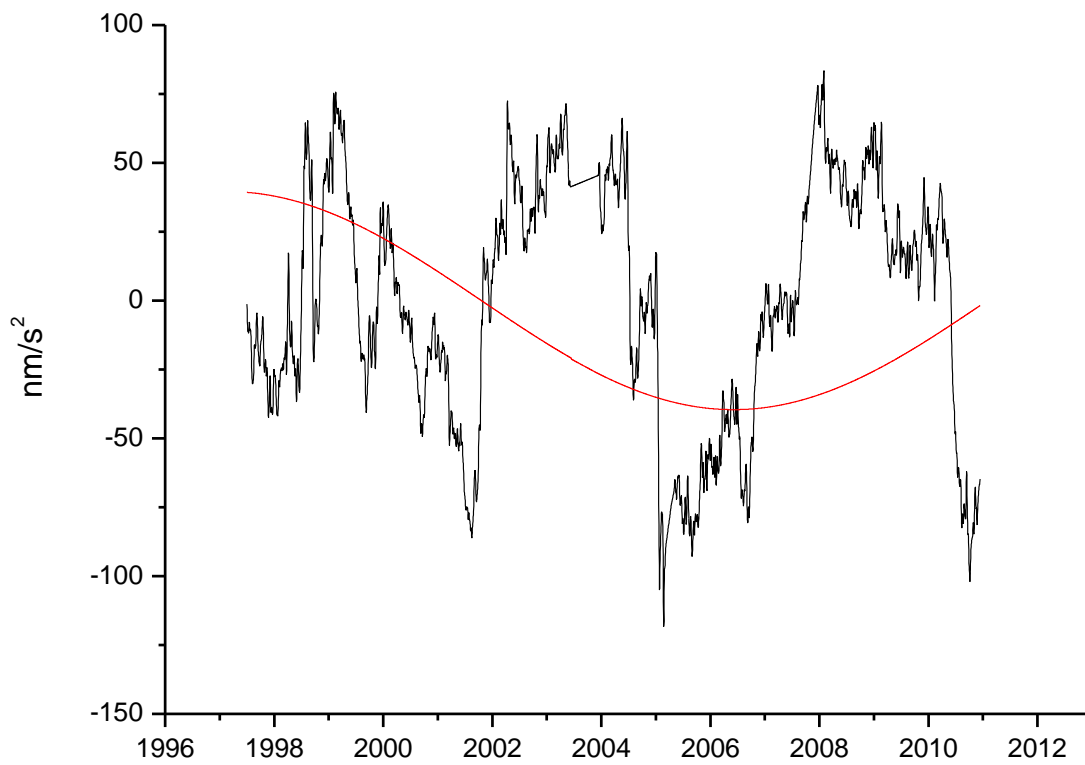
Fig. 5.13: Superposition of the 13 year gravity residuals (in black) at Metsahovi Observatory (GWR T020) and the theoretical 18.6y wave at the same location (red) (correlation coefficient = 0.02).

5.4.2. Search of the 9.3 year period signal

The 9.3 year wave has also been computed theoretically for the J9 station using PREDICT software. The amplitude of this signal is almost 300 times smaller than the amplitude of 18.6y. Thus, due to the noise in the data series at J9 site, it is completely impossible to visualize it in the residuals, as shown by figure 5.14.

Maybe some stacking procedure could help improve the SNR of the 9.3-year component. This could be part of future perspectives.
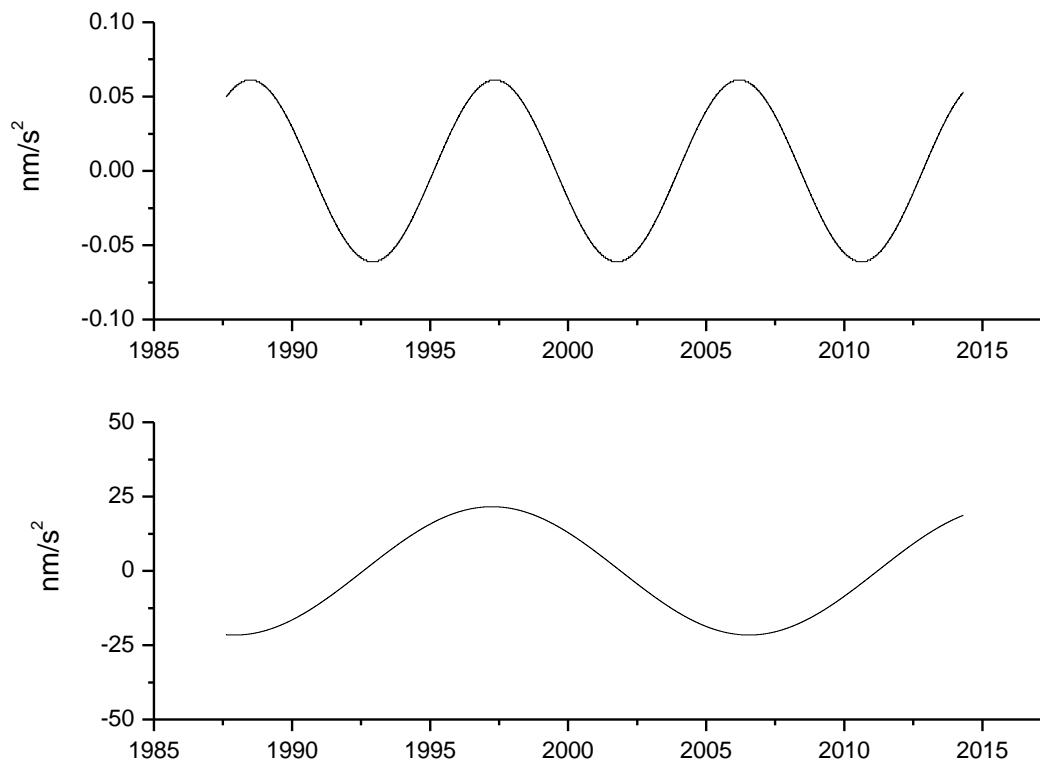
Fig. 5.14: Theoretical amplitudes of the 9.3y (upper plot) and 18.6y (lower plot) waves at J9 Observatory.

The purpose of this chapter was to show some of the benefits that can be obtained from very long gravity records, to detect very weak amplitude signals and low frequency signals.

We mainly use the 27 years gravity data registered at J9 Observatory by two different SGs (T005&C026), which is the longest available series ever recorded by SG at the same site. In fact, at that Observatory, there are available almost 40 years of continuous data (if we consider also the gravity data registered by a spring gravimeter). But we've checked that the SG records are preferred to the long spring gravimeter records, even when they are shorter. This is because of the long-term stability and very small linear instrumental drift of the SGs, as seen previously in chapter 4. And in addition, because the signal-to-noise ratio is not only improved by increasing the length of the data set, but it is also strongly influenced by the quality of the data.

We perform a tidal analysis using ETERNA 3.4 over the SG series, being able to separate several tidal waves in the diurnal, semi-diurnal, ter-diunal and quart-diurnal frequency bands, some of them with very low amplitude, with a high precision.

We also show the spectral analysis from both SGs series separately and for the merged series, obtaining in all cases a high spectral resolution in the tidal bands. Due to the higher noise in the T005 data relative to the C026, we still have to wait 5 more years, until the SNR of the merged series (T005+C026) will be larger than the SNR of the C026 series. So in just 5 years we will be able to get even more advantage of this merger. In these spectral analyses we can detect several low amplitude tidal waves that were hidden in the shorter series. Clear examples of small amplitude tides in the semi-diurnal and diurnal frequency bands are pointed out.

To conclude, the long-period part of the gravity spectrum is discussed. Unfortunately, despite the length of our series, we are not able to retrieve the tidal waves of 18.6 year period. In addition, we try with the data from the 8 SGs European stations previously studied in Chapter 4, obtaining also negative results. Furthermore, as the long-period tides have their maximum amplitudes values at the poles (due to the latitude dependence of the tidal potential) we try with the data from Metsahovi station (60.22ºN), but even at that location, the results were not satisfactory.

In the case of the tidal wave of 9.3 year period is even more complicated; its amplitude is almost 300 times smaller than the amplitude of the 18.6y.

Chapter 6

Contribution of the gravimetry to rotational modes (FCN&FICN)

We have already mentioned in the previous chapters some effects of tidal forces on a solid Earth, but there are actually other effects that are related to the mechanics of a spherical shell enclosing a fluid.

If a slight rotational motion is applied to such a shell, it will produce another slight inertial rotational movement of the fluid, relative to the shell. If the shell is ellipsoidal, there will be then a coupled rotation between the fluid part and the solid shell.

In the case of the Earth, we can consider that the <u>shell is the mantle</u> and <u>the fluid is the core</u>. The small rotational movement of the mantle is produced by Earth's tides, hence inducing a rotational movement of the fluid part if there is a coupling between the core and the mantle. The core-mantle system like all coupled systems will have a number of eigenmodes which are denoted Rotational Normal Modes.
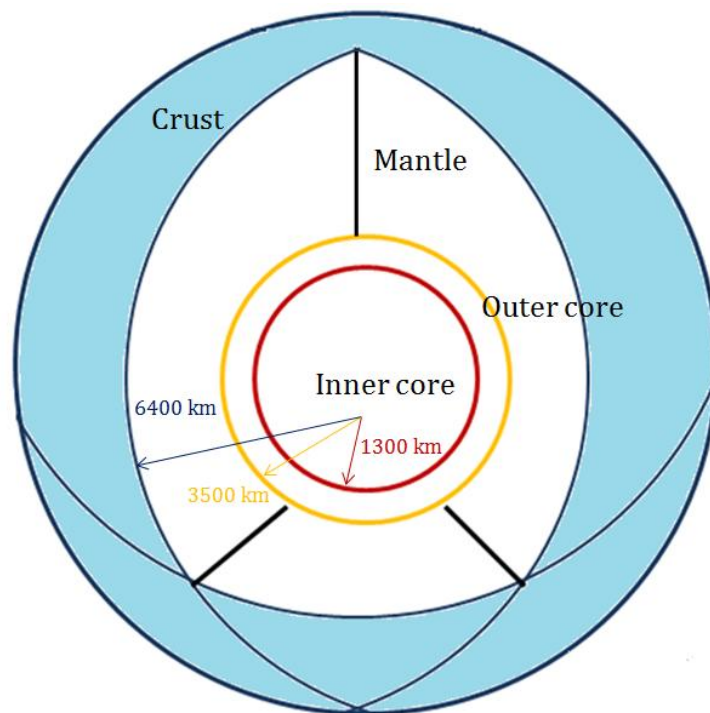
Fig. 6.1: Diagram of the different rotating layers in which the Earth can be divided (the anelastic mantle, the liquid outer core and the solid inner core).

The existence of more than one rotational normal mode for the Earth is due to the presence of the fluid core and the consequent possibility of differential rotations between different regions (Dehant 2007). These three regions (each one having an instantaneous rotation vector), interact with each other because of pressures on the boundaries, gravitational, electromagnetic and viscous couplings.

The principal rotational modes, which are presently known, are the following (Mathews et al. 1991a, b):

• **The Chandler Wobble (CW)**, which was discovered in 1891 by the astronomer Seth Carlo Chandler. It is a small deviation of the Earth's axis of rotation relative to the solid Earth (e.g. Mueller 1969) related to the ellipticity of the Earth. For a rigid Earth, this mode corresponds to the **Euler Wobble** (Euler, 1758) and it exists also for an Earth without a fluid core.

• **The Free Core Nutation (FCN)**, which is a retrograde (opposite to the Earth's rotation) mode, related to the existence of a flattened fluid core inside the Earth. This normal mode involves a relative rotation between the core and mantle. If observed in the terrestrial reference frame its frequency is nearly diurnal, so this mode is also called the **Nearly Diurnal Free Wobble (NDFW).** The existence of this nearly diurnal free wobble mode was discovered by Hough (1895).

• **The Free Inner Core Nutation (FICN)**, which is a mode related to the existence of a flattened inner core inside the fluid core. Similarly to the FCN, the FICN has a nearly diurnal prograde period in a terrestrial reference frame. The theoretical existence of this mode was undoubtedly demonstrated in 1991 by Mathews et al. (1991a), but its existence was already proposed by Toomre (1974) and is present in the results of Jeffreys and Vicente (1957). This mode has not yet been clearly observed.

• **The Inner Core Wobble (ICW),** which is the longest free mode of rotation also related to the existence of a flattened inner core inside the fluid core. It consists of a prograde precession of the tilted figure of the inner core with respect to a fixed mantle. This long-period oscillation of the inner core was first studied by Busse (1970) who proposed a period around 7 years. This mode has never been observed.
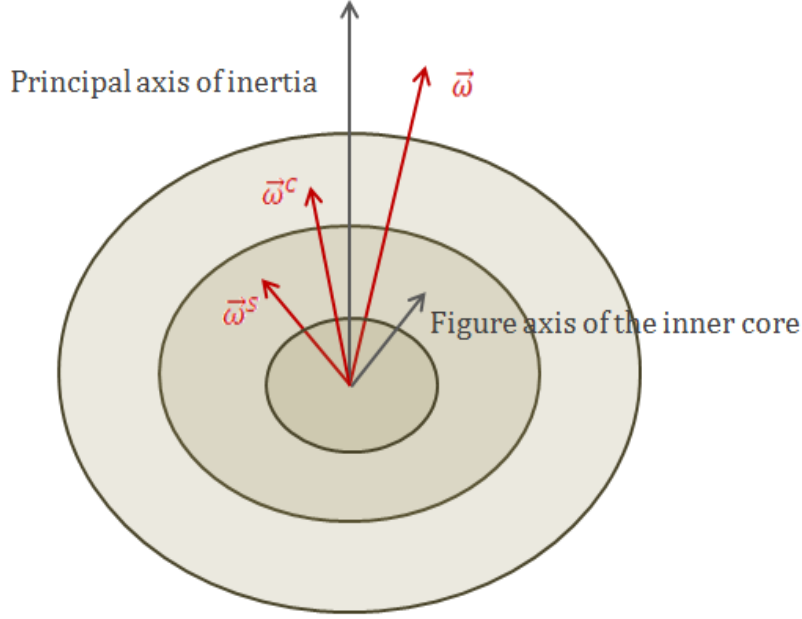
Fig. 6.2: Diagram of the whole-Earth axis of rotation, the axis of rotation of the inner core, the angular velocity of the mantle and the differential rotation of the outer and inner core with respect to the mantle.

The FCN and the CW were computed using the angular momentum conservation equations in a reference frame tied to the Earth, for an elliptical uniformly rotating Earth model with an elastic mantle and a liquid core (Sasao et al. 1980, Hinderer et al. 1982). The other two modes (ICW and FICN) were investigated later, once a solid inner core was added to the model (Kakuta et al. 1975, Mathews et al. 1991b, Herring et al., 1991).

To obtain the approximate frequencies of these rotational modes, we start with the classical Liouville equations (1858) (that is, Euler's equations modified to allow for deformation and internal flow) in a form given by Dehant et al. (1993) (eq. 6.1).

The Liouville equations are applied to three rotating bodies (the mantle, the liquid outer core and the solid inner core). If the Earth is submitted to a tidal volumic potential (involving an external torque $\vec{L}$), we have, in the lack of topographic torque at the core-mantle boundary (CMB) and at the inner core boundary (ICB):

$$
\begin{cases}
\dfrac{d\vec{H}}{dt} + \vec{\omega} \wedge \vec{H} = \vec{L} \\[2mm]
\dfrac{d\vec{H}^C}{dt} - \vec{\omega}^C \wedge \vec{H}^C = \vec{T}^C \\[2mm]
\dfrac{d\vec{H}^S}{dt} + \vec{\omega} \wedge \vec{H}^S = \vec{\Gamma}^S + \vec{T}^S
\end{cases}
\tag{6.1}
$$

Where $\vec{\omega}$ is the angular velocity of the mantle, $\vec{\omega}^C$ and $\vec{\omega}^S$ the differential rotation of the fluid core and of the inner core, respectively, with respect to the mantle (figure 6.2).

$\vec{T}^C$ and $\vec{T}^S$ are the frictional torques which may appear at the CMB and ICB and $\vec{\Gamma}^S$ is the sum of the gravitational torque and the pressure torque acting on the inner core.

The angular momentum for the global Earth, the fluid outer core and the inner core respectively ($\vec{H}, \vec{H}^C$ and $\vec{H}^S$) can be expressed as the product of its angular rotation and its mass redistribution, which is described by the inertia tensor for the entire Earth, for the core and for the inner core respectively. So, to obtain the equatorial part of the angular momentum equations for the global Earth, the liquid outer core and for inner core, we note:

$(A, A, C), (A^C, A^C, C^C)$ and (A^S, A^S, C^S) as the mean moments of inertia of the Earth, of the outer core and of the inner core respectively

$\vec{\omega} = (\omega_1, \omega_2, \Omega + \omega_3)$, $\vec{\omega}^C = (\omega_1^C, \omega_2^C, \omega_3^C)$ and $\vec{\omega}^S = (\omega_1^S, \omega_2^S, \omega_3^S)$ being Ω the sidereal rotation (in a linear approximation, we have: $\omega_i \ll \Omega, \omega_i^C \ll \Omega$ and $\omega_i^S \ll \Omega$).

We also noted α, α^C and α^S the dynamic flattening of the Earth, fluid core and inner core respectively ($\alpha, \alpha^C, \alpha^S \ll 1$)

If we introduce now the complex notations for these components, such as:

$$\omega = \omega_1 + i\omega_2, \qquad \omega^C = \omega_1^C + i\omega_2^C, \qquad \omega^S = \omega_1^S + i\omega_2^S$$

$$C = C_{13} + iC_{23}, \qquad C^C = C_{13}^C + iC_{23}^C, \qquad C^S = C_{13}^S + iC_{23}^S$$

$$L = L_1 + iL_2, \qquad \Gamma^S = \Gamma_1^S + i\Gamma_2^S, \qquad T^S = T_1^S + iT_2^S, \qquad T^C = T_1^C + iT_2^C$$

In that case, the equatorial parts of the angular momentum equation can be written as:

(6.2)

$$\begin{cases} A\dot{\omega} - i\alpha A\Omega\omega + \dot{C}\Omega + i\Omega^2 C + A^C\dot{\omega}^C + A^S\dot{\omega}^S + i\Omega(A^C\omega^C + A^S\omega^S) = L \\ A^C\dot{\omega} + A^C\dot{\omega}^C + i(1 + \alpha^C)A^C\Omega\omega^C + \dot{C}^C\Omega = T^C \\ A^S\dot{\omega} + A^S\dot{\omega}^S - i\alpha^S\Omega A^S\omega + \dot{C}^S\Omega + i\Omega^2 C^S + i\Omega A^S\omega^S = \Gamma^S + T^S \end{cases}$$

We should point that the instantaneous figure axis of the inner core is tilted with respect to the principal axis of inertia by two instantaneous rotations.

We refer to Dehant et al. (1993) for the solution of this equatorial system to obtain the approximate frequencies of the rotational modes:

$$\lambda_{CW} = \Omega \frac{A}{A^m} \alpha \left(1 - \frac{k}{k_f}\right)$$

$$\lambda_{ICW} = \Omega \frac{\rho^s - \rho^C}{\rho^s} \alpha^s \left(1 + \frac{\gamma^s}{\Omega^2}\right)$$

$$\lambda_{FCN} = -\Omega \left[1 + \frac{A}{A^m} \left(\alpha^C - \frac{q_0 h_1^C}{2}\right)\right]$$

$$\lambda_{FICN} = -\Omega \left[1 - \frac{\rho^C}{\rho^s} \left(\alpha^s - \frac{q_0 h_2^s}{2}\right) + \frac{\rho^s - \rho^C}{\rho^s} \left(\frac{\alpha^s \gamma^s}{\Omega^2} - \frac{q_0 \delta^s}{2\Omega^2}\right)\right]$$

(6.3)

Where

A, A^m are the principal equatorial moments of inertia of the whole Earth and mantle $(A^m = A - A^c)$

α^C is the dynamical ellipticity of the core, α^s of the inner core and α of the Earth

h, δ and γ are elastic parameters related to the deformations of the boundaries, to mass redistribution, or to the tilt of the inner core

ρ^C is the outer core density

ρ^s is the inner core density

q_0 is the ratio of the centrifugal acceleration and the gravity at the Earth's surface

$q_0 h_1^C / 2$ represents the effect of deformation of the core

There is an additional rotational mode which depends on the rotation of the whole Earth, which eigenperiod is not dependent of the shape, and which yields no information on the inner structure or the shape of the body:

• **The Tilt-Over Mode (TOM).** This mode exists for every rotating body, and is basically a rigid rotation of the body about an axis that does not match any of the axes of the relative reference system. Its period corresponds to the spin period of the body.

The period of all these five modes are summarized in figure 6.3. The periods of the FCN and FICN are nearly diurnal; the period of the TOM is diurnal; the period of the CW is about 430 sidereal days. As for the ICW, its period has not yet been observed either directly or indirectly (through the resonance effects). It has been computed of the order of a few years (e.g. 7.5 yrs for PREM by Rochester and Crossley 2009, later confirmed by Rogister 2010).
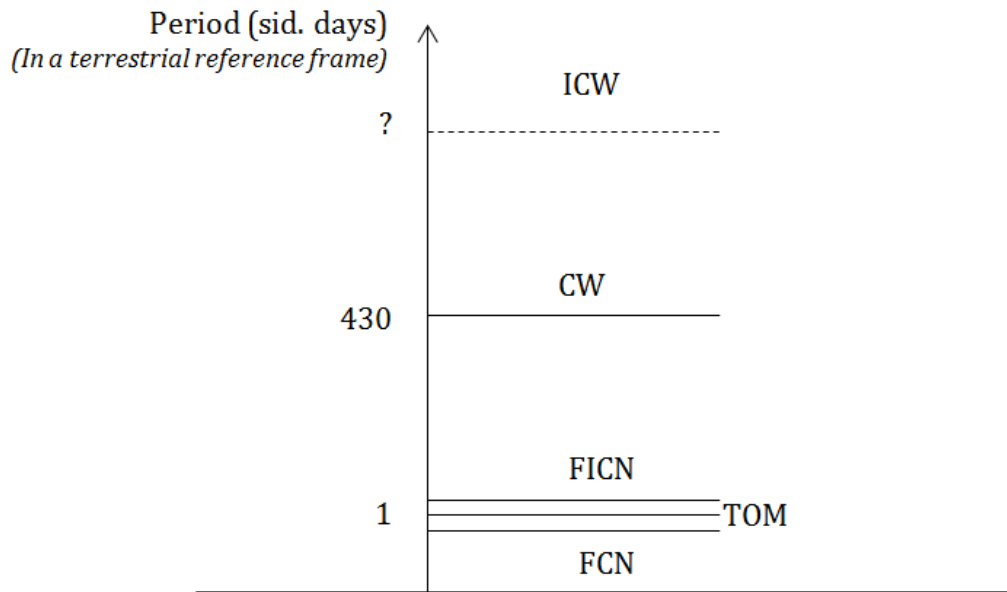
Fig. 6.3: Diagram of the periods (in a terrestrial reference frame) for the principal rotational modes (FCN, TOM, FICN, CW and ICW).

In this chapter we focus only on two of these rotational modes; the Free Core Nutation and the Free Inner Core Nutation, which are nearly diurnal wobbles in a rotating reference frame.

These free oscillations are associated with free nutations in space in addition to the nutations forced by the Sun, the Moon and the planets *(we call precession and nutation the motions of the Earth's rotation axis in the space reference frame)*.

Free Core Nutation

This rotational normal mode of the Earth involves a relative rotation between the core and mantle; it is caused by the misalignment of the rotational axis of the Earth's mantle and of the rotational axis of the fluid core (figure 6.4).

If we consider a rotating elliptical Earth model, this mode will cause both, displacement and deformation of the Earth simultaneously. However, the displacement component related to the nutation is much larger (about 300 times) than the deformation component related to the body tides. That is why this normal mode is usually called Free Core Nutation (Wahr, 1981a) *(and it is also called <u>Nearly Diurnal Free Wobble</u>, when looking at its effect on Earth)*.
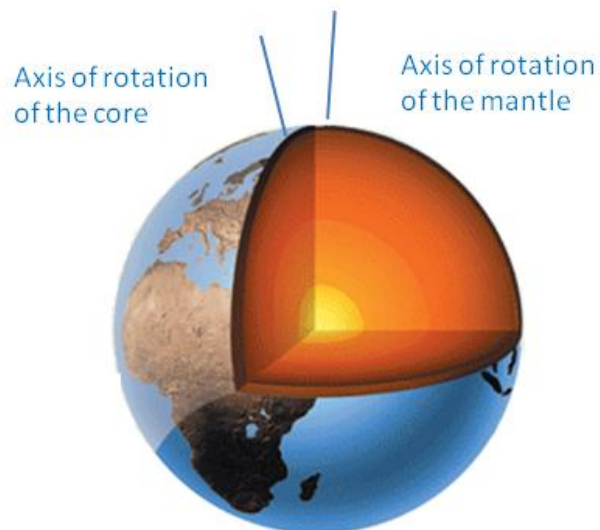
Fig. 6.4: Diagram of the misalignment of the rotational axis of the Earth's mantle and the rotational axis of the fluid core.

From the first theoretically discovery in 1895 until observational evidence was obtained, it took a long way. Despite the fact that this mode has been studied for a long time, the accuracy of the estimates of the most relevant parameters has improved rather slowly.

The physical origin of this mode is due to the pressure coupling between the liquid core and the solid mantle which acts as a restoring force (Florsch and Hinderer 2000). Its eigenperiod directly depends on the core–mantle boundary (CMB) ellipticity, as well as on the Earth's elasticity (Toomre, 1974; Sasao et al., 1980; Sasao and Wahr, 1981). Hence, its observation can be considered as a useful tool to study the Earth's deep interior dynamics and structure.

The attenuation of the mode (defined by a quality factor Q) is a direct consequence of damping and coupling mechanisms at the CMB, so it is also important to compute it.

Based on a given Earth's model, the eigenperiod of the FCN can be theoretically predicted. In a terrestrial reference frame, this normal mode has an eigenperiod T_{FCN} close to one sidereal day (sd). In the celestial reference frame, this mode corresponds to a retrograde motion (in the opposite way of the Earth's rotation) with a period close to 435 sd. The luni-solar tidal forcing at such frequencies leads to an amplification of the Earth's nutational and deformational responses to the tidal forcing (Hinderer et al., 1993a).

The difference obtained between the theoretical period of this mode (~460 sd) and the observed period (~430 sd), has been attributed to violation of the hydrostatic equilibrium at the core-mantle boundary: Herring et al. (1986) proposed a small increase of about 500 m in the difference between the core equatorial and polar ratio in order to explain the observed FCN period (see also Gwinn, Herring & Shapiro 1986; Dehant 1990).

Because of the presence of dissipation processes in the Earth, such as the viscosity of the mantle, the tidal friction in the bottom of oceans, the electro-magnetic and viscous coupling between the core and the mantle, the FCN is a damped oscillation. As a result, the attenuation of the mode amplitude is a direct consequence of damping and coupling mechanisms at the CMB. So it should be taken into account when the FCN is investigated by introducing a complex frequency.

Theoretical models of the rheological behavior of the mantle result in a Q-value not less than 78000 (Wahr, 1987). However, there are large discrepancies in the quality factor values obtained with different kinds of data or even with similar data but from different areas. In general, Q values estimated from body tide observations (eg. Neuberg et al. 1987; Sato et al. 1994; Hinderer, 1997) are much smaller than those estimated from nutation data (e.g. Herring et al., 1986; Gwin et al. 1986; Defraigne et al. 1994, 1995b). Rosat et al. (2009b) have demonstrated that the inadequation between ground gravity estimates and space nutation estimates of Q comes from the large uncertainties obtained on the estimate of the small amplitude PSI1 tidal wave. Recently, Rosat and Lambert (2009) have reached an agreement between the nutation observation and the gravimetric estimates of the Q value of the FCN. Also, it has been pointed out the important impact of inaccurate ocean loading corrections in the gravity observation, on the determination of the damping of the eigenmode (Neuberg et al., 1990; Florsch and Hinderer 1998, 2000).

There have been several studies trying to identify if there is a time variation of the frequency of the FCN resonance, either in VLBI nutation or in SG gravity data (e.g. Roosbeek et al. 1999; Hinderer et al. 2000; Lambert and Dehant, 2007; Vondràk and Ron, 2009; Cui et al., 2014). Most of these authors concluded that the apparent time-variation is not real but rather due to the time-variable excitation of the free mode. However, the analysis of VLBI observations performed by some other authors (Malkin 2004; Shirai et al. 2005; Malkin and Terentev 2007) showed that not only the FCN amplitude and phase vary in time but also its period. Vondràk and Ron (2009)

clearly distinguish the problem of the FCN mode which is forced mainly by atmosphere and oceans through angular momentum exchanges from the observed resonance of the FCN. Indeed, the latter depends only on physical properties of the Earth (ellipticity at the CMB, Love numbers, etc.) and coupling mechanisms acting at the CMB. So a varying resonant period would mean that such mechanisms are changing in time (Cui et al. 2014). Such variability has never been computed or demonstrated yet.

6.2. Theoretical approach to FCN

The consequences of the FCN can be observed both in the motion of the celestial intermediate pole in the celestial reference frame, and also in the resonance behavior of the frequency-dependent Earth tidal response (in its diurnal band). Its period has been deduced from the resonance effects found in nutation observations as well as in tidal observations.

We are going to focus on its signature on the diurnal Earth tides. So we should consider it in the rotating frame.

Theoretical investigations have evolved from the initial computations for hydrostatic seismologically constrained Earth models (e.g. Jeffreys & Vicente 1957; Sasao et al. 1980; Wahr 1981a; Wu & Wahr 1997; Dehant et al. 1999), to the most current MHB model (named after Mathews, Herring and Buffet), obtained from the VLBI observations of non-rigid nutation (Mathews et al. 2002).

There are different models for the FCN resonance. We consider the use of a reference gravimetric factor in the resonance model. In that case, the basic equation which holds for describing the resonance model in tidal gravity can be written as equation 6.4 (Hinderer et al., 1991b), where the FCN resonance parameters (strength amplitude, eigenperiod and quality factor) are combined in a resonance equation involving some Earth's interior properties. In the diurnal band, we can express the complex gravimetric factor $\tilde{\delta}_j$ (observed data) of a wave with frequency σ_j, as the sum of the part independent from frequency (the normal amplitude factor which would not be affected by the resonance, $\tilde{\delta}_0$) and a part which is frequency-dependent with the tidal frequency σ and the FCN resonant frequency $\bar{\sigma}_{FCN}$ (Neuberg et al., 1987; Hinderer et al., 1991b):

(6.4)

$$\tilde{\delta}_j = \tilde{\delta}_{ref} + \frac{\tilde{a}}{\sigma_j - \tilde{\sigma}_{nd}}$$

Where $\tilde{\delta}_{ref} = \tilde{\delta}_{ref}^R + i\tilde{\delta}_{ref}^I$ is the amplitude factor independent of the frequency (not influenced by the resonance),

$\tilde{\delta}_{ref}$ can be obtained by $\tilde{\delta}_{ref} = 1 + h_0 - \frac{3}{2}k_0$

$\tilde{\sigma}_{nd} = \sigma_{nd}^R + i\sigma_{nd}^I$ is the complex eigenfrequency of the FCN,

$\tilde{a} = a^R + ia^I$ refers to the resonance strength corresponding to the response of the whole Earth to the FCN *(the resonance strength relating to the geometric shape of the Earth and the rheological properties of the mantle)*.

It is real for an elastic Earth model. However, for an anelastic model, both the resonance strength and the FCN eigenfrequency should be complex with a very small imaginary part.

$\tilde{a}$ can be written as: $\tilde{a} = -\left(\frac{A}{A_m}\right)\left(h_1 - \frac{3}{2}k_1\right)\left(\alpha - q_0\frac{h^c}{2}\right)\Omega$

Where

h_0 and k_0 are the classical Love numbers (effect of deformation + perturbation of potential) which characterize the Earth's response to the tidal forcing,

h_1 and k_1 are the diurnal internal pressure Love numbers which characterize the elastic response (effect of deformation + mass redistribution) of the Earth to the inner pressure acting at the CMB

h^c is the secular Love number expressing the deformation of the CMB induced by a volumic potential evaluated at the CMB,

A and A_m are the equatorial moments of inertia of the entire Earth and the solid mantle respectively,

α is the dynamical ellipticity of the Earth,

q_0 is the ratio of the centrifugal force to gravity at the equator,

Ω is the sidereal frequency of the Earth's rotation.

Therefore, the eigenperiod of the FCN and the quality factor can be expressed in sidereal days in the rotating frame by (Defraigne et al., 1994):

$$T_{FCN} = \frac{2\pi}{\sigma_{nd}^R} \tag{6.5}$$

$$Q = \frac{\sigma_{nd}^R}{2\sigma_{nd}^I}$$

In order to retrieve the FCN parameters (Q and T_{FCN}) from observations, we have to solve the non-linear equation (6.4). Hereafter, we will introduce two methods classically used to deal with this inverse problem.

6.2.1. Linearized least-squares approach

The frequency of the wave O_1 is far away from the resonant one, so this wave is less influenced by the FCN resonance ($\sim$ in the order of 10^{-4}). Moreover, with a large amplitude and high signal to noise ratio, this wave can be observed very accurately. Therefore, it can be considered as quasi-static, and we can use it as a reference in the retrieval of the FCN parameters.

In that case, the fitting equations can be deduced by modeling the observed complex diurnal tidal gravity parameter (more than three waves should be considered) to theoretical ones and removing the signals of wave O_1, obtaining:

$$\delta(\sigma, j) - \delta(O_1, j) = \frac{a^R + ia^I}{\sigma - (\sigma_{nd}^R + i\sigma_{nd}^I)} - \frac{a^R + ia^I}{\sigma(O_1) - (\sigma_{nd}^R + i\sigma_{nd}^I)} \tag{6.6}$$

where j stands for the station number (in the case that data from several stations are analyzed). This will eliminate systematic errors such as a general bias in the tidal factors.

This equation is still non-linear, so to solve these equations when n tidal waves are included, the error function χ^2 should be minimized after linearization using the Marquardt's optimization algorithm (Marquardt 1963): $\tag{6.7}$

$$\chi^2 = \sum_{\sigma, j} \omega(\sigma, j) \left\| \left[\delta(\sigma, j) - \delta(O1, j) - \left[\frac{a^R + ia^I}{\sigma - (\sigma_{nd}^R + i\sigma_{nd}^I)} - \frac{a^R + ia^I}{\sigma(O1) - (\sigma_{nd}^R + i\sigma_{nd}^I)} \right] \right] \right\|^2$$

with $\omega(\sigma, j) = 1/\varepsilon(\sigma, j)$ being the weight function, where $\varepsilon(\sigma, j)$ is the standard deviation of the amplitude factor of a tidal wave with frequency σ at the jth station.

This method has been widely used in FCN retrieval studies like in Neuberg et al., (1987); Richter and Zürn (1986); Zürn and Rydelek (1991) and Defraigne et al. (1994, 1995a).

6.2.2. Bayesian approach

The Bayesian approach (Florsch and Hinderer 2000; Sato et al. 2004) is an improvement of the previous technique, allowing a precise determination of the quality factor Q (expressing the damping due to all physical processes involved in the resonance). The Bayesian inversion is the method which best propagates the data information to the parameters. This inversion is explained more in detailed in **Annex F.**

This is the approach that we will use later with our data in section 6.4, since such a probabilistic view allows the most complete and reliable information (Tarantola and Valette, 1982) on the FCN resonance. Besides, using the Bayesian approach, the resonance equation does not need to be linearized.

Florsch and Hinderer (2000) used the basic equation that describes the resonance of the FCN in the tidal gravity (equation 6.4) and performed the inversion by treating $\tilde{\delta}_{ref}$ as an unknown parameter, showing that a correlation exists between the real parts δ_j^R and σ_{nd}^R, and between δ_j^R and a^R, and that a strong correlation also exists between a^R and T.

The equation relative to the resonance model become:

$$
\begin{cases}
\delta_j^R = \tilde{\delta}_{ref}^R + \dfrac{a^R\left(\sigma_j - \sigma_{nd}^R\right) - \dfrac{a^I \sigma_{nd}^R 10^{-x}}{2}}{\left(\sigma_j - \sigma_{nd}^R\right)^2 + \left(\dfrac{\sigma_{nd}^R 10^{-x}}{2}\right)^2} \\[5ex]
\delta_j^I = \tilde{\delta}_{ref}^I + \dfrac{a^R\left(\sigma_j - \sigma_{FCN}\right) + \dfrac{a^R \sigma_{nd}^R 10^{-x}}{2}}{\left(\sigma_j - \sigma_{nd}^R\right)^2 + \left(\dfrac{\sigma_{nd}^R 10^{-x}}{2}\right)^2}
\end{cases}
\tag{6.8}
$$

The observed gravimetric factors are then inverted to retrieve the FCN resonance parameters; the real and imaginary parts of the resonance strength, a^R and a^I, the resonance eigenfrequency $\tilde{\sigma}_{nd}$, and $x = log_{10}(Q)$

The sensitivity study of the FCN parameters to the diurnal tidal waves demonstrates that the quality factor Q is strongly dependent on the accuracy of the imaginary part estimates of the gravimetric factors close to the resonance.

Positivity of the quality factor

Florsch and Hinderer (2000) also introduced the positivity of the quality factor Q of the FCN, which was previously underestimated or even found negative in past gravity

studies using the standard least squares technique. They suggested that when estimating such a parameter, one should include that a priori information.

$$(6.9)$$

$$Q = \frac{\sigma_r}{2\sigma_i} = 10^x$$

So that inverting $x = log_{10}(Q)$ instead of Q insures the positivity of Q.

Rosat et al. (2009b) showed that by inverting $log_{10}(Q)$ instead of Q, the result using the least-squares method optimized using the Levenberg–Marquardt algorithm are in good agreement with the Bayesian probabilistic results.

* Oceanic loading correction

One of the major problems for the retrieval of the FCN parameters from surface observations is the accuracy of oceanic corrections applied to the analyzed data. It is known that, because of the Earth's elasticity, the surface gravity observations are influenced by ocean tide loading (OTL). The ocean loading effect can contribute to 10% of the total signal (Francis and Melchior, 1996). Hinderer et al. (1993a) indicated that errors in oceanic correction would lead to significant variations of the retrieved Q value of the FCN. Ducarme et al. (2007) also showed that the uncertainty in oceanic models will lead to some discrepancies in the determination of the FCN parameters. As a consequence, it is important to remove the OTL signals from tidal gravity parameters for a better determination of the FCN parameters.

In this study, we only use gravimetric stations located in Europe, where the ocean load effects on gravity-tides are known to be very small for diurnal tides (0.5 per cent of body tides). Nevertheless, it is of great importance for the FCN determination to compute corrected amplitude factors and phase differences by subtracting the OTL effect (Ducarme et al. 2009 state that the only way to improve the estimation of the FCN using tidal gravity observations is to improve the ocean tide models). In our case, we have used the FES2004 ocean model (Lyard et al., 2006) to correct our data, based on the computation by Boy et al. (2002).

As the oceanic tides have the same forcing sources and similar spectral characteristics as the body tides, we are not able to separate them in a harmonic analysis. So, we should calculate the oceanic influence through the loading theory and the suitable oceanic co-tidal models. As the tidal models are given only for some tidal waves, we need to interpolate the OTL corrections to all diurnal waves used in the inversion for the FCN parameters. We have used a regression method proposed by Xu et al. (2002) defined by:

$$(6.10)$$

$$\begin{cases} L(\sigma) \cdot \cos(\lambda(\sigma))/[T(\sigma) \cdot R(\sigma)] = \alpha^R + \beta^R \cdot \sigma \\ L(\sigma) \cdot \sin(\lambda(\sigma))/[T(\sigma) \cdot R(\sigma)] = \alpha^I + \beta^R \cdot \sigma \end{cases}$$

Where $T(\sigma), L(\sigma)$ and $\lambda(\sigma)$ are respectively the height of equilibrium tides, the amplitude and the phase of gravity signal caused by oceanic tides at the frequency σ.

$R(\sigma)$ is a parameter describing the effects of the FCN resonance on the oceanic tidal wave at the frequency σ.

$\alpha^R, \beta^R, \alpha^I$ and β_i are the unknown regression coefficients.

Some other techniques as the analytical solution (Florsch et al., 1994) or the stochastic inversion (Cummins and Wahr, 1993; Defraigne et al., 1994) have been used to retrieve the FCN parameters using gravity data.

6.3. Historical quest for the FCN resonance in gravity data

The possibility that the Earth, or more accurately, the Earth's mantle, exhibits a free nutation with a period of about one day, in a rotating reference frame, was discovered theoretically, independently and almost simultaneously, by Hough (1895) and by Sloudsky (1896). This mode of nutation can exist only for an Earth with a rigid mantle and a liquid compressed core (Pariiskii, 1963). It took nearly 15 years until Poincaré (1910) revisited this phenomenon, considering a schematic model of a rigid mantle and a liquid core. In 1949, H. Jeffreys published his study about the dynamical effects of a liquid core. He showed that a resonance effect should occur on the tidal waves which periods are sufficiently close to that of the movement in the liquid core, i.e. close to the sidereal day.

In 1957, Jeffreys and Vicente considered a more realistic model, consisting of a compressible and non-uniform mantle and two simplified models of the structure of the Earth's core. They discussed about the diurnal nutation for each model (the first with a homogeneous core, and the second with a density distribution inside the core), obtaining disparate values for the period of the diurnal nutation. They also gave for the first time the numerical values of the gravimetric factors, showing in particular that the amplitude of the Earth's response at O_1 frequency should be larger than at K_1 frequency, resulting in:

$$(6.11)$$

$$\delta(O_1) > \delta(K_1)$$

In 1961, Molodensky considered the general unified theory of nutation and diurnal tides for an inhomogeneous Earth with a liquid core, obtaining results quite similar to those of Jeffreys and Vicente (1957).

According to their theoretical calculations (Molodensky 1961, Jeffreys & Vicente 1957), the three main diurnal waves that it was possible to observe with enough precision from the available records (K_1, O_1 and O_1), should have the amplitudes given in figure 6.5.

TABLE 38

Components \\ Waves	horizontal $\gamma = 1 + k - h$				vertical $\delta = 1 + h - \dfrac{3}{2}k$			
	JV1	JV2	MO1	MO2	JV1	JV2	MO1	MO2
OO_1	0·658	0·661	0·685	0·684	1·221	1·210	1·161	1·165
O_1	0·654	0·658	0·688	0·686	1·224	1·211	1·159	1·164
P_1	0·695	0·696	0·699	0·697	1·196	1·172	1·154	1·158
K_1	0·714	0·693	0·730	0·727	1·183	1·185	1·137	1·143
semi-diurnal	0·704	0·675	0·686	0·685	1·152	1·188	1·160	1·164
$\gamma(O_1) - \gamma(K_1)$ $\delta(O_1) - \delta(K_1)$	− 0·060	− 0·035	− 0·042	− 0·041	+ 0·041	+ 0·026	+ 0·022	+ 0·021

Fig. 6.5: Table 38 extracted from Melchior (1966) comparing the values obtained for the models: JV1 (Jeffreys and Vicente 1957), JV1 (Jeffreys and Vicente 1957b), MO1 and MO2 (Molodensky 1961). Differences in the two models of Molodensky (1961) derive from the conditions applied at the Core-Mantle Boundary.

These last 2 publications (Jeffreys and Vicente, 1957b; Molodensky 1961) stimulated the gravity community to search for an evidence of the existence of the FCN in their gravity records. Unfortunately, the precision of the observations at that time was still insufficient. Several groups hence began to concentrate their efforts on improving the quality of the observations. Among these groups, we can cite the one from Strasbourg, which made several technical improvements on their spring gravimeters, as already mentioned in section 2.3.

We can consider that the discovery of the FCN effect in gravity data is divided into two different stages as already mentioned in paragraph 3.2.2:

- In a first step, the attempts to observationally prove the existence of the FCN focused on the comparison of the observed amplitude of the largest diurnal tidal constituents (O_1, P_1 and K_1) with theoretical amplitudes. At that time, little was known and done to correct the observed amplitudes for the atmospheric and oceanic effects. Unfortunately, the first results published by Lecolazet (1957) and Melchior (1957) using the 5-month data recorded in Strasbourg with the North American AG 138 gravimeter were in disagreement with the theoretical models.

Thanks to the great improvements obtained in both instrumentation and techniques of analysis, two years later Lecolazet published the first clear observation of $\delta(O_1) > \delta(K_1)$ in agreement with Jeffreys' theory, using a new series recorded at the same Strasbourg observatory, from 1957 to 1958 (Lecolazet, 1959). We illustrate these 2 determinations, incorrect and correct, of $\delta(O_1)$ and $\delta(K_1)$, by the figure 6.6, which is a picture of Table II extracted from Lecolazet (1959).

One year later, using the complete series of 860 days of the NA 138 gravimeter (registered between August 1957 and December 1960) he obtained even better results (Lecolazet 1960).

TABLEAU II

Résultats des analyses globales

	Anciens résultats				Nouveaux résultats	
	H/H$_1$		$\varphi - \varphi_1$		H/H$_1$	$\varphi - \varphi_1$
K$_1$	1,204 $\pm$ 0,006		$-$ 1,48 $\pm$ 0,27		1,165	$-$ 1,275
O$_1$	1,178 $\pm$ 0,006		$-$ 1,59 $\pm$ 0,27		1,180	$-$ 1,297
P$_1$	1,150 $\pm$ 0,017		0,9 $\pm$ 0,9		1,158	$-$ 1,351
M$_2$	1,211 $\pm$ 0,005		0,16 $\pm$ 0,21		1,215	$+$ 1,398
S$_2$	1,217 $\pm$ 0,013		$-$ 2,95 $\pm$ 0,61		1,216	$-$ 1,542

Fig. 6.6: Table II extracted from Lecolazet (1959) showing the first incorrect (left two columns) and then correct (right two columns) determination of $\delta(O_1)$ and $\delta(K_1)$ (δ is called H/H$_1$ in this table) respectively obtained by the analyses performed in 1957 and in 1959 using a North American spring meter installed at Strasbourg Observatory.

After these first published results, correct values were found at other stations all around the world. We can cite for example, Pariiskii (1963) who confirmed Lecolazet's results using an Askania GS 11 gravimeter, or Popov (1963). Melchior (1966) compiled these results even though some of them did not achieve the expected results.

As higher quality data were available, the next generation of gravimetric observations dealt not only with these largest waves (O$_1$, P$_1$ and K$_1$), but also with the measurement of minor diurnal tidal constituents, as for example ψ_1 and ϕ_1 which are much closer to the predicted resonance than K$_1$ and hence better constrain the frequency of the FCN.

- In a second step, once the existence of this resonance was proved, <u>the search for the value of the FCN frequency begun</u>. After some failures when Lecolazet and Steinmetz (1973) were not able to locate correctly the frequency, they published the first results of the discovery of the resonance of the core (Lecolazet and Steinmetz, 1974). They determined that the FCN frequency should be either between K$_1$ and PSI$_1$, or between K$_1$ and PHI$_1$.

The wrong estimation of PSI$_1$ amplitude obtained by Lecolazet and Steinmetz in 1973 and the better one obtained in 1974 are illustrated in Figure 6.7.
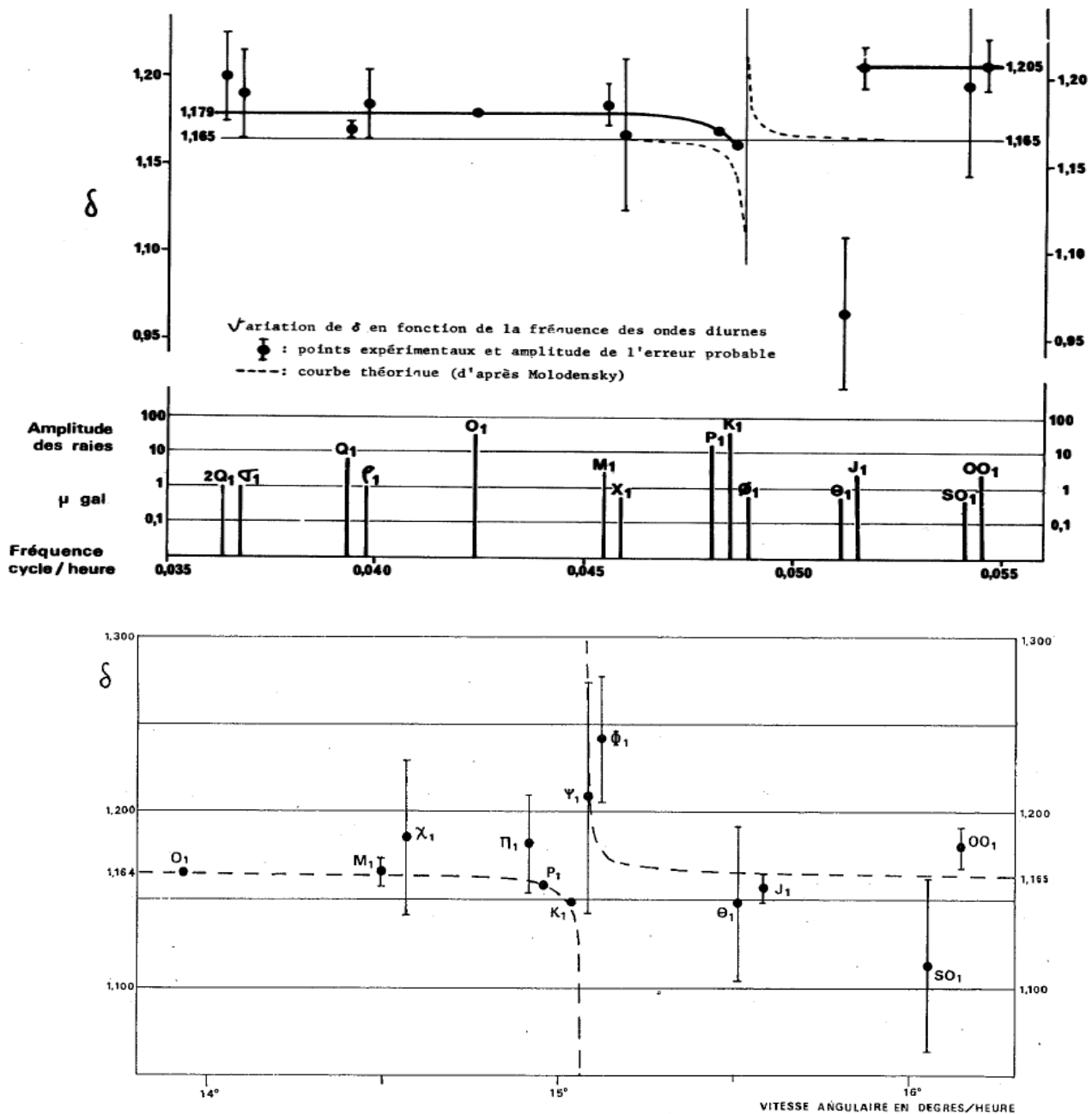
Fig. 6.7: Diurnal tides amplitude factors obtained by Lecolazet and Steinmetz in 1973 (up) and in 1974 (down) illustrating the improvement in PSI1 amplitude determination between these two studies.

In both publications they used the same dataset, i.e. almost 3 continuous years between 1964 and 1967 obtained with the North-American AG 138 installed at the Seismological Observatory in Strasbourg. The major difference in the two studies was the methodology used in the data analysis; in 1974 they performed a tidal analysis method based on the T. Chojnicki's least-squares technique (Chojnicki, 1972) which was a major improvement for tidal analysis.

These results were then much improved by using a longer series recorded between 1973 and 1975 with a LaCoste-Romberg Earth-Tide gravimeter (LR-ET005), equipped with a feedback system installed at the J9 Gravimetric Observatory of Strasbourg, definitively confirming that the FCN frequency lies between K_1 and PSI_1 frequencies (Lecolazet and Melchior, 1977; Abours and Lecolazet, 1978).

The instrumental precision of the LR-ET005 was not only better than that of the North American, but also the tidal analysis technique was improved with the help of computer processing conducted at the International Center for Earth Tides, where the Chojnicki's least-squares procedure was applied and complemented with a spectral analysis of the residuals. Their analysis was also compared with the Venedikov's method (Venedikov, 1966a), leading to similar results. At that time, the analysis technique improved with the introduction of the computer processing, which was a major breakthrough.

At the same epoch, a theory for calculating the normal modes and the forced motion of a deformable, slightly ellipsoidal, rotating body, described by an isotropic elastic constitutive relation was developed by Smith (1974). Also, Lecolazet (1983) correlated observed amplitude variations of the FCN (also called NDFW) with variations of the length-of-day and speculated about a temporal variation of the NDFW eigenfrequency.

Neuberg and Zürn (1986) suggested stacking data from different instruments at a single station. But it was already identified that in addition to the importance of having long gravity records, it was necessary to use observations at more than one station to reduce the effects of local systematic errors. Because the FCN is a global phenomenon, stacking data from gravimeters located in different areas, can reduce effectively the discrepancy of the retrieved FCN resonance parameters. These differences are mainly caused by atmospheric and oceanic loading effects and by some local environmental perturbations surrounding the stations. Neuberg et al. (1987) first proposed an inversion of stacked gravity tide measurements in central Europe. They used the Marquardt optimized linearized least squares. A few years later, Defraigne et al. (1994) added to the gravity stack the nutation observations.

Another breakthrough occurred with a better understanding of the atmospheric and oceanic effects and with the emergence of the superconducting gravimeters during the 80s. With the arrival of this new generation of gravimeters, a new observational window on Earth's deep interior was opened. (See section 2.2.2 for a description of the advantages and improvements brought by SGs), and the first precise determinations of the eigenfrequency and quality factor Q of the mode were proposed (Warburton and Goodkind 1978; Goodkind 1983; Zürn et al., 1991b; Richter et al., 1995).

6.4. Observations of the FCN resonance using other geodetic techniques

Most of the experimental studies for the determination of the FCN parameters are based on the analysis of tidal gravity data and Very Long Baseline Interferometry nutation data. However, some other geodetic observational techniques have also been used to try to determine these parameters (up to now the more reliable results, especially concerning the quality factor of the resonance, are derived from the VLBI observations).

Borehole water-level data

Zaske et al. (1999) performed a tidal analysis on a quasi-continuous 665 day dataset of well-level variations recorded at the European Hot-Dry-Rock test-site in Soultz-sous-Forêts, France. Their results clearly showed the influence of the NDFW on the borehole water level data. However, they obtained a period $T_{FCN} \approx 380$ days which is in disagreement with other studies.

Strainmeters / extensometers

Although tidal signal-to-noise ratio for strain is usually lower than for gravity, the analysis of strain data is promising since the relative perturbations due to the FCN in strain tides are about 10 times larger than in gravity tides (Amoruso et al., 2012).

Levine (1978) first used strain tide data (almost two years, using a 30 meter laser strainmeter located in a gold mine close to Boulder, Colorado) and found a significant structure in the response of the Earth to tidal excitations near 1 cycle/sidereal day, which corresponds to the predicted resonance behavior. Unfortunately, his results at ϕ_1 and ψ_1 frequencies where the resonance has the largest effect, were not accurate. The corroboration for this frequency shift was provided by Sato (1991) in his study of strain tides in Japan.

Later, Polzer et al. (1996) used strain tide data from the Schiltach observatory in southwestern Germany, together with high quality gravity data. They found a T_{FCN} period of about 410 sidereal days, which is much lower than the gravimetric and VLBI obtained values. More recently, Mukai et al. (2004) estimated the FCN parameters using 7.1-year strain data observed with a laser extensometer in a deep tunnel, located at the Rokko-Takao station, Kobe, Japan. They obtained a $T_{FCN} = 427.5$ days and $Q^{-1} = 1.7 \cdot 10^{-4} (Q \sim 5880)$. They also pointed out the difficulty of using strain data to estimate the FCN parameters because tidal strain data are often contaminated by environmental noise such as meteorological variations. Ping et al. (2010) used 17-year data recorded with three identical quartz tube extensometers, located at the

Esashi station, Japan, obtaining values between 410 and 421 days for the T_{FCN}, and between 6670 and 10500 for the quality factor.

More recent results have been published by Amoruso et al. (2012), using eight years of discontinuous strain records from two crossed 90-m long laser extensometers, operating in the Gran Sasso underground observatory, Italy. They obtained $T_{FCN} = 429$ days and Q values between 10000 and 50000.

VLBI technique

The FCN can be observed not only by its resonance effect on the diurnal tidal waves using gravimeter records, but also by its associated resonance effects on the forced nutations of the Earth's figure axis. Such forced nutations are usually observed by Very Long Baseline Interferometry (VLBI) technique relying on the determination of the space reference frame. VLBI technique has been widely used to measure the resonance effect on nutation amplitudes and, as well, to observe and model the forced FCN oscillation (e.g. Lambert 2006, http://syrte.obspm.fr/~lambert/fcn/index.php). This direct FCN effect cannot be observed in surface gravity measurements because its amplitude is about 300 times smaller on Earth than its nutation amplitude in a space reference frame.

Since 1984, series of VLBI measurements have been available with high precision and high resolution. The FCN was probably first detected using VLBI observations by Herring et al. (1986), Eubanks et al., (1986) and Gwinn et al. (1986).

Up to now, the most reliable results for the values of the FCN parameters, especially concerning the quality factor, are derived from VLBI observations. The discrepancy between gravity and nutation is due to the large errors arising from the diurnal tidal wave determinations that are the closest to the FCN resonance. In particularly, the PSI$_1$ wave has small amplitude at the Earth's surface while its corresponding annual retrograde nutation is 300 times larger in space. Another reason is that the oceanic, atmospheric and hydrological effects are much lower on VLBI observations (differential global technique) (angular momentum exchange) than on surface gravity (direct Newtonian effect + mass redistribution + deformation). So, while the ocean loading effect is a main source of error on the gravity signal, the effect of the ocean tides on the Earth's nutation is much weaker.

Sato et al. (1994) pointed out that the error in the correction for the ocean tide effects could strongly affect the estimated FCN parameters when using SG data. Furthermore, Rosat and Lambert (2009) have shown that a joint inversion (using SG + VLBI data) did not improve the results that they obtained using VLBI data alone.

Nowadays, owing to the accumulation of VLBI data it has become possible to improve significantly these results. Modern theory of nutation predicts a steady FCN period of

431.2 sidereal days (Dehant and Defraigne, 1997), and the most recent estimations from VLBI observations have been found to be about 430–431 sidereal days or about 429–430 solar days (Mathews et al., 2002; Koot et al., 2010).

Please note that all along this chapter, we have employed a sign + for the FCN period, but we should remember that the movement is retrograde (so its period should be around - 430 days) with respect to the Earth's rotation.

Response in nutation to the tidal forcing

Following the modern theory of the Earth's rotation (Mathews et al., 2002) we can determine the period not directly from an analysis of the observations but indirectly, through the transfer function. This function expresses the ratio between rigid and non-rigid nutation amplitudes (η_R and η)

(6.12)

$$T^{(n)}(\sigma) = \frac{\eta(\sigma)}{\eta_R(\sigma)}$$

wherein, neglecting the Inner Core Wobble effects,

(6.13)

$$T^{(n)}(\sigma) = \frac{e - \sigma}{e + 1}\left[1 - \frac{\sigma' \, s_1/e}{\sigma - s_1} + \frac{\sigma' N_2}{\sigma' - s_2} + \frac{\sigma' N_3}{\sigma' - s_3}\right]$$

where σ is the luni-solar nutation frequency in a rotating terrestrial reference frame and is given in cycle per sidereal day

$\sigma' = \sigma + \Omega$

$\eta(\sigma)$ are the theoretical amplitudes of the nutation for the real Earth,

$\eta_R(\sigma)$ are the rigid Earth nutation (REN) amplitudes (Souchay et al. 1999) and

$e = 0.0032845479$ is the dynamical oblateness of the rigid Earth,

The last three bracketed terms express the CW, FCN and FICN resonance, respectively, with their corresponding frequencies:

$$s_1 = \frac{A}{A_m}(e - \kappa)$$

$$s_2 = -\frac{A}{A_m}(e_f - \beta) - 1 \qquad s_3 = \frac{A}{A_m}(\alpha_2 e_s + v)$$

174

Where A and A_m are the equatorial inertia moments of the whole Earth and the mantle respectively.

$$N_2 = \frac{A_f}{A_m}(e - \gamma)$$

s_2 is the complex resonant frequency of the FCN, e and e_f the flattenings of the Earth and the fluid outer core, respectively, and A, A_m and A_f the equatorial moments of inertia of the whole Earth, of the mantle and of the fluid outer core, respectively.

The complex parameter N_2 represents the strength of the FCN resonance.

The flattening e_s is relevant to the solid inner core and e_f to the fluid outer core.

The compliance κ is expressed as $\kappa = ek/k_s$, where k and k_s are the elastic and fluid Love number, respectively. It expresses the deformability at the surface under the tidal forcing of degree 2.

The compliances $\gamma = q_0 h^f/2$ and $\beta = q_0 h_1/2$, where $h^f \approx 1.14$ and $h_1 \approx 0.35$, respectively characterize the deformability of the CMB by a volumic potential and under an inertial pressure acting at the CMB (Dehant et al. 1993).

The sensitivity analysis of $T^{(n)}$ to parameters N_2, s_1, s_2 and s_3 shown by Rosat and Lambert (2009), reveals that the nutations are primarily sensitive to the FCN frequency s_2, then to its amplitude N_2, and less sensitive to the Chandler frequency s_1 and to the FICN frequency s_3.

Please note that we have omitted the compliances associated with the electro-magnetic coupling at the CMB and that should be added in the frequency expression of the FCN and FICN (cf. Mathews et al. 2002 for the complete expression of the eigenfrequencies).

Table 6.1: Summary of some of the most relevant estimations of the period T, and the quality factor Q, of the FCN, from theoretical models and experimental results using different types of data (SG stations: B=Brussels, Belgium; BH=Bad Homburg, Germany; CA=Cantley, Canada; CB=Canberra (Australia); ES=Esashi (Japan); J=three Japanese stations; MA=Matsushiro (Japan); MB=Membach (Belgium); ST=Strasbourg, France. "OPA solution" refers to the nutation series obtained at the Observatoire de Paris VLBI analysis center.

Author	Data	T (sid. day)	Q
Neuberg et al. (1987)	Stacked gravity (B+BH)	431 ± 6	2800 ± 500
Sasao et al. (1980)	Theory elastic	465	∞
Wahr and Bergen (1986)	Theory inelastic	474	78000
Herring et al. (1986)	VLBI	435 ± 1	22000 – 100000
Cummins and Wahr (1993)	Stacked gravity IDA	428 ± 12	33000 – 37000
Sato et al. (1994)	Stacked gravity (J)	437 ± 15	$3200 - \infty$
Defraigne et al. (1994)	Stacked gravity (B+BH+ST) VLBI Stacked gravity + VLBI	424 ± 14 432 ± 4 433 ± 3	2300 – 8300 $Q > 15000$ $Q > 17000$
Florsch et al. (1994)	Gravity ST	431 ± 1	1700 – 2500
Merriam (1994)	Gravity CA	430 ± 4	5500 – 10000
Hinderer et al. (1995)	Stacked gravity (ST+CA)	429 ± 8	$7700 - \infty$
Roosbeek et al. (1999)	VLBI	431- 434	Not estimated
Polzer (1997)	Gravity	412.6 ± 4.2	≈ -10000
Florsch and Hinderer (2000)	Gravity ST (Bayes)	428	$Q > 20000$
Hinderer et al. (2000)	Gravity + VLBI	431- 434	15000 – 30000
Mathews et al. (2002)	MHB2000 model	430.20 ± 0.28	20000
Sato et al. (2004)	Stacked gravity (ES+MA+CB+MB)	429.70 ± 1.40	9350 – 10835
Mukai et al. (2004)	Strain	427.50 ± 11.1	5000 ± 12500
Vondràk and Ron (2006)	VLBI	430.32 ± 0.07	20600 ± 340
Ducarme et al. (2007)	Mean gravity	429.70 ± 2.40	Not estimated
Lambert and Dehant (2007)	VLBI	430 ± 0.40	17000 ± 3000
Ducarme et al. (2009)	Mean gravity in Europe	430 ± 2.00	15000 ± 8000
Rosat et al. (2009)	Stacked gravity of 7 European SGs (Bayes)	428 ± 3.00	$7762 < Q < 31989$ (90% C.I)
Rosat and Lambert (2009)	VLBI Gravity	429.6 ± 0.6 426.9 ± 1.2	16683 ± 884 16630 ± 3562
Koot et al. (2010)	VLBI (Bayes)(OPA solution)	429 ± 0.07	19716 ± 288
Amoruso et al. (2012)	Strain	429 ± 10	10000 - 50000

The predicted values of the FCN parameters have evolved from the $T_{FCN} \approx 470$ sidereal days and $Q \approx 40000$ in Wahr (1981)'s early papers to the $T_{FCN} \approx 429.93 - 430.48$ sidereal days and $Q \approx 20000$ obtained by Mathews et al. (2002) by fitting their nutation model to VLBI data up to 1999. Ducarme et al. (2006) pointed out that the most recent models (Dehant et al. 1999; Mathews et al. 2002) do not recover the exact observed resonance shape.

The FCN resonance in gravity data is commonly represented by a damped harmonic oscillator model.

A good example was shown in figure 5.5, section 5.2, where the amplitude factors in the diurnal frequency band using the complete SG record (T005 + C026) in Strasbourg J9 Observatory are shown, and there is a clear evidence of the FCN resonance.

Now, we are going to invert these data in order to estimate the FCN frequency, quality factor Q and the transfer function of the mantle (or the resonance strength). First, we are going to use individual gravimetric series recorded at J9, our study site; in a first analysis we have fitted the resonant admittances for each instrument separately and later we present a stacking of the data for the two SGs.

The data to be inverted are the complex gravimetric factors calculated in section 5.3, corrected for the ocean tide loading effect according to the FES 2004 ocean model (Lyard et al. 2006). All these inversions will be done using the Bayesian approach proposed by Florsch and Hinderer (2000) and previously commented in section 6.2.2.

To realize these inversions, we have used a FORTRAN code initially developed by N. Florsch and revised by S. Rosat in 2007 (this code is also used to subtract the OTL effect in our gravity observed data before estimating the inversion).

This code firstly converts the observed gravimetric factors (amplitude, phase) and their errors resulting from our analysis realized with ETERNA 3.4, into real and imaginary parts of the complex gravimetric factor delta with their errors. By default, 9 diurnal tidal waves are used (Q_1, O_1, M_1, P_1, K_1, PSI_1, PHI_1, J_1 and OO_1) and the initial parameter values follow an *a priori* weakly constraining uniform law (Florsch and Hinderer, 2000). In this first step, the ocean loading correction can be also performed using the FES2004 ocean model. Once the real and imaginary parts are computed, the inversion of these parameters is performed through the equation 6.6 resulting in 2D-joint probability density functions. Finally, the 1D-marginal laws are also computed for each parameter. Later on, we used a MATLAB code, developed also by S. Rosat to design and plot the probability density functions.

* Results for various gravimeters recording at J9

Table 6.2: Summary of the estimations of period and quality factor of the FCN using data from different types of gravimeters recording at J9 Observatory.

Series	T_{FCN} (sid. days)	Q
NA 138	423.6 ± 14	$23743 < Q < 71677$ (90% C.I)
LR ET005	424.5 ± 10	$30097 < Q < 76659$ (90% C.I)
T005	429.8 ± 5	$3954 < Q < 27457$ (90% C.I)
C026	430.9 ± 5	$5975 < Q < 47271$ (90% C.I)
T005 + C026	430.3 ± 5	$5862 < Q < 47362$ (90% C.I)

In the case of the North American gravimeter, due to the large uncertainty on the amplitudes and phases of the diurnal tidal waves close to the resonance, we obtained a poor constraint on the FCN parameter values.

Spring gravimeters

North American 138
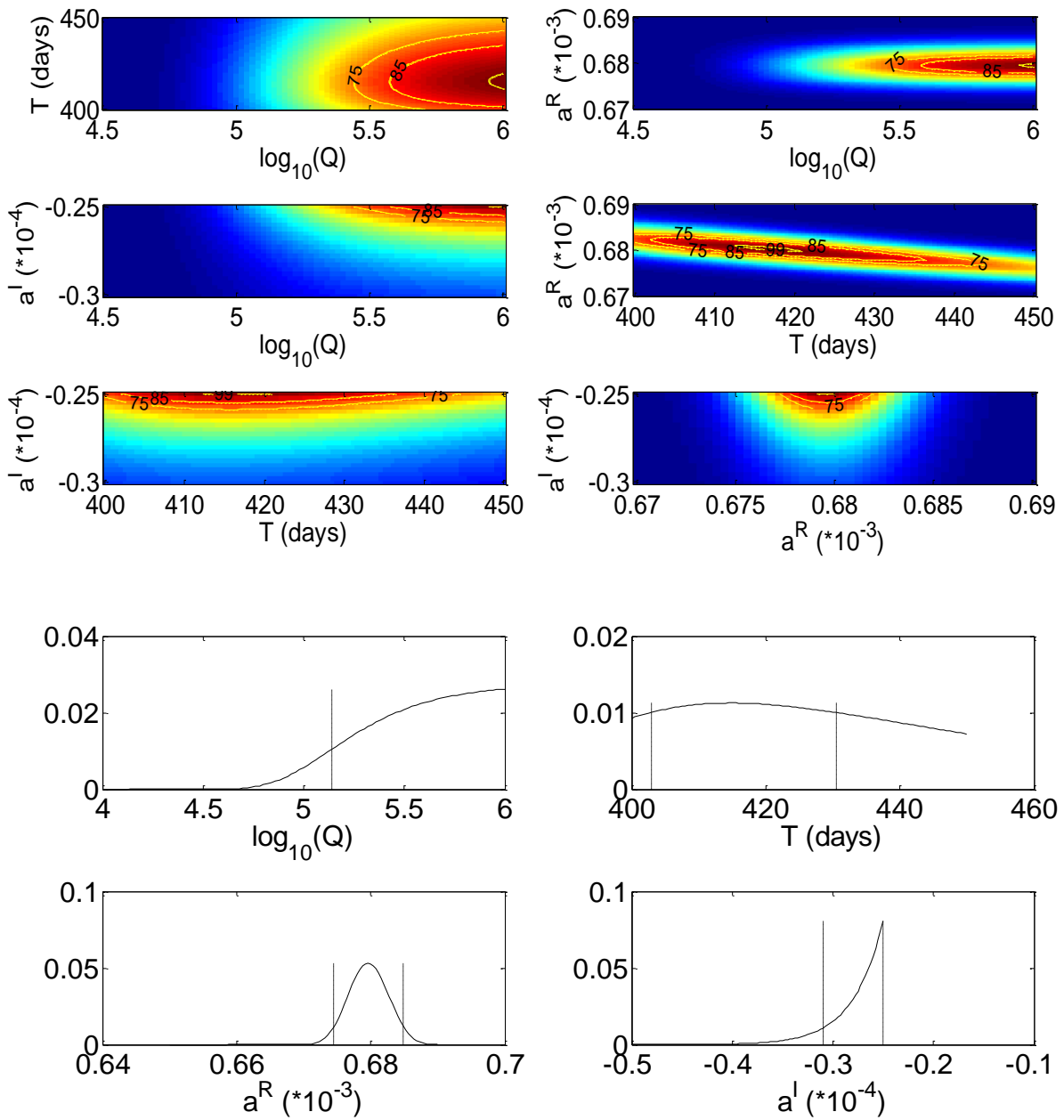
Fig. 6.8: Joint and marginal probability density functions for the FCN parameters $(\mathbf{a_r}, \mathbf{a_i}, \mathbf{T}$ and $\mathbf{x})$ estimated from 34 months of the NA138 data using the Bayesian method. Vertical dotted lines indicate the 90% confidence intervals.
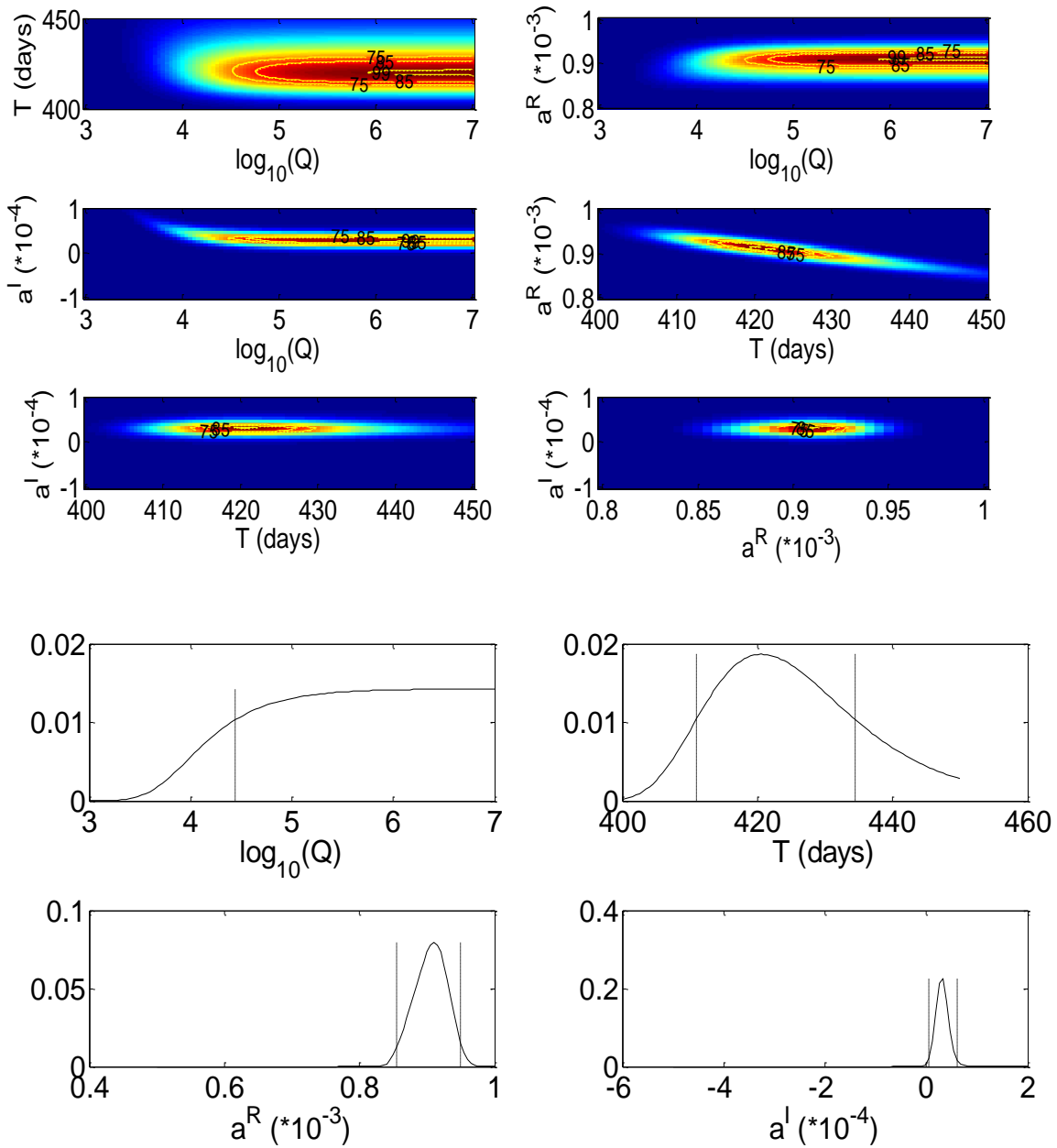
Fig. 6.9: Joint and marginal probability density functions for the FCN parameters ($\mathbf{a_r, a_i, T}$ and $\mathbf{x}$) estimated from 8 years of L&R ET005 data using the Bayesian method. Vertical dotted lines indicate the 90% confidence intervals.
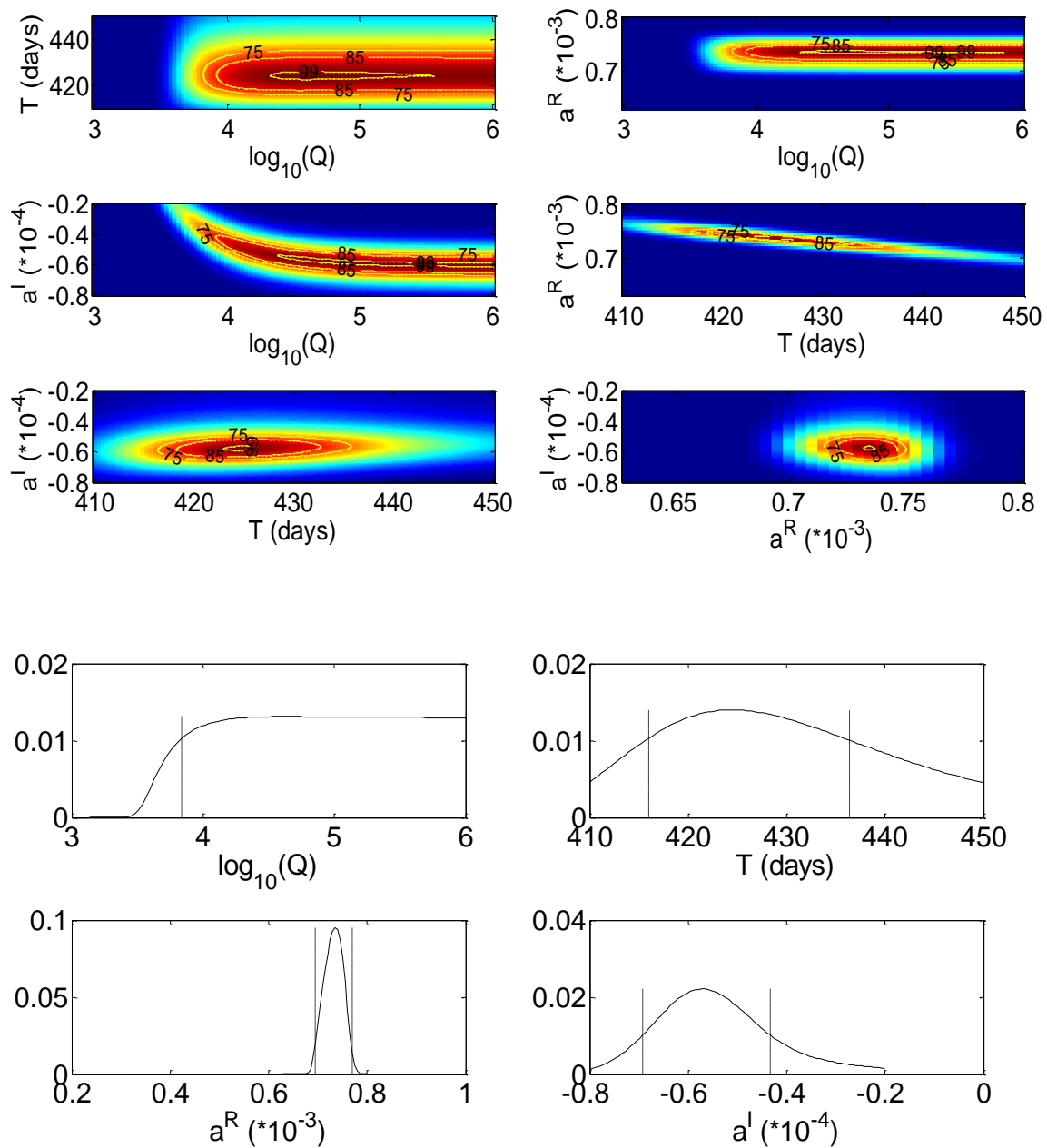
T005

Fig. 6.10: Joint and marginal probability density functions for the FCN parameters (a_r, a_i, **T** and **x**) estimated from 9 years of SG T005 data using the Bayesian method. Vertical dotted lines indicate the 90% confidence intervals.
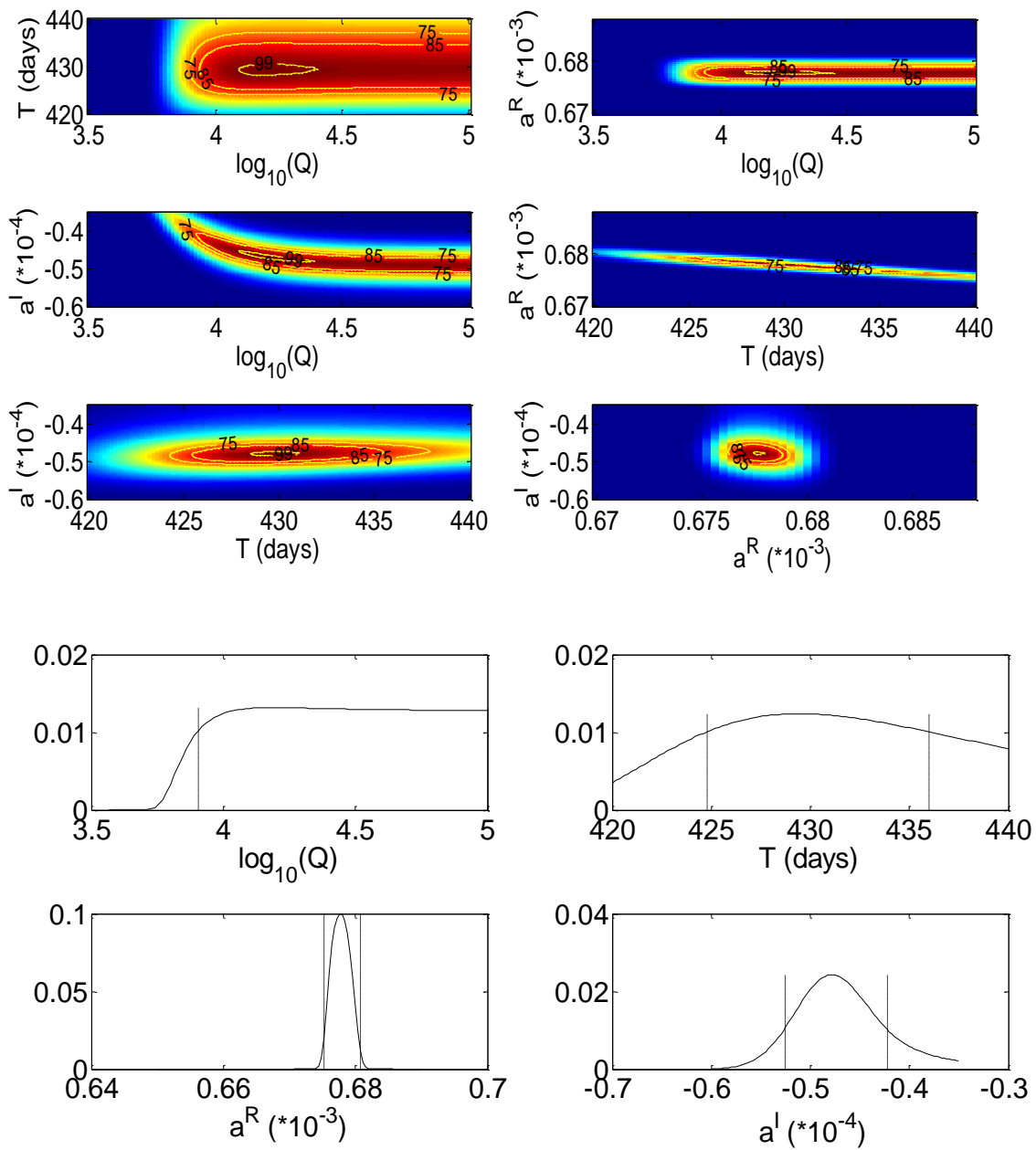
Fig. 6.11: Joint and marginal probability density functions for the FCN parameters ($\mathbf{a_r}, \mathbf{a_i}$, **T** and **x**) estimated from 18 years of SG C026 data using the Bayesian method. Vertical dotted lines indicate the 90% confidence intervals.
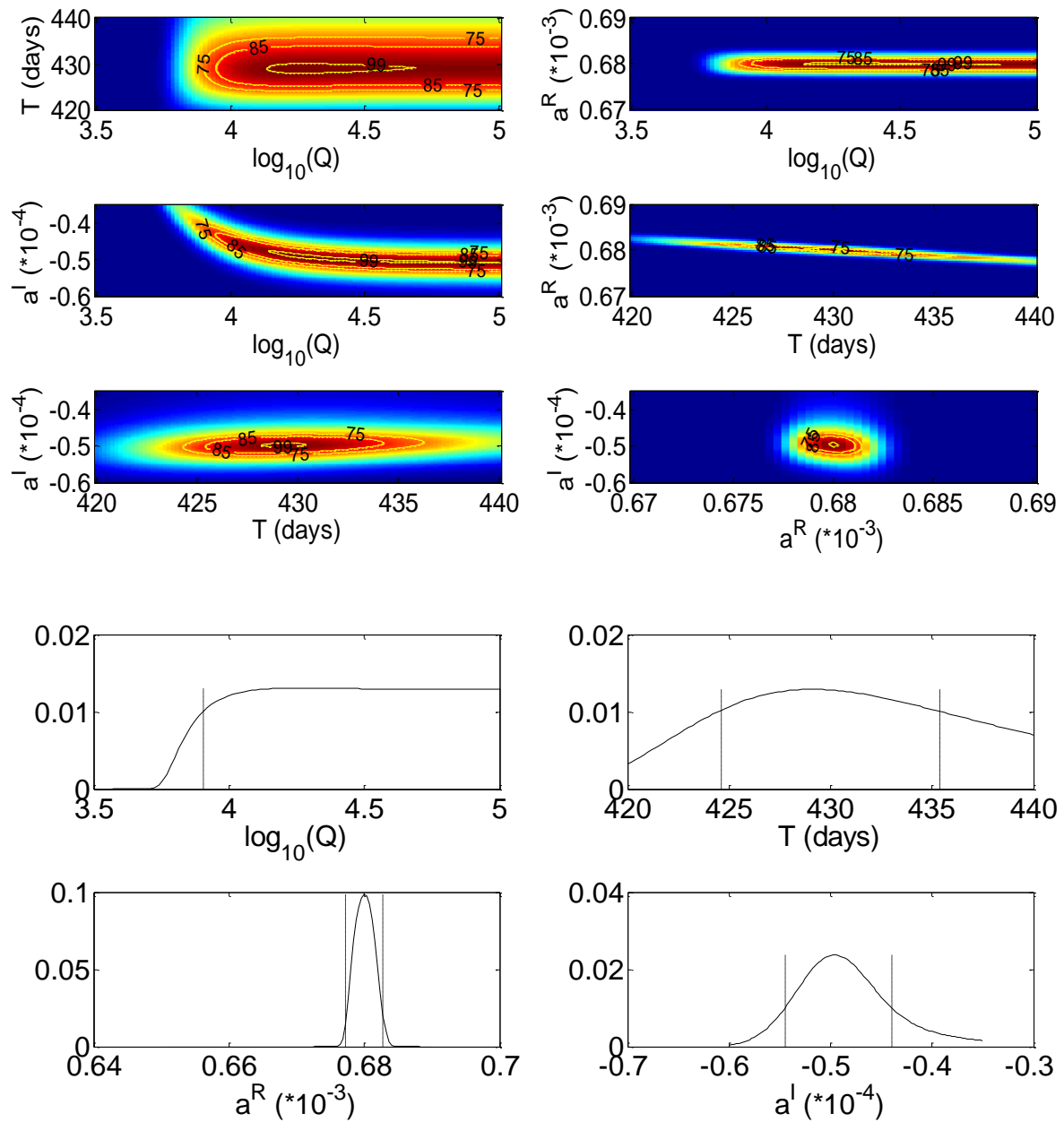
Fig. 6.12: Joint and marginal probability density functions for the FCN parameters ($\mathbf{a_r}, \mathbf{a_i}, \mathbf{T}$ and $\mathbf{x}$) estimated from 27 years of the merged SG series (T005+C026) using the Bayesian method. Vertical dotted lines indicate the 90% confidence intervals.

The FCN period value obtained from the merged SG observations (T005 and C026) at J9 observatory is very close to the period obtained from the theoretical computation, 429.5 sidereal days (Dehant et al., 1999) and is also very close to the one obtained when using VLBI data including the electro-magnetic coupling at the core-mantle boundary, 430.04 sd (Mathews et al., 2002). The best quality factor is obtained from the tidal analysis of SG C026 data alone ($Q = 26613$).

* Results obtained with other European SGs

In a second step, we are going to stack the data from several European SGs. Stacking long-period and high-precision tidal gravity data in different areas can reduce effectively the discrepancy of the retrieved resonance parameters caused by atmospheric and oceanic loading and the local environmental perturbations surrounding the stations. We have performed an independent inversion and a combined inversion of 7 of the GGP European SG data previously analyzed in section 4.4 (Table 6.3).

In a first analysis we fit the resonant admittances for each tidal station separately and later refer to these as the individual fits. In a second analysis we fit the same model function to the resonant admittances of all stations simultaneously.

Table 6. 3: Summary of the estimated period and quality factor of the FCN, using data from 7 European Superconducting gravimeters, and for the stacking of these 7 SGs.

Series	T_{FCN} sid. days	Q
Bad Homburg	429.88 ±5.7	$4201 < Q < 44906$ (90% C.I)
J9 (T005 + C026)	430.91 ±5.1	$5862 < Q < 47362$ (90% C.I)
Medicina	430.03 ±5.7	$1072 < Q < 26819$ (90% C.I)
Membach	429.61 ±5.7	$5156 < Q < 47220$ (90% C.I)
Moxa	429.93 ±5.5	$3507 < Q < 42734$ (90% C.I)
Vienna	429.73 ±5.7	$3671 < Q < 42909$ (90% C.I)
Wettzell	430.38 ±5.7	$2368 < Q < 28911$ (90% C.I)
Stacking of 7 stations	430.32 ±5.2	$3614 < Q < 39742$ (90% C.I)
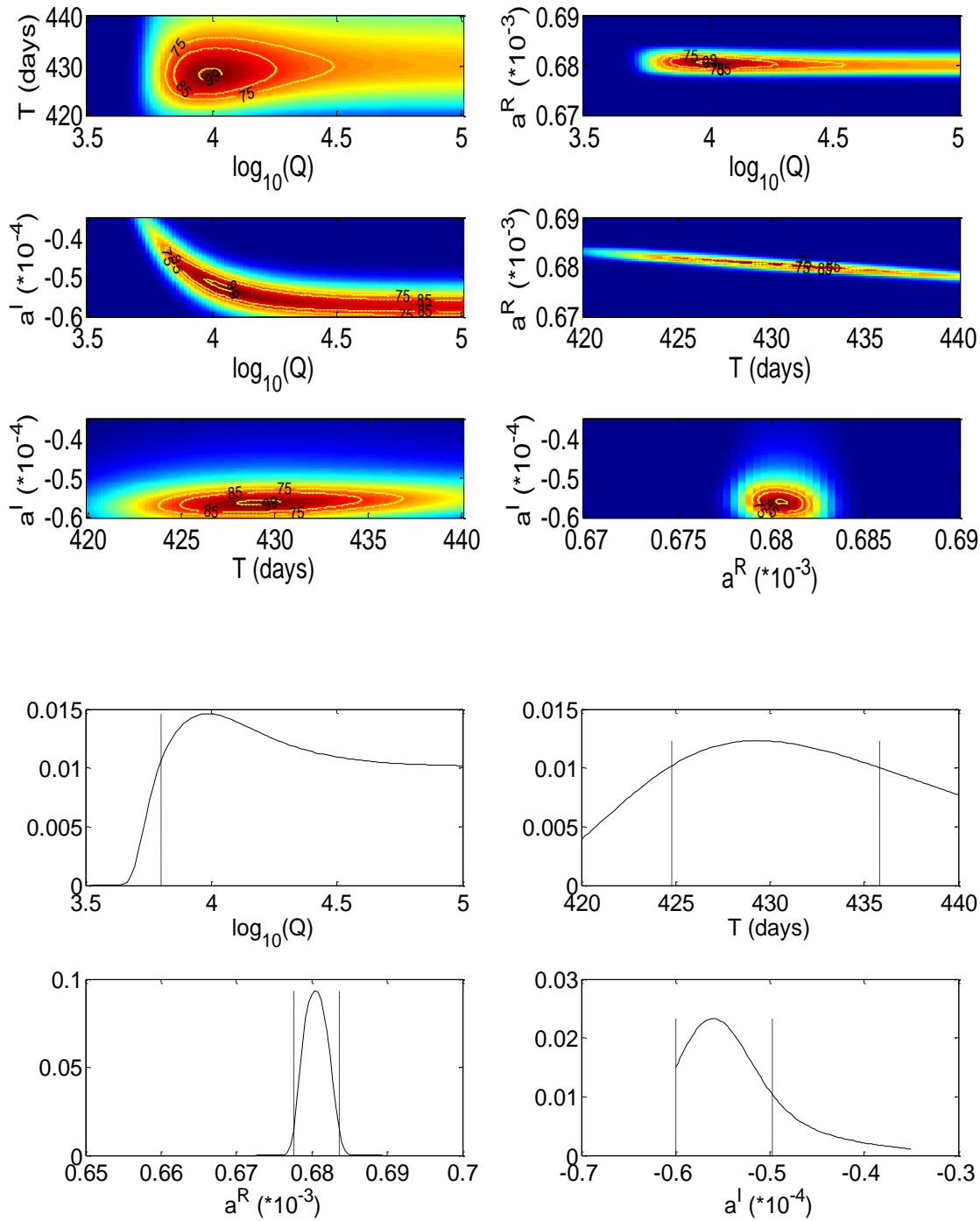
Fig. 6.13: Joint and marginal probability density functions for the FCN parameters $(\mathbf{a_r, a_i, T}$ and $\mathbf{x})$ estimated from stacking 7 European SG (Bad-Homburg, J9 (Strasbourg), Moxa, Membach, Medicina, Strasbourg, Vienna and Wettzell) records using the Bayesian method. Vertical dotted lines indicate the 90% confidence intervals.

Our values obtained from SG gravity data are very consistent with those inferred from VLBI nutation data. The period obtained for all SG stations is slightly lower than the period obtained in our reference site (J9 observatory, 430.91 sd). The higher

quality factors are obtained at Bad Homburg (24553) and Membach (26187) stations.

In the near future, a more accurate determination of the resonance parameters and a more advanced study of the Earth's FCN will depend on the simultaneous utilization of various additional high-precision observations (including strain data) recorded at globally distributed stations.

6.6 Attempt of detection of the FICN

The origin of the existence of the Free Inner Core Nutation (FICN), also called the prograde FCN, is very similar to that of FCN, is caused by the rotation of a slightly tilted solid inner core with respect to the fluid core and the mantle. It has been computed theoretically by Mathews et al. (1991a, 1991b) and Herring et al. (1991) using a semi-analytical method, and by Legros et al. (1993) and Dehant et al. (1993) using a completely analytical method. The theoretical calculations predict a very weak surface amplitude of a few tens of micro-arcseconds (where 1 μas ∼ 0.03 mm of equatorial shift at the Earth surface), a gravity perturbation of ∼ 0.1 nGal and a smaller resonance effect on Earth tides than for the FCN.

As we mentioned in section 2.1.9, this mode has never been observed using gravity data. Several attempts made using VLBI data failed. However, according to Mathews et al. (2002) the FICN period is between 930 and 1140 days, and Koot et al. (2010) estimated the FICN period between 875 and 975 days (1σ interval). The FICN parameters were obtained by fitting a resonance transfer function model like equation 6.13 to the VLBI nutation data including the FICN resonant term. This determination is mostly constrained by the 18.6-yr nutation term, the most sensitive to the FICN, but which amplitude is poorly defined since only 30 years of VLBI data were used.

The parameters involved in the calculation of the FICN are the flattening of the inner core, the densities of the inner core and outer core, and the deformation of the Inner Core Boundary (ICB) due to the fluid dynamic pressure acting on it. The rheological behavior of the inner core seems to play a critical role in its rotation. Theoretically, the geodetic or gravimetric estimations of the period of the FICN simultaneously with its quality factor will permit to determine both, the viscosity of the inner core and the frictional constant at the ICB (Greff-Lefftz et al., 2000).

Similar as the FCN, the FICN has a quasi-diurnal period in the terrestrial reference frame, and a prograde long period in the celestial reference frame. The frequency is very much dependent on the density jump at the inner core-outer core boundary, as well as on the inner-core flattening (Dehant et al. 1997). Therefore, as the density jump at the ICB is not well known, also the period is not well known; an increase in the amplitude of the radial magnetic field at the ICB involves an increase of the period of the FICN. Also, the quality factor associated with the FICN in the different theoretical models varies with several orders of magnitude.

An illustration of the theoretically predicted resonances is shown in figure 6.14 (adapted from Hinderer 1997). The right side shows the FCN resonance and the FICN resonance is shown in the left side. It is evident that the resonance effect of the FICN is significantly lower than the one for the FCN.
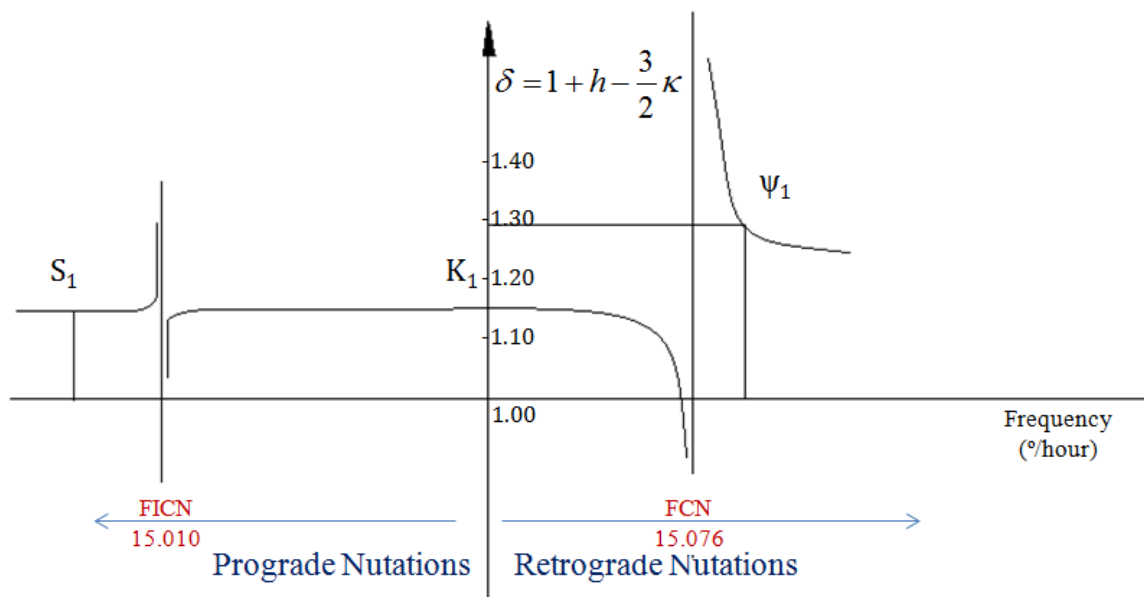
Fig. 6.14: Double theoretical resonance in the tidal gravimetric factor (adapted from Hinderer 1997) including the FICN resonance and the stronger FCN contribution.

Similar as they did in the last century in a first step to try to observationally prove the existence of the FCN, we will use now the 27-year series recorded by the SGs T005 and C026 at J9 to try to prove the existence of the FICN.

We rely on some previous results to estimate in which frequency intervals we should focus our search. Rogister (2001) estimated that the FICN period should be around 470 sidereal days while Koot et al. (2008) estimated it between 875 and 1100 sidereal days. Considering all these values, we expand the range from 430 to 1400 sidereal days (corresponding to a range between 0.99768 and 0.99928 cpsd) to focus the search of a possible resonance effect in diurnal tidal amplitudes.

Using the spectral analysis of the merged 27-year series recorded by T005 and C026 at J9, there are three waves (A, B and C) between S_1 (0.99727 cpsd) and K_{1x-} (0.99985 cpsd) (K_{1x-} is a lunar nodal wave of K_1 with a 18.6 year sidereal period), that we could try to separate performing a more detailed tidal analysis for those frequencies, than the analysis performed in section 5 using ETERNA 3.4 (Fig 6.15).
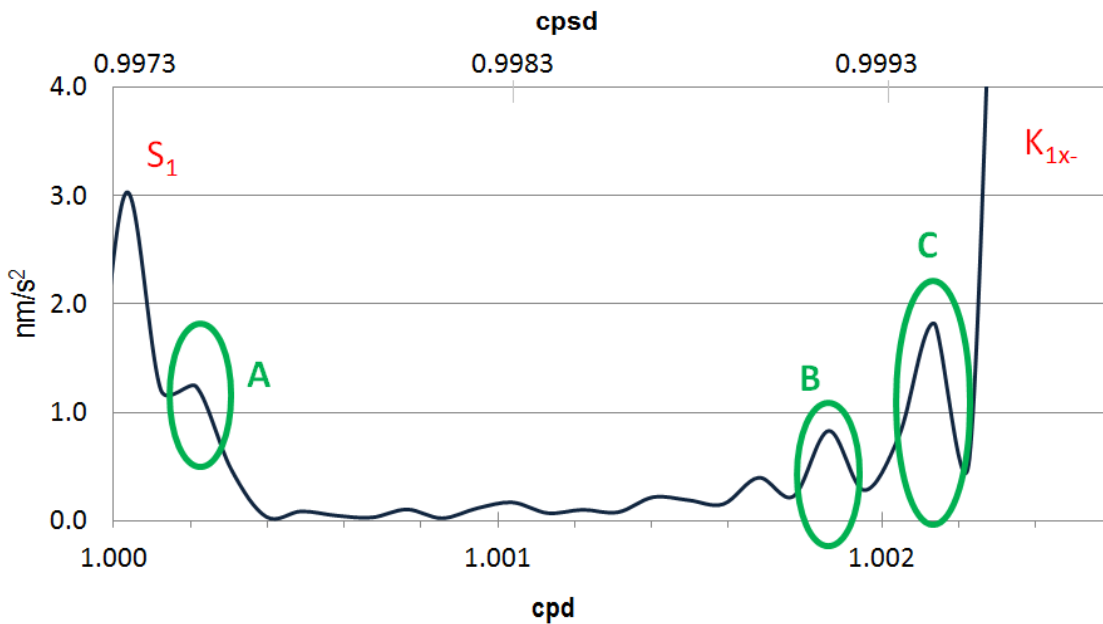
Fig. 6.15: Amplitude spectra of the complete (9760 days, 26.7 years) SG record (T005 + C026) in Strasbourg J9 Observatory between S1 and K1x- waves.

These three waves correspond to the wave 551 (A), wave 553(B) and wave 554 (C) in the potential catalogue of Tamura. A and B are derived from the potential of degree 2, while C wave derives from the potential of degree 3. As expected from the theory, the resonance only alters the amplitude of the degree 2 tides (e.g. Hinderer & Legros 1989). So we try to identify any resonance phenomenon in the amplitudes of the A and B waves.

Despite the length of the series, the results obtained for 'A' and 'C' waves are not accurate enough to consider that there could be a real resonance effect. However despite its large error, the 'B' wave seems to exhibit a resonance near 0.99924 cpsd (1.00198 cpd) (Fig 6.16).
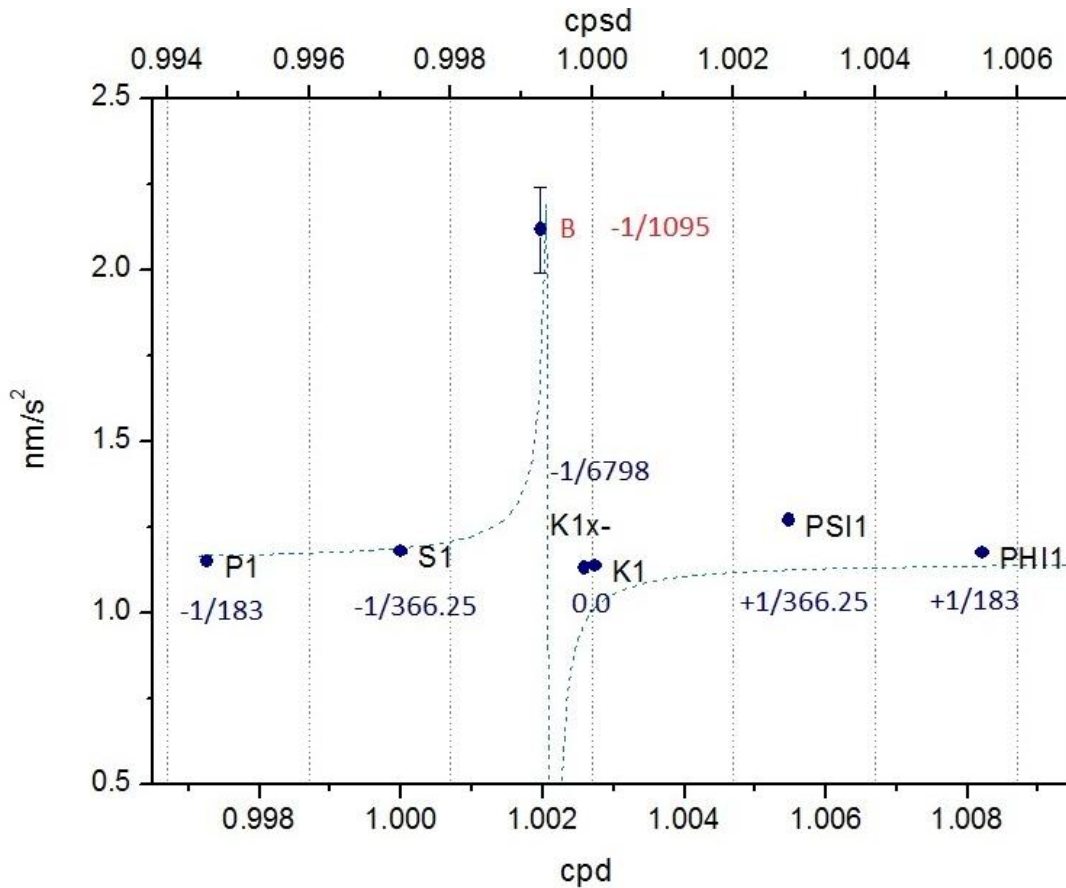
Fig. 6.16: Amplitude factors using the complete (9800 days, ~27 years) SG record (T005 + C026) in Strasbourg J9 Observatory, between P1 and PHI1 frequency bands. A possible resonance curve (least squares fitted) is superimposed with dotted line, with frequency ~ 0.99924 cpsd. For each wave is expressed the x value with respect to the frequency of K_1 (1 cpsd) derived from $f = -\Omega(1 + x)$, where $\Omega = 1$ cpsd.

In addition to Strasbourg, we consider now other SG sites in Europe in order to investigate the possible resonance effect in the amplitude of the diurnal waves, caused in the proximity of this frequency (1.00198 cpd). We perform a precise tidal analysis for all those series using ETERNA 3.4. For some of these stations, such as Bad Homburg, Medicina and Moxa, a similar behavior is indeed found for nearby frequencies (figures 6.17, 6.18, and 6.19).
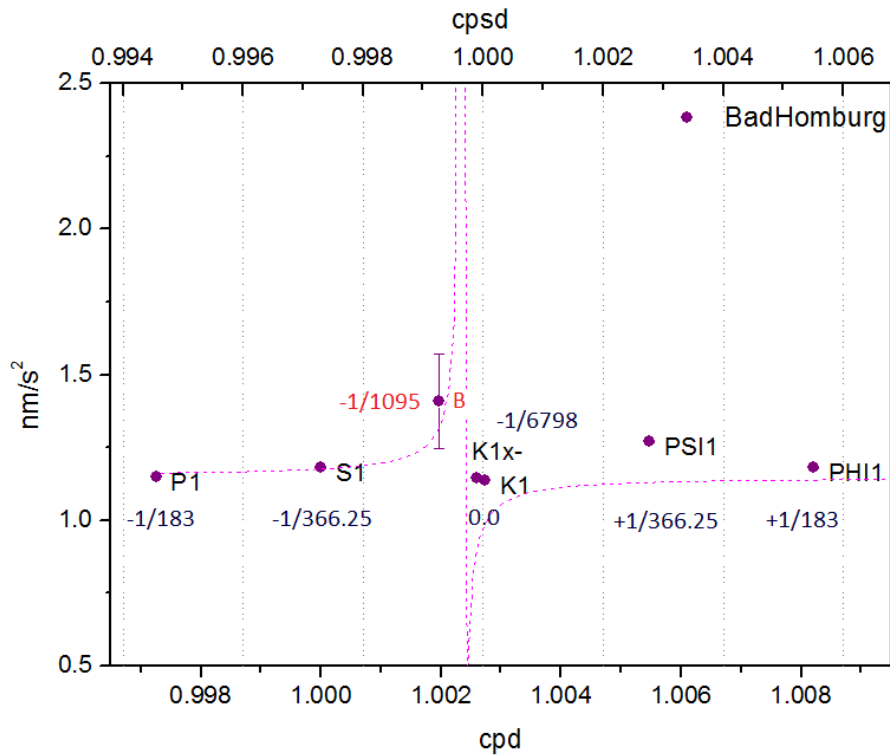
Fig. 6.17: Amplitude factors using the SG record in Bad Homburg Observatory, between P1 and PHI1 frequency bands. A possible resonance curve (least squares fitted) is superimposed with dotted line, with frequency ~ 0.99927 cpsd. For each wave is expressed the x value with respect to the frequency of K_1 (1 cpsd) derived from $\boldsymbol{f} = -\boldsymbol{\Omega}(\boldsymbol{1} + \mathbf{x})$, where $\boldsymbol{\Omega} = 1$ cpsd.
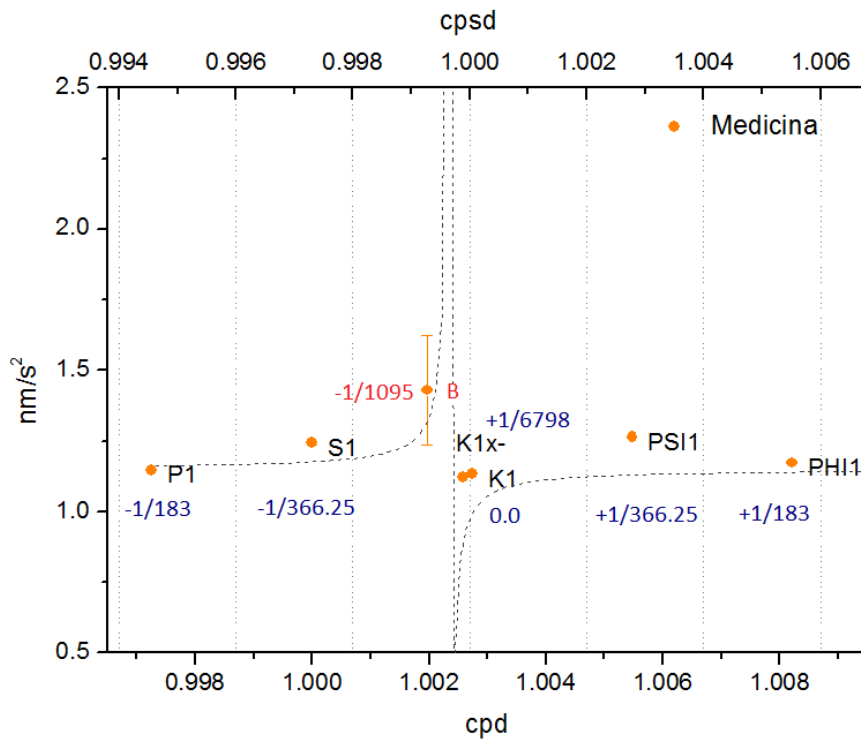
Fig. 6.18: Amplitude factors using the SG record in Medicina Observatory, between P1 and PHI1 frequency bands. A possible resonance curve (least squares fitted) is

superimposed with dotted line, with frequency ~ 0.99931 cpsd. For each wave is expressed the x value with respect the frequency of K_1 (1 cpsd) derived from $f = -\Omega(1 + x)$, where $\Omega = 1$ cpsd.
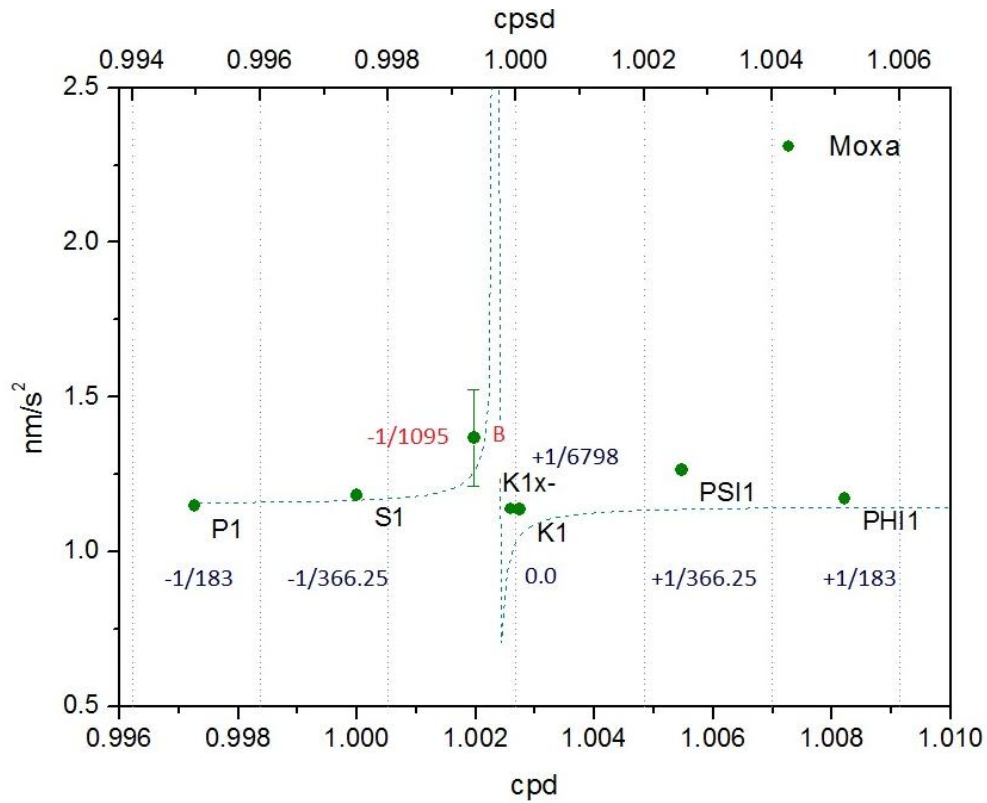
Fig. 6.19: Amplitude factors using the SG record in Moxa Observatory, between P1 and PHI1 frequency bands. A possible resonance curve (least squares fitted) is superimposed with dotted line, with frequency ~ 0.99925 cpsd. For each wave is expressed the x value with respect the frequency of K_1 (1 cpsd) derived from $f = -\Omega(1 + x)$, where $\Omega = 1$ cpsd.

Even if all these results are promising, the theoretical prediction of the FICN period is not sufficiently accurate to unambiguously link those oscillations with the FICN resonance. Hence, it seems to be necessary to improve the theoretical estimates of the FICN period to make its search in the observational data more efficient.

Besides the FICN resonance effect in diurnal gravimetric tides , another way to detect this mode is to analyse the most accurate nutation series obtained from the VLBI observations, especially when the determination of the 18.6 year term will become more accurate thanks to longer data sets.

6.7. Chapter's summary

The objective of this chapter was to determine the characteristics of the core resonance through the gravity data that we have used throughout the previous chapters.

The diurnal tidal amplitudes are resonant at the FCN frequency, and hence we can use the measurements of tidal amplitudes to determine the FCN frequency. The frequency of this mode is particularly sensitive to the flattening of the core-mantle boundary, which is the largest compositional discontinuity within the Earth, at a depth of 2889 km (Young and Lay 1987). So observing the FCN is thus very useful to infer the CMB flattening from its period and to obtain information about the dissipation effects at this interface from the determination of its damping.

After reviewing the history of the first observations of the FCN resonance on gravity data (that casually was carried out using gravity data recorded at the Observatory of Strasbourg), special efforts are undertaken in order to estimate the FCN parameters (Q and T_{FCN}) from our observations, using the Bayesian approach, proposed by Florsch and Hinderer (2000).

We use firstly individual gravimetric series recorded at J9, from both spring and superconducting gravimeters. In a first analysis, we fit the resonant admittances for each instrument separately and for the stacking of the two SGs data. In a second step, we stack the data from different European SGs data we have already used in chapter 4 to study their stability, and in chapter 5 to try to detect the 18.6 year period signal. The values obtained (for all the SG stations) are very close to those estimated from the theoretical computations, and are also in very good agreement with those obtained through VLBI observations.

We also review the observations of the FCN resonance using other techniques, as for example observations obtained using borehole water-level or strainmeter data and in more details, using the VLBI technique, which is the most accurate.

Regarding the FICN, this mode has never been observed in gravity records, and the theoretical calculations predict a very weak resonance effect on Earth tides and nutations. Detecting this signal in the data will allow us to substantially improve our knowledge about the Earth's interior and its dynamics. During last years several attempts to find the FICN component in VLBI nutation series have failed, only its resonance effect on the long-period nutations (mostly the 18.6 year term) could be used to try to constrain its parameters.

We use here the 27-year series recorded by the superconducting gravimeters T005 and C026 at J9 Observatory to try to prove the existence of the FICN, in a similar way as in a first step to try to prove the existence of the FCN on gravity data:

Relying on the frequency interval estimated in previous studies, we focus on the range from 430 to 1400 sidereal days for the FICN period. The spectral analysis of the merged 27-year series is analyzed to check if there are more waves detected in that period range than the waves already obtained in the complete tidal analysis done in chapter 5. Indeed there are several small amplitude tidal waves that can be separated now.

Several tests, modifying the frequency limits of the wave groups, are done to try to separate these new waves in the diurnal tidal band in the ETERNA 3.30 analyses. We focus on the period range $[S_1, K_{1x-}]$ and check if a resonance effect appears. One possible resonance is found near 1.00198 cpd (0.99924 cpsd) using the long Strasbourg series. Similar tidal analyses are performed using the European SG records which have been already used in chapters 4 and 5, and we obtain comparable results in some of these stations (Bad Homburg, Medicina and Moxa). If such observation corresponds to a resonance associated with the FICN, it would correspond to a period for the FICN around 1300 sidereal days that is larger than the latest theoretical predictions and slightly larger than the VLBI nutation estimates.

Progress on the theoretical estimates of the FICN period on one side and the VLBI nutation observations on the other side will also help in the future the search for the resonance effect in the surface gravity data.

Improvement in the observational determination of the FCN and FICN parameters is important in geodynamics, because they give us useful and unique information to constrain the parameters related to the physical process of coupling at the core-mantle boundary (CMB) and at the inner core-fluid core boundary (ICB).

Chapter 7

Conclusions
&Perspectives

Conclusions

In Strasbourg, the first gravimeter with the main purpose of recording Earth's tides was installed in 1954. Since then, 8 different models of gravimeters (relative spring gravimeter, relative superconducting gravimeter and absolute gravimeter) have been recording at different consecutive periods. In the meanwhile, the sensors, the acquisition systems and the computational methods have been drastically improved.

We have used all these series recorded at Strasbourg observatory to verify these improvements, concluding that the measurements accuracy has been increased by more than 10 times with respect to the first models. The time stability and the noise level of all these series have been studied, mainly in terms of long term stability of the tidal parameters (amplitude and phase) and instrumental drift.

Similar studies are carried on 8 superconducting relative gravimeters installed in central Europe, all of them belonging to the worldwide network of superconducting relative gravimeters (Global Geodynamics Project).

We obtained temporal evolutions of the tidal delta factors in Strasbourg found to be very similar to other European SG stations with stability between 0.03% and 0.3%. Some time fluctuations with a seasonal oscillation appear at a few sites. In case that these temporal variations reflect a geophysical process, they should reflect it in a similar way at most European site, or at least at close stations, but it is not the case in our results.

As the variations obtained for the ratio $\delta M_2/\delta O_1$ are much smaller than the variations for each individual gravimetric factor, it led us to consider that some part of the tidal factor fluctuations could be due to changes of instrumental origin (e.g. calibration factor). However, we used all the calibration experiments performed at J9 observatory since 1996, when an absolute gravimeter was acquired, to check the temporal stability of the calibration factors (all these experiments are derived from a direct comparison of the SG data with repeated absolute gravity measurements).

We conclude that the internal SG C026 stability ($\sim 0.1\%$), obtained from the study of the tidal parameters, is more than 10 times better than the one that can be achieved by SG /AG calibration repetitions ($\sim 1.4\%$). Consequently, it is highly possible that the observed time variations of delta factors are due mostly to the noise variations as shown by the correlation found between delta factor deviations and noise level changes.

Taking into account all these results, we show that thanks to its stability, the superconducting gravimeters can uniquely contribute to the study of the low frequency Earth's tides, and small amplitude waves.

It is evident that the ability of SGs to reliably measure effects at the 0.1 μGal level has opened up many interesting scientific possibilities. Therefore, using the long superconducting series studied before, we obtain a high resolution spectral analysis in the tidal bands, which allows us to:

- separate contributions of near frequencies that were never observed before

- search for very weak signals (especially, waves derived from tidal potential of degree 3)

- exhibit very low frequency terms

Unfortunately, despite the 27-year length of our data series, we are still not able to retrieve the tidal waves of 9.3 and 18.6 year periods, which are of special interest for investigating the rheological behavior of the solid Earth at such periods.

In the last part, we have reviewed the history of the first observations of the Free Core Nutation resonance on gravity data. We have estimated the values of the FCN parameters using data from all series at Strasbourg, and also from all SGs series in central Europe. Our results are in very good agreement with those estimated both from theoretical computations and from VLBI observations.

We searched also for the rotational normal mode called Free Inner Core Nutation, which has never been observed using gravity data before. For this purpose we developed a methodology to constrain the possible frequency range, through the detailed tidal analysis of the diurnal frequency band (using the 27-year superconducting gravity series recorded at J9 observatory), to separate small amplitude waves that have never been studied before, and which could be close enough to the frequency period of the FICN to be affected in terms of amplitude resonance.

We focused on the period range $[S_1, K_{1x-}]$, where a possible candidate is found close to the frequency of 1.00198 cpd (0.99924 cpsd). Applying the same detailed tidal analysis in the diurnal frequency band, we obtained comparable results in some of the European SGs stations (Bad Homburg, Medicina and Moxa).

Perspectives

To use the different data series analyzed in this study (both data recorded by spring gravimeters and by superconducting gravimeters) it has been necessary to make a previous huge work of preprocessing. Thanks to this preprocessing, we now have several sets of high-quality gravity residuals distributed in central Europe. All series can be further used in a wide range of studies conducted at the regional level, such as:

- Correlation studies with the oceanic tide loading to check if there is any possible time variation in the loading.

- Correlation studies with the hydrological information available for Central Europe.

- Comparative studies surface gravity - GRACE gravity at the European regional scale

- Studies of the effect of ocean noise on the gravity records,

besides many other studies in a wide frequency range.

A new Superconducting gravimeter model (iOSG) will be installed at J9 observatory in 2015 ensuring the continuity of the long series. The continuity of this long series of high quality data, will allow us to further identify different waves of small amplitude and separate neighboring waves with very close frequencies; new opportunities to better detect the 9.3 and 18.6 year long-period waves will appear, and similarly for all long period waves which will be detected more precisely.

We will continue working on the possible detection of the FICN resonances in our data series. An inversion of the FICN, using a Bayesian approach similar to which has been applied for the FCN parameters, will be applied. Also, in a near future; a combination of longer series and improvement in the theoretical prediction of the FICN period will make the search of the frequency of this rotational mode more promising.

Annexes

Influence of pre-processing on tidal analysis results

Test performed to estimate the impact that the manual correction of the disturbances in the raw data (using Tsoft) could have on the stability of the tidal analysis performed with ETERNA 3.4:

- ✓ We have generated a synthetic series for J9 station using DDW99 non hydrostatic Earth's model (Dehant et al., 1999) and NAO99 ocean model (Matsumoto et al. 2000).
- ✓ This series has been degraded by adding Gaussian white noise (with a standard deviation of 10 nm/s^2), random gaps (up to 2500h in total, corresponding to about 3% of our time length), 4 offsets of different size (5, 10, 15 and 20 nm/s^2) and 10% of spikes distributed all along the series.
- ✓ We have corrected this degraded series manually with the help of TSOFT, in a similar way as we have done for all the observed series used in this study.
- ✓ We have performed similar tidal analysis on all these synthetic signals on yearly segments shifted month by month.
- ✓ We computed the variability of the main diurnal and semi-diurnal tides using the result of these analyses.
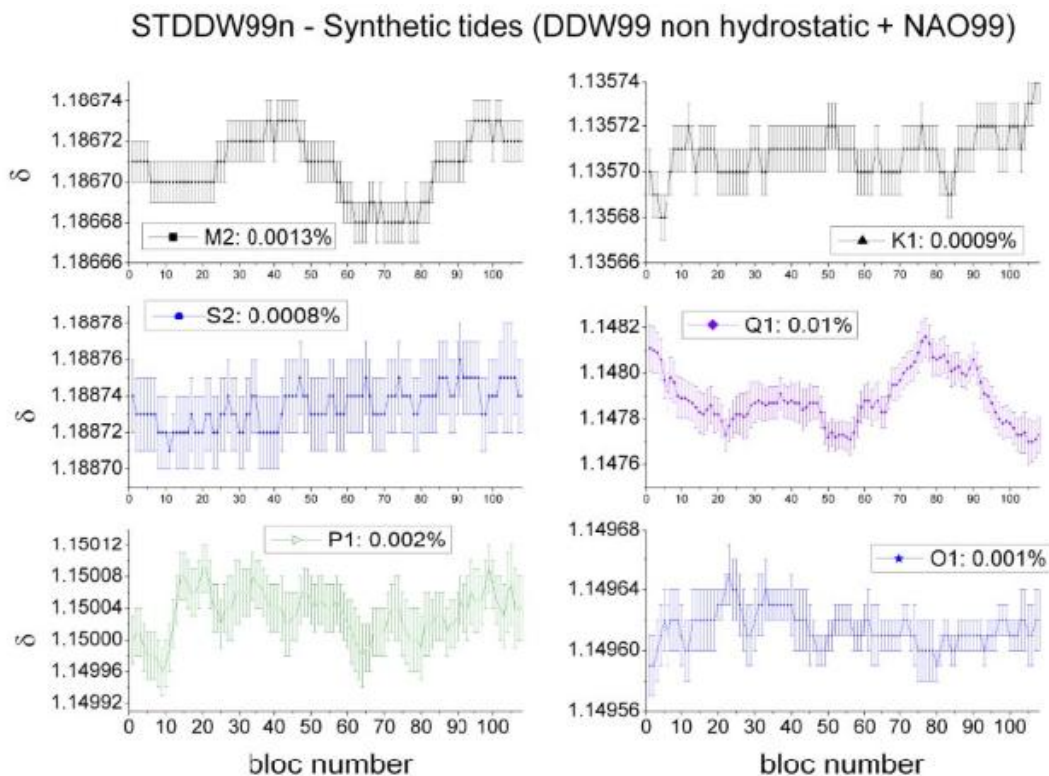
Fig. A.1: Time variability of the delta factors for a synthetic tidal model (DDW99+NAO99) at J9 showing the numeric and ETERNA analysis effects.
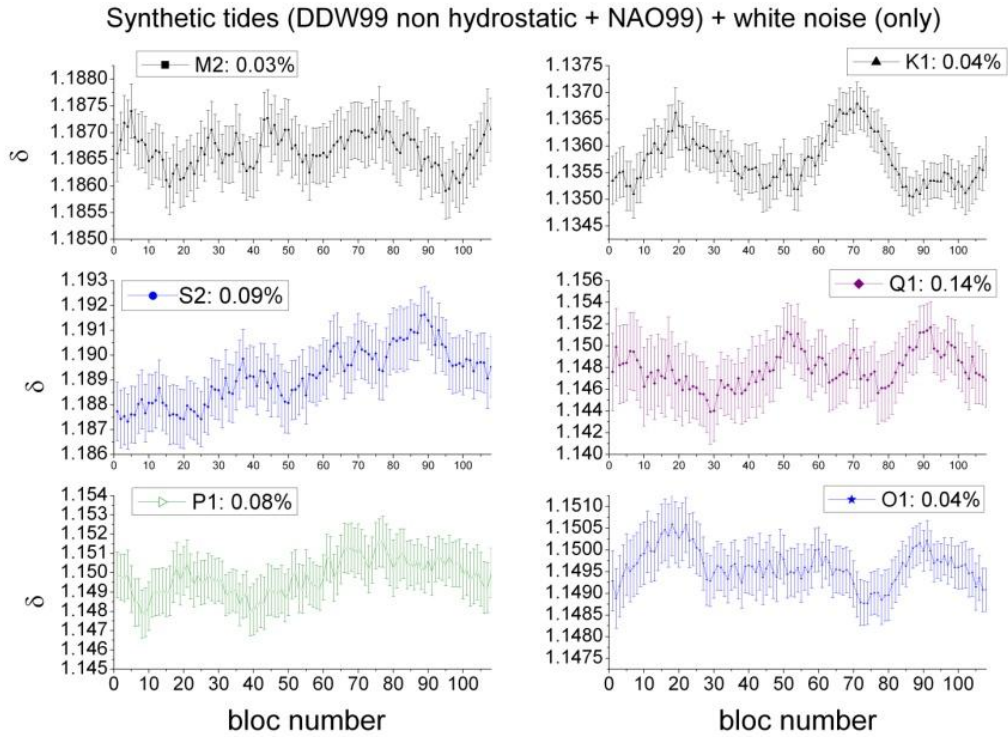
Fig. A.2: Time variability of the delta factors for the same synthetic tidal model at J9, degraded only with Gaussian white noise (10nm/s^2).
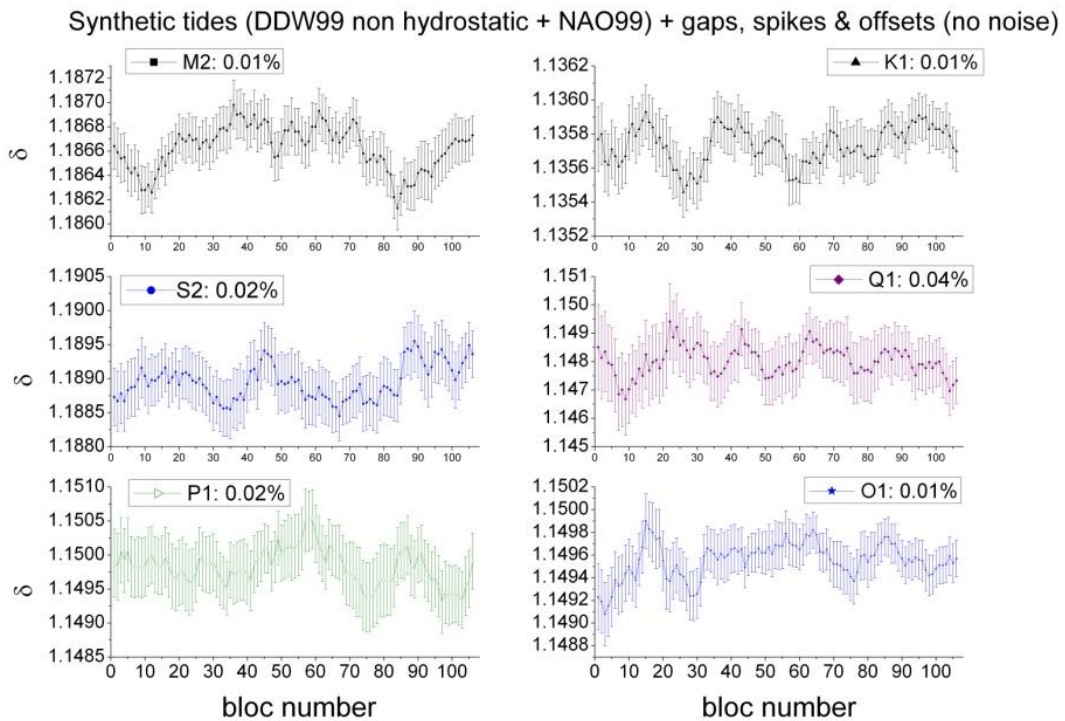
Fig. A.3: Time variability of the delta factors for the same synthetic tidal model at J9, degraded only with disturbances (gaps, spikes and offsets).
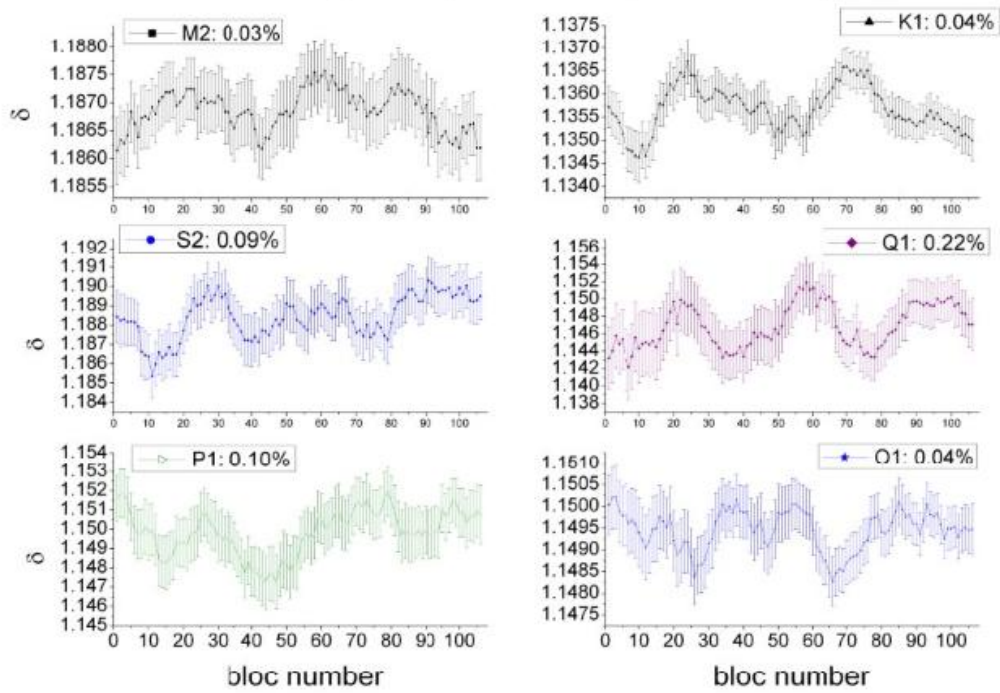
Fig. A.4: Time variability of the delta factors for a synthetic tidal model (DDW99+NAO99) at J9 showing the pre-processing effect.

Synthetic data

* 1-year data

Table B.1: Comparison of the results (amplitude factor ,phase differences and standard deviations) obtained in the diurnal band (up) semi diurnal band (middle) and ter diurnal band (down) for the same synthetic data series (1 year data) using VAV 06 (left columns), ETERNA 3.4 with TAMURA's catalogue (middle columns) and ETERNA 3.4 with HW catalogue (right columns)

Diurnal	VAV 06				ETERNA (TAMURA)				ETERNA (HW)			
	δ	stdv	κ	stdv	δ	stdv	κ	stdv	δ	stdv	κ	stdv
Q1	1.1541	0.0004	-0.0210	0.0220	1.1535	0.0001	-0.0216	0.0032	1.1534	0.00002	0.0004	0.0010
O1	1.1531	0.0001	-0.0020	0.0040	1.1532	0.0000	-0.0046	0.0006	1.1532	0.00000	0.0003	0.0002
K1	1.1460	0.0024	0.0410	0.1230	1.1494	0.0004	0.0218	0.0193	1.1524	0.00012	-0.0366	0.0062
J1	1.1476	0.0002	0.0050	0.0090	1.1476	0.0000	0.0003	0.0012	1.1477	0.00001	0.0003	0.0004
OO1	1.1558	0.0009	-0.0130	0.0430	1.1552	0.0001	-0.0223	0.0071	1.1552	0.00005	0.0008	0.0023

Semi diurnal	VAV 06				ETERNA (TAMURA)				ETERNA (HW)			
	δ	stdv	κ	stdv	δ	stdv	κ	stdv	δ	stdv	κ	stdv
2N2	1.1566	0.0003	-0.0180	0.0150	1.1564	0.0002	-0.0188	0.0072	1.1574	0.00003	0.0016	0.0014
N2	1.1577	0.0001	-0.0100	0.0030	1.1575	0.0000	-0.0137	0.0014	1.1575	0.00001	0.0005	0.0003
M2	1.1575	0.0000	0.0000	0.0010	1.1574	0.0000	-0.0072	0.0003	1.1575	0.00000	0.0004	0.0001
L2	1.1561	0.0006	0.1310	0.0320	1.1589	0.0003	0.1155	0.0148	1.1575	0.00006	0.0018	0.0028
S2	1.1575	0.0000	0.0040	0.0030	1.1575	0.0000	-0.0052	0.0006	1.1575	0.00000	0.0002	0.0001
K2	1.1589	0.0001	0.0070	0.0060	1.1573	0.0001	-0.0044	0.0026	1.1575	0.00001	0.0000	0.0005

Ter diurnal	VAV 06				ETERNA (TAMURA)				ETERNA (HW)			
	δ	stdv	κ	stdv	δ	stdv	κ	stdv	δ	stdv	κ	stdv
M3	1.0697	0.0003	-0.0860	0.0180	1.0692	0.0001	-0.0848	0.0058	1.0694	0.00001	0.0004	0.0003

* 10-year data

Table B.2: Comparison of the results (amplitude factor ,phase differences and standard deviations) obtained in the diurnal band (up) semi diurnal band (middle) and ter diurnal band (down) for the same synthetic data series (10 year data) using VAV 06 (left columns), ETERNA 3.4 with TAMURA's catalogue (middle columns) and ETERNA 3.4 with HW catalogue (right columns).

Diurnal	VAV 06				ETERNA (TAMURA)				ETERNA (HW)			
SGQ1	δ	stdv	κ	stdv	δ	stdv	κ	stdv	δ	stdv	κ	stdv
2Q1	1.1478	0.0018	-0.3210	0.0900	1.1477	0.0005	-0.3222	0.0262	1.1482	0.0002	-0.3301	0.0086
SGM1	1.1475	0.0008	-0.3860	0.0380	1.1478	0.0002	-0.3443	0.0082	1.1481	0.0001	-0.3349	0.0027
Q1	1.1470	0.0005	-0.3400	0.0270	1.1474	0.0001	-0.3350	0.0067	1.1481	0.0000	-0.3333	0.0022
RO1	1.1478	0.0001	-0.3330	0.0040	1.1481	0.0000	-0.3416	0.0010	1.1480	0.0000	-0.3339	0.0003
O1	1.1482	0.0003	-0.3430	0.0170	1.1481	0.0001	-0.3367	0.0054	1.1481	0.0000	-0.3336	0.0018
TAU1	1.1488	0.0000	-0.0180	0.0010	1.1488	0.0000	-0.0190	0.0002	1.1488	0.0000	-0.0158	0.0001
NO1	1.1485	0.0009	-0.0310	0.0460	1.1481	0.0003	-0.0381	0.0145	1.1488	0.0001	-0.0179	0.0047
CHI1	1.1554	0.0002	-0.0410	0.0090	1.1548	0.0000	-0.0366	0.0022	1.1545	0.0000	-0.0269	0.0007
PI1	1.1534	0.0008	0.0100	0.0370	1.1535	0.0003	0.0014	0.0125	1.1540	0.0001	0.0058	0.0041
P1	1.1515	0.0005	0.1180	0.0250	1.1514	0.0001	0.1127	0.0072	1.1515	0.0001	0.0994	0.0023
S1	1.1498	0.0000	0.1100	0.0020	1.1498	0.0000	0.1106	0.0004	1.1498	0.0000	0.1130	0.0001
K1	1.1503	0.0021	-0.6110	0.1760	1.1505	0.0005	-0.5850	0.0259	1.1469	0.0002	-0.4650	0.0085
PSI1	1.1371	0.0000	0.1770	0.0010	1.1371	0.0000	0.1734	0.0001	1.1370	0.0000	0.1772	0.0000
PHI1	1.2622	0.0012	-0.5800	0.0540	1.2624	0.0004	-0.5888	0.0160	1.2635	0.0001	-0.5877	0.0052
TET1	1.1679	0.0006	0.2880	0.0280	1.1676	0.0002	0.3159	0.0097	1.1676	0.0001	0.3242	0.0032
J1	1.1595	0.0008	-0.0360	0.0390	1.1593	0.0003	-0.0051	0.0127	1.1595	0.0001	0.0059	0.0042
SO1	1.1585	0.0002	0.0130	0.0100	1.1594	0.0001	0.0122	0.0025	1.1595	0.0000	0.0135	0.0008
OO1	1.1555	0.0009	0.0980	0.0470	1.1556	0.0003	0.0905	0.0150	1.1556	0.0001	0.0980	0.0049
NU1	1.1559	0.0003	0.1190	0.0150	1.1559	0.0001	0.0934	0.0037	1.1557	0.0000	0.0909	0.0012

Semi diurnal	VAV 06				ETERNA (TAMURA)				ETERNA (HW)			
	δ	stdv	κ	stdv	δ	stdv	κ	stdv	δ	stdv	κ	stdv
EPS2	1.1548	0.0003	2.5250	0.0120	1.1546	0.0002	2.5161	0.0120	1.1553	0.0000	2.5662	0.0012
2N2	1.1552	0.0001	2.5570	0.0040	1.1549	0.0001	2.5506	0.0038	1.1553	0.0000	2.5667	0.0004
MU2	1.1550	0.0001	2.5570	0.0030	1.1549	0.0001	2.5535	0.0031	1.1553	0.0000	2.5664	0.0003
N2	1.1746	0.0000	2.4250	0.0000	1.1746	0.0000	2.4190	0.0005	1.1745	0.0000	2.4294	0.0001

	δ	stdv	κ	stdv	δ	stdv	κ	stdv	δ	stdv	κ	stdv
NU2	1.1742	0.0001	2.4250	0.0030	1.1742	0.0001	2.4187	0.0025	1.1745	0.0000	2.4292	0.0003
M2	1.1871	0.0000	1.9660	0.0000	1.1871	0.0000	1.9616	0.0001	1.1871	0.0000	1.9684	0.0000
LAM2	1.2126	0.0003	1.3250	0.0120	1.2121	0.0003	1.2986	0.0120	1.2118	0.0000	1.3137	0.0013
L2	1.2130	0.0001	1.3420	0.0030	1.2122	0.0001	1.3272	0.0026	1.2118	0.0000	1.3114	0.0003
T2	1.1893	0.0001	0.4610	0.0040	1.1894	0.0001	0.4551	0.0033	1.1891	0.0000	0.4534	0.0003
S2	1.1892	0.0000	0.4510	0.0000	1.1892	0.0000	0.4459	0.0002	1.1892	0.0000	0.4524	0.0000
K2	1.1915	0.0000	0.7360	0.0010	1.1915	0.0000	0.7282	0.0007	1.1915	0.0000	0.7271	0.0001
ETA2	1.1935	0.0004	0.8400	0.0180	1.1920	0.0003	0.7971	0.0120	1.1915	0.0000	0.7263	0.0013
2K2	1.1835	0.0007	0.6780	0.0320	1.1844	0.0006	0.6953	0.0305	1.1915	0.0001	0.7282	0.0032

Ter diurnal	VAV 06				ETERNA (TAMURA)				ETERNA (HW)			
	δ	stdv	κ	stdv	δ	stdv	κ	stdv	δ	stdv	κ	stdv
M3	1.0658	0.0000	-0.0010	0.0020	1.0659	0.0000	0.0002	0.0014	1.0661	0.0000	0.0136	0.0001

Observed data

* 1 year data

Table B.3: Comparison of the results (amplitude factor, phase differences and standard deviations) obtained in the diurnal band (up) semi diurnal band (middle) and ter diurnal band (down) for the same observed data series recorded at J9 (1 year data, 2000/01/01 – 2000/12/31) using VAV 06 (left columns), ETERNA 3.4 with TAMURA catalogue (middle columns) and ETERNA 3.4 with HW catalogue (rigth columns)

Semi diurnal	VAV 06				ETERNA (TAMURA)				ETERNA (HW)			
	δ	stdv	κ	stdv	δ	stdv	κ	stdv	δ	stdv	κ	stdv
SGQ1	1.1594	0.0112	0.3080	0.5550	1.1365	0.0151	2.4310	0.7635	1.1401	0.0150	2.4101	0.7541
2Q1	1.1593	0.0033	-0.5990	0.1640	1.1649	0.0043	-0.4863	0.2092	1.1664	0.0042	-0.5058	0.2067
SGM1	1.1593	0.0029	-0.5300	0.1420	1.1620	0.0037	-0.5286	0.1822	1.1630	0.0037	-0.5437	0.1800
Q1	1.1494	0.0004	-0.2760	0.0220	1.1499	0.0006	-0.2910	0.0280	1.1498	0.0006	-0.2690	0.0277
RO1	1.1515	0.0023	-0.3550	0.1160	1.1506	0.0029	-0.3447	0.1452	1.1505	0.0029	-0.3248	0.1435
O1	1.1502	0.0001	0.0760	0.0040	1.1500	0.0001	0.0750	0.0053	1.1501	0.0001	0.0799	0.0053
TAU1	1.1531	0.0056	-0.2660	0.2770	1.1499	0.0072	-0.7075	0.3609	1.1501	0.0072	-0.7520	0.3565
NO1	1.1476	0.0014	0.2800	0.0680	1.1403	0.0034	-0.1274	0.1685	1.1433	0.0033	-0.1857	0.1665
CHI1	1.1444	0.0051	0.3800	0.2570	1.1447	0.0073	0.4171	0.3646	1.1461	0.0072	0.4009	0.3598
P1	1.1514	0.0002	0.2150	0.0090	1.1515	0.0002	0.2325	0.0106	1.1516	0.0002	0.2324	0.0105
TET1	1.1518	0.0051	0.2740	0.2540	1.1690	0.0071	-0.0864	0.3497	1.1695	0.0071	-0.0426	0.3454
J1	1.1610	0.0009	0.2080	0.0420	1.1613	0.0012	0.2010	0.0611	1.1613	0.0012	0.2241	0.0603
SO1	1.1531	0.0061	-0.4570	0.3020	1.1540	0.0085	-0.6621	0.4207	1.1549	0.0084	-0.5602	0.4155
OO1	1.1572	0.0019	0.1610	0.0950	1.1617	0.0037	0.2331	0.1825	1.1625	0.0037	0.1712	0.1802
NU1	1.1537	0.0088	0.8140	0.4380	1.1427	0.0171	0.1451	0.8553	1.1430	0.0169	-0.1104	0.8451

Semi diurnal	VAV 06				ETERNA (TAMURA)				ETERNA (HW)			
	δ	stdv	κ	stdv	δ	stdv	κ	stdv	δ	stdv	κ	stdv
EPS2	1.1372	0.0032	2.4890	0.1630	1.1417	0.0061	2.1603	0.3036	1.1411	0.0060	2.1531	0.3029
2N2	1.1510	0.0010	2.7300	0.0480	1.1544	0.0012	2.7493	0.0608	1.1554	0.0012	2.7695	0.0607
N2	1.1723	0.0001	2.6360	0.0070	1.1732	0.0002	2.5894	0.0115	1.1732	0.0002	2.6037	0.0115

	δ	stdv	κ	stdv	δ	stdv	κ	stdv	δ	stdv	κ	stdv
M2	1.1883	0.0000	2.1430	0.0010	1.1883	0.0001	2.1391	0.0023	1.1883	0.0001	2.1467	0.0023
L2	1.2000	0.0014	3.1630	0.0690	1.2218	0.0025	3.0039	0.1187	1.2203	0.0025	2.8910	0.1185
S2	1.1900	0.0001	0.6340	0.0060	1.1902	0.0001	0.6383	0.0053	1.1902	0.0001	0.6432	0.0053
K2	1.1929	0.0003	0.8740	0.0120	1.1928	0.0004	0.8733	0.0209	1.1930	0.0004	0.8775	0.0208

Ter diurnal	VAV 06				ETERNA (TAMURA)				ETERNA (HW)			
	δ	stdv	κ	stdv	δ	stdv	κ	stdv	δ	stdv	κ	stdv
M3	1.0641	0.0011	0.3210	0.0620	1.0642	0.0019	0.3313	0.1045	1.0645	0.0019	0.4171	0.1032

* 10 years data

Table B.4: Comparison of the results (amplitude factor, phase differences and standard deviations) obtained in the diurnal band (up) semi diurnal band (middle) and ter diurnal band (down) for the same observed data series recorded at J9 (10 year data, 1997/01/01/ - 2006/12/31) using VAV 06 (left columns), ETERNA 3.4 with TAMURA catalogue (middle columns) and ETERNA 3.4 with HW catalogue (rigth columns)

Semi diurnal	VAV 06				ETERNA (TAMURA)				ETERNA (HW)			
	δ	stdv	κ	stdv	δ	stdv	κ	stdv	δ	stdv	κ	stdv
SGQ1	1.1634	0.0066	-0.7950	0.3240	1.1607	0.0047	-0.8251	0.2340	1.1612	0.0047	-0.8311	0.2325
2Q1	1.1548	0.0026	-0.6450	0.1280	1.1545	0.0015	-0.6701	0.0733	1.1547	0.0015	-0.6610	0.0728
SGM1	1.1521	0.0019	-0.5370	0.0950	1.1520	0.0012	-0.5098	0.0598	1.1527	0.0012	-0.5081	0.0595
Q1	1.1476	0.0003	-0.3090	0.0150	1.1485	0.0002	-0.3062	0.0094	1.1485	0.0002	-0.2985	0.0093
RO1	1.1511	0.0013	-0.2750	0.0620	1.1510	0.0010	-0.2631	0.0488	1.1510	0.0010	-0.2600	0.0485
O1	1.1497	0.0001	0.0000	0.0030	1.1501	0.0000	0.0719	0.0017	1.1501	0.0000	0.0751	0.0017
TAU1	1.1528	0.0035	-0.1330	0.1720	1.1548	0.0026	0.0489	0.1298	1.1554	0.0026	0.0681	0.1290
NO1	1.1559	0.0007	0.1110	0.0320	1.1545	0.0004	0.1871	0.0194	1.1542	0.0004	0.1969	0.0193
CHI1	1.1505	0.0028	0.0610	0.1370	1.1496	0.0023	0.1913	0.1133	1.1501	0.0023	0.1957	0.1126
PI1	1.1522	0.0018	-0.0670	0.0910	1.1513	0.0013	-0.1163	0.0646	1.1514	0.0013	-0.1298	0.0642
P1	1.1507	0.0001	0.1060	0.0070	1.1511	0.0001	0.2062	0.0038	1.1511	0.0001	0.2085	0.0038
S1	1.1572	0.0079	-0.0130	0.6510	1.1735	0.0046	0.7481	0.2286	1.1698	0.0046	0.8676	0.2272
K1	1.1369	0.0001	0.1650	0.0030	1.1382	0.0000	0.2546	0.0013	1.1382	0.0000	0.2584	0.0012
PSI1	1.2638	0.0044	1.3200	0.2000	1.2634	0.0032	1.3346	0.1439	1.2645	0.0032	1.3351	0.1429
PHI1	1.1703	0.0021	0.2460	0.1040	1.1717	0.0018	0.2545	0.0873	1.1717	0.0018	0.2630	0.0867
TET1	1.1580	0.0029	0.1070	0.1450	1.1597	0.0023	0.1915	0.1145	1.1599	0.0023	0.2031	0.1138
J1	1.1582	0.0007	0.0280	0.0360	1.1598	0.0005	0.1361	0.0222	1.1598	0.0005	0.1375	0.0221
SO1	1.1559	0.0034	-0.1170	0.1700	1.1561	0.0027	0.0689	0.1353	1.1561	0.0027	0.0761	0.1344
OO1	1.1577	0.0011	0.0000	0.0540	1.1580	0.0007	0.0973	0.0337	1.1578	0.0007	0.0948	0.0335
NU1	1.1595	0.0049	0.4470	0.2400	1.1558	0.0036	0.5511	0.1761	1.1565	0.0035	0.5638	0.1750

Semi diurnal	VAV 06				ETERNA (TAMURA)				ETERNA (HW)			
	δ	stdv	κ	stdv	δ	stdv	κ	stdv	δ	stdv	κ	stdv
EPS2	1.1383	0.0035	2.2750	0.1760	1.1367	0.0029	2.4239	0.1459	1.1375	0.0029	2.4755	0.1449
2N2	1.1558	0.0010	2.8310	0.0510	1.1552	0.0009	3.0252	0.0452	1.1555	0.0009	3.0412	0.0449
MU2	1.1560	0.0009	2.6650	0.0430	1.1558	0.0008	2.8084	0.0376	1.1561	0.0008	2.8213	0.0373
N2	1.1754	0.0001	2.5810	0.0070	1.1750	0.0001	2.7169	0.0058	1.1749	0.0001	2.7274	0.0058
NU2	1.1742	0.0007	2.6050	0.0360	1.1745	0.0006	2.7055	0.0304	1.1749	0.0006	2.7160	0.0302
M2	1.1878	0.0000	1.9750	0.0020	1.1878	0.0000	2.1193	0.0011	1.1878	0.0000	2.1261	0.0011
LAM2	1.1912	0.0036	1.4920	0.1740	1.1899	0.0031	1.6447	0.1467	1.1897	0.0030	1.6599	0.1457
L2	1.1877	0.0008	0.9360	0.0400	1.1860	0.0007	1.0963	0.0320	1.1856	0.0007	1.0806	0.0318
T2	1.1894	0.0011	-0.0120	0.0520	1.1899	0.0008	0.2893	0.0399	1.1897	0.0008	0.2877	0.0397
S2	1.1897	0.0001	0.4690	0.0060	1.1899	0.0001	0.6153	0.0025	1.1899	0.0001	0.6218	0.0024
K2	1.1915	0.0003	0.7240	0.0120	1.1921	0.0002	0.8780	0.0081	1.1921	0.0002	0.8769	0.0081
ETA2	1.1992	0.0049	0.3130	0.2320	1.1918	0.0030	0.5561	0.1441	1.1914	0.0030	0.4859	0.1431
2K2	1.1847	0.0087	0.1630	0.4210	1.1854	0.0076	0.1976	0.3654	1.1925	0.0076	0.2305	0.3629

Ter diurnal	VAV 06				ETERNA (TAMURA)				ETERNA (HW)			
	δ	stdv	κ	stdv	δ	stdv	κ	stdv	δ	stdv	κ	stdv
M3	1.0641	0.0006	0.0800	0.0310	1.0648	0.0006	0.2582	0.0339	1.0650	0.0006	0.2715	0.0334

<u>Groups of waves used in ETERNA 3.4 analyses</u>

Wave	From (cpd)	To (cpd)
SA	0.001460	0.003425
SSA	0.004710	0.010951
MM	0.025812	0.044652
MF	0.060132	0.080797
MTM	0.096423	0.249951
Q1	0.501370	0.911390
O1	0.911391	0.947991
M1	0.947992	0.981854
P1	0.981855	0.998631
S1	0.998632	1.001369
K1	1.001370	1.004107
PSI1	1.004108	1.006845
PHI1	1.006846	1.023622
J1	1.023623	1.057485
OO1	1.057486	1.470243
2N2	1.470244	1.880264
N2	1.880265	1.914128
M2	1.914129	1.950419
L2	1.950420	1.984282
S2	1.984283	2.002736
K2	2.002737	2.451943
M3	2.451944	3.381478
M4	3.381379	4.000000
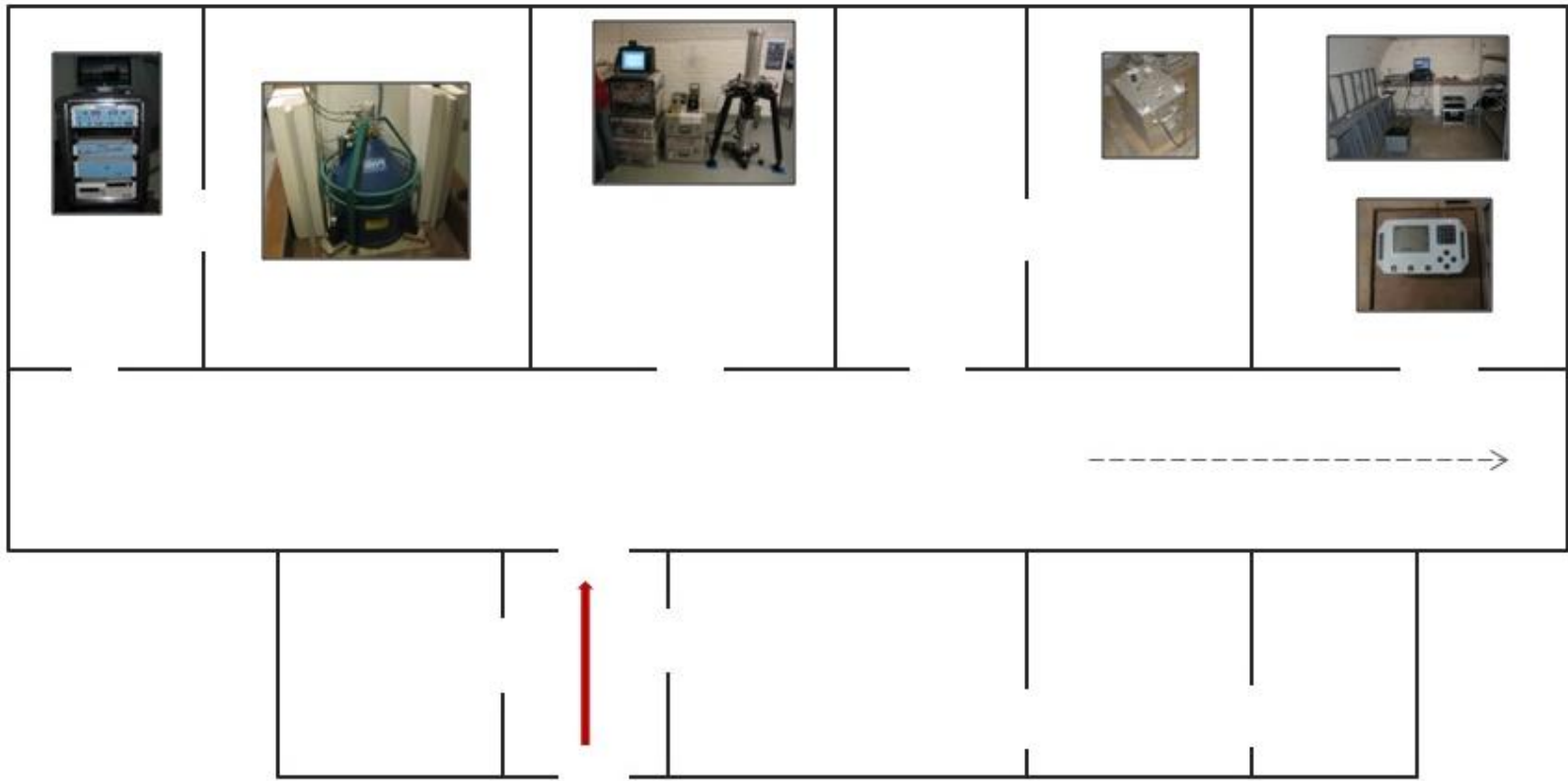
More examples of detection of weak amplitudes tidal signals at J9
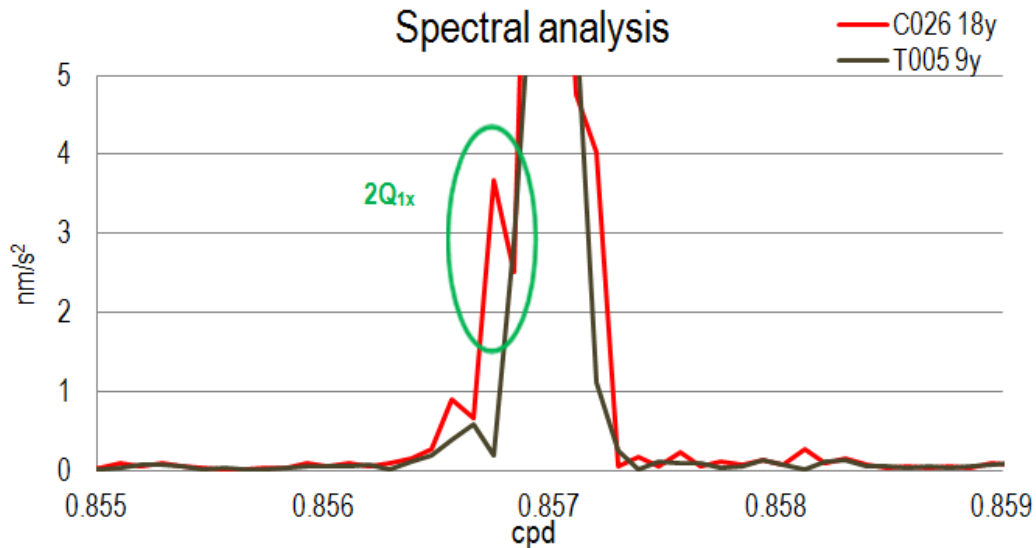
Fig. E.1: Spectral analyses in the diurnal frequency band of the 18 years series of the SG C026 in red, and of the merged 27 year series recorded both by T005 and C026 in black, at Strasbourg J9 Observatory.
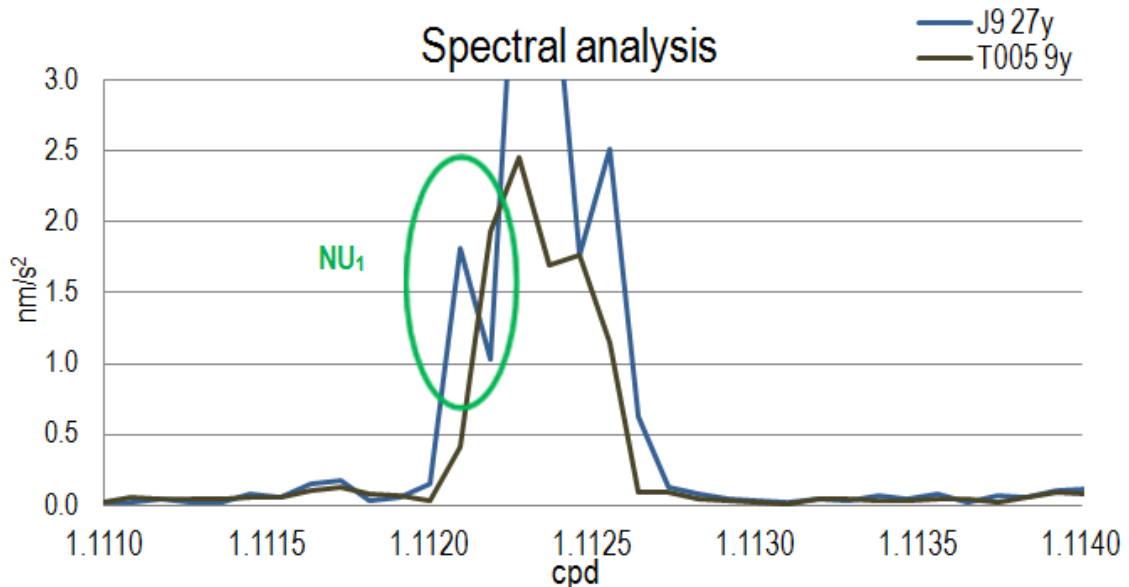
Fig. E.2: Amplitude spectra of J9 gravity series, 9 year of T005 in brown, and 27 years of T005&C026 in blue, in the diurnal frequency band.
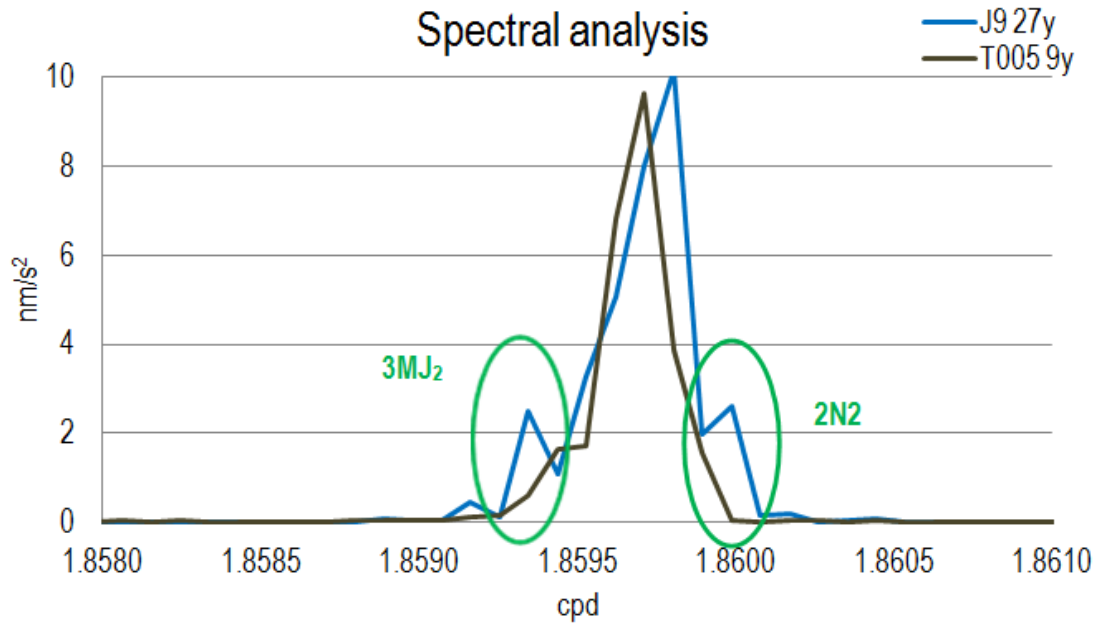
Fig. E.3: Amplitude spectra of J9 gravity series, 9 year of T005 in brown, and 27 years of T005&C026 in blue, in the semidiurnal frequency band.

Bayesian estimation of the free core nutation parameters (gravity data)

The Bayesian approach that we have used in chapter 6 for estimate the free core nutation parameters was a probabilistic inversion method proposed by Florsch and Hinderer (2000). This method does not rely on the assumption that the model is linear in its parameters; it is thus particularly well-suited for the highly nonlinear nutation model (*in the nutation model, the earth interior parameters enter in the model in a highly nonlinear way*).

The Bayesian inversion consists in propagating the information provided by the measurements through an assumed physical model (perfectly or probabilistically known) to the parameters and to include the *a* priori knowledge of the model parameters. The results are probability distributions on the parameters, which is more general than a single numerical value and an associated error on the parameter. The result is indeed the knowledge of the probability law for each parameter.

The Bayesian probability distribution of the parameter vector $\boldsymbol{\theta}$ is given by:

$$p(\boldsymbol{\theta}) = p(x, \sigma_{nd}^R, a^R, a^I) = k \exp\left\{-\frac{1}{2}\sum_j\left[\left(\frac{\text{Re}\left(\delta_j^{\text{th}}\right) - \text{Re}(\delta_j)}{\Delta\text{Re}(\delta_j)}\right)^2 + \left(\frac{\text{Im}\left(\delta_j^{\text{th}}\right) - \text{Im}(\delta_j)}{\Delta\text{Im}(\delta_j)}\right)^2\right]\right\}$$

Where k is a normalization factor in order that the integral of this equation is unity. Re and Im denote the real and imaginary part respectively of the measurement value of the gravimetric factor δ, and δ^{th} the theoretical values.

The general probability laws for the parameter vector $\boldsymbol{\theta}$ is obtained by the previous formula, so in order to obtain the law for one or two parameters, we should compute the marginal probability density functions (pdf) by integration of the probability function over selected parameters. For instance, the joint pdf integrated with respect to σ_{nd}^R is defined by:

$$p_{x,\,a^R,a^I}(x, a^R, a^I) = \int p(x, \sigma_{nd}^R, a^R, a^I)d\sigma_{nd}^R$$

Two further integrations of the pdf lead to the marginal probability law for each of the parameters.

Bibliography

Abd El-Gelil, M., Pagiatakis, S., El-Rabbany, A., 2008. Frequency-dependent atmospheric pressure admittance of superconducting gravimeter records using least squares response method. Phys. Earth Planet. Inter. 170, 24-33.

Abe M., Kroner C., Neumeyer J. and Chen X. D., 2010. Assessment of atmospheric reductions for terrestrial gravity observations Bull. d'Inf. Marées Terr. 146 11817–38.

Abours S., 1977. Exploitation des enregistrements de marée gravimétrique à Strasbourg - aout 1973/février 1977. Diplôme d'Ingénieur Géophysicien. Univ. De Strasbourg, Strasbourg

Abours S., Lecolazet, R., 1978. New results about the dynamical effects of the liquid outer core as observed at Strasbourg, in Proc. 8th Int. Symp. Earth Tides, pp. 689–697, eds Bonatz M., Melchior P., Bonn.

Achilli, V., Baldi, P., Casula, G., Errani, M., Focardi, S., Guerzoni, M., Palomorani, F., Raguní, G., 1995. A calibration system for superconducting gravimeters. Bull. Géodésique, 69(2), 73-80.

Agnew D., 2007, Earth tides Treatise on Geophysics vol 3 ed T Herring, Gen ed. G Schubert (Amsterdam: Elsevier) pp 163–195.

Akaike, H., 1979. A Bayesian extension of the minimum AIC procedure of autoregressive model fitting. Biometrika 66, 237–242.

Amalvict, M., Hinderer, J., & Boy, J.P., 1999. A comparative analysis between an absolute gravimeter (FG5-206) and a superconducting gravimeter (GWR C026) in Strasbourg: new results on calibration and long term gravity changes, Boll. Geofisica Geodetica, 40, n°2-3, 519-525.

Amalvict M., Hinderer J., Boy J-P., Gegout P., 2001. A 3 year comparison between a superconducting gravimeter (GWRC026) and an absolute gravimeter (FG5#206) in Strasbourg (France). J. Geod. Soc. Jpn. 47, 334 – 340.

Amalvict M., Hinderer J., Gegout P., Rosat S., Crossley D., 2002. On the use of AG data to calibrate SG instruments in the GGP network: example of Strasbourg - J9. Bull. Inform. Marees Terr. 135, 10621– 10626.

Amalvict, M., Hinderer, J., Mäkinen, J., Rosat, S., Rogister, Y., 2004. Long-term and seasonal gravity changes at the Strasbourg station and their relation to crustal deformation and hydrology. J. Geodyn. 38 (3-5), 343–353.

Amoruso A., Botta V., Crescentini L., 2012. Free Core Resonance parameters from strain data: sensitivity analysis and results from the Gran Sasso (Italy) extensometers. Geophys. J. Int. 189, 923-936.

Arnoso, J., Riccardi, U., Hinderer, J., Córdoba, B. Montesinos, FG (2014). Analysis of co-located measurements made with a LaCoste&Romberg Graviton-EG gravimeter and two superconducting gravimeters at Strasbourg (France) and Yebes (Spain). Acta Geodaetica et Geophysica, doi: 10.1007/s40328-014-0043-y

Bacon, F., 1620. Novum organum scientiarum. Johannes Billius, London, UK (cit: L. Jardine and M. Silverthorne, eds 2000. The new organon.–Cambridge Univ. Press, Cambridge, UK.), 1910.

Banka, D., 1997. Noise levels of superconducting gravimeters at seismic frequencies, PhD thesis, GDMB – Informationgesellschaft mbH, Clausthal, Germany.

Baker, T.F., 1980. Tidal gravity in Britain: tidal loading and the spatial distribution of the marine tide. Geophys. J.R. Astron. Soc. 62, 249–267.

Baker, T. F., Bos, M. S., 2003. Validating Earth and ocean tide models using tidal gravity measurements. Geophys. J. Int., 152(2), 468-485.

Bendat, J.S. and Piersol, A.G., 1986. Random data, 2nd edn., Wiley, New York, pp.566.

Boy, J-P., Hinderer, J. and Gegout, P., 1998. Global atmospheric loading and gravity Phys. Earth Planet. Int. 109 161–77.

Boy J-P., Hinderer J., Amalvict M., Calais E., 2000. On the use of long records of superconducting and absolute gravity observations with special application to the Strasbourg station, France. Cahiers Centre Eur. Géodyn. Séismol. 17, 67–83.

Boy J.P., Gegout, P. and Hinderer Jacques, 2001. Gravity variations and global pressure loading, Journal of the Geodetic Society of Japan, 47, 267-272.

Boy, J.P., Gegout, P., Hinderer, J., 2002. Reduction of surface gravity data from global atmospheric pressure loading. Geophys. J. Int. 149, 534–545.

Boy, J.-P., M. Llubes, R. Ray, J. Hinderer, N. Florsch, S. Rosat, F. Lyard and T. Letellier, 2004. Non-linear oceanic tides observed by superconducting gravimeters in Europe, J. Geodyn., 38, 391-405.

Boy, J-P., and Chao, B., 2005. Precise evaluation of atmospheric loading effects on Earth's time-variable gravity field J. Geophys. Res. 110 B08412.

Boy, J.-P., Hinderer J., 2006a. Study of the seasonal gravity signal in superconducting gravimeter data J. Geodyn. 41 227–33

Boy, J.-P., Ray, R., Hinderer, J., 2006b. Diurnal atmospheric tide and induced gravity variations J. Geodyn. 41 253–8.

Boy, J.-P., Llubes, M., Ray, R., Hinderer, J., Florsch, N., 2006c. Validation of long-period oceanic tidal models with superconducting gravimeters, Journal of Geodynamics, 41, 112–118.

Bollo R., Gougenheim A., 1949. Variation périodique de la gravité en un lieu. Annales de Géophysique 1949. T5, 2, 176-180.

Breiner, S., Corbett, J.D., Daniels, J.J., Hansen, D.A., Horsnail, R.F., and Morrison, H.F., 1981. American mining geophysics delegation to the People's Republic of China: GEOPHYSICS, v. 46, p. 347-356.

Büllesfeld, FJ. 1985. Ein Beitrag zur harmonischen Darstellung des gezeitenerzeugenden Potentials. Reihe C, Heft 314, Deutsche Geodätische Kommission, München.

Busse, F. H., 1970. The dynamical coupling between inner core and mantle of the Earth and the 24-year libration of the pole, pp. 88-98. Springer Netherlands.

Calvo M., Hinderer, J., Rosat, S., Legros H., Boy J-P., Ducarme, B., Zürn, W., 2014a. Time stability of spring and superconducting gravimeters through the analysis of very long gravity records. J. Geodyn., 80, 20-33.

Calvo, M., S. Rosat, J. Hinderer, Legros, H., Boy, J.-P., Riccardi, U., 2014b. Study of the time stability of tides using a long term (1973-2011) gravity record at Strasbourg, France. Earth on the Edge: Science for a Sustainable Planet, vol. 139, Rizos C. and Willis P. (Ed.), Springer-Verlag, Berlin Heidelberg, pp 377-381, doi: 10.1007/978-3-642-37222-3_50

Cartwright D.E., Tayler, R. J., 1971. New computations of the tide generating potential, Geophys. J. R. Astron. Soc, 23, 45-74.

Cartwright, D. E., Edden A. C., 1973. Corrected tables of tidal harmonics, Geophys. J. R. Astron. Soc, 33, 253-264.

Chapin D., 1998, Gravity instruments: past, present, future. Leading Edge 17 100–12.

Chojnicki, T., 1972. Détermination des paramètres de marée par la compensation des observations au moyen de la méthode des moindres carrés. Publications of the Institute of Geophysics, Polish Academy of Sciences, Marées Terrestres, 55, pp. 43-79.

Cook, A.H., 1967, A new absolute determination of the acceleration due to gravity at the National Physical Laboratory, England: Phil. Trans. R. Soc. London, v. A261, p. 211-252.

Crossley D, Jensen O Hinderer J 1995 Effective barometric admittance and gravity residuals Phys. Earth Planet Int. 90 221–41.

Crossley, D., Hinderer, J., Casula, G., Francis, O., Hsu, H.T., Imanishi, Y., Jentzsch, G., Kääriäinen, J., Merriam, J., Meurers, B., Neumeyer, J., Richter, B., Shibuya, K., Sato, T., Van Dam, T., 1999. Network of superconducting gravimeters benefits a number of disciplines. EOS 80 (11), 121–126.

Crossley, D., Hinderer, J., Rosat, S., 2002. Using the atmosphere-gravity correlation to derive a time-dependent admittance. BIM 136, p. 10809–10820.

Crossley, D., Hinderer, J., Riccardi, U., 2013. The measurement of surface gravity. Rep. Prog. Phys. 76 046101 doi:10.1088/0034-4885/76/4/046101.

Crovini, L., Quinn, T.J., 1992. Metrology at the Frontiers of Physics and Technology. Amsterdam: North-Holland.

Cui, X., Sun, H., Rosat, S., Xu, J., Zhou, J., Ducarme, B., 2014. Investigation of the time variability of diurnal tides and resonant FCN period. Journal of Geodynamics, 79, p. 30-38.

Cummins, P.R., Wahr, J.M., 1993. A study of the Earth's free core nutation using international deployment of accelerometers gravity data. Journal of Geophysical Research: Solid Earth (1978–2012), 98(B2), 2091-2103.

D'Agostino, G., Desogus, S., Durando, G., Germak, A., Origlia C., 2002. Improvements of IMGC absolute gravimeter. Cahiers du Centre Européen de Géodynamique et de Séismologie, Vol. 22, pp. 117-122.

Darwin, G.H., 1883. The harmonic analysis of tidal observations. (Report of a Committee consisting of Proffesors G.H. Darwin and J.C. Adams for the harmonic analysis of tidal observations. Brit. Assoc. Report for 1883, 49-118) Reprinted in Scientific papers, 1, 1-70. Cambridge, 463 pp. 1907.

Darwin G.H., 1886. 0n the dynamic theory of tides of long period, Proc.. R. Soc. London, 41, 337-342.

Defraigne P., Dehant V., Hinderer J., 1994. Stacking gravity tide measurements and nutation observations in order to determine the complex eigenfrequency of nearly diurnal free wobble. Journ.of Geophys. Res., vol.99, (B5), pp 9203-9213.

Defraigne P., Dehant V., Hinderer J., 1995a. Correction to "stacking gravity tide measurements and nutation observations in order to determine the complex eigenfrequency of the nearly diurnal free wobble". Journ.of Geophys.Res., vol.100, n°b2, pp 2041-2042.

Defraigne P., Dehant V., Hinderer J., 1995b. FCN period and Q deduced from a global stacking tidal and nutation data. Proc.12th Int. Symp. on Earth Tides, Science Press,; Beijing, China, pp 381-386.

Dehant, V., 1986. Earth models and earth rotation, in Proceedings od NATO Workshop on Earth Rotation: Solved and Unsolved Problems, Bonas, France, ed. A. Cazenave, D. Reidel, Norwell, Mass., pp. 269-275.

Dehant, V., 1987. Tidal parameters for an Inelastic Earth, Phys. Earth Planet. Inter., 49, 97 - 116.

Dehant, V., Ducarme, B., 1987. Comparison between the theoretical and observed tidal gravimetric factor. Phys. Earth Planetary Inter. 49, 192-212.

Dehant, V., 1990. On the nutations of a more realistic Earth model. Geophysical Journal International, 100(3), 477-483.

Dehant V., Hinderer J., Legros H., Lefftz M. 1993. Analytical approach to the computation of the earth, the outer core and the inner core rotational motions. Physics of the Earth and planetary interiors, 76, pp 259-282.

Dehant V., Feissel M., Defraigne P., Roosbeek F., Souchay J. 1997. Could the energy near the FCN and the FICN be explained by luni-solar or atmospheric forcing? Geophysical journal inter.,130, pp 535-546.

Dehant V., Defraigne P., 1997. New Nutation for a non-rigid Earth. Proc. Journees Systemes de Reference, 1996, Paris, France, ed.: Capitaine n., pp 180-184.

Dehant V., Defraigne P. and Wahr J.M., 1999. Tides for a convective Earth. J. Geophys. Res. 104, B1, 1035–1058.

Dehant V., Mathews PM., 2007. Earth rotation variations. In Treatise on Geophysics, ed. Herring TA, vol. 3 Geodesy, Amsterdam, Pays-Bas : Elsevier, 295-349.

Desruelle, B., Menoret, V., Bouyer, P., Landragin, A., 2013. Development of a portable matter-wave gravimeter. American Geophysical Union, Fall Meeting 2013, abstract #G11A-0888.

Dickman, S.R., 2005. Rotationally consistent Love numbers. Geophysical Journal International, v 161, Issue 1, pp. 31-40.

Dierks, O., Neumeyer, J., 2002. Comparison of Earth Tides Analysis Programs. Bulletin d'Information des Marées Terrestres, 135, p. 10669-10688.

Dittfeld, H-G., 1991. Analysis of third degree waves with diurnal and semidiurnal frequencies. Bull. Inf. Marées Terr. 111, 8053–8061.

Doi, K., Shibuya, K., Ikeda, H., Fukuda, Y., 2008. Continuous Gravity Observation with the Superconducting Gravimeter CT #043 at Syowa Station, Antarctica. Geodetic and geophysical Observation in Antartica, pp. 237-247.

Doodson A.T., 1921. The harmonic development of the tide-generating potential Proc. R. Soc. Lond. Series A 100, 306–329. Reprint in International Hydrographic Revue, vol. 31, No. 1, Monaco 1954.

Doodson, A.T., 1928. The analysis of tidal observations. Philosophical Transactions of the Royal Society of London A227, 223-279.

Doodson, A.T., Warburg, H.D., 1941. Admiralty Manual of Tides. H.M. Stationary Office, London.

Doodson A.T., 1954. The analysis of tidal observations for 29 days. Int. Hydrogr. Rev., 31 (1), pp. 63-71.

Ducarme B., Sun H-P., Xu J.Q., 2002. New investigation of tidal gravity results fromGGPnetwork. In: Proceedings of the GGP Workshop, Jena, March 11–15. Bull. Inf. MaréesTerrestres 136: 10761–10776.

Ducarme, B., Venedikov, A.P., Arnoso, J., Vieira, R., 2004. Determination of the long period tidal waves in the GGP superconducting gravity data. J. Geodyn 38 p. 307 – 324.

Ducarme B., Venedikov A., Arnoso J., Chen X-D., Sun H-P. and Vieira R., 2006a. Global analysis of the GGP superconducting gravimeters network for the estimation of the pole tide gravimetric amplitude factor. J. Geodyn. 41, 1-3, pp. 334–344.

Ducarme, B., Neumeyer, J., Vandercoilden, L., Venedikov, A.P., 2006b. The analysis of long period tides by ETERNA and VAV programs with or without 3D pressure correction. Bull. Inf. Marées Terrestres 141, 11201–11210.

Ducarme, B., Sun, H.-P., Xu, J.-Q., 2007. Determination of the free core nutation period from tidal gravity observations of the GGP superconducting gravimeter network; J. Geodesy, 81, 179–187, doi:10.1007/ s00190-006-0098-9.

Ducarme, B., Rosat, S., Vandercoilden, L., Jian-Qiao, X., Heping, S. 2009. European tidal gravity observations: Comparison with Earth tide models and estimation of the Free Core Nutation (FCN) parameters. International Association of Geodesy Symposia Volume 133, 2009, pp 523-532, doi:10.1007/978-3-540-85426-5.

Ducarme, B., 2011. Determination of the main Lunar waves generated by the third degree tidal potential and validity of the corresponding body tides models. J. DOI: 10.1007/s00190-011-0492-9. Journal of Geodesy, Vol. 86 Issue 1, p. 65-75.

Dziewonski A. M. and Anderson D. L., 1981. Preliminary reference Earth model Phys. Earth Planet Int. 25 297–356.

Eötvös, R. von, 1896, Untersuchungen uber Gravitation und Erdmagnetismus: Ann. Phys., v. 59, p. 354-400.

Eubanks, T.M., Steppe, J.A., Sovers, O.J., 1986. An analysis and intercomparison of VLBI nutation estimates. In: I.I. Mueller (Editor), Proc. Int. Conf. Earth rotation and terrestrial reference frame (IAU), Vol. 1, Ohio, Ohio State University, OH, pp. 326-340.

Euler L., 1758. Du mouvement de rotation des corpes solides autour d'un axe variable Memoires de l'Académie des Scinces de Berlin. 14, 154-193.

Faller, J. E., 1965. Results of an absolute determination of the acceleration of gravity. Journal of Geophysical Research, vol.70, pp. 4035–4038.

Falk, R., Harnisch, M., Harnisch, G., Nowak, I., Richter, B., Wolf, P., 2001. Calibration of the superconducting gravimeters SG103, C023, CD029 and CD030. J. Geod. Soc. Jpn. 47, 22-27

Farrell, W.E., 1972. Deformation of the Earth by surface load. Rev. Geophys. Space Phys. 10, 761–797.

Florsch, N., Chambat F., Hinderer, J., Legros H., 1994. A simple method to retrieve the complex eigenfrequency of the earth's nearly diurnal-free wobble. Application to the Strasbourg superconducting gravimeter data. Geophys. J. Int., Vol.116, pp 53-63.

Florsch N., Hinderer, J., Legros, H., 1995. Mise en évidence d'ondes de marée quart-diurnes de quelques pico-g d'amplitude à l'aide de gravimètres supraconducteurs. C. R. Acad. Sci. Paris, t. 321, 279-285.

Florsch, N., Hinderer, J., 1998. Estimation of the free core nutation Q factor from tidal analysis. In *Proc. 13th Int. Symp. Earth Tides, Brussels,* pp. 315-322.

Florsch, N., Hinderer, J., 2000. Bayesian estimation of the free core nutation parameters from the analysis of precise tidal gravity data. . Physics of the Earth and Planetary Interiors. Volume 117, (1), p. 21–35.

Francis, O., Melchior, P., 1996. Tidal loading in south western Europe: A test area. Geophysical research letters, 23(17), 2251-2254.

Francis, O., 1997. Calibration of the C021 superconducting gravimeter in Membach (Belgium) using 47 days of absolute gravity measurements. In: International Association of Geodesy Symposia. Springer-Verlag, 117, 212–219.

Francis, O., van Dam, T., 2002. Evaluation of the precision of using absolute gravimeters to calibrate superconducting gravimeters. Metrologia 39, 485–488.

Francis, O., van Dam, T., Amalvict, M., Andrade de Sousa, M., Bilker, M., Billson, R. , D'Agostino, G., Desogus, S., Falk, R., Germak, A., Gitlein, O., Jonhson, D., Klopping, F., Kostelecky, J., Luck, B., Mäkinen, J., McLaughlin, D., Nunez, E., Origlia, C., Palinkas, V., Richard, P., Rodriguez, E., Ruess, D., Schmerge, D., Thies, S., Timmen, L., Van Camp, M., van Westrum, D. and Wilmes, H.: 2005, Results of the International Comparison of Absolute Gravimeters in Walferdange (Luxembourg) of November 2003. IAG Symposia, Volume 129, Gravity, Geoid and Space Missions, 272–275.

Francis, O., van Dam, T., Germak, A., M. Amalvict, R. Bayer, M. Bilker-Koivu la, M. Calvo, G.-C. D'Agostino, T. Dell'Acqua, A. Engfeldt, R. Faccia, R. Falk, O. Gitlein, Fernandez, J. Gjevestad, J. Hinderer, Jones, J. Kostelecky, N. Le Moigne, B. Luck, J. Mäkinen D. Mclaughlin, T. Olszak, P. Olsson, A. Pachuta, V. Palinkas, B. Pettersen, R. Pujol, I. Prutkin, D. Quagliotti, R. Reudink, C. Rothleitner, D. Ruess, C. Shen, V. Smith, S. Svitlov, L. Timmen, C. Ulrich, M. Van Camp, J. Walo, L. Wang, H., Wilmes, L. and Xing: 2010, Results of the European Comparison of Absolute Gravimeters in Walferdange (Luxembourg) of November 2007. Gravity, Geoid and Earth observation. Springer Berlin Heidelberg, p. 31-35.

Francis, O., Baumann, H., Volarik, T., Rothleitner, C., Klein, G., Seil, M., Dando, N., Tracey, R., Ullrich, C., Castelein, S., Hua, H., Kang, W., Chongyang, S., Songbo, X., Hongbo, T., Zhengyuan, L., Pálinkás, V., Kostelecký, J., Mäkinen, J., Näränen, J., Merlet, S., Farah, T., Guerlin, C., Pereira Dos Santos, F., Le Moigne, N., Champollion, C., Deville, S., Timmen, L., Falk, R., Wilmes, H., Iacovone, D., Baccaro, F., Germak, A., Biolcati, E., Krynski, J., Sekowski, M., Olszak, T., Pachuta, A., Agren, J., Engfeldt, A., Reudink, R., Inacio, P., McLaughlin, D., Shannon, G., Eckl, M., Wilkins, T., van Westrum, D., Billson, R. 2013. The European Comparison of Absolute Gravimeters 2011 (ECAG-2011) in Walferdange, Luxembourg: results and recommendations. Metrologia vol. 50, 3, p. 257.

Fukuda, Y., Iwano, S., Ikeda, H., Hiraoka, Y., Doi, K., 2005. Calibration of the superconducting gravimeter CT#043 with an absolute gravimeter FG5#210 at Syowa Station, Antarctica. Polar Geosci. 18, 41–48.

Goodkind, J.M., 1983. Q of the nearly diurnal free wobble, In: J.T. Kuo (Editor), Proc. Ninth. Int. Symp. Earth Tides. Schweizerbart, Stuttgart, pp. 569-575.

Goodkind, J.M., 1991a. The Superconducting Gravimeters. principles of operation, current performance, and future prospects. In: Proc. of the Workshop Won-Tidal Gravity Changes. Intercomparison Between Absolute and Superconducting Gravimeters'. Cahiers du Centre Europeen de Geodynamique et de Seismologie ,Vol. 3, Luxemburg, pp. 81–90.

Goodkind, J.M., Young, C., Richter, B., 1991b. Comparison of two superconducting gravimeters and an absolute meter at Richmond, Florida, in Proc. Workshop: Non tidal gravity changes: intercomparison between absolute and superconducting gravimeters, Vol. 3, pp. 91-98, ed. Poitevin, C., Cahiers du Centre Europeén de Géodynamique et de Seismologie, Luxembourg.

Goodkind, J.M., 1996. Test of theoretical solid earth and ocean gravity tides. Geophys. J. Int., 125: 106–114.

Goodkind, J.M., 1999. The superconducting gravimeter Rev. Sci. Instrum. 70 4131–52.

Gostoli J., 1970. Etude et construction d'un dispositif d'asservissement pour un gravimètre LaCoste–Romberg. Enregistrement numérique de la marée gravimétrique. Thèse de Dr. Ing, Univ de Strasbourg, Strasbourg.

Greff-Lefftz M., Legros H., Dehant V., 2000. Influence of the inner core viscosity on the rotational eigenmodes of the Earth. Physics of the Earth and Planetary Interiors 122, p 187-204.

Gross, R.S., 2007. Earth Rotation Variations, Long Period. In Physical Geodesy, ed. T.A. Herring, Treatise on Geophysics, Vol. 11, Elsevier, Amsterdam.

Gwinn C.R., Herring T. A., Shapiro I.I., 1986. Geodesy by radiointerferometry: Studies of the forced Nutations of the Earth. 2. Interpretation. Journ. of Geophys. Res., vol.91, n°b5, pp 4755-4765.

GWR-Manual, 1985. Superconducting gravity meter, model TT70, cryogenic refrigeration, Operating Manual, GWR Instruments, San Diego.

Hammond, J.A., and Faller, J.E., 1967, Laser interferometer system for the determination of the acceleration of gravity: IEEE J. Quant. Elec., v. 3, p. 597-601.

Harnisch M. and Harnisch G., 2006. Study of long-term gravity variations, based on data of the GGP cooperation J. Geodyn. 41 318–25.

Harrison, P.J. and Stevens, C.F. (1976). Bayesian forecasting (with discussion). Journal of the Royal Statistical Society Series B, 38, 205-247.

Harrison, J.C., Sato, T., 1984. Implementation of electrostatic feedback with a LaCoste & Romberg model G gravity meter. J. Geophys. Res. 89, 7957-7961.

Hartmann, T., Wenzel, H.-G., 1995. The HW95 tidal potential, Geophys. Res. Let., Vol. 22, No. 24, p. 3553-3556.

Herring T. A., Gwinn C.R., Shapiro I.I., 1986. Geodesy by radiointerferometry: Studies of the forced Nutations of the Earth. 1. Data Analysis. Journ. of Geophys. Res., vol.91, n°b5, pp 4745-4754.

Herring, T. A., Buffett, B. A., Mathews, P. M. and Shapiro, I. I., 1991. Forced Nutations of the Earth: Inuence of Inner Core Dynamics, 3. Very Long Interferometry Analysis, J. Geophys. Res., 91, 4755 - 4765.

Hinderer, J., Legros, H. and Amalvict, M., 1982. A search for Chandler and nearly diurnal free wobbles using Liouville equations, Geophys. J. R. astr. Soc., 71, 303 - 332.

Hinderer, J., Legros, H., 1989. Elasto-Gravitational Deformation, Relative Gravity Changes and Earth dynamics. Geophysical Journal International, v. 97, I. 3, p. 481-495.

Hinderer, J., Florsch, N., Mäkinen, J. , Legros, H. & Faller, J.E., 1991a. On the calibration of a superconducting gravimeter using absolute gravity measurements, Geophys. J. Int., 106, 491-497.

Hinderer, J., Legros, H., Crossley, D., 1991b. Global Earth dynamics and induced gravity changes. Journal of Geophysical Research, 96, doi: 10.1029/91JB00423.

Hinderer J., Crossley D., 1993a. Core dynamics and surface gravity changes. Dynamics of Earth's. Int.& Earth Rotation; I.U.G.G. & the American Geophys. Union; Geoph. Monograph 72, IUGG vol.12, pp 1-16.

Hinderer, J., Crossley, D., Xu, H., 1993b. Gravity noise levels from a 2-year comparison of two superconducting gravimeter data. Bull. Inf. Mare´es Terrestres 116, 8612–8626.

Hinderer, J., Crossley, D., Xu, H., 1994. A two-year comparison between the French and Canadian superconducting gravimeter data, Geophys. J. Int., 116, 252-266.

Hinderer J., Crossley D., Hui Xu. 1995. The accuracy of tidal gravimetric factors and nearly diurnal free wobble resonance parameters in superconducting gravimetry. Proc.12th Int. Symp. on Earth tides, Science Press, Beijing, China, pp 289-310.

Hinderer J., 1997. Constraints on the Earth's deep structure and dynamics from superconducting gravimetry. Earth's Deep Interior, Doornbos Memorial Volume, Gordon&Breach, 167-195.

Hinderer J., Boy, J.O. Legros, H. 1998. A 3000 day registration of the superconducting gravimeter GWR T005 in Strasbourg (France). In Proc. 13th Int., Symp. Earth Tides, eds. B. Ducarme and P. Pâquet, Brussels, p. 617-624.

Hinderer J., Boy JP., Defraigne P., Roosbeek F., Dehant V., 2000. Are free core nutation parameters variable in time? Phys. Earth Planet Int 117:37–49.

Hinderer, J., Rosat, S., Crossley, D., Amalvict, M., Boy, J.-P. and Gegout, P., 2002. Influence of different processing methods on the retrieval of gravity signals from GGP data, Bull. Inf. Marees Terr., 135, 10653-10668.

Hinderer, J., Crossley, D., 2004. Scientific achievements from the first phase (1997-2003) of the Global Geodynamics Project using a worldwide network of superconducting gravimeters. Journal of Geodynamics, v 38, n 3-5, pp. 237-262.

Hinderer, J., Crossley, D., Warburton, R., 2007. Superconducting gravimetry. Treatise on Gheophysics. Amsterdam: Elsevier, Vol. 3, pp. 65-122.

Hinderer J., Hector B., Boy J.-P., Riccardi U., Rosat S., Calvo M., Little F., 2014. A search for atmospheric effects on gravity at different time and space. J. Geodyn. 80, 50-57.

Hobson, E.W., 1931. The theory of spherical and ellipsoidal harmonics, Cambridge University Press., Cambridge.

Hough S. S., 1895. The oscillations of a rotating ellipsoidal shell containing fluid. Philos. Trans. Royal Soc. London, vol.186, 1 pp 469-506.

Hu, X.-G; Liu, L.-T; Hinderer, J.; Sun, H.P , 2005. Wavelet filter analysis of local atmospheric pressure effects on gravity variations. Journal of Geodesy, 79 (8): 447-459.

Huygens, C., 1888. Oeuvres complètes de Christiaan Huygens. Correspondance [de Christiaan Huygens], 1638-1656.

Imanishi, Y., Higashi, T., Fukuda, Y., 2002. Calibration of the superconducting gravimeter T011 by parallel observation with the absolute gravimeter FG5#210 – a Bayesian approach. Geophys. J. Int. 151, p. 867-878.

Iwano, S., Fukuda, Y., Sato, T., Tamura, Y., Matsumoto, K. and Shibuya, K., 2005. Long-period tidal factors at Antarctica Syowa Station determined from 10 years of superconducting gravimeter data. Journal of Geophysical Research 110: doi: 10.1029/2004JB003551.

Jeffreys H., 1949, Dynamic effects of a liquid core. Monthly Notices of the Royal Astronomical Society, Vol. 109, No. 6, p.670.

Jeffreys, H., Vicente R.O., 1957. The theory of Nutation and the Variation of Latitude. The roche model core. Monthly Notices of the Royal Astronomical Society, Vol. 117, p.162-173.

Jeffreys, H., 1976. The Earth. Its Origin, History and Physical Constitution, Cambridge University Press, Cambridge, 1924 (reprinted with additions 1976).

Kakuta, C., Okamoto, I., & Sasao, T., 1975. Is the nutation of the solid inner core responsible for the 24-year libration of the pole. Publications of the Astronomical Society of Japan, 27, 357-365.

Kater, H., 1818. An account of experiments for determining the length of the pendulum vibrating seconds in the latitude of London. Philosophical Transactions of the Royal Society of London, vol. 108, pp. 33–102.

Koot, L., Rivoldini, A., de Viron, O., Dehant, V., 2008. Estimation of Earth interior parameters from a Bayesian inversion of very long baseline interferometry nutation time series. J. Geophys. Res. 113, B08414, doi:10.1029/2007JB005409.

Koot, L., Dumberry, M., Rivoldini, A., de Viron, O., Dehant, V., 2010. Constraints on the coupling at the core-mantle and inner core boundaries inferred from nutation observations, Geophys. J. Int., 182, pp. 1279–1294.

Klügel T. and Wziontek H., 2009. Correcting gravimeters and tiltmeters for atmospheric mass attraction using operational weather models J. Geodyn. 48 204–10.

Kroner C. and Jentzsch G. 1999 Comparison of different pressure reductions for gravity data and resulting consequences Phys. Earth Planet. Int. 115 205–18.

Kroner C., Dierks O., Neumeyer J. and Wilmes H., 2005.Analysis of observations with dual sensor superconducting gravimeters. Physics of the Earth and Planetary Interiors 153, 210–219.

Kudryavtsev, S.M., 2004. Improved harmonic development of the Earth tide generating potential J. Geodyn. 77 829–38.

LaCoste, L. J. B., 1934. A new type long period vertical seismograph. Physics, vol. 5, no. 7, pp. 178–180.

LaCoste, L. J. B., 1988. The zero-length spring gravity meter. The leading Edge, 7, p. 20-24.

Lambert, W.D., 1936. Rapport sur les marées de l'écorce Terrestre. Association de Géodésie de l'UGGI

Lambert, W.D., 1939. Rapport sur les marées de l'écorce Terrestre. Association de Géodésie de l'UGGI

Lambert, A., 1974. Earth Tide Analysis and Prediction by the response Method. J. Geophys. Res., 79, 4952-4960.

Lambert, S.B., Mathews P.M., 2006. Second-order torque on the tidal redistribution and the Earth's rotation, Astron. Astrophys., 453, 363.

Lambert, S.B., Dehant, V., 2007. The Earth's core parameters as seen by the VLBI. Astron. Astrophys. 469, 777–781.

Larson, J. V., and Harrison, J. C., 1986. An improved analysis of the electrostatic feedback of LaCoste and Romberg gravity meters, Proc. 10th Int. Symp. Earth Tides, Madrid 1985, Consejo Superior de Investigaciones Cientificas, Madrid, 1-8.

Lecolazet R., 1956a. L'enregistrement de la marée gravimétrique avec un gravimètre North-American. Bull. d'Inf. Marées Terr. 1, 4–16

Lecolazet, R., 1956b. Application, a l'analyse des observations de la marée gravimétrique, de la méthode de H. et Y. Labrouste, dite par combinaisons linéaires d'ordonnées. Extrait des ANNALES DE GÉOPHYSIQUE. Tome 12, p. 59-71.

Lecolazet, R., 1957. Enregistrement et analyse harmonique de la marée gravimétrique à Strasbourg. Extrait des ANNALES DE GÉOPHYSIQUE. Tome 13, p. 186-202.

Lecolazet R., 1958a. La méthode utilisée à Strasbourg pour l'analyse harmonique de la marée gravimétrique-Instructions pratiques pour l'application de la méthode a un mois d'observations horaires-Avant-propos. Bull. d'Inf. Marées Terr. 10, 153–185.

Lecolazet, R., 1958b. Résultats provisoires des enregistrements de la marée gravimétrique, effectués à Strasbourg d'aut 1957 à février 1958. Deuxième Colloque international de la commission du CSAGI pour l'étude des marées terrestres.

Lecolazet, R., 1959. Résultats des observations de marée gravimétrique effectuées à Strasbourg jusqu'en 1958. Third International Symposium on Earth Tides. Trieste 1959.

Lecolazet, R., 1960. Rapport sur les observations de marée gravimétrique faites à Strasbourg en 1957, 1958 et 1959. B.I.M Nº21, p. 387-395.

Lecolazet, R., Steinmetz L., 1966. Premiers résultats expérimentaux concernant la variation semi-mensuelle lunaire de la pesanteur à Strasbourg. C. R. Acad. Sci. Paris, t. 263, p. 716-719.

Lecolazet, R., Steinmetz L., 1973. Nouveaux résultats expérimentaux concernant les ondes diurnes de la marée gravimétrique. Journal of the international association of geodesy. Nº 109, p. 301-307.

Lecolazet, R., Steinmetz L., 1974. Sur les ondes diurnes de la marée gravimétrique observée à Strasbourg. C. R. Acad. Sci. Paris, t. 278, p. 295-297.

Lecolazet, R., Melchior, P., 1977. Experimental determination of the dynamical effects of the liquid core of the Earth. Ann. Geophys., t.33, fasc. 1 / 2, p. 11-22.

Lecolazet, R., 1983. Correlation between diurnal gravity tides and the Earth's rotation rate. Proc. 9th Int. Symp. Earth Tides. N.Y., p. 527-530.

Legros H., Hinderer J., Lefftz M., Dehant V. 1993. The influence of the solid inner core on gravity changes and spatial nutations induced by luni-solar tides and surface loading. Physics of the Earth and Planetary Interiors, 76, pp 283-315.

Levine J., 1978. Observation of the nearly diurnal resonance of the earth using a laser strainmeter applications of geodesy to geodynamics. Geop 9; Ohio Univ. Dept Geodetic SC, Report 280, pp 341-343.

Liouville, J., 1858. Développements sur un chapitre de la Mécanique de Poisson. Journal de Mathématiques Pures et Appliquées, T3, 1-25.

Lomb, N.R., 1976. Least-Squares Frequency Analysis of Unevenly Spaced Data," Astrophysical and Space Science, 39, pp. 447-462. Geophysical Journal of the Royal Astronomical Society, v 71, issue 1, pp. 173-186.

Longuevergne L., Boy J-P., Florsch N., Viville D., Ferhat G., Ulrich P., Luck B., Hinderer J., 2009. Local and global hydrological contributions to gravity variations observed in Strasbourg. J. Geodyn 48 p. 189 – 194.

Love, A.E.H., 1911. Some problems of geodynamics. First published in 1911 by the Cambridge University Press and published again in 1967 by Dover, New York, USA.

Loyer S., Hinderer J. and Boy J.-P., 1999. Determination of the gravimetric factor at the Chandler period from Earth's orientation data and superconducting gravimetry observations. Geophys. J. Int. 136 1–7.

Lozhinskaya, A.M., 1959, The string gravimeter for measurement of gravity at sea: Bull. Acad. of Sci. USSR, Geophys. Ser. 3, p. 398-409.

Lyard, F., Lefevre, F., Letellier, T., Francis, O., 2006. Modelling the global ocean tides: modern insights from FES2004. Ocean Dynam. 56, 394–415.

Malkin, Z., 2004. A New Free Core Nutation Model with Variable Amplitude and Period. arXiv preprint physics/0407153.

Malkin Z., Terentev, D., 2007. Parameters of the Free Core Nutation from VLBI data. arXiv preprint physics/0702152.

Malkin, Z., 2013. Free core nutation and geomagnetic jerks. Journal of Geodynamics, 72, 53-58.

Marquardt, D.W., 1963. An algorithm for least-squares estimation of non-linear parameters. J. Soc. Ind. Appl. Math. 11 (2), 431– 441.

Martsyniak, A.Y., 1956. Opredelenje absoliutnoi velichiny uskoreniia sily trax zhesti po paderniiu zhezla v vakuume, Izmer. Tekh. Poverochn Delo, vol. 5, p. 11.

Mathews, P. M., Buffett, B. A., Herring, T. A. and Shapiro, I. I., 1991a. Forced nutations on the Earth: Influence of inner core dynamics, 1. Theory, J. Geophys. Res., 96, 8219 - 8242.

Mathews, P. M., Buffett, B. A., Herring, T. A. and Shapiro, I. I., 1991b. Forced nutations of the Earth: Influence of inner core dynamics: 2. Numerical results and comparisons, J. Geophys. Res., 96, 8243– 8257.

Mathews, P.M., Dehant, V. and Gipson, J.M., 1997. Tidal station displacements. Journal of Geophysical Research 102: doi: 10.1029/97JB01515.

Mathews, P. M., 2001. Love numbers and gravimetric factor for diurnal tides. Proc. 14th Int. Symp. Earth Tides. J. Geod. Soc. Jpn., 47(1), 231–236.

Mathews, P.M., Herring, T.A., Buffett, B.A., 2002. Modeling of nutation-precession: New nutation series for nonrigid Earth and insights into the Earth's interior. J. Geophys. Res. 107 (B4): ETG3-1-3-30.

Matsumoto, K., Takanezawa T., Ooe M., 2000. Ocean tide models developed by assimilating TOPEX/Poseidon altimeter data into hydro dynamical model: A global model and a regional model around Japan, J. Oceanogr., 56(5), 567–581.

McCarthy, DD., 1996. IERS Conventions 1996, IERS Technical Note 22.

Melchior, P., 1957. Rapport sur les marées terrestres. B.I.M Nº8, p. 1-30.

Melchior, P., 1966. The earth tides. Pergamon Press. Ltd., New York.

Melchior, P., Venedikov, A., 1968. Derivation of the wave M3 (811.279) from the periodic tidal deformations of the Earth. Phys. Earth Planet. Inter., 1, p. 363-372.

Melchior, P., Kuo, J.T., Ducarme, B., 1976. Earth tide gravity maps for Western Europe. Physics of the Earth and Planetary Interiors. Volume 13, Issue 3, p. 184–196.

Melchior, P., 1978. The Tides of the Planet Earth. Pergamon Press., Oxford, 609 pp.

Melchior, P., Moens, M., Ducarme, B., Van Ruymbeke, M.,1981. Tidal loading along a profile Europe-East Africa-South Asia-Australia and the Pacific Ocean. Physics of the Earth and Planetary Interiors. Volume 25, Issue 1, p. 71–106.

Melchior, P., De Becker, M., 1983. A discussion of world-wide measurements of tidal gravity with respect to oceanic interactions, lithospheric heterogeneities, Earth's flattening and inertial forces, Phys. Earth Planet. Int., 31, p. 27-53.

Melchior, P., Ducarme, B., Francis, O. 1996. The response of the Earth to tidal body forces described by second- and third-degree spherical harmonics as derived from a 12 year

series of measurements with the superconducting gravimeter GWR/T3 in Brussels, Phys. Earth Planet. Inter., 93(3– 4), 223–238.

Merriam J.B., 1992. Atmospheric pressure and gravity. Geophys. J. Int. 109 488–500

Merriam, J.B., 1993. A comparison of recent tide catalogues and the consequences of catalogue errors for tidal analysis. Bull. Inf. Marées terrestres, 115, 8515-8535.

Merriam J.B., 1994. The nearly diurnal free wobble resonance in gravity measured at Cantley, Quebec. Geophys. J. Int., 119, pp 369-380.

Merriam J.B., 1995. Non-linear tides observed with the superconducting gravimeter at Cantley, Quebec Geophys. J. Int. 123 529–40.

Metivier, L., Conrad, C.P., 2008. Body tides of a convecting, laterally heterogeneous, and aspherical Earth. J. Geophys. Res. 113, B11405.

Meurers, B., 2004. Investigation of temporal gravity variations in SG-records. Journal of geodynamics, v. 38, p. 423-435.

Meurers, B., 2012. Superconducting Gravimeter Calibration by Colocated Gravity Observations: Results fromGWRC025. International Journal of Geophysics, v 2012. doi:10.1155/2012/954271.

Molodensky, M.S., 1961. The theory of nutations and diurnal earth tides. IVme Symp. International sur les marées terrestres. Obs. Roy. Belg. Comm.n°188, S. Geoph.58, pp 25-56.

Mueller, I.I., 1969. Spherical and Practical Astronomy. Frederick Ungar Publ. Co., New York.

Müller, T.. and Zürn, W., 1983. Observation of gravity changes during the passage of cold fronts J. Geophys. 53, 155–162.

Müller, M., Arbic, B. K., Mitrovica, J. X., 2011. Secular trends in ocean tides: Observations and model results. Journal of Geophysical Research: Oceans (1978–2012), vol. 116, C5.

Mukai, A., Higashi, T., Takemoto, S., Nakagawa, I. and Naito, I., 1995. Accurate estimation of atmospheric e_ects on gravity observations made by a superconducting gravity meter at Kyoto, Phys. Earth Planet. Inter., 91, 149 - 159.

Mukai, A., Takemoto, S., Higashi, T., Fukuda, Y., 2001. Oceanic tidal loadings estimated from gravity observations in Kyoto and Bandung. J. Geod. Soc. Japan 47, 261–266.

Mukai A., Takemoto S., Yamamoto T., 2004. Fluid core resonance revealed from a laser extensometer at the Rokko-Takao station, Kobe, Japan. Geophys. J. Int 156, 22-28.

Munk, W., MacDonald, G.J.F., 1960. The Rotation of the Earth: A Geophysical Discussion, Cambridge University Press. (revised 1975) ISBN 0-521-20778-9.

Munk, W .H., and D. E. Cartwright (1966), Tidal Spectroscopy and Prediction, Phil. Trans. Roy.Soc., Ser.A., 259, pp. 533-581.

Nabighian M. N., Ander M. E., Grauch V. J. S., Hansen R. O., LaFehr T. R., Li Y., Pearson W. C., Peirce J. W., Phillips J. D. and Ruder M. E., 2005, Historical development of the gravity method in exploration Geophysics 70 63–89.

Neuberg J., Zürn, W., 1986. Investigation of the nearly diurnal resonance using gravity, tilt and strain data simultaneously. Proc. 10th Int. Symp. Earth tides. Consejo sup. de invest. Cient., Madrid, pp 305-312.

Neuberg J., Hinderer J., Zürn, W., 1987. Stacking gravity tide observations in central Europe for the retrieval of the complex eigenfrequency of the nearly diurnal free-wobble. Geophys. J. R. Astr. Soc., vol 91, pp 853-868.

Neuberg, J., Hinderer, J., Zürn, W., 1990. On the complex eigenfrequency of the "nearly diurnal free wobble" and its geophysical interpretation. Variations in Earth Rotation, 11-16.

Neumeyer J., 1995 Frequency-dependent atmospheric pressure correction on gravity variations by means of cross-spectral analysis Bull. Inf. Mar. Terr. 122 9212–20.

Neumeyer J., Hagedoorn J., Leitloff J. and Schmidt T., 2004. Gravity reduction with three-dimensional atmospheric pressure data for precise ground gravity measurements J. Geodyn. 38 437–50

Newton, I., 1687. Philosophiæ naturalis principia mathematica (Mathematical principles of natural philosophy) London. 1687. William Dawson, 1978.

Niebaur, H.J., 1998. Variability in Bering Sea ice cover as affected by a regime shift in the North Pacific in the period 1947-1996. Journal of Geophysical Research, 103(C12): 27, 717-27, 737.

Niebauer, T.M., 1987. New absolute gravity instruments for physics and geophysics [Ph.D. Dissertation], University of Colorado, Boulder, USA, 155pp.

Niebauer T. M., Sasagawa G. S., Faller J. E., Hilt R. and Klopping F., 1995. A new generation of absolute gravimeters Metrologia, 32, 159.

Pagiatakis, S.D., 2000. Application of the least-squares spectral analysis to superconducting gravimeter data treatment and analysis. Cahiers Du Centre Europeen De Geodynamique et de Seismologie (ECGS) 17, 103–113.

Pariiskii, N.N., 1963. The discovery of the Earth's Diurnal Nutation. Soviet Astronomy, Vol. 7, No.3, p.424.

Pertsev, B.P., 1958. Analyse Harmonique des marées. Izvestia Acad. Sc. URSS. Ser. Geoph.,n°8, pp 946-958.

Pertsev, B.P., 1961. Analyse harmonique de séries de 50 jours d'observations de variations des marées de la force de pesanteur. Bull. d'Inf. Marées Terr. 26, 554–571.

Peters A., Chung K.Y., Chu S., Nature, 1999, 400, 849-852.

Ping, Z., 2010. Analysis of very weak signals in seismic, climatic and tidal observations. (Doctoral dissertation, PhD thesis). Université catholique de Louvain.

Plantamour, E., 1864. Détermination télégraphique de la difference de longitude entre les observatories de Genève et de Neuchâtel. Extrait des Mémoires de la Société de physique et d'histoire naturelle de Genève. T. XVII.

Pliny (the Elder.), Jones, W. H. S., & Eichholz, D. E., 1949. Natural history (Vol. 2). Cambridge, Mass.: Harvard University Press.

Poincaré H., 1910. Sur la précession des corps déformables. Bull. Astron., vol.27, pp 321-356.

Polzer, G., Zfirn, W., Wenzel, H.-G. 1996. NDFW Analysis of Gravity, Strain and Tilt Data from BFO. Bull. Inf. Marées Terrestres 125:9514 - 9545.

Polzer, G., 1997. Analysis of earth tide observations for the determination of core resonance parameters (Doctoral dissertation, PhD thesis).

Popov, N. A., 1963, Nutational motion of the Earth's axis. Nature, 193, 1153.

Preston-Thomas H., Turnbull, L.G., Green, E., Dauphinee, T.M., and Kalra, S.N., 1960, An absolute measurement of the acceleration due to gravity at Ottawa: Canad. J. Phys., v. 38, p. 824-852.

Prothero, W.A., Goodkind, J. M., 1968, "A superconducting gravimeter," Review of Scientific Instruments, vol. 39, no. 9, pp.1257–1262.

Rebeur Paschwitz E., 1895. Horizontalpendel Beobachtungen auf der Kaiserlichen Universitäts-Sternwarte zu Strassburg 1892-1894. Beitrage zur Geophysik 2, pp 211-535.

Riccardi, U., Rosat, S., Hinderer, J., 2011. Comparison of the Micro-g LaCoste gPhone-054 spring gravimeter and the GWR-C026 superconducting gravimeter in Strasbourg (France) using a 300-day time series. Metrologia, 48, 28-39.

Riccardi, U., Rosat, S., Hinderer, J., 2012. On the Accuracy of the Calibration of Superconducting Gravimeters Using Absolute and Spring Sensors: a Critical Comparison, Pure Appl. Geophys., doi:10.1007/s00024-011-0398-8.

Richter, B., 1983. Three years of registration with the superconducting gravimeter. Bull. Inf. Mar. Terr. 93, 1–9.

Richter B., Zürn W., 1986. Chandler effect and nearly diurnal free wobble as determined from observations with a superconducting gravimeter. The Earth's rotation and reference frames for geodesy and geodynamics, pp 309-315, Kluwer, Dordrecht.

Richter, B.,Wenzel, H.-G., Zürn, W. and Klopping, F., 1995. From Chandler wobble to free oscillations: comparison of cryogenic gravimeters and other instruments in a wide period range, Phys. Earth Planet. Inter., 91, 131 - 148.

Richter, B., Warburton, R.J., 1997. A new generation of superconducting gravimeters. Proceedings of the 13th International Symposium on Earth Tides, Observatoire Royal de Belgique, Brussels. 545–555.

Rochester, M.G., Crossley D.J., 2009. Earth's long period wobble modes: a Lagrangian description, Geophys. J. Int., 176, 40–62.

Rogister Y., 2001. On the diurnal and nearly diurnal free modes of the Earth. Geophys J Int 144, 459-470.

Rogister, Y., 2010. Multiple inner core wobbles in a simple Earth model with inviscid core. Physics of the Earth and Planetary Interiors, 178(1), 8-15.

Roosbeek, F., 1996. RATGP95: An analytical development of the tide generating potential. Geophysical Journal International. V 126, Issue 1, p. 197-204.

Roosbeek, F., Defraigne, P., Feissel, M., Dehant, V., 1999. The free core nutation period stays between 431 and 434 sidereal days. Geophysical research letters, 26(1), 131-134.

Rosat, S., Hinderer, J., Crossley, D., 2002. A comparison of the seismic noise levels at various GGP stations. Bull. Inf. Marées Terr. 135, 10689–10700.

Rosat, S., Hinderer, J., Crossley, D. and Boy, J.P., 2004. Performance of superconducting gravimeters from long-period seismology to tides, J. of Geodyn., 38, (3-5), 461-476.

Rosat, S., Boy, J.-P., Ferhat, G., Hinderer, J., Amalvict, M., Gegout, P. and B. Luck, 2009a. Analysis of a ten-year (1997-2007) record of time-varying gravity in Strasbourg using absolute and superconducting gravimeters: new results on the calibration and comparison with GPS height changes and hydrology, J. of Geodyn., 48, 360-365.

Rosat, S., Florsch, N., Hinderer, J., Llubes, M. 2009b. Estimation of the Free Core Nutation parameters from SG data: sensitivity study and comparative analysis using linearized

Least-Squares and Bayesian methods, J. of Geodyn., 48, 331-339, doi:10.1016/j.jog.2009.09.027.

Rosat, S., Lambert, S.B., 2009. Free core nutation resonance parameters from VLBI and superconducting gravimeter data. Astron. Astrophys. 503, 287–291. Doi: 10.1051/0004-6361/200811489.

Rosat, S., Hinderer, J., 2011. Noise Levels of Superconducting Gravimeters: Updated Comparison and Time Stability, *Bull. Seism. Soc. Am.*, vol. 101, no. 3, June 2011, doi: 10.1785/0120100217.

Rosat, S., Calvo, M., Hinderer, J., Riccardi, U., Arnoso, J., W., Zürn, 2014. A comparison of the performances of some Gravimeters and a STS-2 Seismometer at the Gravimetric Observatory of Strasbourg. In Press. Studia Geophysica et Geodaetica.

Roosbeek, F., Defraigne, P., Feissel, M., Dehant, V., 1999. The Free Core Nutation period is between 431 and 434 sidereal days. Geophys. Res. Lett. 26 (1), 131–134.

Rydelek, P.A., Knopoff, L., 1982. Long-period lunar tides at the South Pole. J. Geophys. Res. 87, 3969-3973.

Sakuma A., 1963. Etat actuel de la nouvelle détermination absolue de la pesanteur au Bureau International des Poids et Mesures, Sevres:Bull. Geod., v. 69, p. 249-260.

Sakuma, A., 1970. Nat. Bur. Stand. (US) Spec. Pub. 343, p. 447-456.

Sakuma, A., 1973. A permanent station for the absolute determination of gravity approaching one micro-gal accuracy: in Mather, R.S., and Angus-Leppan, P.V. eds., Proc. Symp. On Earth's Gravitational Field and Secular Variations in Position: U. of New South Wales, p. 674-684.

Sasao, T., Okubo, S. and Saito, M., 1980. A simple theory on the dynamical effects of a stratified fluid core upon nutational motion of the Eart, Proc. IAU Symp.: Nutation and the Earth's rotation, (Eds.: Fedorov, E. P., Smith, M. L. and Bender, P. L.), Reidel, Dordrecht, 165 – 183.

Sasao T., Wahr J.M., 1981. An excitation mechanism for the free 'core nutation'. Geophys. J. R. Astr. Soc., vol 64, nr 3, pp 729-746.

Sato, T. 1991. Fluid Core Resonance Measured by Quartz Tube Extensometers at Esashi Earth Tide Station. In: Proc. 11th Int. Syrup. Earth Tides.. pp. 573 - 582. J. Kakkuri (ed.). Schweizerbart, Stuttgart.

Sato, T., Shibuya, K., Okano, K., Kaminuma, K., Ooe, M., 1993. Observation of Earth tides and Earth's free oscillations with a superconducting gravimeter at Syowa Station (status report). Proc. NIPR Symp. Antarct. Geosci. 6, 17-25.

Sato T., Tamura Y., Higashi T., Takemoto S., Nakagawa I., Morimoto N., Fukuda Y., Segawa J., Seama N., 1994. Resonance parameters of the free core nutation measured from three superconducting gravimeters in Japan. J. Geomag. Geoelectr., vol.46, pp 571-586.

Sato, T., Ooe, M., Nawa, K., Shibuya, K., Tamura, Y., Kaminuma, K. 1997a. Long-period tides observed with a superconducting gravimeter at Syowa Station, Antarctica, and their implication to global ocean tide modeling, Phys. Earth Planet. Inter., 103(1– 2), 39-53.

Sato, T., Nawa, K., Shibuya, K., Tamura, Y., Ooe, M., Kaminuma, K., Aoyama, Y., 1997b. Polar motion effect on gravity observed with a superconducting gravimeter at Syowa station, Antarctica. In: IAG Symposia. Segawa et al. (eds.) Gravity, Geoid, and Marine Geodesy, vol. 117, pp. 99–106. Berlin: Springer-Verlag.

Sato T., Tamura Y., Matsumoto K., Imanishi Y., Mac Queen H., 2002. Parameters of the fluid core resonance estimated from superconducting data. Bull. Inf. Marées Terrestres 136 p 10751–10759.

Sato T., Tamura Y., Matsumoto K., Imanishi Y., Mac Queen H., 2004. Parameters of the fluid core resonance inferred from superconducting gravimeter data. J Geodyn 38:375–389.

Shida, T., 1912. On the elasticity of the earth and the earth's crust, Memoirs of the College of Science and Engineering, Kyoto Imperial University, 4, 1-286.

Shirai, T., Fukushima, T., Malkin, Z., 2005. Detection of phase disturbances of Free Core Nutation of the Earth and their concurrence with geomagnetic jerks, Earth Planets Space, vol. 57, pp. 151-155.

Schweydar, W., 1914a. Harmonische Analyse d. Lotstörungen durch Sonne u. Mond. Ed. Potsdam, 4, 72 S.OBr. Umschl. leicht angeschmutzt. (Veröffentl. d. Königl. Preusz. Geodät. Inst. N.F. 59).

Schweydar, W., 1914b. Beobachtung der Änderung der Intesität der Schwerkraft durch der Mond. Sitzungsber Preuss. Akad. Wiss. XIV 454 – 465.

Schüller, K., 1977. Tidal analysis by the hybrid least squares frequency domain convolution method. In: Proceedings Eighth International Symposium on Earth Tides, Bonn, Germany, pp. 103-128.

Sloudsky TH., 1896. De la rotation de la terre supposee fluide a son interieur. Bull. Soc. Imp. Nat. Moscou, IX, pp 285-318.

Smith, M. L., 1974. The scalar equations of infinitesimal elastic-gravitational motion for a rotating, slightly elliptical Earth. Geophysical Journal International, 37(3), 491-526.

Souchay, J., Loysel, B., Kinoshita, H., Folgueira, M., 1999. Corrections and new developments in rigid Earth nutation theory. III. Final tables 'REN-2000' including crossed-nutation and spin-orbit coupling effects. Astron. Astrophys. 318, 639–652.

Spratt, R.S., 1982. Modelling the effect of atmospheric pressure variations os gravity. Geophys. J. R. Astron. Soc. 71, 173-186.

Standish, E. M., Jr., 1990. The observational basis for JPL's DE 200, the planetary ephemerides of the Astronomical Almanac. Astronomy and Astrophysics (ISSN 0004-6361), vol. 233, no. 1, July 1990, p. 252-271.

Steiner, A., 1988. : Bevezetés az alkalmazott geofizikába. I. J. 14-1642, Budapest.

Sterneck R. von, 1887. Der neue Pendelapparat des k.u.k. Militär-Geographischen Institutes. Mitt d. K.K. Milit.-Geogr. Inst.,VII, Wien 1887.

Sun H.-P., 1995. Static deformation and gravity changes at the Earth's surface due to the atmospheric pressure. Observatoire Royal del Belguique, Serie Geophysique Hors.Serie, Bruxelles.

Sun, H.-P., Hsu, H.-Z., Jentzsch, G., Xu, J.-Q., 2002. Tidal gravity observations obtained with superconducting gravimeter and its application to geodynamics at Wuhan/China. J. Geodyn. 33 (1–2), 187–198.

Swenson, S., and J. Wahr, 2002. Estimated effects of the vertical structure of atmospheric mass on the time-variable geoid, J. Geophys. Res., 107, pp. 2194-2205. doi: 10.1029/2000JB000024.

Tai, A., Tanaka, K., 2014. Secular Changes in the Tidal Amplitude and Influence of Sea-Level Rise in the East China Sea, Journal of Disaster Research Vol.9 No.1, 48-54.

Tamura, Y., 1987. A Harmonic Development of the Tide-Generating Potential, Bull. Inf. Mar. Terr., 99, 6813 - 6855

Tamura, Y., 1990. BAYTYP-G Users Manual. National Astronomical Observatory, Mizusawa.

Tamura, Y., Sato, T., Ooe, M., Ishiguro, M., 1991. A procedure for tidal analysis with a Bayesian information criterion. Geophys. J. Int., 104 (3), 507-516.

Tamura, Y., 1993. Additional terms to the tidal harmonic tables. In: Hsu HT (ed) Proc, 12th Int. Symp. Earth Tides. Science Press, Beijing, pp. 345-350.

Tamura, Y., Sato, T., Fukuda, Y., Higashi, T., 2001. Scale factor calibration of a superconducting gravimeter at Esashi Station, Japan, using absolute gravity measurements. J. Geodesy. 71, doi:10.1007/s00190-004-0415-0.

Tarantola, A., Valette, B., 1982. Inverse problems-quest for information. J. Geophys., 50, 159–170.

Tarantola, A., Valette, B., 1982b. Generalized non-linear inverse problems solved using the least squares criterion. Rev. Geophys. Space Phys. 20 (2), 219–232.

Thulin, A., 1960, Une détermination absolue de g au pavillon de Breteuil, par la méthode de la chute d'une règle divisée: Ann. Géophys., v. 16, p. 105-127.

Tomaschek, R. , and Schaffernicht, W., 1932. Tidal Oscillations of Gravity, Nature Volume 130, 165-166 (1932)

Tomaschek, R. 1937. Die Messungen der zeitlichen Änderung der Schwerkraft (Springer).

Toomre A., 1974. On the -nearly diurnal wobble- of the Earth. Geophys. J. R. Astr. Soc., vol.38, pp 335-348.

Torge W., 1989. Gravimetry. Walter de Gruyter. Berlin 465 pp.

Truman O.H. 1939. Variations in gravity at one place. Astrophysical Journal. Vol. 89. P 445-462.

Uppala, S.M., Kallberg, P.W., Simmons, A.J., Andrae, U., Costa Bechtold, V. Da, Fiorino, M., Gibson, J.K., Haseler, J., Hernandez, A., Kelly, G.A., Li, X., Onogi, k., Saarinen, S., Sokka, N., Allan, R.P., Andersson, E., Arpe, K., Balmaseda, M.A., Beljaars, A.C.M., Berg, L. van D., Bidlot, J., Bormann, N., Caires, S., Chevallier, F., Dethof, A., Dragosavac, M., Fisher, M., Fuentes, M., Hagemann, S., Holm, E., Hoskins, B.J., Isaksen, L., Janssen, P.A.E.M., Jenne, R., Mcnally, A.P., Mahfouf, J-F., Morcrette, J-J., Rayner, N.A., Saunders, R.W., Simon, P., Sterl, A., Trenberth, K.E., Untch, A., Vasiljevic, D., Viterbo, P., Woollen, J. 2005. The ERA-40 re-analysis. In: Quarterly Journal of the Royal Meteorological Society, 131 pp, 2961-3012.

Van Camp, M., Wenzel, H.-G., Schott, P., Vauterin P. and Francis O., 2000. Accurate transfer function determination for superconducting gravimeters, Geophys. Res. Lett. 27 (1), 37–40.

Van Camp, M., Vauterin, P., 2005. Tsoft: graphical and interactive software for the analysis of time series and Earth tides, Computers & Geosciences, 31(5) 631-640. doi:10.1016/j.cageo.2004.11.015.

Venedikov, A.P., 1961. Application à l'analyse harmonique des observations des marées terrestres de la méthode des moindres carrées. Comptes Rendues Académie Bulgare des Sciences 14 (7), 671-674.

Venedikov, A.P., 1966a. Une méthode d'analyse des marées terrestres à partir d'enregistrements de longueurs arbitraires. Observatoire Royal de Belgique, Série Géophysique 71, 463–485.

Venedikov, A.P., 1966b. Sur la constitution de filtres numeriques pour le traitement des enregistrements des marées terrestres. Acad. Roy. Belg. Bull. Cl. Sc.,5e Ser.t.LII,6 pp 827-845.

Venedikov, A.P., Vieira, R., de Toro, C., 1997. On the determination of the D and SD Earth tides generated by the tidal potential of third degree. Bulletin d'Informations des Marées Terrestres 126, 9635–9637.

Venedikov, A.P., Arnoso, J., Vieira, R., 2001. Program VAV/2000 for tidal analysis of unequally spaced data with irregular drift and colored noise. J. Geodetic Soc. Jpn. 47 (1), 281–286.

Venedikov, A.P., Arnoso, J., Vieira, R., 2003. VAV: a program for tidal data processing. Comput. Geosci. 29, 487–502.

Venedikov A.P., Arnoso J., Vieira R., 2005. New version of program VAV for tidal data processing. Computer & Geosciences, 31, 667-669.

Volet, Ch., 1963. Mesure de l'acceleration due à la pesanteur, au Pavillon de Breteuil: Comptes Rendus Acad. Sci. Paris, v. 235, p. 442-444.

Vondràk, J., Ron, C., 2006. Resonant period of free core nutation—its observed changes and excitations. Acta Geodyn. Geomater. 3 (143), 53–60.

Vondràk, J., & Ron, C., 2009. Stability of period and quality factor of free core nutation. Acta Geodyn. Geomater, 6(3), 217-224.

Wahr, J.M., 1979. The tidal motions for a rotating, elliptical, elastic and oceanless Earth, Ph.D. thesis, 216 pp., Univ. of Color., Boulder.

Wahr, J.M., 1981a. Body Tides on an Elliptical, Rotating, Elastic and Oceanless Earth, Geophys. J. R. Astron. Soc., 64, 677 - 703.

Wahr J.M., 1981b. A normal mode expansion for the forced response of a rotating Earth. Geophys. J. R. Astr. Soc., vol 64, nr 3, pp 651-675

Wahr, J.M., 1985. Deformation induced by polar motion J. Geophys. Res. 90 9363–8.

Wahr, J.M., and Bergen, Z., 1986. The effects of mantle inelasticity on nutations, Earth tides, and tidal variations in rotation rate, Geophys. J. R. Astron. Soc., 87, 633 - 668.

Wahr J.M., 1987. The theory of the earth's orientation, with some new results for the nutation. Proc. IAU Symp. N. 129; The impact of BLVI on Astrophysics and Geophysics, ed. J. Moran, Academic Publisher, p. 381-390.

Warburton R. J., and Goodkind J. M., 1977. The influence of barometric-pressure variations on gravity, Geophys. J. R. astr. Soc., 48, 281-292.

Warburton, R. J., Goodkind, J. M., 1978. Detailed gravity-tide spectrum between one and four cycles per day. Geophysical Journal International, 52(1), 117-136.

Warburton, R.J., Pillai, H., Reineman, R.C., 2010a. Initial results with the new GWR iGravTM superconducting gravity meter Extended Abstract Presented at 2nd Asia Workshop on Superconducting Gravimetry Taipei, Taiwan, (20-22 June 2010)

Warburton, R.J., Pillai, H., Reineman, R.C., 2010b. Initial results with the new iGravTM superconducting gravity meter. International Association of Geodesy (IAG) Symposium Proceedings Russia, St Petersburg 22–25 June 2010.

Wang, R., 1994 Effect of rotation and ellipticity on earth tides Geophys. J. Int. 117 562–5

Wang, R., 1997. Tidal response of the Solid Earth, Tidal Phenomena, (Eds.: Wilhelm, H., Zürn, W. and Wenzel, H.-G.), Springer, Berlin, 27-26.

Wenzel, H.G.and Zürn, W., 1990. Errors of the Cartwright-Tayler-Edden 1973 tidal potential displayed by gravimetric Earth tide observation at BFO Schiltach. Bull. Inf. Marées. Terr., 107, 7555-7574.

Wenzel, H.-G., 1994a. PRETERNA - a preprocessor for digitally recorded tidal data, Bull. Inf. Mar. Terr., 118, 8722-8734.

Wenzel, H.-G., 1994b. Earth tide analysis Package ETERNA 3.0, Bull. Inf. Mar. Terr., 118, 8719-8721.

Wenzel, H.-G., 1994c. Earth tide data processing package ETERNA 3.2, Bull. Inf. Mar. Terr., 120, 9019-9022.

Wenzel, H.-G., 1996a. Accuracy assessment for tidal potential catalogues. Bull. Inf. Mar. Terr., vol. 124, 9394-9416.

Wenzel, H.-G., 1996b. The nanogal software: Earth tide data processing package ETERNA 3.30. Bull. Inf. Mar. Terr., 124, 9425–9439

Wenzel, H.-G., 1997a. Tide-generating potential of the Earth. In: Wilhelm, H., Zürn, W., and Wenzel, H.-G. (Eds.), Tidal Phenomena, Lecture Notes in Earth Sciences, 66, 9–26, Springer, Berlin

Wenzel, H.-G., 1997b. Analysis of Earth tide observations. In: Wilhelm, H., Zürn, W., Wenzel, H.-G. (Eds.), Tidal Phenomena. Lecture Notes in Earth Sciences 66. Springer, Berlin, pp. 59–75.

Westerhaus, M. 1997. In: Helmut W, Zuern W, and Wenzel H-G (eds.) Tidal response of the Earth, in Tidal Phenomena, Lecture Notes in Earth Sciences, pp. 311-340. Berlin: Springer

Widmer, R., Zürn, W., Masters, G., 1992. Observation of low order toroidal modes from the 1989 Macquarie rise event. Geophys. J. Int., 111, 226-236.

Wu X.P., Wahr J.M., 1997. Effects on non-hydrostatic core-mantle boundary topography and core dynamics on Earth rotation. Geophys. J. Int., vol.128, pp 18-42.

Xi, QW., 1987. A new complete development of the tide-generating potential for the epoch J2000.0. Bull Inf Mar Terrest 99: 6766-6812

Xi, QW., 1989. The precision of the development of the tidal generating potential and some explanatory notes. Bull Inf Mar Terrest 105: 7396-7404.

Xu, J.-Q., Sun, H.-P., Luo, S.-C., 2002. Study of the Earth's free core nutation by tidal gravity data recorded with international superconducting gravimeters. Sci. China (Series D) 45 (4), 337.

Yoder, C.F., Williams, J.G., Dickey, J.O. , Schutz, B.E., Eanes, R.J., TapIcy, B.D., 1983. Secular variation of the Earth's gravitational harmonic J2 coefficient from LAGEOS and nontidal acceleration of Earth rotation, Na,ure, 303, 747-762.

Young, C.J., Lay, T., 1987. The Core-Mantle Boundary. Ann. Rev. Earth Planet. Sci. 1987, 15, pp. 25-46.

Zaske J., Zürn W., Wilhelm H., 1999. NDFW Analysis of Borehole Water level data from the hot-dry-rock test site Soultz-sous-Forêts. Bull. d'Informations Marees Terrestres 132, 10241–10270.

Zürn, W., Wenzel, H. G., Laske, G., 1991a. High quality data from LaCoste- Romberg gravimeters with electrostatic feedback: A challenge for superconducting gravimeters, Bull. Inf. Maréees Terrestres, 110, 7940–7952.

Zürn W., Rydelek P.A., 1991b. Investigation of the "nearly diurnal free wobble" -resonance in individual tidal records. Proc.11th Symp. Earth tides, Helsinki 1989; Schweizerbartsche verlagsbuchhandlung Stuttgart, pp 521-530.